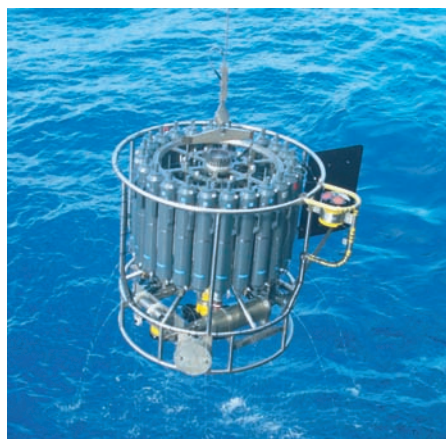




# The Effect of Halogens on Global Tropospheric Ozone

Gabriela Sousa Santos



## Hinweis

Die Berichte zur Erdsystemforschung werden vom Max-Planck-Institut für Meteorologie in Hamburg in unregelmäßiger Abfolge herausgegeben.

Sie enthalten wissenschaftliche und technische Beiträge, inklusive Dissertationen.

Die Beiträge geben nicht notwendigerweise die Auffassung des Instituts wieder.

Die "Berichte zur Erdsystemforschung" führen die vorherigen Reihen "Reports" und "Examensarbeiten" weiter.



## Notice

*The Reports on Earth System Science are published by the Max Planck Institute for Meteorology in Hamburg. They appear in irregular intervals.*

*They contain scientific and technical contributions, including Ph. D. theses.*

*The Reports do not necessarily reflect the opinion of the Institute.*

*The "Reports on Earth System Science" continue the former "Reports" and "Examensarbeiten" of the Max Planck Institute.*

## Anschrift / Address

Max-Planck-Institut für Meteorologie  
Bundesstrasse 53  
20146 Hamburg  
Deutschland

Tel.: +49-(0)40-4 11 73-0  
Fax: +49-(0)40-4 11 73-298  
Web: [www.mpimet.mpg.de](http://www.mpimet.mpg.de)

## Layout:

Bettina Diallo, PR & Grafik

Titelfotos:

vorne:

Christian Klepp - Jochem Marotzke - Christian Klepp

hinten:

Clotilde Dubois - Christian Klepp - Katsumasa Tanaka

# The Effect of Halogens on Global Tropospheric Ozone

Dissertation zur Erlangung des Doktorgrades der Naturwissenschaften  
im Departement Geowissenschaften der Universität Hamburg  
vorgelegt von

Gabriela Sousa Santos

Hamburg 2008

Gabriela Sousa Santos  
Max-Planck-Institut für Meteorologie  
Bundesstrasse 53  
20146 Hamburg  
Germany

Als Dissertation angenommen  
vom Department Geowissenschaften der Universität Hamburg

auf Grund der Gutachten von  
Prof. Dr. Guy P. Brasseur  
und  
Dr. Sebastian Rast

Hamburg, den 24. November 2008  
Prof. Dr. Jürgen Oßenbrügge  
Leiter des Departments für Geowissenschaften

# The Effect of Halogens on Global Tropospheric Ozone

---



Gabriela Sousa Santos

Hamburg 2008

Picture of frost flowers taken by Rachel Obbard at Kuujjuarapik-Whapmagoostui, Québec, Canada, in the framework of the International Polar Year.

---

# Contents

<b>1</b>	<b>Introduction</b>	<b>1</b>
1.1	Halogens in the troposphere . . . . .	2
1.2	Bromine sources in the troposphere . . . . .	6
1.3	Modelling bromine chemistry in the troposphere . . . . .	9
<b>2</b>	<b>Model Development</b>	<b>13</b>
2.1	Photolysis of Halogenated Species . . . . .	13
2.1.1	New photolysis reactions added to MOZART4 . . . . .	15
2.1.2	Simulations performed to test the photolysis in MOZART4 and its comparison to MOZART3 . . . . .	15
2.2	Heterogeneous Reactions of Halogens . . . . .	22
2.2.1	Mathematical description of heterogeneous chemical reactions . . . . .	23
2.2.2	Modelling heterogeneous chemical reactions . . . . .	27
2.2.3	Heterogeneous chemistry of BrONO <sub>2</sub> on aqueous aerosols . . . . .	28
2.2.4	Heterogeneous chemistry of bromine species on sulphate . . . . .	28
2.2.5	Heterogeneous chemistry of bromine species on sea salt . . . . .	30
2.2.6	Choice of the total reactive uptake . . . . .	35
2.3	Oceanic Emissions for the Very Short-Lived Halocarbons . . . . .	36
2.3.1	Bromoform observations used in the compilation of the emission inventory . . . . .	36
2.3.2	Calculation of emissions . . . . .	38
2.3.3	Resulting emission distribution and its evaluation . . . . .	40
2.3.4	The additional equatorial enhancement study . . . . .	42
2.3.5	The final run . . . . .	44
2.3.6	The other natural organohalogens . . . . .	46
2.3.7	Final global annual emissions . . . . .	48
2.3.8	Conclusion . . . . .	49
2.4	Dry Deposition of Halogens . . . . .	49
2.4.1	Parameters added to MOZART4 . . . . .	50
2.4.2	Deposition velocity results . . . . .	51
2.4.3	Conclusions . . . . .	54
2.5	Wet Deposition of Halogens . . . . .	54
2.5.1	Below-cloud scavenging in MOZART4 . . . . .	56
2.5.2	In-cloud scavenging in MOZART4 . . . . .	59
2.5.3	Simulations performed to test the reliability of the wet deposition rates for halogen species . . . . .	60
2.5.4	Analysis of the wet deposition simulation results . . . . .	61
2.5.5	Conclusion . . . . .	68

---

<b>3</b>	<b>The Effect of Bromine on Tropospheric Chemistry</b>	<b>71</b>
3.1	Simulations . . . . .	71
3.2	Bromine emissions from the simulations . . . . .	73
3.3	Evaluation of BrO . . . . .	74
3.4	Br <sub>x</sub> , partitions and chemistry . . . . .	89
3.5	Comparison with other modelling experiments . . . . .	97
3.6	Evaluation of ozone . . . . .	106
3.7	Evaluation of NO <sub>x</sub> and HO <sub>x</sub> . . . . .	109
3.8	Comparison with data composites . . . . .	111
<b>4</b>	<b>Summary</b>	<b>121</b>
<b>5</b>	<b>Outlook</b>	<b>125</b>
<b>A</b>	<b>Additional Chemistry in MOZART4</b>	<b>127</b>
<b>B</b>	<b>The Atmospheric Chemistry of Bromoform</b>	<b>131</b>

# List of Figures

1.1	Most important sources of reactive halogen species in the atmosphere. The size of the ellipses indicates the relative atmospheric burden of reactive halogens generated by the respective organohalogen. If a substance contains various halogens the size of the ellipse refers to the contribution of this organohalogen to the burden of reactive bromine only. Bromine is probably the most important halogen in the global troposphere. Solid ellipses mean that those substances contain bromine. Empty ellipses mean no bromine and the burden will come from Cl or I; green means natural origin; grey/black means anthropogenic origin of the respective compounds. . . . .	3
1.2	Scheme of the expected effect of halogen oxide radicals on the oxidation capacity of the troposphere (X=Br,Cl,I). Figure taken from Platt and Hönniger, 2003 [88]. . . . .	6
1.3	The spatial and temporal scales of trace gases in the atmosphere. Figure of W.L. Chameides in Brasseur <i>et al.</i> , 1999, page 113 [36]. . . . .	11
2.1	Photolysis rates for O <sub>2</sub> , O <sub>3</sub> (→ O( <sup>1</sup> D)), NO <sub>2</sub> , and N <sub>2</sub> O <sub>5</sub> for the MOZART4 model simulation (left side) and the MOZART3 model simulation (right side). Instantaneous output. . . . .	16
2.2	Photolysis rates (s <sup>-1</sup> ) for NO <sub>3</sub> for MOZART4 (top) (→ 0.89 NO <sub>2</sub> + 0.11 NO + 0.89 O <sub>3</sub> ) and MOZART3 (→ NO <sub>2</sub> + O – bottom left; → NO + O <sub>2</sub> – bottom right). Instantaneous output. . . . .	18
2.3	Photolysis rates (s <sup>-1</sup> ) for Br <sub>2</sub> in MOZART4. Instantaneous output. . . . .	18
2.4	Photolysis rates (s <sup>-1</sup> ) for Cl <sub>2</sub> and ClONO <sub>2</sub> (→ Cl + NO <sub>3</sub> ; → ClO + NO <sub>2</sub> ) for MOZART4 (left side) and MOZART3 (right side). Instantaneous output. . .	19
2.5	MOZART4 photolysis rates (s <sup>-1</sup> ) for the reactive bromine species BrONO <sub>2</sub> (→ Br + NO <sub>3</sub> – left; → BrO + NO <sub>2</sub> – right) and HOBr at the bottom. Instantaneous output. . . . .	20
2.6	MOZART4 photolysis rates (s <sup>-1</sup> ) for the very short lived halocarbons at the 1 <sup>st</sup> February 2000. Instantaneous output. . . . .	21
2.7	Zonal average of the sulphate weight percent (wt) calculated according to the parameterization of Tabazadeh <i>et al.</i> (1997) [120], and the total uptakes (Γ) for: the hydrolysis of BrONO <sub>2</sub> , the heterogeneous reactions of HOBr with HCL and of HOBr with HBr. . . . .	29

2.8	Analysis of the Br <sub>2</sub> and BrCl yield dependence from Br <sup>-</sup> concentration and pH by Fickert and co-workers [33]. The left panel shows Br <sub>2</sub> and BrCl yields (per HOBr) as a function of the Br <sup>-</sup> concentration at pH = 5.5. The yields were calculated for long exposure times when HOBr had decayed to almost zero. The right panel shows the ratio of Br <sub>2</sub> /HOBr counts (counts are proportional to concentration) as a function of pH. The dots represent the results of the experiment using a solution containing a Cl <sup>-</sup> concentration of 1 M and a Br <sup>-</sup> concentration of 10 <sup>-3</sup> M. The stars represent the results for sea water. Also shown in the right panel as a full line (right axis) is the representation of the calculated acid-dissociation curve of HOBr, based on a pKa=8.5. . . . .	33
2.9	Bromoform atmospheric mixing ratios in air at the surface (pptv) at coastal locations. Values reported by Quack and Wallace (2003) [92] are represented by circles; those from PEM Tropics campaigns A and B are represented by squares [109]. . . . .	36
2.10	Bromoform atmospheric mixing ratios in air at the surface (pptv) at open ocean locations. Values reported by Quack and Wallace (2003) [92] are represented by circles; those from PEM Tropics campaigns A and B are represented by squares [109]. . . . .	37
2.11	Bromoform boundary layer measurements done during the Pacific Exploratory Mission in the Tropical Pacific (PEM-Tropics) in phase A (August and September 1996) and B (March and April 1999) [109]. . . . .	38
2.12	Map of the bromoform emission areas used in the simulations: areas with zero surface emissions are in blue; the <i>left panel</i> represents simulation A with spatially homogeneous emissions over the ocean (green shaded area); the <i>right panel</i> represents simulation B or C in which coastal emissions (yellow shaded areas) are higher than over the open ocean (green shaded area). . . . .	39
2.13	Time evolution (1 February 2001 to 31 December 2002) for bromoform atmospheric mixing ratios (pptv), zonal mean at the surface for, from top clockwise: <b>simulation A</b> - spatially homogeneous oceanic emission - <b>simulation B</b> - coastal regions with 2.5 times higher emissions than open ocean - <b>simulation C</b> -coastal regions with 10 times higher emissions than open ocean. . . . .	41
2.14	Bromoform monthly average atmospheric mixing ratios (pptv) at the surface for March 2002 and 2003 (1 <sup>st</sup> column) and June 2002 and 2003 (2 <sup>nd</sup> column) for, top to bottom, <b>simulation A</b> , <b>simulation B</b> , and <b>simulation C</b> . . . .	42
2.15	Bromoform monthly average atmospheric mixing ratios (pptv) at the surface for March and July 2002 and 2003, for simulations B and C. Modelled data as box plots; observed mean values as individual points from Quack and Wallace, 2003 [92]. . . . .	43
2.16	Bromoform monthly average atmospheric mixing ratios (pptv) at the surface for March and July 2002 and 2003 from the simulations. The results are for the Pacific Ocean (longitude 150-290°, latitude 50°N – 50°S). . . . .	44
2.17	Bromoform atmospheric mixing ratios (pptv) at the surface of the ocean: the blue crosses are measurements from the PEM-Tropics campaign phase B (March and April 1999), and the polygons are medians for the results for March 2002 and 2003 for the Pacific Ocean (longitude 150-290°, latitude 50°N – 50°S) for each of the simulations. . . . .	45

2.18	Bromoform atmospheric mixing ratios (pptv) at the surface of the ocean: the red crosses are measurements from the PEM-Tropics campaign phase A (August and September 1996), and the polygons are medians for the results for September 2002 and 2003 for the Pacific Ocean (longitude 150-290°, latitude 50°N – 50°S) for each of the simulations. . . . .	45
2.19	Satellite data composites (Nov. 1978 June 1986) for phytoplankton pigment concentration ( $\text{mg}\cdot\text{m}^{-3}$ ) [lower values at the top of the legend bar], SeaWiFS Project, NASA). . . . .	46
2.20	Bromoform surface air concentrations versus SST ( <i>left</i> ) and versus Solar radiation ( <i>right</i> ) over the Pacific. The data is from the PEM-Tropics campaign B [109]. . . . .	46
2.21	Bromoform surface air concentrations versus Phytoplankton Pigment Concentration over the Pacific. The bromoform data is from the PEM-Tropics campaign B [109]. PPC data is from the SeaWiFS project. . . . .	47
2.22	Simulated bromoform monthly mixing ratio at the surface (pptv) for March 2001 - <i>left panel</i> . Comparison of the median of the simulated bromoform zonal mean concentrations for March 2001 with the PEM-Tropics boundary layer measurements in campaign B (March and April 1999) - <i>right panel</i> . . . . .	47
2.23	Simulated bromoform monthly mixing ratio at the surface (pptv) for September 2001 - <i>left panel</i> . Comparison of the median of the simulated bromoform zonal mean concentrations for September 2001 with the PEM-Tropics boundary layer measurements in campaign A (August and September 1996) - <i>right panel</i> . . . . .	48
2.24	MOZART4 result for O <sub>3</sub> dry deposition velocity [cm/s] (left panel). MOZECH result for OX dry deposition velocity [m/s] (right panel). Monthly average for January 2000. . . . .	52
2.25	MOZART4 result for NO <sub>2</sub> dry deposition velocity [cm/s]. Monthly average for January 2000. . . . .	52
2.26	MOZART4 result for HNO <sub>3</sub> dry deposition velocity [cm/s] (left panel). MOZECH result for HNO <sub>3</sub> dry deposition velocity [m/s] (right panel) Monthly average for January 2000. . . . .	53
2.27	MOZART4 result for CO dry deposition velocity [cm/s] (left panel). MOZECH result for CO dry deposition velocity [m/s] (right panel). Monthly average for January 2000. . . . .	53
2.28	MOZART4 result for the dry deposition [cm/s] of (from the top left clockwise): HBr, HCl, HOBr, and HOCl. Monthly average for January 2000. . . . .	55
2.29	Henry Effective Coefficient ( $k_H^*$ ) for HNO <sub>3</sub> (black) and other species (CH <sub>3</sub> COOH, HBr, HOBr, HCl, and HOCl) considered in this report [M/atm]. Note different scales. . . . .	62
2.30	MOZART4 results for the wet deposition rates on the surface for HNO <sub>3</sub> , CH <sub>3</sub> OOH, HBr, and HCl [ $\text{s}^{-1}$ ]: time evolution of the longitudinal average from 3 <sup>rd</sup> to 13 <sup>th</sup> March 2000 (left side), and global distribution for the first day of the simulation (right side). . . . .	63
2.31	Diurnal average for the precipitation [m/s]: convective (left panel) and stratiform (right panel). . . . .	64
2.32	Global surface cloud water content distribution for the 3 <sup>rd</sup> of March of 2000 [kg/kg] (diurnal average). . . . .	64

2.33	Volume mixing ratio for HNO <sub>3</sub> at the surface on the 3 <sup>rd</sup> of March 2000 [ppt] (diurnal average). . . . .	65
2.34	Global surface distribution of the rate of conversion of condensate to precipitation for the 3 <sup>rd</sup> of March of 2000 [K] (diurnal average). . . . .	66
2.35	Global surface temperature distribution for the 3 <sup>rd</sup> of March of 2000 [K] (diurnal average). . . . .	66
2.36	The difference in percent of the wet deposition rates of HNO <sub>3</sub> and HBr. . . . .	67
2.37	Diurnal average on the surface for the HBr volume mixing ratio [ppt] used in simulation 1 (equal to the volume mixing ratio of HNO <sub>3</sub> ) - left panel - and simulation 2 (equal to the volume mixing ratio of CH <sub>3</sub> COOH - right panel). . . . .	67
2.38	MOZART4 results for the wet deposition rates on the surface for HOBr in each of the experiments (simulation 1 at the top, simulation 2 middle row, and simulation 3 at the bottom): time evolution of the longitudinal average from 3 <sup>rd</sup> to 13 <sup>th</sup> March 2000 (left side), and global distribution for the first day of the simulation (right side). . . . .	68
2.39	Diurnal averages of volume mixing ratios (up) and wet deposition rates (bottom) for HOBr in simulation 1 (left side) and 2 (right side), on the 3 <sup>rd</sup> of March 2000, at meridian 90°. . . . .	69
2.40	MOZART4 results for the wet deposition rates on the surface for HOCl in each of the experiments (simulation 1 at the top, simulation 2 middle row, and simulation 3 at the bottom): time evolution of the longitudinal average from 3 <sup>rd</sup> to 13 <sup>th</sup> March 2000 (left side), and global distribution for the first day of the simulation (right side). . . . .	70
3.1	BrO vertical column density [molecules/cm <sup>2</sup> ] retrieved by GOME. . . . .	75
3.2	BrO vertical column density [molecules/cm <sup>2</sup> ] in the troposphere from the MOZART4 simulation <i>SS1</i> . Monthly averages of daily instantaneous results at 10h30 local time. . . . .	76
3.3	BrO vertical column density [molecules/cm <sup>2</sup> ] in the troposphere from the MOZART4 simulation <i>SS1ice</i> . Monthly averages of daily instantaneous results at 10h30 local time. . . . .	77
3.4	BrO vertical column density [molecules/cm <sup>2</sup> ] in the troposphere from the MOZART4 simulation <i>SS2ice</i> . Monthly averages of daily instantaneous results at 10h30 local time. . . . .	78
3.5	BrO vertical column density [molecules/cm <sup>2</sup> ] in the troposphere from the MOZART4 simulation <i>SS3ice</i> . Monthly averages of daily instantaneous results at 10h30 local time. . . . .	79
3.6	Surface area density of sea salt particles in MOZART4 [cm <sup>2</sup> /cm <sup>3</sup> ] in the simulation year 2000. . . . .	80
3.7	Bromine production from sea salt in MOZART4 simulations <i>SS1</i> [molecules/cm <sup>3</sup> /s] at the surface level. Monthly averages. . . . .	81
3.8	BrO volume mixing ratio [ppt] at MOZART4 surface level for simulation <i>SS1</i> . Monthly averages. Beware different scales. . . . .	82

3.9	Surface Area Density (SAD) of sea salt [ $\text{cm}^2/\text{cm}^3$ ] in MOZART4, simulation <i>SS1</i> at the surface. Each symbol represents a value at a certain grid point. The Northern hemispheric grid points are located between $32^{\circ}$ - $46^{\circ}$ N and $156^{\circ}$ - $176^{\circ}$ E. The Southern hemispheric grid points are located between $46^{\circ}$ - $60^{\circ}$ S and $184^{\circ}$ - $204^{\circ}$ E. . . . .	83
3.10	BrO volume mixing ratio [ppt] at the model surface level in simulation <i>SS1</i> . Each symbol represents a value at a certain grid point. The Northern hemispheric grid points are located between $32^{\circ}$ - $46^{\circ}$ N and $156^{\circ}$ - $176^{\circ}$ E. The Southern hemispheric grid points are located between $46^{\circ}$ - $60^{\circ}$ S and $184^{\circ}$ - $204^{\circ}$ E. . .	84
3.11	BrONO <sub>2</sub> volume mixing ratio [ppt] at the model surface level in simulation <i>SS1</i> . Each symbol represents a value at a certain grid point. The Northern hemispheric grid points are located between $32^{\circ}$ - $46^{\circ}$ N and $156^{\circ}$ - $176^{\circ}$ E. The Southern hemispheric grid points are located between $46^{\circ}$ - $60^{\circ}$ S and $184^{\circ}$ - $204^{\circ}$ E. . .	85
3.12	HOBr volume mixing ratio [ppt] at the model surface level in simulation <i>SS1</i> . Each symbol represents a value at a certain grid point. The Northern hemispheric grid points are located between $32^{\circ}$ - $46^{\circ}$ N and $156^{\circ}$ - $176^{\circ}$ E. The Southern hemispheric grid points are located between $46^{\circ}$ - $60^{\circ}$ S and $184^{\circ}$ - $204^{\circ}$ E. . .	86
3.13	Southern hemispheric view for September and October 2000 of the sea ice cover fraction in MOZART4, VTCD of BrO [ $\text{molecules}/\text{cm}^2$ ] for simulations <i>SS2ice</i> and <i>SS3ice</i> , and GOME retrievals. . . . .	87
3.14	BrO concentration profiles [ $\text{molecules}/\text{cm}^3$ ] resulting from measurements [35] (circles) and from Mozart4 simulations <i>SS2ice</i> (squares) and <i>SS3ice</i> (triangles) at Kiruna (model grid: $67.1^{\circ}$ N, $22.5^{\circ}$ E); monthly averages of daily instantaneous outputs at 10h30 local time. Symbols on the Y-axis represent small values below $1 \times 10^5$ . The standard deviation of the measurements is roughly 30%. . . . .	88
3.15	Monthly zonal averages of the total gas phase inorganic bromine Br <sub>x</sub> VMR [ppt] for simulation <i>SS1</i> . . . . .	90
3.16	Monthly zonal averages of the total gas phase inorganic bromine Br <sub>x</sub> [ppt] for simulation <i>S1</i> . . . . .	91
3.17	Monthly zonal averages of the total gas phase inorganic bromine Br <sub>x</sub> [ppt] for simulation <i>SS1ice</i> . . . . .	92
3.18	Monthly zonal averages of the total gas phase inorganic bromine Br <sub>x</sub> [ppt] for simulation <i>SS2ice</i> . . . . .	93
3.19	Monthly zonal averages of the total gas phase inorganic bromine Br <sub>x</sub> [ppt] for simulation <i>SS3ice</i> . . . . .	94
3.20	Meridional slice at longitude $180^{\circ}$ of HBr instantaneous VMR at the 1 <sup>st</sup> of March and the 1 <sup>st</sup> of September 2000 for simulation <i>SS2ice</i> . . . . .	94
3.21	Vertical distribution of the partitioning of the seven inorganic bromine species in the gas phase at longitude $180^{\circ}$ . Monthly average of the daily instantaneous outputs at 00:00 UCT in March 2000 for simulation <i>SS1ice</i> . . . . .	95
3.22	Vertical distribution of the partitioning of the seven inorganic bromine species in the gas phase at longitude $180^{\circ}$ . Monthly average of the daily instantaneous outputs at 00:00 UCT in March 2000 for simulation <i>SS2ice</i> . . . . .	96

3.23	Concentrations of the bromine species [molecules/cm <sup>3</sup> , ppt in square brackets] and highest chemical fluxes [molecules/cm <sup>3</sup> /s] calculated for some gridboxes in the region of high bromine production rates from sea salt in the Southern Pacific at the surface. Instantaneous output at the 1 <sup>st</sup> of April, 00:00 UTC (corresponding to local noon). . . . .	97
3.24	Distribution of monthly mean Br <sub>x</sub> [pptv] obtained by Yang <i>et al.</i> [138] near the surface in the simulation with an annual Br production from sea salt of 14 Gmol/yr. The model surface layer has an average height of about 65m over the surface. . . . .	99
3.25	Simulation <i>SS2ice</i> : Distribution of monthly mean Br <sub>x</sub> [pptv] at about 94m altitude above the surface for March, June, September, and December 2000. .	99
3.26	Simulation <i>SS1</i> results: horizontal distribution of monthly mean Br <sub>x</sub> [ppt] at 982hPa (94m altitude) for March, June, September, and December 2000. . . .	100
3.27	Vertical distribution of the monthly mean of the seven inorganic bromine species at 00:00h UTC in March for the simulation of Yang and co-workers [138]. The left panels are for concentrations (pptv), and the right panels are for percentages of total Br <sub>x</sub> . For the left panels, the minimum value for the various solid lines is 1 pptv increasing in steps of 1 pptv; for the right panels, the minimum value of the solid line is 10% increasing in steps of 10%. . . . .	102
3.28	Vertical distribution of monthly mean concentrations [pptv] of the seven inorganic bromine species at 00:00 UTC in March in simulation <i>SS2ice</i> . . . . .	103
3.29	Distribution of monthly mean tropospheric column BrO [ $\times 10^{13}$ molecules/cm <sup>2</sup> ] in daytime (09:00-15:00 LT) in <i>p</i> -TOMCAT [138]. . . . .	104
3.30	BrO profiles [pptv] resulting from measurements [35] and by Yang <i>et al.</i> [138] ( <i>p</i> -TOMCAT) at Kiruna (68 <sup>o</sup> N, 21 <sup>o</sup> E). The curve "Model(SMI)" represents the simulation including an equation for the sea salt droplet production rate that produces a bromine emission of 14 Gmol/yr; curve "Model(MON)" is the simulation with the bromine emission of 26 Gmol/yr. . . . .	105
3.31	The percent difference in ozone [%] between the simulations <i>G1</i> and the <i>Base run</i> (left) and <i>S1</i> and the <i>Base run</i> (right). Monthly average for September 2000. . . . .	106
3.32	Top: vertical tropospheric column density of BrO [molecules/cm <sup>2</sup> ] (left) and volume mixing ratio [pptv] of BrO at the surface (right). Bottom: volume mixing ratio [ppbv] of ozone at the surface and the percent difference in ozone between the simulations <i>SS3ice</i> and the <i>Base run</i> . Monthly average for September 2000. . . . .	107
3.33	Top: zonal average of the volume mixing ratio [pptv] of BrO. Bottom: volume mixing ratio [ppbv] of ozone at the surface and the percent difference in ozone between the simulations <i>SS3ice</i> and the <i>Base run</i> . Monthly average for September 2000. . . . .	108
3.34	Top: vertical tropospheric column density of BrO [molecules/cm <sup>2</sup> ] (left) and volume mixing ratio [pptv] of BrO at the surface (right). Bottom: volume mixing ratio [ppbv] of ozone at the surface and the percent difference in ozone between the simulations <i>SS3ice</i> and the <i>Base run</i> . Monthly average for September 2000. . . . .	109

3.35	Top: vertical tropospheric column density of BrO [molecules/cm <sup>2</sup> ] (left) and volume mixing ratio [pptv] of BrO at the surface over the South pole (right). Bottom: volume mixing ratio [ppbv] of ozone at the surface level and the percent difference in ozone between the simulations <i>SS3ice</i> and the <i>Base run</i> . Monthly average for September 2000. . . . .	110
3.36	Ozone monthly averages [ppb] at four stations of the CMDL group in the year 2000, and corresponding values for MOZART4 simulations. . . . .	111
3.37	Percent ozone difference between simulations <i>SS3ice</i> and <i>SS2ice</i> in September 2000. Clockwise we have the horizontal distribution, the zonal average, and a zonal slice at 180 <sup>0</sup> . . . . .	112
3.38	Horizontal distribution and zonal average of the percentage difference [%] between simulations <i>SS3ice</i> and <i>Base run</i> of the ratios NO <sub>2</sub> /NO and HO <sub>2</sub> /OH for September 2000. . . . .	113
3.39	Sea ice fraction in MOZART4 [0 to 1] and the distribution of BrO VMR [pptv] in simulation <i>SS3ice</i> at the surface for September 2000. . . . .	113
3.40	Comparison of methyl hydroperoxide (six upper panels) and formaldehyde (six lower panels) VMR profiles for the simulation <i>G1</i> (red) and the <i>Base run</i> (blue) with measurements from the TOPSE campaign (black). We present the profiles obtained at Boulder (left), Churchill (middle), and Thule (right) for the months of February and May. Boxes and whiskers indicate the central 50% and 90% of the observations, the vertical bar representing the median, the star indicating the mean. The dotted lines represent the standard deviation in time for the simulations. . . . .	115
3.41	Comparison of ethane (six upper panels) and propane (six lower panels) VMR profiles for the simulation <i>G1</i> (red) and the <i>Base run</i> (blue) with measurements from the TOPSE campaign (black). We present the profiles obtained at Boulder (left), Churchill (middle), and Thule (right) for the months of February and May. For further explanations, see Fig. 3.40. . . . .	116
3.42	Comparison of carbon monoxide (six upper panels) and PAN (six lower panels) VMR profiles for the simulation <i>G1</i> (red) and the <i>Base run</i> (blue) with measurements from the TOPSE campaign (black). We present the profiles obtained at Boulder (left), Churchill (middle), and Thule (right) for the months of February and May. For further explanations, see Fig. 3.40. . . . .	117
3.43	Comparison of H <sub>2</sub> O <sub>2</sub> (six upper panels) and SO <sub>2</sub> (six lower panels) VMR profiles for the simulation <i>G1</i> (red) and the <i>Base run</i> (blue) with measurements from the TOPSE campaign (black). We present the profiles obtained at Boulder (left), Churchill (middle), and Thule (right) for the months of February and May. For further explanations, see Fig. 3.40. . . . .	118
3.44	Comparison of (from top to bottom) methyl hydroperoxide, formaldehyde, ethane, and propane VMR profiles for the simulation <i>G1</i> (red) and the <i>Base run</i> (blue) with measurements from the PEM-Tropics A campaign (black), with the exception of formaldehyde, where we only have data from PEM-Tropics B. We present the profiles obtained at Easter Island (left), Fiji (middle), and Hawaii (right). For further explanations, see Fig. 3.40. . . . .	119

- 3.45 Comparison of (from top to bottom) monoxide carbon, PAN, H<sub>2</sub>O<sub>2</sub>, and SO<sub>2</sub> VMR profiles for the simulation *G1* (red) and the *Base run* (blue) with measurements from the PEM-Tropics A campaign (black). We present the profiles obtained at Easter Island (left), Fiji (middle), and Hawaii (right). For further explanations, see Fig. 3.40. . . . . 120
- B.1 Schematic oxidation path for bromoform till it releases all its bromine atoms. 131

# List of Tables

2.1	Photolysis of new species using aliases to the photolysis of existing species . . .	15
2.2	Global, 5-km altitude, mean photolysis rates $\bar{j}$ from MOZART4 (the base data was instantaneous output for the 1 <sup>st</sup> February 12:00 UTC) and in WMOs Scientific Assessment for Ozone [85] . . . . .	20
2.3	Review of literature about heterogeneous reactions of BrONO <sub>2</sub> and HOBr on sea salt . . . . .	34
2.4	Percentiles calculated for the air observations compiled by Quack and Wallace, 2003 [92] . . . . .	37
2.5	Bromoform fluxes for the different regions for each simulation . . . . .	39
2.6	The emission ratios of several halocarbons to bromoform according to Carpenter and Liss (2003) [21] and the data measured during the PEM-Tropics campaigns A and B [109] . . . . .	48
2.7	Global annual emissions of Br for each halocarbon simulated with MOZART2	48
2.8	Dry deposition velocities of HBr and HOBr (cm/s) used by Yang <i>et al.</i> , 2006 [138] . . . . .	50
2.9	Parameters introduced for the interactive halogen dry deposition computation	51
2.10	Average dry deposition velocities of HBr and HOBr (cm/s) resulting from MOZART4 . . . . .	54
2.11	Correspondence between the symbology in this report and the one in the model	57
2.12	Constant values in the wet deposition parameterization in MOZART4 . . . . .	58
2.13	Parameters for the computation of gas uptake by rain water . . . . .	60
3.1	Main experiments performed with MOZART4 for this study . . . . .	72
3.2	The global emissions obtained in MOZART4 simulations for the year 2000 . . .	73
3.3	The global emissions obtained from various MOZART4 simulations for the year 2000 and for the <i>p</i> -TOMCAT simulation of Yang and co-workers[138] . . .	98
A.1	Halogenated species and processes in which they interact . . . . .	127
A.2	Gaseous reactions . . . . .	128
A.2	Gaseous reactions — continued . . . . .	129
A.3	Photolysis reactions . . . . .	129
A.4	Heterogeneous reactions . . . . .	130



## Abstract

The aim of this work is to investigate the effects of halogens on tropospheric ozone and related tracers. Observations made in the polar regions have shown that large and episodic bromine emissions from sea ice in spring lead to substantial ozone depletion in the atmospheric boundary layer. It has been therefore postulated that the lack of halogen processes in chemistry-transport models of the troposphere could explain some discrepancies with observations.

We focus on bromine chemistry, because it is more efficient in ozone depletion than chlorine in the troposphere, and it has potentially higher emissions than iodine in the global tropospheric scale.

We chose the three-dimensional global chemistry transport model MOZART4 for our investigations, and expanded it with the relevant bromine chemistry, emissions and losses to the atmosphere. The use of a global model allows us to study the relative importance of the most relevant sources of bromine in the troposphere: bromocarbons, sea salt aerosols, and frost flowers. Frost flowers are sources of bromine located in the polar regions. Our experiments indicate that polar sources roughly account for 65% of yearly global bromine emissions, bromocarbons for 26%, and sea salt aerosol emissions for 9%. The latter emissions are probably underestimated. However, to improve the bromine emissions from sea salt particles, we need to take into consideration the acidity of the particles. This is a crucial characteristic of the particles that determines how much bromine is available for oxidation, thus producing bromine species that will be released from the particle into the gas phase.

Bromine oxide (BrO) concentrations associated with a vertical tropospheric total column density (VTCD) in the order of  $10^{13}$  molecules/cm<sup>2</sup> correspond to an ozone loss of 40-100% compared to a case in which the bromine chemistry is ignored. GOME satellite retrieves values of BrO VTCD in the order of  $10^{13}$  molecules/cm<sup>2</sup> over the polar regions at local spring. The effect of bromine chemistry on ozone is regional, and is due to polar emissions. Effects on species other than ozone are visible in larger geographical areas, and are mainly due to emissions of bromocarbons, mostly by the ocean.

The inclusion of the bromine chemistry in the model decreases the simulated oxidising capacity of the atmosphere. The performance of MOZART4 improves for species associated with the oxidation capacity of the atmosphere (CH<sub>3</sub>OOH, PAN, H<sub>2</sub>O<sub>2</sub>), which usually are overpredicted, and for species that are oxidised (CO, alkanes), which are usually underpredicted. The over and underprediction are in some cases greatly reduced.

The effects of bromine chemistry on the HO<sub>2</sub>/OH and NO<sub>2</sub>/NO concentration ratios are different from other modelling experiments and predictions reported in the literature. The expected effect is an increase for HO<sub>2</sub>/OH and a decrease for NO<sub>2</sub>/NO. We observe the same behaviour in the model, except in locations where the rate of bromine emission is high. We parameterise the emissions of bromine from sea salt aerosols and sea ice (proxy for the frost flowers and sea salt in the snowpack) using heterogeneous chemical reactions with BrONO<sub>2</sub> and HOBr reactants. This implies that the NO<sub>2</sub> and the OH that are part of the reactant molecules are removed from the atmosphere. Therefore the values of the concentration ratios have a different tendency than in model experiments in which bromine is produced as a simple flux.



# Chapter 1

## Introduction

This work aims to describe the impact of halogenated species on tropospheric ozone ( $O_3$ ). Halogenated species are in the focus of this study, because they are involved in the ozone destruction in the atmosphere. Despite the relatively small concentration of halogenated species in the atmosphere, their ozone destruction potential is high, because of the catalytic mechanism of ozone depletion that regenerates halogenated species making them available for further reactions with ozone.

Ozone is a reactive oxidant gas produced naturally in trace amounts in the Earth's atmosphere. In the troposphere, it is formed by photochemical reactions in the presence of so-called precursors such as CO, NO<sub>x</sub> and volatile organic compounds. In the stratosphere it is formed mainly by the reaction of molecular oxygen and atomic oxygen, the latter of which is a product of O<sub>2</sub> photolysis. A fraction of the ozone present in the troposphere is advected from the stratosphere. Ozone is central to the chemical and physical properties of both the stratosphere and troposphere. Most ozone (about 90%) is found in the stratosphere, where it constitutes a protective layer against the penetration of biologically harmful UV-B radiation. In the troposphere, ozone concentrations are about 10-100 ppb (parts per billion) in volume mixing ratio. Despite this low concentration, it plays an important role in the troposphere as a greenhouse gas and serves as a source of OH radicals, which drive the tropospheric chemistry during the day. OH radicals are the most important cleansers of the atmosphere, converting species like the pollutant CO, the greenhouse gas CH<sub>4</sub> or CH<sub>3</sub>Br, which depletes stratospheric ozone, into oxidized forms, which may be removed from the atmosphere rather rapidly. Thus, tropospheric O<sub>3</sub> plays a critical role in determining the oxidising and cleansing efficiency of the atmosphere [18]. Ozone is commonly known for being toxic for biological organisms. The use of fossil fuels by humans has led to an increase in the concentration of ozone precursors. The effect on the complex chemical cycles that form and remove ozone from the troposphere means that, since the industrial revolution, the net chemical source<sup>1</sup> of ozone globally increased by a factor of 5 ([133], page 262, table 5.8). Toxic levels of ozone are found locally, posing a threat to human health, animals [84], and plants, in this last case lowering agricultural yields.

The models that simulate ozone in the troposphere show significant discrepancies with observations. With this work, we like to contribute to the fundamental scientific understanding of tropospheric ozone, and improve the modelling of chemistry. For this purpose, we study possible mechanisms for the O<sub>3</sub> destruction by halogens.

---

<sup>1</sup>Net chemical source is the excess of production over destruction through chemistry. The ozone budget includes also the transport into the troposphere from the stratosphere and deposition on the Earth's surface.

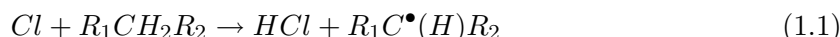
The troposphere is the lowest level of the atmosphere, extending from the Earth's surface up to the tropopause, which is at 10 to 15 km altitude depending on latitude and season. The troposphere is characterised by decreasing temperature with height and rapid vertical mixing. The next layer is the stratosphere, characterised by increasing temperature with altitude and low mixing. We will focus on tropospheric chemistry, in particular how it is affected by halogens.

Halogens including chlorine (Cl), bromine (Br), and iodine (I) are very reactive and are injected in the atmosphere mostly as organic compounds named halocarbons or organohalogenes. The higher the atomic weight of the halogen the lower the lifetime of the respective halocarbon due to its lower chemical stability. Another straightforward rule (and as every rule with exceptions) is that the higher the number of a kind of halogen in a compound, the lower the lifetime, corresponding again to its lower chemical stability. Figure 1.1 sketches the relative importance of halocarbons as sources of reactive halogens in the troposphere and stratosphere. We can observe that halocarbons of anthropogenic origin generally are more stable than halocarbons of natural origin. Consequently, their atmospheric lifetimes are different and they determine the atmospheric regions where the reactive inorganic halogenated species are released. The main degradation path for halocarbons is the photolysis and the oxidation through reaction with OH. In the troposphere, the halocarbons of anthropogenic origin (CFCs - chlorofluorocarbons, halons) as sources of reactive halogens are not important, since their chemical structures are too stable to be affected by the penetrating solar ultraviolet radiation. Only at higher altitudes, the energy of radiation is sufficiently high to dissociate them. The consequent release of the inorganic halogens leads to the so called stratospheric "Ozone hole", the ozone depletion produced by stratospheric halogen-induced photochemistry [115]. The halocarbons that may have an impact on the troposphere are mostly from natural origin. When compared to anthropogenic halocarbons, natural halocarbons contain a higher mole fraction of bromine and iodine atoms than chlorine, and contain no fluorine.

The ozone destruction in the troposphere is linked to catalytic reactions dominated by bromine [13, 16, 126, 93]. The explanation for the bromine proeminence in the tropospheric halogen chemistry lies in the particular reaction pathways of each halogen compound in the troposphere, and specifically reaction with organic compounds and NO<sub>x</sub><sup>2</sup>. Heterogeneous chemistry also plays a very important role. Its effect, however, remains poorly quantified, and will be examined in this study.

## 1.1 Halogens in the troposphere and their possible impact on ozone

Chlorine plays a role in the VOC<sup>3</sup>-NO<sub>x</sub> cycle that leads to ozone formation in the troposphere (R<sub>1</sub>, R<sub>2</sub> are arbitrary organic radicals):




---

<sup>2</sup>NO<sub>x</sub> = NO + NO<sub>2</sub>

<sup>3</sup>VOC - Volatile Organic Carbons

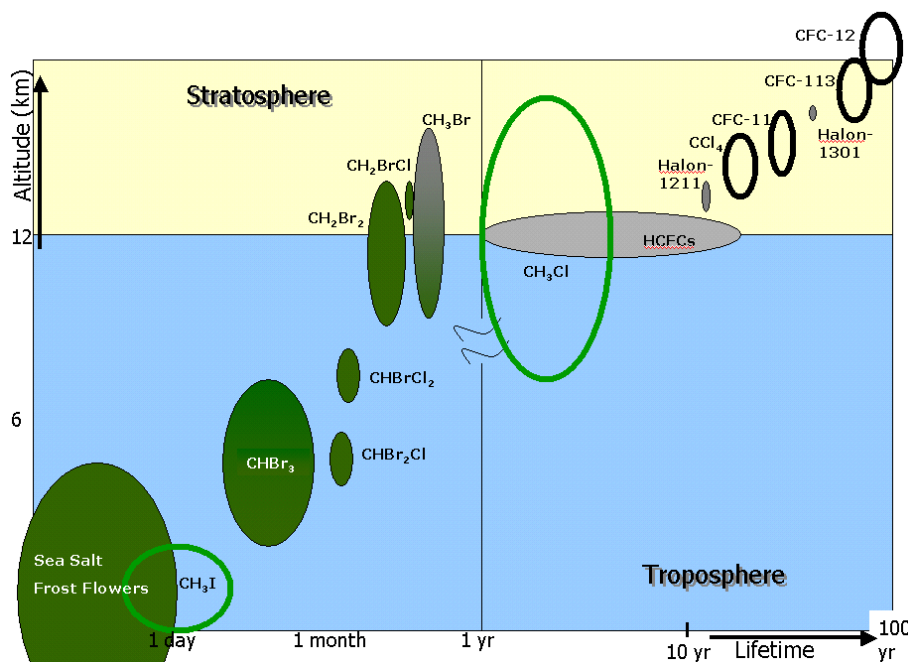
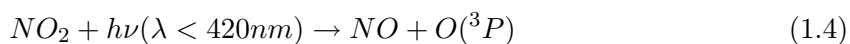


Figure 1.1: Most important sources of reactive halogen species in the atmosphere. The size of the ellipses indicates the relative atmospheric burden of reactive halogens generated by the respective organohalogen. If a substance contains various halogens the size of the ellipse refers to the contribution of this organohalogen to the burden of reactive bromine only. Bromine is probably the most important halogen in the global troposphere. Solid ellipses mean that those substances contain bromine. Empty ellipses mean no bromine and the burden will come from Cl or I; green means natural origin; grey/black means anthropogenic origin of the respective compounds.



Bromine does not play a similar role, because its reaction rates with organic compounds are generally much slower than similar reactions with chlorine [6]. On the contrary, bromine has an efficiency of ozone depletion in the troposphere that is 40% higher than that of chlorine. Iodine is even more efficient, but, because there are many unknowns regarding chemical kinetics, sources and sinks, its impact on ozone is still very uncertain. The best known organoiodide is  $CH_3I$ , with a global annual emission of around 2 Gmol/year [19]. However, many other organoiodine compounds exist, but due to their high photochemical instability they normally occur in atmospheric concentrations below the detection limit of current instrumentation. The high photochemical instability of the iodine halocarbons limits the chemical impact of iodine to the boundary layer, and due to their main origin in coastal regions, to the coastal marine boundary layer. McFiggans and co-workers [75] made a simulation study with a box model of the marine boundary layer including iodine chemistry. They tuned the model in order to achieve a good agreement between observations in Mace Head and Tenerife and the simulation results. They found that iodine-catalysed chemistry could account for up to 13% of  $O_3$  net destruction in the marine boundary layer. The impact of iodine is closely

linked to heterogeneous chemistry of bromine and chlorine. This permits the recycling of the iodine to the gas phase in the form of IX ( $X = \text{Cl}$  and  $\text{Br}$ ). However, because iodine is not an important element in sea salt, it is not emitted in similar quantities like chlorine and bromine. Therefore, it is unlikely that it will have a significant effect on the global tropospheric chemistry.

Consequently, bromine with relatively high emissions coming from natural halocarbons, relatively high content in sea salt, and low reaction rates with organic molecules, is in principle the most important halogen regarding its potential influence on ozone concentrations. This is supported by observations (see for example reference [11]), since Barrie and co-workers [13] first proposed it based on measurements of bromine<sup>4</sup> collected on cellulose aerosol filters at Alert (Canada).

The first evidence of the effect of reactive halogen species (RHS) on the tropospheric chemistry came in the mid-eighties with the observation of ozone depletion episodes in the Arctic region, when ozone concentration levels reached very low values (a few ppb or even less) [83, 17]. In later years, more field work showed that these episodes are consistently observed year after year at polar sunrise (e.g. [122, 114]). They were called "Polar Tropospheric Ozone Hole" episodes, and are observed for periods of hours to weeks over a large horizontal and vertical domain. The ozone concentration levels observed during the "Polar Tropospheric Ozone Hole" episodes were anti-correlated with bromine sampled in collected particles and with BrO concentration levels measured through long-path optical absorption (the reaction of Br with ozone yields BrO - reaction (1.6), so that the presence of BrO in the troposphere is an indication of ozone depletion). Similar ozone depletion events occur in the Antarctic region during local spring [48, 38, 131], but they are less pronounced [52]. These episodes are generally associated with weather situations that trap the air at the planetary boundary layer, promoting the accumulation of reactive bromine species to high concentration levels. The vertical structure of the ozone depleted layer was found to be distinct between the polar regions: in the Arctic the trapping is due to boundary layer temperature inversions, in the Antarctic this is observed due to catabatic surface winds [137, 122]. The existence of light during the ozone depletion events is necessary because bromine chemistry is driven by photolysis reactions.

Satellite retrieval allows to follow the vertical tropospheric column density of BrO globally all along the year<sup>5</sup>. The annual cycle of BrO distribution over the globe is observed, and shows a strong seasonal cycle in the polar regions. During polar spring, the chemical activation gives rise to enhancements of more than  $6 \times 10^{13}$  molecules/cm<sup>2</sup>. From February to May high column densities are retrieved over the North Pole, and similarly over the South Pole during September-December. This is due to the unique one-day/one-night light regime and, as already mentioned, due to the fact that BrO chemistry is driven by sunlight.

The ozone destruction by bromine occurs through the chemical reaction:



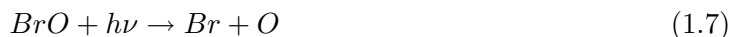
The reconversion of BrO to Br takes place over several cycles, the relative importance of

---

<sup>4</sup>Barrie and co-workers indicate that this bromine is the sum of particulate Br and gaseous HBr, and that from measurements at Alert they assume that 50-93% of it is gaseous.

<sup>5</sup>GOME and SCHIAMACHY satellite products that can be accessed at <http://www.oma.be/BIRA-IASB/Molecules/BrO/level3.php> or [http://www.iup.uni-bremen.de/doas/bro\\_from\\_gome.htm#Data](http://www.iup.uni-bremen.de/doas/bro_from_gome.htm#Data). Due to the uncertainties inherent to the instruments, retrieval, and the product derivation, the products should be used carefully (personal communication Andreas Richter). Last accessed April 24, 2008

which depends on the environmental conditions. During the day, the main pathway is the photolysis of BrO:



The self-reaction of BrO is important for locations and situations as the "Polar Tropospheric Ozone Hole" episodes, when bromine oxide concentrations are high <sup>6</sup>:



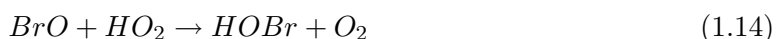
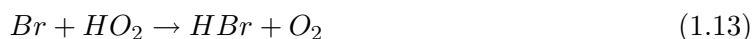
A second cycle is effective at low reactive halogen concentrations, e.g., in the free troposphere:



In regions with high NO<sub>x</sub> levels, the following reactions are predominant:



During the day, BrONO<sub>2</sub> is photolysed to BrO or Br relatively fast. During the night, it is a reservoir species, and may disappear through hydrolysis on aerosols. In this way, bromine is transferred to the aqueous phase. Other losses to the aqueous phase are due to wet deposition of two other reservoir species: HBr and HOBr. The conversion of Br into HBr, and BrO into HOBr, can take some hours through the reactions:



HBr and HOBr are both very soluble in water, and constitute the main loss of bromine from the gas phase.

An interesting and essential aspect of bromine chemistry in the atmosphere is the heterogeneous chemistry, i.e., chemical reactions of gas phase species on or in particles suspended in the atmosphere. First, multiphase reactions allow the recycling of bromine that was lost from the gas phase by deposition or reaction onto the particles. Second, from particles with bromine anions in their composition (as sea salt or shattered frost flowers - ice crystals formed from sea water over young sea ice), bromine may be emitted into the gas phase through heterogeneous chemistry. The heterogeneous reactions are considered to be essential for the formation of large concentrations of inorganic bromines (in the order of 25-35 ppt for Br<sub>2</sub>, BrCl, and BrO [88, 34]) observed in the Arctic during the "Polar Tropospheric Ozone Hole" episodes. This autocatalytical release of bromine into the gas phase is often called "bromine explosion". Besides the catalytic destruction of ozone, the chemistry of bromine in the troposphere may induce various changes in the chemical composition of the troposphere. Through the reactions described so far, the stationary state ratios of NO/NO<sub>2</sub> and HO<sub>2</sub>/OH decrease as it is indicated in Figure 1.2. Two important consequences result: 1) the production of

<sup>6</sup>The product of the self-reaction of BrO is Br<sub>2</sub>, but this product is rapidly photolysed into atomic bromine.

ozone in the troposphere is suppressed because NO and HO<sub>2</sub> concentrations decrease, and these are the products intervening in the limiting step reaction (1.15) of the ozone production in the troposphere; 2) OH concentration levels increase.

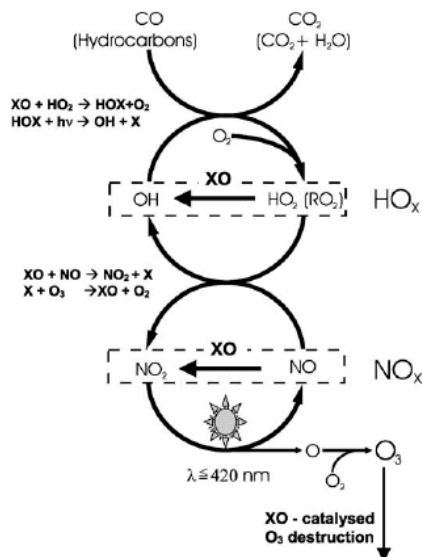
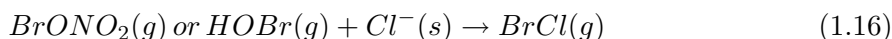


Figure 1.2: Scheme of the expected effect of halogen oxide radicals on the oxidation capacity of the troposphere (X=Br,Cl,I). Figure taken from Platt and Hönninger, 2003 [88].



Other effects of the bromine chemistry in the troposphere are the activation of chlorine through the heterogeneous reaction:



Chlorine, as already mentioned, reacts efficiently with organic molecules, and is a strong oxidant in the atmosphere. Moreover, bromine oxide reacts with mercury at the poles, accelerating its deposition; bromine oxide reacts with dimethyl sulfide (DMS) leading to a faster formation of sulfate aerosols, which in turn have an influence on cloud formation processes and ultimately on climate.

## 1.2 Bromine sources in the troposphere

The already mentioned bromine measured in filters in the Arctic has peak concentrations in March and April, well after the anthropogenic aerosol constituents have reached a maximum [12]. This hints at a local source for bromine. Initially, it was suggested that the source could be halocarbons, especially bromoform (CHBr<sub>3</sub>) [13]. Halocarbons are halogenated organic compounds, the atmospheric degradation of which releases reactive halogen species.

There are several reasons for which CHBr<sub>3</sub> was thought as the most important source of bromine in the troposphere: it is the most abundant halocarbon detected in the Arctic and its measurements are anti-correlated with ozone during the "Polar Tropospheric Ozone

Hole” episodes [13]; it has a high photodissociation rate[77]; it is the main halocarbon being emitted by algae, not only in the Arctic, but all over the ocean [92]; it may even have an impact on lower stratospheric chemistry [64, 109, 118].

Bromoform has a 58% contribution to the total tropospheric bromine burden. Other organic sources of bromine are dibromomethane ( $\text{CH}_2\text{Br}_2$ ), bromochloromethane ( $\text{CH}_2\text{BrCl}$ ), dibromochloromethane ( $\text{CHBr}_2\text{Cl}$ ), bromodichloromethane ( $\text{CHBrCl}_2$ ), and methyl bromide ( $\text{CH}_3\text{Br}$ ) [109]. Methyl bromide has natural and anthropogenic sources, and has the highest lifetime of the group. Therefore, it degrades in the higher troposphere and lower stratosphere (Figure 1.1). All the other molecules have a local lifetime of 0.5 years or less, and are called very short-lived species (VSLS), according to the definition of the World Meteorological Organisation [85].

These VSLS are mainly formed in the oceans. From measurements it is found that the abundance of most of the natural organic bromine compounds spatially correlates with the oceanic regions with high primary productivity [85]. The biogenic production seems to come from marine creatures (sponges, corals, sea slugs, tunicates, sea fans), seaweed, plants, fungi, phytoplankton, algae, bacteria, microbes, and some mammals. Their function seems to be chemical defence, facilitation of food gathering, or hormones [43]. Concerning bromoform in particular, the main sources seem to be seaweed, algae [20] (from which it is the main emission [24, 30, 98]) and phytoplankton[81, 91]. Bromoform emissions show a positive linear response to light and photosynthesis [43, 68, 25]. It is expected that one effect of the warming of the oceans will be the increase of primary production in the ocean [108]. This would probably enhance the release of natural halocarbons into the atmosphere. There may also be an abiotic chemical and photochemical bromoform production by UV-irradiation of sea water, bromide oxidation in water by chlorine, hypochlorite, ozone, and hydrogen peroxide, or by direct photochemistry in oxygenated and acidified sea water ([92], and work cited herein). The other natural halocarbons mentioned above seem to have a similar concentration distribution pattern as bromoform [9, 109]. Carpenter and Liss [20] analysed the ratios of concentration measurements of the less abundant natural halocarbons with bromoform in sea water. They observed that the ratios were remarkably constant in the open ocean, coastal waters and macroalgal beds. They added that this suggested a common source over the whole ocean or multiple sources with very similar emission patterns. The same analysis was made by us for the PEMTROPICS measurement campaign for the atmospheric volume mixing ratios and the results were similar to those reported in Carpenter and Liss.

The highest concentration levels of bromoform are observed in the equatorial region [109], where deep convection events occur. This process is characterised by rapid updrafts with sustained high vertical wind velocities covering an area of around 1 km in diameter. It can rapidly transport bromoform to the upper troposphere and the lower stratosphere. However, there is a counter-balancing slow downdraft outside the convectively active regions. Moreover, there is also frequent formation of heavy precipitation in convective clouds and anvil cirrus clouds that efficiently scavenge soluble gases [85]. The average mixing ratios of  $\text{CHBr}_3$  for the 8-12 km height region for all latitudes in the Pacific are 0.4-0.6 ppt [109]. Concomitantly, the global tropospheric burden of Br from the sum of halons and methyl bromide peaked in 1998 and since then declined by nearly 5% [80]. Decrease is also detected in the stratosphere [85]. The latter effect is due to international agreements and consequent measures to curtail the anthropogenic emissions. The decline in anthropogenic halocarbons in the atmosphere and the detection of natural halocarbons in the upper troposphere and lower stratosphere attracted the attention of the scientific community to their potentially

significant effect on chemistry in these high altitude regions [29, 85, 113].

However, in the polar troposphere, the analysis of the bromoform impact on chemistry soon showed that it did not yield enough RHS to account for the "Polar Tropospheric Ozone Hole" phenomenon. According to Moorgat *et al.*[82], the photodissociation rate constant of bromoform would result in a lifetime of three months under polar conditions<sup>7</sup>. The negative correlation found between the concentrations of ozone and bromoform during the ozone depletion events are probably due to simultaneous advection of air masses from the Arctic Ocean [139].

Besides VLSL, sea salt has been studied as a source of bromine. Sea salt is a relatively large atmospheric aerosol (particle diameter  $> 0.1 \mu\text{m}$ ), which means that its importance is limited to the marine boundary layer, due to fast removal by sedimentation and wet scavenging. It scatters solar radiation and constitutes reaction sites for reactive gases (as  $\text{HNO}_3$ ,  $\text{SO}_2$ ) and, most important for us, RHS. The heterogeneous reactions with the anion halides ( $\text{Cl}^-$ ,  $\text{Br}^-$ ) in sea salt transfer the halides into the atmosphere in the form of  $\text{Br}_2$  and  $\text{BrCl}$  and sequential formation of  $\text{BrO}$ . The contribution of atmospheric Cl species is less important, because  $\text{Br}_2$  formation and desorption from the particles is favored over the formation and release of  $\text{BrCl}$ . This is mainly due to a larger molecular dipole of  $\text{BrCl}$ , which makes it more probable that it will react before it diffuses out of the particle, producing  $\text{Br}_2$  [5]. Also, at the air-water interface of the particles, the presence of bromine anions is favored over the presence of chlorine, and thus the ratio  $\text{Cl}^-/\text{Br}^-$  is much lower than the 650:1 found in sea water [59, 60].

The reactions in the particle take place in the bulk aqueous phase and in the gas-liquid interface. Finlayson-Pitts [34] points out that the most important reactions in the aqueous phase are 1) acid-base reactions, 2) reactions initiated by  $\text{O}_3$ , 3) reactions with  $\text{OH}$ , 4) reactions with sulfur compounds, and 5) reactions with  $\text{NO}_3$  and  $\text{N}_2\text{O}_5$ . For 1) the products are  $\text{HCl}$  and  $\text{HBr}$ , which are very soluble and not expected to pass into the gas phase in a significant amount. Reactions 2) would lead to the formation of  $\text{HOBr}$ , but the uptake of  $\text{HOBr}$  from the gas phase or the formation through the hydrolysis of  $\text{BrONO}_2$  is more important. Reactions with  $\text{OH}$  would only be significant in the tropics. Processes 3) and 4) are important for the acid-base equilibrium in the particle, a key property of the particle for halogen heterogeneous chemistry. However, because the gas phase concentrations of species like  $\text{NO}_3$ ,  $\text{N}_2\text{O}_5$  or  $\text{NO}_2$  [116] do not make the reactions fast enough to result in an efficient bromine activation. The bromine activation is more an autocatalytic process so that chemically active bromine in the gas phase can activate additional bromine from the particles. Moreover, there is an increasing evidence that the reactions in the gas-liquid interface is more important for halides [34] than its reactions in the bulk phase, which makes heterogeneous reactions even more relevant.

Sea salt as a source of halogens has been studied in various thermodynamic states, as it was assumed that the bromide existing in suspended sea salt particles is insufficient to cause the "Polar Tropospheric Ozone Hole" episodes. Moreover, the highest  $\text{BrO}$  amounts have been observed in the polar regions over the sea ice[101, 141, 38]. It was proposed that frost flowers, and sea salt aerosols that have been deposited and incorporated in the snowpack [121], serve as additional sources of the halogens observed in the polar troposphere. Frost flowers are ice crystals formed from sea water, that grow over young sea ice, on frozen leads (linear breaks

---

<sup>7</sup>Globally, the atmospheric removal of bromoform is dominated by photolysis (lifetime 36 days) and by reaction with  $\text{OH}$  (lifetime 100 days). Both return an estimate for local lifetime of 26 days[85].

in the sea ice cover) and polynyas (openings between drift ice and fast ice or the coast). This additional source presents higher salinity and lower ratios of  $\text{Cl}^-/\text{Br}^-$  [65, 87, 94], and so potentially represent a higher source of halogens. Frost flowers last normally some days before being blown away or being covered by snow [87].

The process through which frost flowers release halogens into the gas phase is not clear. Its high surface area would mean high reaction rates for the surface heterogeneous reactions which are important for the catalytical cycle of bromine release. The measured pH of frost flowers is in the alkaline regime, which would mean a bromine activation process distinct from that on sea salt particles. Sander and co-workers [105] proposed a process in which the precipitation of calcium carbonate from the freezing sea water triggers acidity and the reactivation of the bromide. Recently, crystals of calcium carbonate were observed supporting this hypothesis (personal communication Lars Kaleschke).

Apart from the poles, BrO enhancement is locally detected at salt lakes [51, 73, 131, 119] and in volcano emissions [40, 7, 69, 14].

Until the end of the 90s, bromine chemistry was considered to be relevant for the tropospheric chemistry only within local scales. The evidence for BrO in the free troposphere was very limited. In 1998, Harder and co-workers [49] comparing ground-based observations and satellite column measurements found that the integrated stratospheric balloon profiles of BrO did not account for all the column BrO. They proposed that the missing quantities were BrO in the background troposphere, and they estimated its volume mixing ratios at 1-2 ppt. Subsequently, other comparative studies pointed to similar conclusions (for example [74, 103]). The supposed background volume mixing ratios of BrO proposed would have an important effect on tropospheric chemistry [88], as discussed in the last section. The major sources of halogens in the free troposphere would be halocarbons, sea salt particles, and transport from the poles. Actually, GOME observations show BrO transport from the poles to lower latitudes (personal communication Jens Hollwedel and published data [132, 102]). An analysis of BrO plumes observed by the GOME satellite between 1996-2001 shows an increasing area covered by these plumes occurring near both poles. In the Northern hemisphere the relative increase was 10% per year in the studied period [54]. Tarasick and Bottenheim [122] show the same trend with the analysis of historical ozonesonde records at stations located in the Arctic<sup>8</sup> and Antarctic. They link the increase of the frequency of boundary-layer ozone depletion episodes to the increase in mercury levels in Arctic biota observed in the last decades. The increase of ozone depletion events may be due to climate change effects, which are accompanied by a decrease in the area covered by old ice opening new areas for the formation of new ice which is rich in bromine. This would mean that the polar source of bromine in the atmosphere may increase in the future.

### 1.3 Modelling bromine chemistry in the troposphere

Modelling is the attempt to describe complex phenomena in nature with mathematical methods. In the case of this study, the complex processes are the chemistry of the atmosphere. We have to make simplifications, because of the lack of complete knowledge of the atmosphere, and the lack of computer resources that could perform the computation of all the connecting and feedback effects. However, a simplification does not necessarily weaken the conclusions. The most important issue for the modeller is to control which assumptions are in the model

---

<sup>8</sup>Start of regular ozone soundings in the Canadian Arctic: 1966.

and how they are used in the model, in order to interpret his results. The main purpose is to gain deeper insight in the importance of the various processes and not to give absolute correct values.

As scientists, we have questions regarding something intertwined in a complex system. In order to find and use the best suited model to answer our questions, we need to know what we can simplify in our complex system. In our case, the simplifications concern two main areas: the physical and/or chemical processes, and the spatial and temporal resolution. Some of the physical or chemical processes should be incorporated into the model in a more complete way, and others can just be ignored. E.g., in our particular case, we need a complete description of the chemical equations that govern ozone in the troposphere, but we do not need the description of the carbon cycle. We do not need the inclusion of ocean processes, but we need to prescribe information regarding ocean properties that influence the atmosphere or the chemistry we are studying, in particular sea surface temperatures and halocarbon emissions, for example.

As already mentioned, the other simplification is the use of a relatively low spatial and temporal resolution in the model. The scientific question has to be posed in such a way that we can answer it with our corresponding model resolution or we have to change the model. If we are interested in the German climate, we do not really need a description of the whole world. We can simplify the world and describe in more detail the climate over Germany. Furthermore, physical and chemical processes evolve in the atmosphere at different scales. For example, the wind has various scales of space and time. We have trade winds running distances of 1000 to 40,000 km in weeks, and on the other side, we have turbulence, which are wind motions within 1 km and developing in minutes, even seconds. The construction of a model implies the integration of the significant processes in different degrees of simplification depending on the scientific question. For chemistry, we show in Figure 1.3 a sketch of the spatial and temporal scales associated with trace gases in the atmosphere. As it can be seen, a model of tropospheric ozone should have a more detailed description of processes that evolve at the local scale and mesoscale. We can also observe the direct relation between the spatial and temporal scales. The temporal resolution of a model is determined by the integration timestep of the evolution equations. If we would like to resolve fast evolving processes with our model, we need to have a small timestep, that is at least two or three times shorter than the characteristic time scale of the processes we would like to describe.

A chemical system is the perfect example for the need of a model for understanding the interactions between the various chemical and physical processes. The main problem is that knowing the concentration of a species in the atmosphere does not mean to have knowledge about its relative importance in the chemical system. A species with low concentration interacting in a catalytic cycle may modify the concentration of another species that is much more abundant. For example, the OH concentration is very low compared to other species, however OH is the main cleanser of the atmosphere. In order to determine the concentration of the species in the atmosphere we need to integrate a large amount of variables, like temperature, pressure, and/or solar radiation that affect the reaction rates, like Earth surface characteristics affecting dry deposition, like precipitation rates affecting wet deposition, and so on. Without a model, the calculation of all the equations that govern such a chemical system would be fastidious and it is improbable that it gives the comprehensive understanding needed at atmospheric scales.

Therefore, our study of the effect of halogen chemistry on ozone chemistry demanded the use of a mathematical model. As already exposed, a model needs informed simplification. We

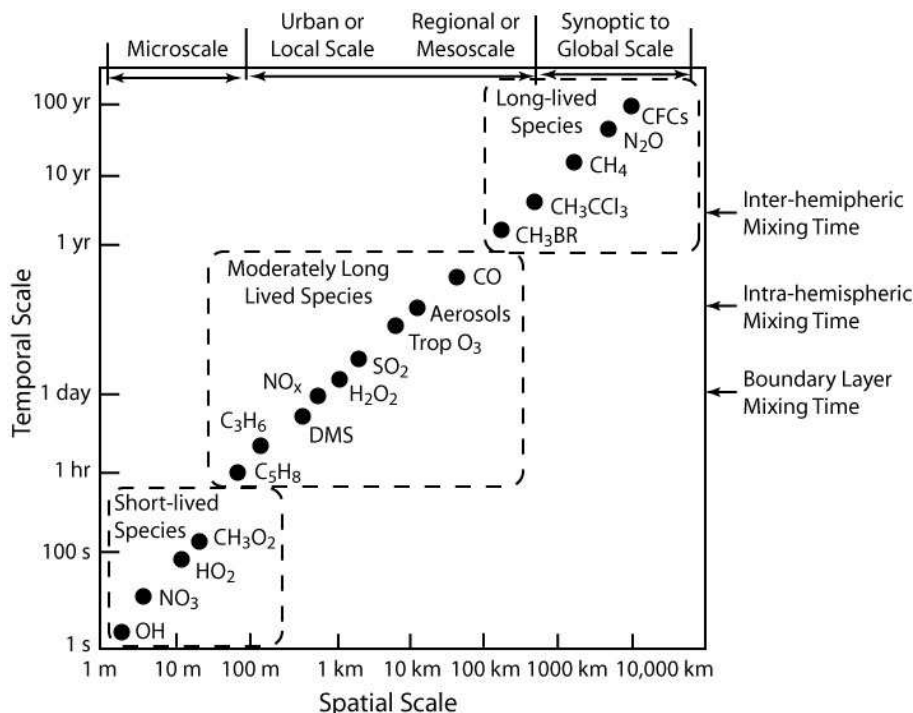


Figure 1.3: The spatial and temporal scales of trace gases in the atmosphere. Figure of W.L. Chameides in Brasseur *et al.*, 1999, page 113 [36].

could not introduce all the chemical reactions that are known to happen in the atmosphere. For the investigation of ozone and halogens, we need a model that includes the important reactions for these species. Moreover, our scientific question is the assessment of an impact of halogens on tropospheric ozone on a global scale, consequently it is mandatory to use a global model of the atmosphere containing the processes relevant to our scientific questions. However, we still can try to interpret local observations (e.g.: spectroscopic BrO measurements at Kiruna). The interpretation of our model results is reported in Chapter 3.

One model that is suitable for our work is MOZART4 (Model for OZone And Related Tracers, version 4). MOZART4 is a three-dimensional global chemistry transport model designed to simulate tropospheric ozone and its precursors. The model has been developed at the National Center for Atmospheric Research (NCAR, Boulder, U.S.A.), the Geophysical Fluid Dynamics Laboratory (GFDL, Princeton, U.S.A.), and the Max-Planck Institute for Meteorology in Hamburg (MPI-Met, Germany). It is an expansion of version 2 [55] with the inclusion of a more complete description of anthropogenic hydrocarbon chemistry, the inclusion of tropospheric aerosols (extended from the work of Tie *et al.* [124, 125]), and online calculations of dry deposition, water vapour, and biogenic emissions. For our work, the use of MOZART4 is more appropriate than the use of MOZART2, because it contained the interactive calculation of sea salt concentrations.

MOZART4 simulates the concentrations of 80 chemical trace species from the surface up to the middle/upper stratosphere (2 hPa), comprising a detailed chemistry scheme for tropospheric ozone, nitrogen oxides and hydrocarbon chemistry. In the standard configuration, the model simulations are performed at a  $2.8^0 \times 2.8^0$  horizontal resolution (128 longitude  $\times$  64 latitude grid boxes), 28 vertical levels extending up to approximately 42 km, and with a 20

minutes timestep. The meteorological fields for driving the dynamical core of the model are taken from the National Center for Environmental Prediction (NCEP) and NCAR Reanalysis [63] and are interpolated from a 6-hour time resolution to the 20-minutes timestep of the simulations. The emissions are taken from the European Union project POET (Precursors of Ozone and their Effects in the Troposphere)[42].

MOZART4 did not contain the halogen chemistry. We added a chemical scheme (our own simplification) that contains gas-phase, photolysis and heterogeneous reactions on sulfate and sea-salt particles. A total of 21 additional species and 83 additional reactions were introduced, which are listed in appendix A. We also needed to include the sources and sinks for these compounds. The description of the model development is provided in Chapter 2.

---

## Chapter 2

# Model Development

MOZART4 is a global chemical transport model designed to simulate the chemistry of ozone and its precursors in the troposphere. In the present study, we have extended the scope of the model, and we have introduced an additional scheme that accounts for the chemistry of halogens (listed in Appendix A). This includes the source species - short-lived halocarbons - and inorganic bromine and chlorine species and the relevant chemistry:

1. gas phase chemistry with ozone, nitrogen and hydrogen oxides, low mass hydrocarbons, chlorine and bromine inorganic species. The chemical parameters were taken from the JPL Publication 06-02 [6].
2. Photolysis reactions, which are essential for a radiation driven chemistry as is the halogen one (Section 2.1). Degradation by radiation is the main loss pathway for halocarbons and, with the exception of HBr and ClO, all the other inorganic halogen molecules are decomposed by light.
3. Heterogeneous reactions on sulphate and sea salt were included for the bromine species HOBr and BrONO<sub>2</sub> (Section 2.2).

The longest lived halocarbon considered in the model is CH<sub>3</sub>Br (atmospheric lifetime of circa 1.7 years). The surface concentration of this species is fixed using lower boundary conditions. For the remaining species (CHBr<sub>3</sub>, CH<sub>2</sub>Br<sub>2</sub>, CH<sub>2</sub>BrCl, CHBr<sub>2</sub>Cl, CHBrCl<sub>2</sub>) input files of surface emissions were prepared as described in Section 2.3.

Dry deposition and wet deposition are the two processes which constitute the atmospheric losses for halogen species from the gas phase. Dry deposition consists of the chemical species transport onto surfaces in the absence of precipitation and wet deposition, in the presence of precipitation. The inclusion of both processes into the model is explained in Sections 2.4 and 2.5.

### 2.1 Photolysis of Halogenated Species

Atmospheric chemistry is driven by the sun. The sun radiates electromagnetic energy into the atmosphere of the Earth. The elementary particle that carries the electromagnetic energy is called a photon. The energy of a photon of wavelength  $\lambda$  (or frequency  $\nu$ ) is described by Planck's law:

$$E = \frac{hc}{\lambda} = h\nu \quad (2.1)$$

where  $h$  is Planck's constant and  $c$  is the speed of light.

Photolysis is a reaction in which photons break down the bond that maintains atoms in a molecule, e.g.:



The photolysis rate  $j$  is a first-order rate constant for photolysis (units:  $s^{-1}$ ). It depends on the intensity of the actinic flux<sup>1</sup> and the photochemical and photophysical properties of the absorbing molecules. The radiation can lead to photolysis only if the bonding and antibonding orbitals in the molecule are separated by an energy that is equal to that of the energy of the incoming photon and if the transition is allowed (in quantum mechanics).

To calculate  $j$ , it is necessary to know the spectral actinic flux ( $I$ ), the quantum yield ( $\phi$ ) and the absorption cross sections ( $\sigma$ ), the latter two for each respective species. The quantum yield is the probability that the molecule will dissociate after the absorption of a photon. The absorption cross section is

$$\sigma = \frac{b}{n} \quad (2.3)$$

where  $b$  is the absorption coefficient of the gas ( $m^{-1}$ ) and  $n$  is the number of absorbing molecules per unit volume (molecules  $cm^{-3}$ ), also called the number density. The quantum yield  $\phi$  may be pressure dependent,  $\sigma$  may be temperature dependent, and both are wavelength dependent. These two quantities are experimentally determined. Then,  $j$  is calculated from:

$$j = \int_{\lambda_1}^{\lambda_2} \sigma(\lambda, T) \phi(\lambda, p) I(\lambda) d\lambda \quad (2.4)$$

where  $\lambda_1$  and  $\lambda_2$  are the shortest and longest wavelengths at which absorption occurs.

In MOZART4, the photolysis frequencies can be calculated interactively or by interpolation from tabulated values. In the former case, MOZART4 uses a fast-version of the Tropospheric Ultraviolet-Visible Model (TUV) [125]; this interactive photolysis calculation takes into account the presence of aerosols, in addition to the effect of clouds. Interpolation from tables are used in MOZART3 [86]: lookup table provides clear sky photolysis frequencies as a function of pressure, the ozone column above the current location, solar zenith angle, surface albedo, and temperature profile; these photolysis rates are then adjusted for the presence of clouds following Madronich [72].

Short-lived halocarbons absorb at  $\lambda > 290nm$ , which means that their photolytic loss occurs mostly in the troposphere. Nevertheless, removal by reaction with OH is the dominant loss process, with the exception of bromoform and dibromochloromethane for which photolysis has a similar importance [85].

---

<sup>1</sup>Actinic flux is the quantity of light available to molecules at a particular point in the atmosphere and which, by absorption, drives photochemical processes in the atmosphere.

### 2.1.1 New photolysis reactions added to MOZART4

For the photolysis of the halocarbons and Br<sub>2</sub>, we introduced in the model aliases to already existing photolysis reactions in the code (see table 2.1). We chose the aliases on the basis of calculations with TUV, version 4.1. We used quantum yields and absorption cross sections which are a function of wavelength. These quantities are tabulated in JPL [6]. We emphasise that it is important to make sure that the integration region in equation (2.4) is similar for all the photolysis rates that we wish to compare in order to establish aliases.

Table 2.1: Photolysis of new species using aliases to the photolysis of existing species

New species	Alias species	$j_{new}/j_{alias}$
CHBr <sub>3</sub>	PAN <sup>2</sup>	1.2
CH <sub>2</sub> Br <sub>2</sub>	PAN	$2.4 \times 10^{-4}$
CHBr <sub>2</sub> Cl	PAN	$6.1 \times 10^{-1}$
CHBrCl <sub>2</sub>	PAN	$3.8 \times 10^{-1}$
CH <sub>2</sub> BrCl	PAN	$3.1 \times 10^{-8}$
Br <sub>2</sub>	NO <sub>3</sub>	$1.4 \times 10^{-1}$

The other photolysis rates listed in table A.3 were already implemented in MOZART4.

### 2.1.2 Simulations performed to test the photolysis in MOZART4 and its comparison to MOZART3

Instantaneous photolysis rates were calculated for the 2<sup>nd</sup> of February 2001, 12:00 UCT for MOZART4. We chose several chemical species and analysed their values in comparison to the instantaneous results for February 2001, 12:00 UCT for MOZART3 or the literature. We chose:

- important atmospheric chemistry species as O<sub>2</sub>, O<sub>3</sub>, NO<sub>2</sub>, NO<sub>3</sub>, and N<sub>2</sub>O<sub>5</sub>;
- new species whose photolysis is calculated through tables existing in MOZART4, as Cl<sub>2</sub>, ClONO<sub>2</sub>, BrONO<sub>2</sub>, and HOBr;
- new species whose photolysis is calculated through aliases (table 2.1).

From the analysis, we concluded that there is a very good agreement between the photolysis rates produced by MOZART4 and the reference that we used for comparison. The comparison between the results of the two MOZART versions assures that the introduction of the photolysis of the new species in MOZART4 was done properly. We like to mention that a comparison between the results is possible even when we compare two simulations computed with different dynamic fields.

Figure 2.1 shows the photolysis rates for both models for the following reactions:




---

<sup>2</sup>Peroxyacetyl nitrate, CH<sub>3</sub>C(O)OONO<sub>2</sub>.

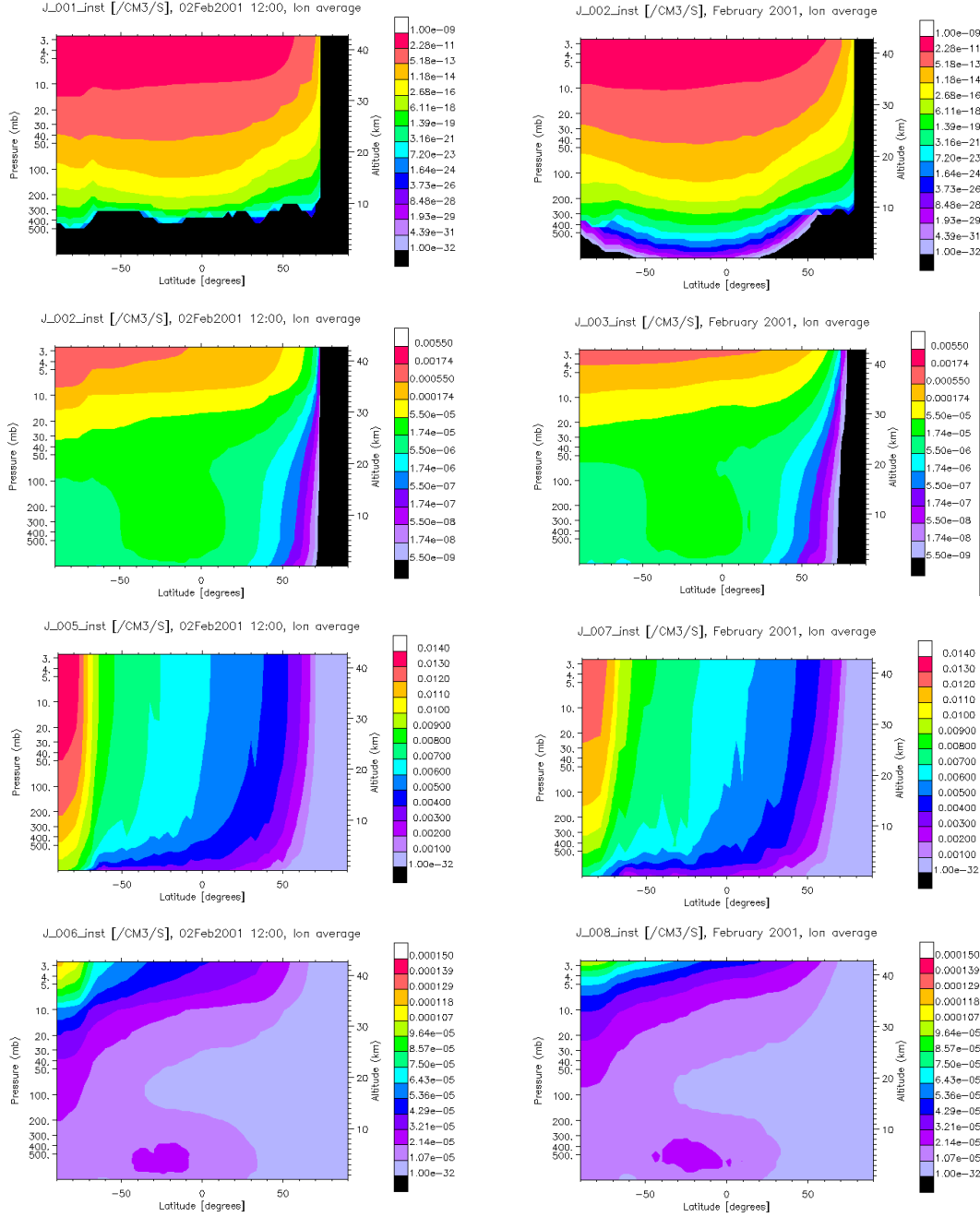


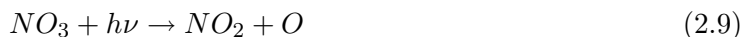
Figure 2.1: Photolysis rates for  $O_2$ ,  $O_3$  ( $\rightarrow O(^1D)$ ),  $NO_2$ , and  $N_2O_5$  for the MOZART4 model simulation (left side) and the MOZART3 model simulation (right side). Instantaneous output.

In MOZART4, the photolysis reactions that are important for very low wavelengths are restricted to model levels with pressure below 300-500 hPa, which is not the case in MOZART3. Therefore, the photolysis rates are zero for  $O_2$  in MOZART4 while there are (low) values in

MOZART3. This is demonstrated in Figure 2.1 (first row).

According to NCAR publication [36] (table on page 98 and appendix N), the photolysis rates for molecular  $O_2$  varies between 20 to 40 km altitude within  $10^{-12}$ – $10^{-15(3)}$   $s^{-1}$  and within  $10^{-11}$ – $10^{-9(3)}$   $s^{-1}$ , respectively. This corresponds well to the results of both MOZART3 and MOZART4.  $O_3$ ,  $NO_2$  and  $N_2O_5$  are also in fairly good agreement with the references. All show vertical profiles similar to those found in the literature.  $O_3$  has a slight *S* shape,  $NO_2$  is mostly constant, and  $N_2O_5$  is an elbow shaped curve, with the minimum around 100 hPa and a flattening of the curve occurring around 5 hPa. The absolute values for the model results and of the plots shown in the NCAR publication [36] are of the same order of magnitude.

Let us look into another atmospherically important photolysis process: the photodissociation of  $NO_3$ . We checked both photolysis channels, with a branching ratio of 90% for (2.9) and 10% for (2.10):



In MOZART4, both reactions are joined into a single reaction:



The literature indicates that the photolysis rates under clear sky conditions for (2.9) is  $1.9 - 3 \times 10^{-1}$   $s^{-1}$  and for (2.10)  $1.6 - 4 \times 10^{-2}$   $s^{-1}$  [112, 36]. The results for both models (Figure 2.2) show generally lower values than these, but the difference is the one expected when we take into consideration that the models take cloud and aerosol scattering into account.

Using TUV, we obtain a photolysis rate for  $Br_2$  which is about 1.4 times of that of reaction (2.10). On the other side,  $j_{NO_3}$  for the overall reaction (2.11) is 10 times the  $j$  for reaction (2.10). Combining these two relations, we obtain  $j_{Br_2} = 0.14 \times j_{NO_3}$  for MOZART4. The result is shown in Figure 2.3. Again using TUV, we derive a ratio  $j_{Br_2}/j_{Cl_2}$  around 15, which the model also shows (see Figures 2.3 and 2.4, first row, left panel).

$ClONO_2$  photolysis rates are shown in Figure 2.4, the second row showing the results for reaction (2.12) and the third row for reaction (2.13). TUV and the NCAR publication put the photolysis rates for these species at  $10^{-6}$ – $10^{-5}$   $s^{-1}$ , which is confirmed by the results.



The results for the reactive species  $BrONO_2$  and  $HOBr$  are shown in Figure 2.5. The photolysis rates of the short lived halocarbons are shown in Figure 2.6. We calculated the global photolysis rate for the first five km altitude in order to compare with values tabulated in WMOs Scientific Assessment for Ozone [85] (see table 2.2). Both estimates are rough estimates and strongly depend on the exact meteorological conditions even if it is a global average. Nevertheless, we obtained a fairly good agreement. The largest differences are found for the

---

<sup>3</sup>These two ranges for the photolysis rates at two altitudes are due to the consideration of different solar zenith angles.

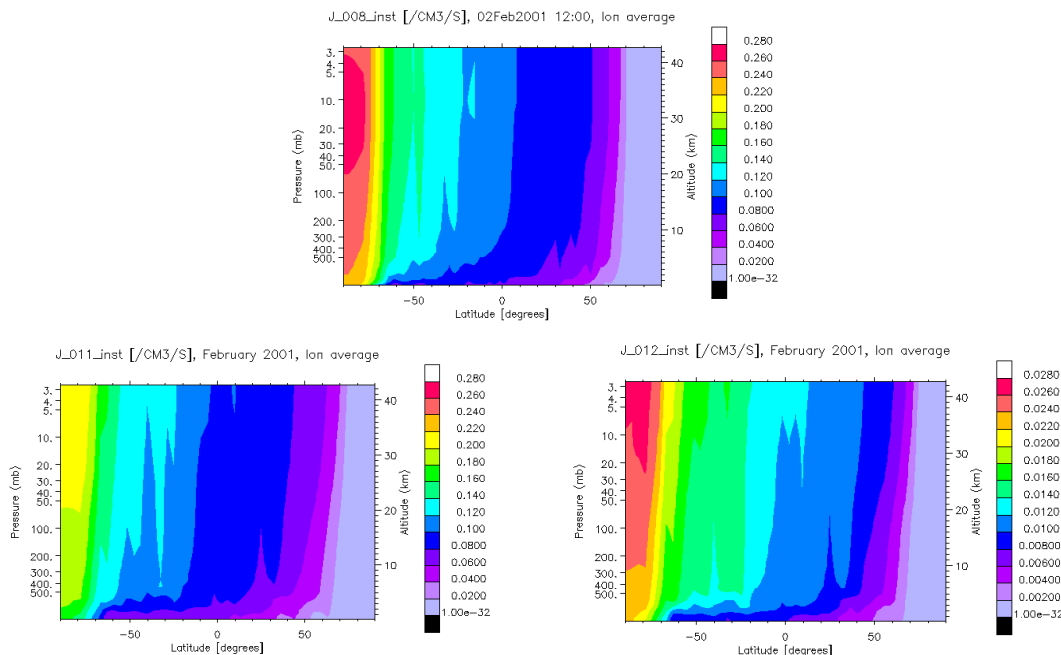


Figure 2.2: Photolysis rates ( $\text{s}^{-1}$ ) for  $\text{NO}_3$  for MOZART4 (top) ( $\rightarrow 0.89 \text{NO}_2 + 0.11 \text{NO} + 0.89 \text{O}_3$ ) and MOZART3 ( $\rightarrow \text{NO}_2 + \text{O}$  - bottom left;  $\rightarrow \text{NO} + \text{O}_2$  - bottom right). Instantaneous output.

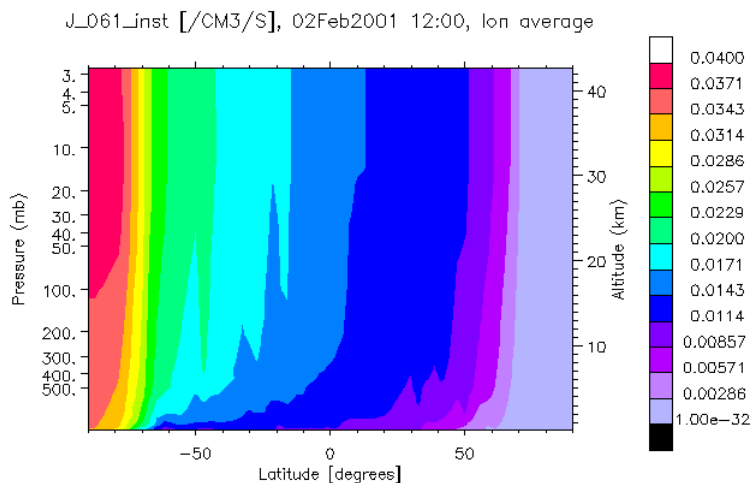


Figure 2.3: Photolysis rates ( $\text{s}^{-1}$ ) for  $\text{Br}_2$  in MOZART4. Instantaneous output.

reactive species  $\text{BrONO}_2$ ,  $\text{HOBr}$ , and for the VSLs  $\text{CH}_2\text{BrCl}$ . Concerning the VSLs, the decreasing order of the stability of their chemical compositions found in the laboratory (personal communication of John Orlando) is as follows:  $\text{CHBr}_3$ ,  $\text{CHBr}_2\text{Cl}$ ,  $\text{CHBrCl}_2$ ,  $\text{CH}_2\text{Br}_2$ ,  $\text{CH}_2\text{BrCl}$ . This is reflected in the photolysis rates calculated by MOZART4 (table 2.2).

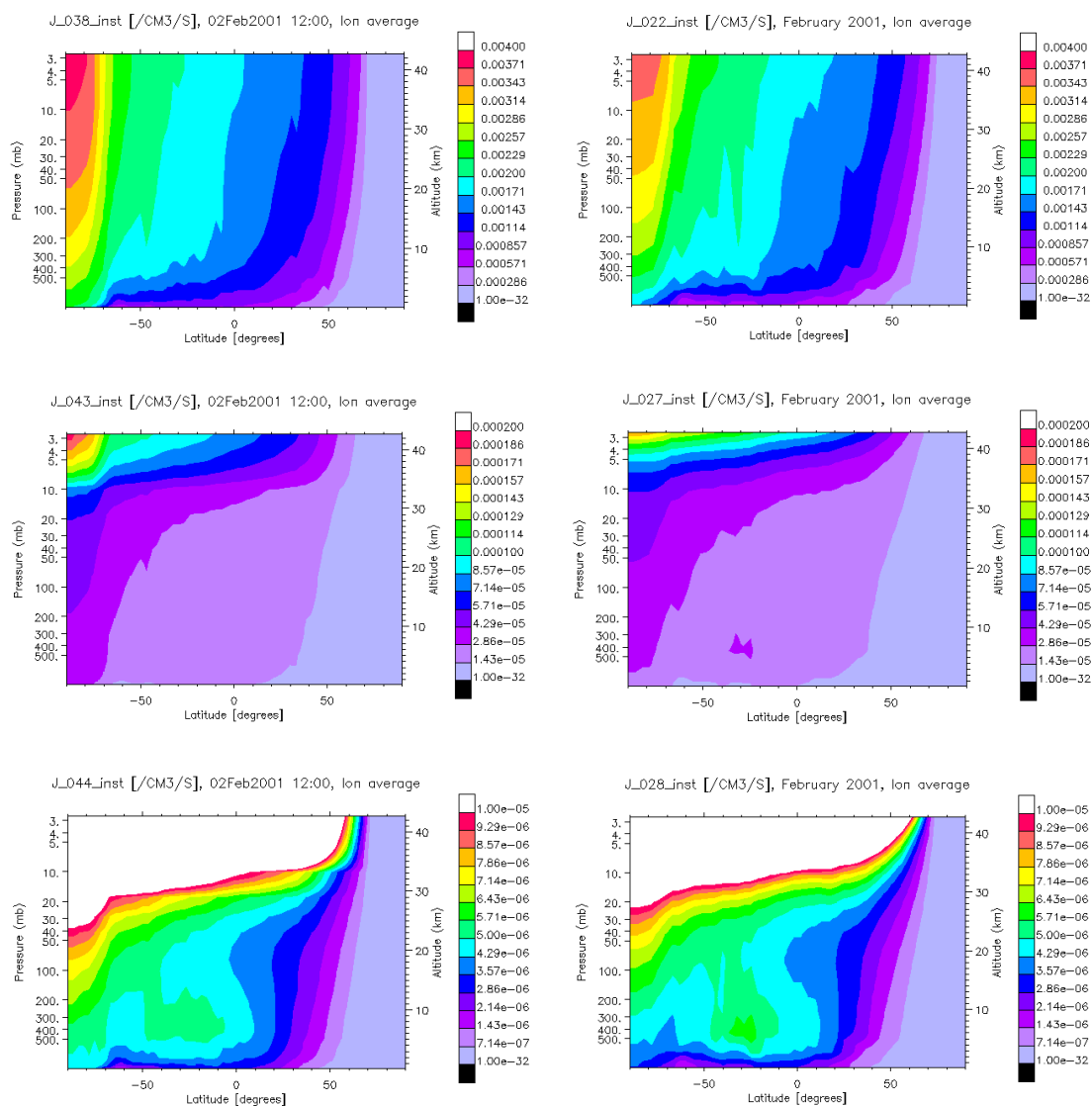


Figure 2.4: Photolysis rates ( $\text{s}^{-1}$ ) for  $\text{Cl}_2$  and  $\text{ClONO}_2$  ( $\rightarrow \text{Cl} + \text{NO}_3$ ;  $\rightarrow \text{ClO} + \text{NO}_2$ ) for MOZART4 (left side) and MOZART3 (right side). Instantaneous output.

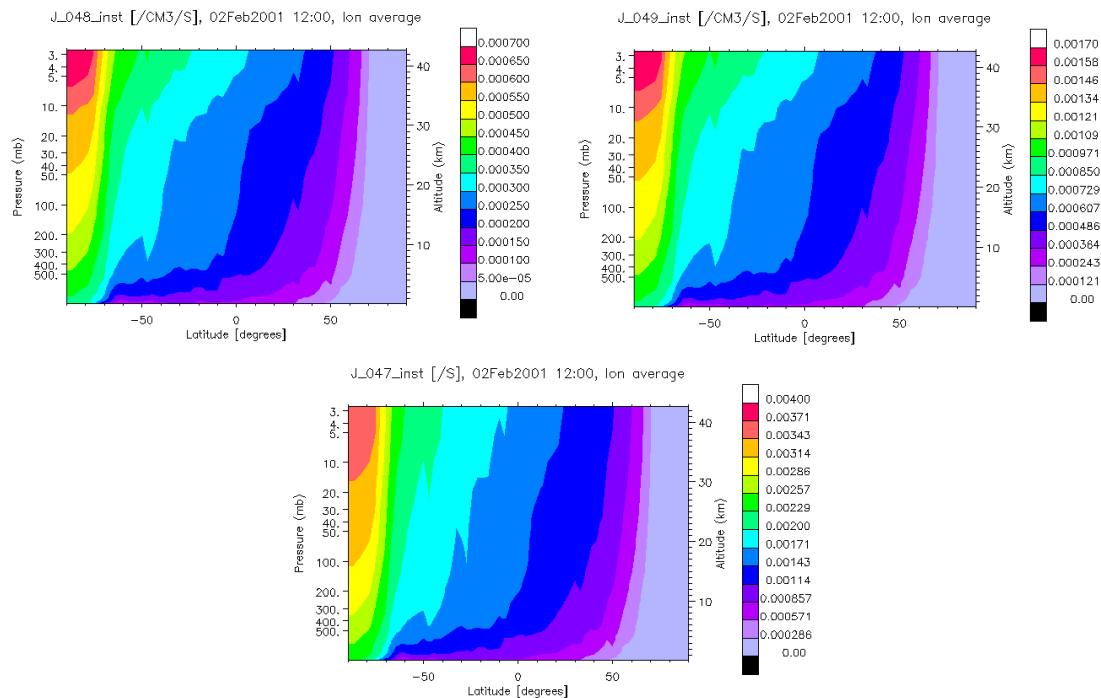


Figure 2.5: MOZART4 photolysis rates ( $\text{s}^{-1}$ ) for the reactive bromine species  $\text{BrONO}_2$  ( $\rightarrow \text{Br} + \text{NO}_3$  – left;  $\rightarrow \text{BrO} + \text{NO}_2$  – right) and  $\text{HOBr}$  at the bottom. Instantaneous output.

Table 2.2: Global, 5-km altitude, mean photolysis rates  $\bar{j}$  from MOZART4 (the base data was instantaneous output for the 1<sup>st</sup> February 12:00 UTC) and in WMOs Scientific Assessment for Ozone [85]

Species	$\bar{j}$ ( $\text{s}^{-1}$ )	
	MOZART4	WMO
$\text{CHBr}_3$	$2.4 \times 10^{-7}$	$1 \times 10^{-6}$
$\text{CH}_2\text{Br}_2$	$4.7 \times 10^{-11}$	$< 1 \times 10^{-8}$
$\text{CH}_2\text{BrCl}$	$6.1 \times 10^{-15}$	$7.7 \times 10^{-10}$
$\text{CHBr}_2\text{Cl}$	$1.2 \times 10^{-7}$	$7.2 \times 10^{-8}$
$\text{CHBrCl}_2$	$7.5 \times 10^{-8}$	$5.2 \times 10^{-8}$
$\text{BrONO}_2$	$\sim 2 \times 10^{-4}$	$\sim 1 \times 10^{-3}$
$\text{HOBr}$	$7.7 \times 10^{-4}$	$3 \times 10^{-3}$

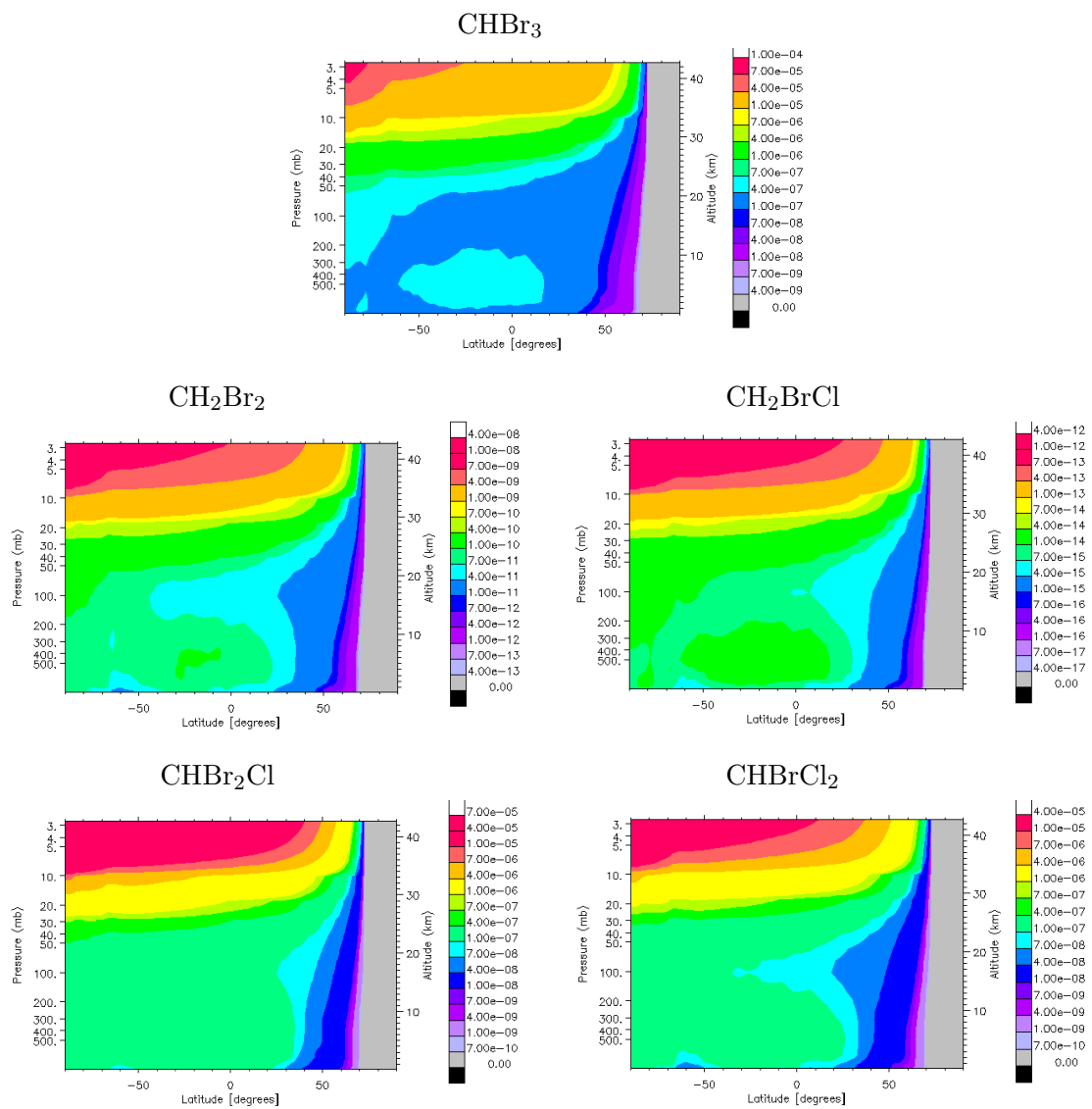


Figure 2.6: MOZART4 photolysis rates ( $\text{s}^{-1}$ ) for the very short lived halocarbons at the 1<sup>st</sup> February 2000. Instantaneous output.

## 2.2 Heterogeneous Reactions of Halogens

The term "heterogeneous chemistry" refers to all chemical reactions of gas phase species on the surface of solid or liquid particles (aerosols <sup>4</sup>) suspended in the atmosphere [96]. Solid particles in the atmosphere are usually wet in the atmospheric boundary layer.

The importance of heterogeneous chemistry is well known for the polar stratosphere, where reactions on particle surfaces in polar stratospheric clouds (PSCs) convert halogen reservoir species into easily photolysed molecules, which then release the radicals that deplete ozone. A large number of available measurements of the ozone column gives a hint that ozone depletion occurs also in lower latitudes [15]. The assumption is that heterogeneous chemistry takes place on background stratospheric sulphate aerosol in the mid-latitudes. In the free troposphere, the same chemistry may efficiently occur on background sulphate aerosol as shown by Abbatt and Nowak's laboratory work [2].

The reaction rates depend on the composition and abundance of the substrates. In particular, we need information about the surface of the particles and the chemical properties of the surface. These are assessed by laboratory and field measurements. In the global model MOZART4, the properties of the aerosols are accessible through parameterized equations derived from measurements.

The two atmospheric substrates considered in this study are sea salt and sulphate. Sea salt aerosols are formed when sea spray evaporates. Sulphate has natural and anthropogenic sources. It is produced in the atmosphere by chemical reactions from gaseous precursors, mainly SO<sub>2</sub> (emitted from fossil and bio-fuels, industry, and volcanos), and DMS (dimethyl sulfide) from oceanic biogenic sources.

In the polar atmosphere, ice crystals can also constitute a substrate for heterogeneous chemistry.

The parameterization in the model comprises only particles of simple composition: SO<sub>4</sub><sup>2-</sup> and NaCl. In nature, the chemical composition is more diversified. The counterion to the sulphate anions in aerosols depends on the environmental conditions. Common sulphates are in the form of H<sub>2</sub>SO<sub>4</sub>, NH<sub>4</sub>HSO<sub>4</sub> or (NH<sub>4</sub>)<sub>2</sub>SO<sub>4</sub>. Sea salt in the marine environment contains more species than just Na<sup>+</sup> and Cl<sup>-</sup>. Mg<sup>2+</sup>, Ca<sup>2+</sup>, K<sup>+</sup>, Br<sup>-</sup>, and others will certainly be present. The sea salt particles are deliquescent because of the high relative humidities in the marine troposphere.

Measurements show that sea salt has a higher content of Br shortly after its formation and that this bromine is gradually depleted [106, 48]. Nevertheless, for submicron particles an enrichment was detected. Enami and co-workers[32] provide a physical explanation for this enrichment: submicrometer marine aerosol drops are, on average, already negatively charged and subsequent water evaporation shrinks them, thereby increasing electrostatic repulsion among excess surface charges. This leads to Coulomb explosions, in which drops shed interfacial charge and mass into smaller droplets, and consequently these smaller particles are enriched in anions.

Acidification of particles is a commonly observed phenomenon, and it promotes the halogen activation<sup>5</sup> that eventually leads to Br release [89, 107, 33, 3]. The acidification of the particles comes from H<sub>2</sub>SO<sub>4</sub> formed from DMS in a clean marine boundary layer and from H<sub>2</sub>SO<sub>4</sub> and

---

<sup>4</sup>Aerosol is defined as a suspension in air of liquid or solid particles.

<sup>5</sup>Halogen activation are all the chemical reactions that convert inorganic, inactive halogens to reactive ones in the atmosphere.

HNO<sub>3</sub> formed from SO<sub>2</sub> and NO<sub>x</sub> in a marine boundary layer affected by anthropogenic pollution.

The heterogeneous chemistry includes several steps: the diffusion in the gas phase of the gas component to the aerosol, the interface transport, the solvation, the liquid phase reaction, and the desorption. If the particle is dry, the process is resumed to gas phase diffusion and reaction on the surface. In this document, we define the equations that determine the consumption of the gas phase species through heterogeneous chemistry, we discuss the experimental values used here for the heterogeneous reactions, we describe the necessary modifications made in the code of MOZART4. We also present results, analysis and conclusions.

### 2.2.1 Mathematical description of heterogeneous chemical reactions

The speed of a chemical reaction is described by the reaction constant  $k$ . For its definition, we consider the situation where a liquid droplet of radius  $r$  is suspended in the atmosphere which contains a gas phase chemical species  $i$  with concentration  $C_i^{(g)}$ . We assume that this species  $i$  is not subjected to any chemical reaction in the atmosphere and that its concentration  $C_i^{(g)}$  is constant with time. On the other hand, we assume that it will be subjected to a first order chemical reaction in the droplet with a rate constant  $k^{(l)}$  ( $l$  for liquid phase). Due to the consumption of  $i$  by the chemical reaction, this compound will first diffuse into the droplet with a diffusion coefficient  $D^{(l)}$ . After some time, a steady state is established so that the concentration profile inside the droplet is not changing. We assume a centrosymmetric situation, so the concentration  $C_i^{(l)}$  of species  $i$  in the droplet depends only on the distance  $r$  from the center of the droplet:

$$C_i^{(l)} : \begin{cases} \mathbb{R}_+ \times [0, r] \mapsto \mathbb{R}_+ \\ (t, r) \mapsto C_i^{(l)}(t, r) \end{cases}$$

where we expect that  $C_i^{(l)}(t, r) = \bar{C}_i^{(l)}(r)$  for all  $t \geq T$ ,  $T$  being the time when steady state is reached.

In a first step, we are interested in establishing the maximum value of the reaction rate. This maximum rate is reached in the case that all the molecules which hit the droplet "deposit" and react, i.e., in the case of an irreversible uptake. The flux  $\sigma_i^{(d)}$  of particles  $i$  on a surface is ( $d$  for deposition):

$$\sigma_i^{(d)} = \frac{n_i}{\Delta t A} \quad (2.14)$$

where  $n_i$  is the number of moles of molecules hitting the finite area  $A$  in a period of time  $\Delta t$ . On the other hand, from overall first order kinetics, we have

$$\dot{C}_i^{(g)}(t) = k C_i^{(g)}(t) \quad (2.15)$$

Multiplying (2.15) by the volume  $V$  of the gas phase, we obtain the rate of change of the mole number  $n_i^{(g)}$ :

$$\dot{n}_i^{(g)}(t) = k C_i^{(g)}(t) \cdot V \quad (2.16)$$

From (2.14), we derive:

$$\dot{n}_i^{(g)}(t) = \sigma_i^{(d)} \cdot A, \quad (2.17)$$

$A$  being the surface of the droplet. We also know from the kinetic gas theory that  $\sigma_i^{(d)}$  is (see Appendix 1):

$$\sigma_i^{(d)} = \frac{1}{4} \cdot C_i^{(g)} \bar{v} \quad (2.18)$$

where  $\bar{v} = \sqrt{\frac{8RT}{\pi M}}$ ,  $R$  being the molar gas constant,  $M$  the molar mass, and  $T$  the temperature.

Combining equations (2.16), (2.17), and (2.18), we obtain the following expression for the first order rate constant associated with the heterogeneous reaction with irreversible uptake:

$$k = \frac{\bar{v}}{4} \cdot \frac{A}{V} \quad (2.19)$$

Setting  $\frac{A}{V} = \mathcal{A}$ , the available surface per volume, we derive for the upper bound:

$$k = \frac{\bar{v}}{4} \cdot \mathcal{A} \quad (2.20)$$

However, not every collision on the surface does lead to a reaction or to solvation and subsequent reaction. The molecule of species  $i$  may escape to the gas phase. We can then formally introduce such a "collision success factor"  $\Gamma$  in equation (2.18),  $0 \leq \Gamma \leq 1$ :

$$\sigma_i^{(d-e)} = \frac{1}{4} \cdot C_i^{(g)} \bar{v} \Gamma, \quad (2.21)$$

so that  $\sigma_i^{(d-e)}$  represents the net flux of species  $i$  onto the drop, which is equal to the rate of chemical consumption at steady state. This leads to a slightly modified equation (2.20), which becomes

$$\boxed{k = \frac{\bar{v}}{4} \cdot \Gamma \cdot \mathcal{A}} \quad (2.22)$$

$\Gamma$  is called the reactive uptake coefficient, and we need an appropriate mathematical expression that describes it quantitatively. For this purpose, we first develop an expression for the net uptake on the droplet in the steady state:

$$\sigma_i^{(d-e)} = \sigma_i^{(d)} - \sigma_i^{(e)} \quad (2.23)$$

Let's consider first  $\sigma_i^{(d)}$ : its upper limit is given by equation (2.18). But as already mentioned, not every collision may lead to absorption. This is taken into account by the introduction of a so-called mass accommodation factor  $\alpha$  ( $0 \leq \alpha \leq 1$ ):

$$\sigma_i^{(d)} = \frac{\alpha}{4} \cdot C_i^{(g)} \bar{v}. \quad (2.24)$$

If there is a chemical reaction in the aqueous phase, the concentration  $C_{i,eq}^{(l)}$  in the droplet reaches an equilibrium value that is governed by the Henry law coefficient ( $k_H$ ):  $C_{i,eq}^{(l)} =$

$k_H \cdot p_{i,eq}$ , with  $p_i = C_i^{(g)} \cdot RT$  (ideal gas law). This means that  $\sigma_{i,eq}^{(e)} = \sigma_i^{(d)}$ , so that the escape of the particles balances  $\sigma_i^{(d)}$  (which is still effective). Then, we can in equilibrium determine the escape rate from the knowledge of the gas phase concentration, because in this case  $\sigma_{i,eq}^{(e)}$  fullfills equation (2.24).

If there is chemical reaction, there is a net flux to the droplet with  $\sigma_i^{(d-e)} > 0$ . In this case, we define  $\sigma_i^{(e)}$  considering that due to the reaction, the concentration at the surface of the droplet  $C_i^{(l)}(r = a)$  established in the steady state is smaller than the equilibrium concentration  $C_{i,eq}^{(l)}$ . On the other hand,  $C_i^{(l)}(a)$  would yield the following hypothetical partial pressure  $\tilde{p}_i$  and thus a hypothetical gas phase concentration  $\tilde{C}_i^{(g)}$  due to Henrys law:

$$C_i^{(l)}(a) = k_H \cdot \tilde{p}_i = k_H \cdot \tilde{C}_i^{(g)} \cdot RT, \quad (2.25)$$

from which we can determine the escape rate of species  $i$  with surface concentration  $C_i^{(l)}(a)$  by

$$\sigma_i^{(e)} = \frac{\alpha}{4} \cdot \tilde{C}_i^{(g)} \bar{v} = \frac{\alpha}{4} \cdot C_i^{(l)}(a) \cdot \frac{1}{k_H RT} \cdot \bar{v} \quad (2.26)$$

Now, we can insert equations (2.24) and (2.26) into equation (2.23) and obtain:

$$\sigma_i^{(d-e)} = \frac{\alpha}{4} \left( 1 - \frac{C_i^{(l)}(a)}{k_H RT C_i^{(g)}} \right) C_i^{(g)} \bar{v} \quad (2.27)$$

Comparing the last equation with equation (2.21), we derive the reactive uptake coefficient:

$$\Gamma = \alpha \left( 1 - \frac{C_i^{(l)}(a)}{k_H RT C_i^{(g)}} \right) \quad (2.28)$$

We have now a link between the overall reaction rate  $k$  and the gas phase and surface concentration of  $i$  by combining (2.22) and (2.28):

$$k = \frac{\bar{v}}{4} \alpha \left( 1 - \frac{C_i^{(l)}(r)}{k_H RT C_i^{(g)}} \right) \mathcal{A} \quad (2.29)$$

Another way to access  $k$  and  $\Gamma$  is based on the concentration profile at steady state within the droplet. For that we assume Fickian diffusion and a first order reaction with reaction constant  $k^{(l)}$ :

$$\partial_t C_i^{(l)}(t, \sqrt{x^2 + y^2 + z^2}) = D^{(l)} \Delta C_i^{(l)}(t, \sqrt{x^2 + y^2 + z^2}) - k^{(l)} C_i^{(l)}(t, \sqrt{x^2 + y^2 + z^2}) \quad (2.30)$$

At steady state,  $\partial_t C_i^{(l)}(t, \sqrt{x^2 + y^2 + z^2}) = 0$ .

Equation (2.30) is easier to solve in spherical coordinates which are defined as

$$\vec{r}: \begin{cases} \mathbb{R}_+ \times [0, \pi] \times [0, 2\pi[ \mapsto \mathbb{R}^3 \\ (r, \vartheta, \varphi) \mapsto a \begin{pmatrix} \sin \vartheta \cos \varphi \\ \sin \vartheta \sin \varphi \\ \cos \vartheta \end{pmatrix} \end{cases}$$

The Laplacian is needed in spherical coordinates. The derivatives with respect to  $\vartheta$  and  $\varphi$  are 0 for our centro-symmetric problem; so, it is sufficient to consider  $\Delta_r = \frac{\partial^2}{\partial r^2} + \frac{2}{r} \frac{\partial}{\partial r} = \frac{1}{r^2} \partial_r (r^2 \partial_r)$ .

The diffusion-reaction equation (2.30) then takes the form:

$$D^{(l)} \frac{1}{r} \partial_r (r^2 \partial_r C_i^{(l)}(t, r)) - k^{(l)} C_i^{(l)}(t, r) = 0 \quad \forall t \geq T \quad (2.31)$$

We recall that  $T$  is the time when steady state is reached, which means that  $C_i^{(l)}(t, r) = \text{constant}$  in time.

For solving the equation we set the following boundary conditions:

$$\begin{cases} C_i^{(l)}(t, a) = C_i^{(l)}(a) \\ C_i^{(l)}(t, 0) = \text{constant in time.} \end{cases}$$

Moreover, we substitute for any time  $t \geq T$  :  $u(r) := r C(t, r)$ , which means for the transformed boundary condition:

$$\begin{cases} u(a) = a \cdot C_i^{(l)}(a) \\ u(0) = 0 \end{cases} \quad (2.32)$$

Inserting  $u$  into equation (2.30), we obtain:

$$D^{(l)} \frac{1}{r} \partial_r^2 u(r) - \frac{1}{r} k^{(l)} u(r) = 0 \quad (2.33)$$

The general solution of equation (2.33) is:

$$u(r) = C_1 \cdot e^{\sqrt{\frac{k^{(l)}}{D^{(l)}}} \times r} + C_2 \cdot e^{-\sqrt{\frac{k^{(l)}}{D^{(l)}}} \times r} \quad (2.34)$$

In the following, we abbreviate  $\frac{k^{(l)}}{D^{(l)}} = K$ .

Taking into account the boundary conditions (2.32), we can determine the integration constants:

$$\begin{cases} C_1 = -C_2 \\ C_1 = \frac{a \cdot C_i^{(a)}}{\sinh(\sqrt{K}a)} \end{cases}$$

Therefore, we obtain for  $u$ :

$$u(r) = \frac{a \cdot C_i^{(a)}}{\sinh(\sqrt{K}a)} \sinh(\sqrt{K}r) \quad (2.35)$$

For  $C_i^{(l)}$ , we derive for any time  $t \geq T$ :

$$C_i^{(l)}(t, r) = \frac{a \cdot C_i^{(l)}(a)}{\sinh(\sqrt{K}a)} \times \frac{\sinh(\sqrt{K}r)}{r} \quad (2.36)$$

From Fickian diffusion, we know that the flux is proportional to the gradient. We calculate from (2.36) the gradient in radial direction:

$$\partial_r C_i^{(l)}(t, a) = \frac{a \cdot C_i^{(l)}(a)}{\sinh \sqrt{K}a} \left( \sqrt{K} \frac{\cosh(\sqrt{K}a)}{a} - \frac{\sinh(\sqrt{K}a)}{a^2} \right) \quad (2.37)$$

$$\sigma_i^{(d-e)} = D^{(l)} \times \partial_r C_i^{(l)}(t, a) = D^{(l)} \sqrt{K} C_i^{(l)}(a) \left( \coth(\sqrt{K}a) - \frac{1}{\sqrt{K}a} \right) \quad (2.38)$$

From the combination of equations (2.27) and (2.38), we obtain

$$\frac{C_i^{(l)}(a)}{C_i^{(g)}} = 1 / \left( \frac{4 D^{(l)} \sqrt{K} \left( \coth(\sqrt{K}a) - \frac{1}{\sqrt{K}a} \right)}{\alpha \cdot \bar{v}} + \frac{1}{k_H RT} \right) \quad (2.39)$$

This result can be inserted into (2.28), in order to derive the reactive uptake dependent on variables related to the liquid phase properties:

$$\boxed{\frac{1}{\Gamma} = \frac{1}{\alpha} + \frac{\bar{v}}{4 k_H RT D^{(l)} \sqrt{K} \left( \coth(\sqrt{K}a) - \frac{1}{\sqrt{K}a} \right)}} \quad (2.40)$$

### 2.2.2 Modelling heterogeneous chemical reactions

The determination of each of the basic physicochemical parameters at any given atmospheric condition is a central effort in the field of heterogeneous chemistry. It is a challenge to make the bridge between values measured in the laboratory and their application to atmospheric conditions, and in this particular case, the small spherical particles on which the reactions actually take place. Hanson *et al.* [47] e.g. state: "When reactive uptake coefficients are measured in the laboratory on thick planar substrates, the concentration gradient in the bulk may be large enough to result in a large measured uptake. The uptake in the atmosphere, however, could be much slower due to a smaller concentration gradient in the atmospheric particles because they are small and spherical. Therefore  $\Gamma$  measured using thick substrates may have to be corrected to apply them to the submicron-sized droplets found in the stratosphere". From our literature review, we see that this is particularly true for sea salt, for which the experiments on solid substrates [8] or bulk solutions [33] result in uptake coefficients ten times higher than the ones determined under more realistic conditions on droplets [28] or natural sea salt [89].

For a planar liquid surface the uptake coefficient  $\gamma$  is (from Danckwerts [26, 27], cited in Hanson and co-workers, 1994 [47]):

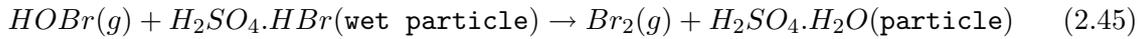
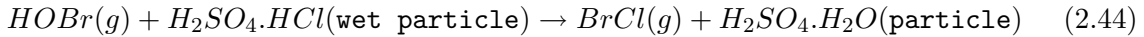
$$\frac{1}{\gamma_{bulk}} = \frac{1}{\alpha} + \frac{\bar{v}}{4 k_H RT \sqrt{D^{(l)} k^{(l)}}} \quad (2.41)$$

Comparing the last equation with equation (2.40), that gives the uptake on spherical aerosol particles, we obtain  $\Gamma$  in terms of  $\gamma_{bulk}$ :

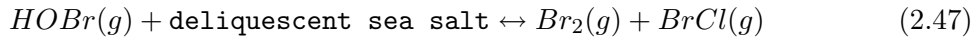
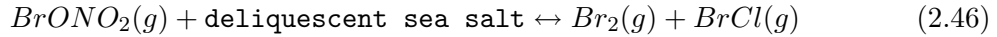
$$\frac{1}{\Gamma} = \frac{1}{\gamma_{bulk} \times \left( \coth(\sqrt{K} a) - \frac{1}{\sqrt{K} a} \right)} + \frac{1}{\alpha} \left( 1 - \frac{1}{\coth(\sqrt{K} a) - \frac{1}{\sqrt{K} a}} \right) \quad (2.42)$$

If we know the parameters  $\alpha$ ,  $k^{(l)}$ ,  $D^{(l)}$ , and  $a$  or we are able to estimate them, we can calculate the uptake and finally the reaction rate.

In the next sections, we will review how we accomplished this for the reactions considered in this work on sulphate aerosols



and on sea-salt aerosols



### 2.2.3 Heterogeneous chemistry of BrONO<sub>2</sub> on aqueous aerosols

Hydrolysis is effective for BrONO<sub>2</sub>, with a high uptake coefficient. It is a chemical species efficiently dissolved in water, however it cannot be considered that the uptake is a wet deposition process as described by the Henry law coefficient.  $k_H$  refers to gases which physically dissolve, but do not undergo a chemical reaction. To include the hydrolysis of BrONO<sub>2</sub><sup>6</sup> on the aqueous phase in the atmosphere, we inserted into MOZART4 the hydrolysis reaction on the aerosols of sulphate, NH<sub>4</sub>NO<sub>3</sub>, organic carbon and secondary organic carbon. The reactive uptake was parameterized for sulphate according to Hanson, 2003 [44] (described in the next section), and  $\Gamma$  was set to 0.032 for the uptake on the remaining aerosols. This reactive uptake is the simple average of the values measured on pure water for various temperatures by Deiber and co-workers, 2004 [28]. To our best knowledge, there are no experiments done on the aerosols relevant to our simulations.

### 2.2.4 Heterogeneous chemistry of bromine species on sulphate

The hydrolysis of BrONO<sub>2</sub> has been shown to be very efficient at submicron aerosols containing 45-70 wt%<sup>7</sup> of H<sub>2</sub>SO<sub>4</sub>, with uptake coefficients  $\Gamma > 0.8$  [46]. For more concentrated aerosols the value for the uptake drops to  $\Gamma < 0.1$  because of the decreased amount of water available for the reaction. Other experiments performed by Hanson and co-workers [45, 44] showed that uptake is a function of sulfuric acid concentration, but independent of temperature in the range of 210-300K. Hanson [44] has fit an empirical expression to the combined data set of measured uptakes, that apply to bulk and aerosol experiments. It has the form:

$$\frac{1}{\Gamma_{BrONO_2}} = \frac{1}{\alpha} + \frac{1}{\gamma_{rxn}} \quad (2.48)$$

<sup>6</sup>The same reasoning stands for ClONO<sub>2</sub>, however its hydrolysis was not included as our work focuses on the bromine tropospheric chemistry.

<sup>7</sup>weight percent

where,

$$\gamma_{rxn} = e^{a+b \times \frac{y_{H_2SO_4}}{100\%} + \gamma_{100}} \quad (2.49)$$

with  $\alpha=0.80$ ,  $a=29.2$ ,  $b=-0.40$ ,  $\gamma_{100}=0.11$ , and  $y_{H_2SO_4}$  being the sulphate weight fraction in the particle.

Using the parameterization of Tabazadeh *et al.* [120] for  $H_2SO_4/H_2O$  aerosols and ECMWF dynamical data for 22 March 2002 (air temperature, specific humidity and surface pressure) the calculated acid weight percent ( $y$ ) is the one represented in Figure 2.7, upper left panel. These values were used for the calculation of the total uptake for the hydrolysis of  $BrONO_2$ , calculated through equations (2.48) and (2.49) (see Figure 2.7, up right panel).

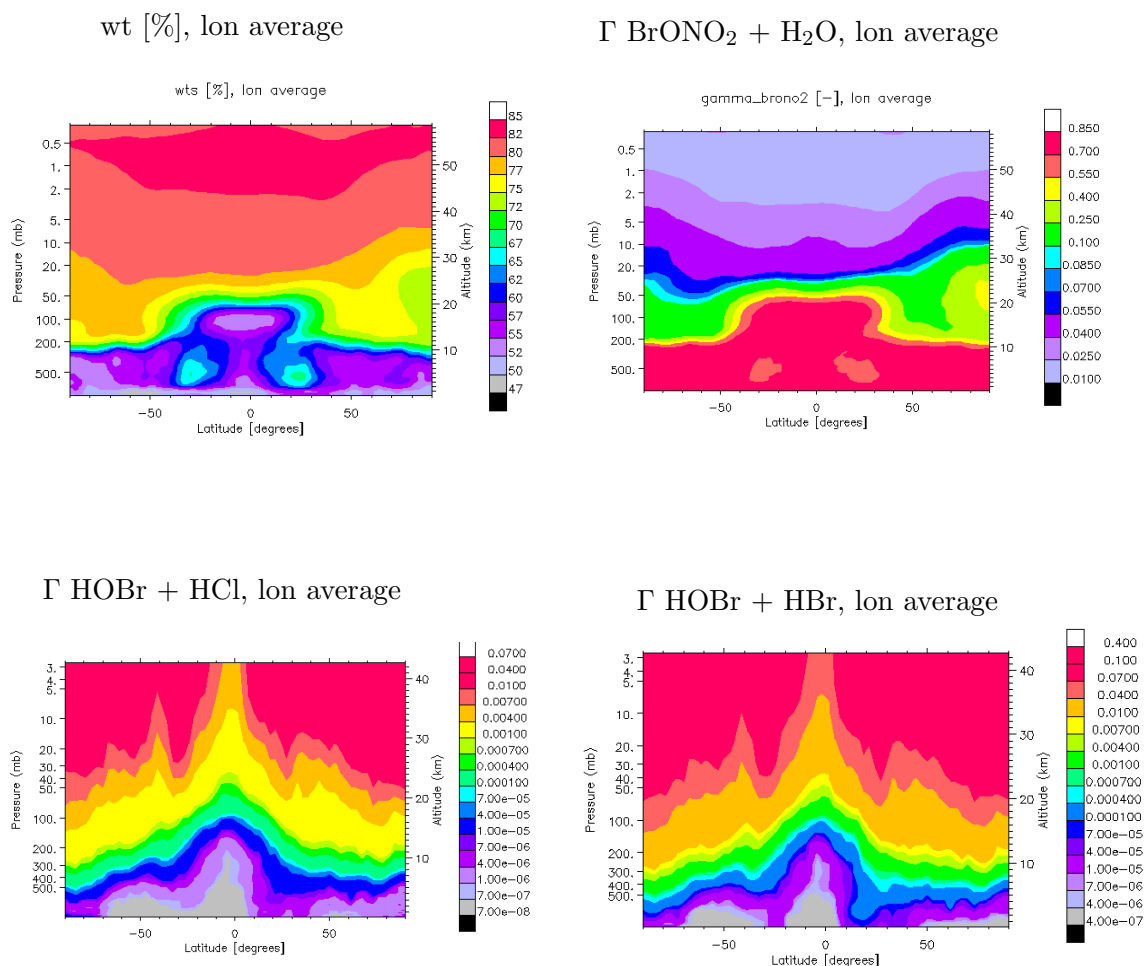


Figure 2.7: Zonal average of the sulphate weight percent ( $wt$ ) calculated according to the parameterization of Tabazadeh *et al.* (1997) [120], and the total uptakes ( $\Gamma$ ) for: the hydrolysis of  $BrONO_2$ , the heterogeneous reactions of  $HOBr$  with  $HCL$  and of  $HOBr$  with  $HBr$ .

The parameterization of Tabazadeh *et al.* [120] was developed for "relative humidities above 1% in the temperature range of 185-260K". The temperature range implies that the validity of the parameterization is under conditions found in the upper troposphere and the stratosphere. However, the relative humidity range is characteristic of the troposphere. The results for  $\gamma$  and the uptake seem reasonable for the troposphere, which gives confidence to use it in MOZART4 runs for the tropospheric chemistry simulation.

Hanson [44] showed that the products of reaction (2.43) that reach the gas phase comprise  $\text{Br}_2$ , HOBr, and  $\text{HNO}_3$ . The production of  $\text{Br}_2$  was significant at high  $y_{\text{H}_2\text{SO}_4}$ , and was attributed to the possible HOBr self-reaction (2.50):



As it can be observed in Figure 2.7 (left panel top), high  $\text{H}_2\text{SO}_4$  weight percentages are present above 30 km altitude. Therefore, reaction (2.50) is of no significance in tropospheric conditions.

The bromine species were, after several minutes of Hanson's experiment [44], at concentrations generally less than 10% of the initially injected  $\text{BrONO}_2$  concentration, while the  $\text{HNO}_3$  concentration remained fairly constant. This means that some of the HOBr stays in the aqueous phase, due to its high solubility. In MOZART4, all the HOBr produced passes immediately to the gas phase. The reactions (2.44) and (2.45) bring HOBr back into the aqueous phase.

The  $\Gamma$  for reactions (2.44) and (2.45) is calculated using equation (2.40). The calculation of each of the parameters in the equation is done according to Hanson, 2003 [44], and Waschewsky and Abbatt [134] for reaction (2.44). The Henry law coefficient is calculated as a function of  $y_{\text{H}_2\text{SO}_4}$  also using Tabazadeh's parameterization.

For reaction (2.45), Iraci *et al.* [58] did not observe the saturation of the substrate, but continued production as long as there is HOBr in the gas phase. The solubility of HBr in water is higher than that of HOBr under tropospheric conditions, indicating that the aerosols should contain concentrations of HBr which exceed those of HOBr in equilibrium. As the partition  $\text{HBr}/\text{HOBr}$  is larger than 1 in the troposphere, it is expected that, as in the laboratory, the reaction on the particle should proceed as long as there is HOBr in the gas phase. The reaction will then proceed in pseudo first-order reaction conditions. The parameters for the calculation of  $\Gamma$  are the same as for reaction (2.44), with the exception of  $k^l$  (considered to be 0.1 times lower according to Abbatt, 1995 [1]), and  $k_H$  chosen to be 100 times higher for HBr. The calculated  $\Gamma$  is shown in Figure 2.7 (bottom panels).

### 2.2.5 Heterogeneous chemistry of bromine species on sea salt

$\text{BrONO}_2$  and HOBr diffuse into sea salt particles and lead to a chemical production of mainly  $\text{Br}_2$  and  $\text{BrCl}$ .  $\text{Br}_2$  and  $\text{BrCl}$  consequently desorb into the atmosphere. Bromine as a minor component of sea salt may be depleted from the particles. Sander and co-workers [107] made a comprehensive analysis of field data observations for several measurement campaigns and concluded that bromine emissions from sea salt depend on particle size and acidity. The observation was that very large particles show a bromine content similar to sea water. This was explained by the fact that the deposition of these large particles is too fast for chemical removal or addition of bromine prior to deposition. Medium sized particles (few micrometers in diameter) showed bromine depletions and submicrometer particles showed bromine

enrichment (higher bromine content than sea water). Sander and co-workers [107] proposed a chemical explanation for the enrichment: at the poles, during severe ozone depletions, the bromine activation chain is interrupted, and so the enrichment in bromine of sea salt particles is favored. In the midlatitudes this drastic ozone depletion events do not occur, but maybe bromine in submicrometer particles is in a chemically inert form. Enami and co-workers [32] proposed a physical explanation for this enrichment based on the electrostatic repulsion within the particles and subsequent break-up into smaller particles with higher population of anions.

The pH of the particles affects the process of solvation of the ions, and as a result affects the dissociation of the gas phase species and the desorption of the products. In particles with very low pH, we expect that weak acids such as HOBr (dissociation constant  $K_a=2\times 10^{-9}$ ) will not dissociate. Indeed, very low dissociation of HOBr was observed below pH 6 [33]. The decreasing degree of dissociation of HOBr with decreasing pH induces a decreasing reactive uptake, because the reactive uptake essentially implies the solvation of  $H^+$  and  $BrO^-$  in a deliquescent sea salt particle. This phenomenon was observed by Abbatt and Waschewsky [3], who measured a reactive uptake  $\Gamma$  of circa 0.2 in a deliquescent solution of NaCl buffered at pH 7.2, but a rapidly decreasing uptake by two orders of magnitude when an unbuffered solution is used. This unbuffered deliquescent solution of NaCl is being acidified by the uptake of HOBr.

After the uptake of HOBr into the particle, the following step is the chemical reaction with the  $Cl^-$  or  $Br^-$  in solution. The chemistry in the aqueous phase is also dependent on the pH, affecting the availability of the ions for reaction. Under alkaline conditions the reaction of HOBr with  $Cl^-$  or  $Br^-$  will not take place as it needs the presence of protons:

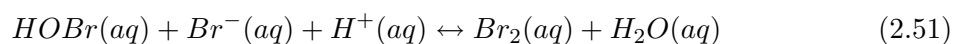


Table 2.3 contains a compilation of the peer-reviewed literature pertaining the measurement of heterogeneous reaction parameters of HOBr and  $BrONO_2$  on sea-salt and the experiments. The latter information permits to evaluate the degree of similarity of laboratory conditions with the natural conditions in the atmosphere.

For  $BrONO_2$ , the substrates used in the two available experiments are rather different from sea salt in composition and, for [8] also in terms of the physical state as the experiments were performed on solid substrates. Deiber *et al.* [28] directly measured  $\Gamma$  as 0.02. Aguzzi and Rossi [8] measured a bulk uptake ( $\gamma$ ) of 0.2. From this, we could calculate the total uptake  $\Gamma$  using equation (2.42) in the following way: We have estimates from Aguzzi and Rossi [8] for the first order reaction (defined by them as the rate of gaseous  $BrONO_2$  loss, which does not take into account the loss due to hydrolysis), and estimates from Deiber *et al.* [28] for the diffusion coefficient in water and the accommodation coefficient. However, their value for the accommodation coefficient is 0.06, which is lower than the reactive uptake  $\gamma$  in [8]. This means that the amount of product that reacts in the particle is higher than the amount that entered the particle, which is not possible, and mathematically translates into a negative total uptake  $\Gamma$ . The conclusion is that both experiments are not compatible.

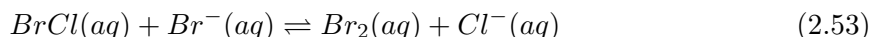
The value of the accommodation coefficient is not only low in [28] compared to that from Aguzzi and Rossi [8], but it is also low compared with experiments with sulphate as a substrate, where values of about 0.8 were found for  $BrONO_2$  [6]. Deiber *et al.* [28] address this

difference and offer an interesting speculation: what impairs the accommodation capacity of  $\text{BrONO}_2$  is the ability of Br atoms to interact with the  $\text{H}_2\text{O}$  molecules in the air/aqueous interface, which means that their concentration on the surface is enhanced and impairs the accommodation of more molecules. Consequently, Aguzzi and Rossi's [8] experiments on dry sea salt particles is not applicable to our situation, and we decided to base our simulations on the  $\Gamma$  of Deiber *et al.*

Moreover, Deiber's speculation also means that the accommodation coefficient  $\alpha$  may depend on the gas phase concentration of the reactant. That could explain the relatively high value of  $\alpha$  obtained by Wachsmuth *et al.* [129] for HOBr, who performed their experiments at an extremely low concentration of 300 molecules/cm<sup>3</sup> (on sulphate  $\alpha > 0.05$  [6]).

For HOBr, we decided to use the measurements on spherical particles for the definition of the total uptake coefficient  $\Gamma$ . Even with this restriction, rather different values for  $\Gamma$  can be found in the literature:  $\Gamma = 1.0\text{-}1.9 \times 10^{-2}$  [89] and  $\Gamma \approx 1.5 \times 10^{-3}\text{-}0.2$  [3]. Pratte and Rossi [89] did not use pH-buffered particles, which then would correspond to Abbatt and Waschewsky's lowest value results [3]. But particles in the atmosphere have a varying composition that implies some pH-buffering. Consequently, the true values of the coefficients would be at the upper level of the scale.

In a last step of our analysis, we have to decide upon the yields of the main products from the reaction of  $\text{BrONO}_2$  and HOBr on sea salt:  $\text{Br}_2$  and  $\text{BrCl}$  [5, 127]. Besides these reactions, the  $\text{BrONO}_2$  hydrolysis with the consequent release of HOBr and  $\text{HNO}_3$  is a very important pathway of heterogeneous destruction of  $\text{BrONO}_2$ , that competes with other loss pathways even under experimental conditions which are claimed to be dry. This is the case in some of Aguzzi and Rossi's experiments [8]. They heated the surfaces up to 550 K *in vacuo* and then conducted their "dry" experiments at low pressure, which means that the gas phase humidity is very low. Even so, the  $\text{BrONO}_2$  hydrolysis competed with the other chemical destruction pathways of halogen exchange and decomposition. In the marine boundary layer the relative humidity is very high meaning that the sea salt particles are generally wet. Therefore, it is expected that the  $\text{BrONO}_2$  hydrolysis will be the main pathway leading to HOBr formation and producing  $\text{Br}_2$  and  $\text{BrCl}$  through reactions (2.51), (2.52), and by the following sequent reaction:



According to our assumption that  $\text{BrONO}_2$  yields  $\text{Br}_2$  and  $\text{BrCl}$  mainly by reaction via HOBr, we assume the yields of  $\text{Br}_2$  and  $\text{BrCl}$  from  $\text{BrONO}_2$  to be equal to those from HOBr.

Fickert and co-workers made the most exhaustive research concerning the reaction yields of reaction (2.47). In one of the experiments, the pH was fixed to 5.5, the  $\text{Cl}^-$  concentration was fixed to 1M, whereas the concentration of  $\text{Br}^-$  was allowed to change. The resulting yields are shown in Figure 2.8 (left panel). Average sea salt contains 0.6M of  $\text{Cl}^-$  and  $8 \times 10^{-4}\text{M}$  of  $\text{Br}^-$  [79]. For this concentration of  $\text{Br}^-$  in the particle, the  $\text{Br}_2$  yield according to Fickert *et al.* results is 90%. In another experiment,  $\text{Cl}^-$  was fixed to 1M,  $\text{Br}^-$  was fixed to  $10^{-3}$ , and the pH was variable (see Figure 2.8 - right panel). The natural average sea water pH is 8, which is also the pH of fresh sea salt particles. Generally, sea salt is acidified by  $\text{H}_2\text{SO}_4$  formed from DMS in a clean marine boundary layer and by  $\text{H}_2\text{SO}_4$  and  $\text{HNO}_3$  formed from  $\text{SO}_2$  and  $\text{NO}_x$  in marine polluted regions. As Figure 2.8 (right panel) shows, the  $\text{Br}_2$  yield is 40% at pH 8, climbing to 90% at just pH 7. Adams and co-workers [5] also found a high  $\text{Br}_2$  yield in their experiments. Moreover, because  $\text{BrCl}$  has a larger molecular dipole than  $\text{Br}_2$

it has a higher residence time on the surface of the particle, which means that if a sufficient amount of  $\text{Br}^-$  exists, the subsequent reaction (2.53) forms even more  $\text{Br}_2$ . Based on these results we set generally the yields in our calculations to 90%  $\text{Br}_2$  and 10%  $\text{BrCl}$ .

Adams *et al.* did not find any impact of the pH on the reaction of HOBr on NaCl/NaBr surfaces, however the other studies found that the acidification of the particle promotes the activation of the chemistry, not only in the laboratory [3, 56, 28, 89], but also in field campaigns [10, 107]. Therefore, the consideration of the pH of the particles in the parameterisation of the heterogeneous reactions in the model may be rather important. However, this is not implemented yet, but should be introduced in the future. The uncertainty that will arise in the model results because of this approximation will probably be lower in the Northern Hemisphere, as the pollution in  $\text{H}_2\text{SO}_4$  and  $\text{HNO}_3$  will promptly acidify the sea salt particles. On the other hand, in the Southern Hemisphere DMS is the main source of acidifying  $\text{H}_2\text{SO}_4$ . However, DMS is a molecule with high seasonal variation of its atmospheric concentration levels, which implies that the acidification of the particles will be uncertain and variable.

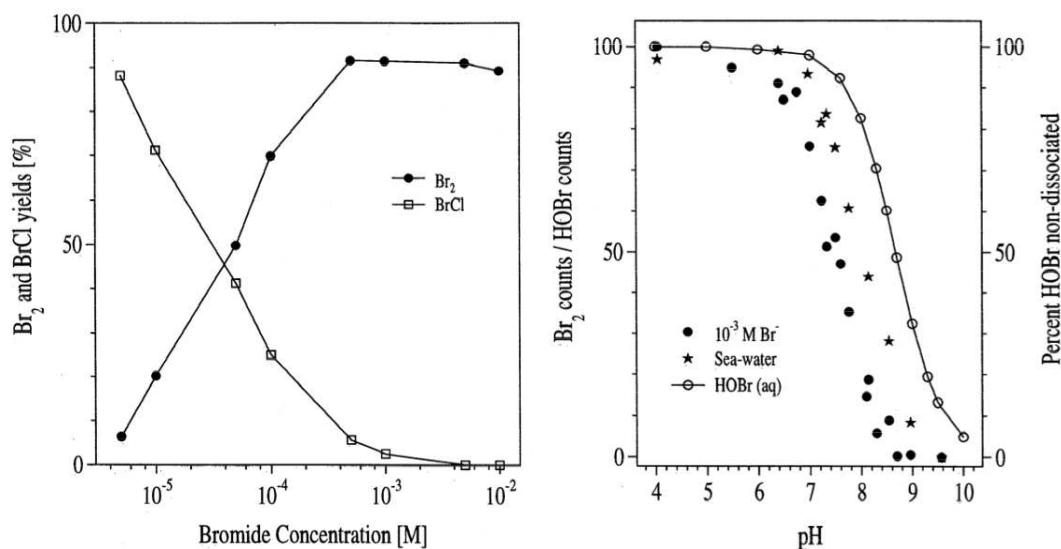


Figure 2.8: Analysis of the  $\text{Br}_2$  and  $\text{BrCl}$  yield dependence from  $\text{Br}^-$  concentration and pH by Fickert and co-workers [33]. The left panel shows  $\text{Br}_2$  and  $\text{BrCl}$  yields (per HOBr) as a function of the  $\text{Br}^-$  concentration at  $\text{pH} = 5.5$ . The yields were calculated for long exposure times when HOBr had decayed to almost zero. The right panel shows the ratio of  $\text{Br}_2$ /HOBr counts (counts are proportional to concentration) as a function of pH. The dots represent the results of the experiment using a solution containing a  $\text{Cl}^-$  concentration of 1 M and a  $\text{Br}^-$  concentration of  $10^{-3}$  M. The stars represent the results for sea water. Also shown in the right panel as a full line (right axis) is the representation of the calculated acid-dissociation curve of HOBr, based on a  $\text{pK}_a=8.5$ .

One of the studies found a link between the product yields of the HOBr heterogeneous reaction and temperature [56]. At 233 K only  $\text{Br}_2$  was detected while both  $\text{BrCl}$  and  $\text{Br}_2$  were detected at 248 K. More experiments are needed in order to clarify this point.

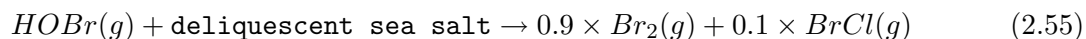
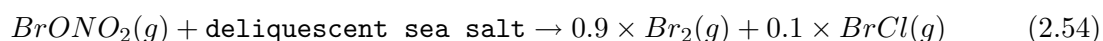
Table 2.3: Review of literature about heterogeneous reactions of BrONO<sub>2</sub> and HOBr on sea salt

Surface	Content	Temperature (K)	Technique	Gas concentration (molecules/cm <sup>3</sup> )	Uptake parameters	Yield	
<b>BrONO<sub>2</sub></b>							
Planar	solid NaCl	Ambient	Knudsen flow reactor	10 <sup>10</sup> -10 <sup>12</sup>	$\gamma_0=0.31\pm 0.12$ $\gamma=0.2$	BrCl (80%±20) Br <sub>2</sub> (~10%)	[8]
"	solid KBr	"	"	"	$\gamma_0=0.33\pm 0.12$	Br <sub>2</sub> +HBr	"
Spherical	NaBr doped droplets	273-280	Droplet train technique	10 <sup>13</sup> -10 <sup>15</sup>	$\alpha=0.063\pm 0.021$ $\Gamma=0.02$	100%Br <sub>2</sub>	[28]
"	NaCl doped droplets	"	"	"		100%BrCl	"
<b>HOBr</b>							
Planar	H <sub>2</sub> O.Br <sup>-</sup> .Cl <sup>-</sup>	274	Wetted-wall flow tube reactor	2×10 <sup>12</sup>	$\alpha > 0.001$	pH=8 (new sea-salt) Br <sub>2</sub> yield circa 40%	[33]
Planar	Frozen salt similar to sea-spray	233-253	Coated-wall flow tube reactor	10 <sup>9</sup> -10 <sup>10</sup>	$\gamma \approx 0.01$	pH<7 Br <sub>2</sub> yield >90% mostly Br <sub>2</sub>	[5]
Planar	H <sub>2</sub> O.Br <sup>-</sup> .Cl <sup>-</sup>	233 and 248	"	10 <sup>12</sup>	$\gamma < 0.01$		[56]
Spherical	Natural sea-salt	Ambient	Laminar flow reactor	1.0×10 <sup>13</sup>	$\Gamma_{max}=0.019$		[89]
"	Recrystallized sea-salt	"	"	"	$\Gamma_{max}=0.010$		"
Spherical	Deliquescent NaCl	Ambient	Aerosol kinetics flow tube	2×10 <sup>12</sup> -1×10 <sup>13</sup>	$\Gamma > 0.2$ acid/pH7.2 $\Gamma < 1.5 \times 10^{-3}$ unbuff		[3]
Spherical	NaBr	Standard	"	300	$\alpha=0.6\pm 0.2$		[129]

### 2.2.6 Choice of the total reactive uptake

For our MOZART4 long simulations including bromine chemistry we need to define a value for the total uptake coefficients of each heterogeneous reaction on sea salt. Therefore, we performed sensitivity tests with MOZART4. We describe these sensitivity tests and the choice of the most reasonable halogen volume mixing ratios.

Three sensitivity experiments were made. All experiments had the simulation duration of 2 months and they had the same yield for the reactions on sea salt, but different values for the reactive uptakes. The heterogeneous reactions on sea salt introduced were:



First, we chose the maximum and minimum of the total reactive uptakes ( $\Gamma$ ) in the literature for both gas phase species:

$$\begin{array}{l} \text{Simulation TRGY1 (maximum scenario)} \\ \Gamma_{\text{BrONO}_2} = 0.02 \\ \Gamma_{\text{HOBr}} = 0.2 \end{array}$$

$$\begin{array}{l} \text{Simulation TRGY2 (minimum scenario)} \\ \Gamma_{\text{BrONO}_2} = 0.01 \\ \Gamma_{\text{HOBr}} = 0.02 \end{array}$$

We compared the individual inorganic species volume mixing ratios (Br, BrO, HOBr, HBr, BrONO<sub>2</sub>, BrCl, and Br<sub>2</sub>), their sum (Br<sub>x</sub>), and partitions (ratio between individual bromine inorganic species and Br<sub>x</sub>) to the results of Yang and co-workers [138], who performed simulations including bromine chemistry using the chemical transport model *p*-TOMCAT.

We observed in the results of simulation *TRGY1* an overall good agreement, with the exception of extremely high maxima of Br<sub>x</sub> over the Northern Hemispheric Oceans. Simulation *TRGY2* showed overall too low values. In terms of individual species, the same is true, with the exception of Br<sub>2</sub> that exhibits always low volume mixing ratios, 10 times lower than Yang and colleagues results. The partitions are similar to the results of Yang and colleagues, with the striking exception that our HBr/Br<sub>x</sub> ratio is much higher in both simulations.

From our analysis, we concluded that the reality should be between these two simulations, which are the extremes, but closer to *TRGY1*. As BrONO<sub>2</sub>/Br<sub>x</sub> was high in *TRGY1* compared to Yang *et al.*, but HOBr/Br<sub>x</sub> was similar, we decided to increase the loss of BrONO<sub>2</sub>. Consequently, we lowered the total uptake of HOBr on sea salt, get lower Br<sub>x</sub> concentrations, and maintain the loss of BrONO<sub>2</sub> relatively high. Thus, the BrONO<sub>2</sub>/Br<sub>x</sub> ratio becomes lower. We tested the following choice of total uptake coefficients in a last short simulation named *TRGY3*:

$$\begin{array}{l} \text{Simulation TRGY3} \\ \Gamma_{\text{BrONO}_2} = 0.02 \\ \Gamma_{\text{HOBr}} = 0.1 \end{array}$$

The results of this last simulation of two months are in reasonable agreement with the study of Yang *et al.* [138]. We performed a longer simulation like *TRGY3*, that we called *SS1* and that we analyse in chapter 3.

## 2.3 Oceanic Emissions for the Very Short-Lived Halocarbons

Other organic sources of bromine are dibromomethane ( $\text{CH}_2\text{Br}_2$ ), bromochloromethane ( $\text{CH}_2\text{BrCl}$ ), dibromochloromethane ( $\text{CHBr}_2\text{Cl}$ ), and bromodichloromethane ( $\text{CHBrCl}_2$ ). These substances seem to have a similar emission pattern as bromoform [20, 109], which permits to establish simple relationships between the emissions of these species and bromoform.

### 2.3.1 Bromoform observations used in the compilation of the emission inventory

We constructed the emissions focusing first on bromoform ( $\text{CHBr}_3$ ). The observations of emission fluxes of halocarbons and their concentration in water and air are sparse. To create the emission inventory for the short-lived halocarbons, we began with the compilation and analysis of approximately 60 publications reporting bromoform measurements in marine seawater and air (for the latter see Figures 2.9 and 2.10) done by Quack and Wallace (2003) [92]. The plots summarize various mean values of air measurements from various campaigns in several oceanic regions. The earliest measurement campaign was done in 1982-83 in the Atlantic and the latest in the winter of 1997 in the Indian Ocean and Western Pacific. The figures also contain the measured values of a second data source: the boundary layer measurements of bromoform done during the Pacific Exploratory Mission in the Tropical Pacific (PEM-Tropics) in phase A (August and September 1996) and B (March and April 1999) described in [109].

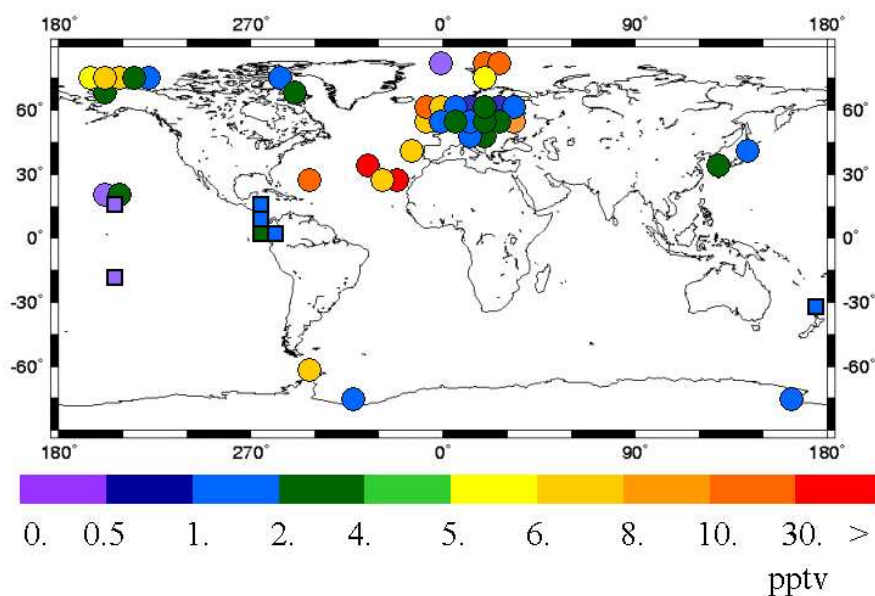


Figure 2.9: Bromoform atmospheric mixing ratios in air at the surface (pptv) at coastal locations. Values reported by Quack and Wallace (2003) [92] are represented by circles; those from PEM Tropics campaigns A and B are represented by squares [109].

From the data, it was possible to conclude that the bromoform concentration shows a significant coast-open ocean contrast, the highest levels being measured in coastal areas. The

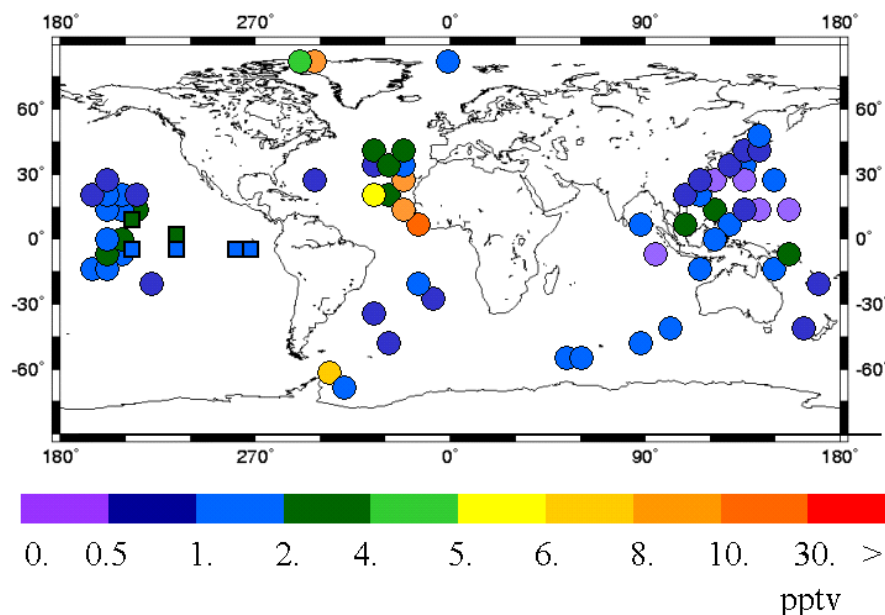


Figure 2.10: Bromoform atmospheric mixing ratios in air at the surface (pptv) at open ocean locations. Values reported by Quack and Wallace (2003) [92] are represented by circles; those from PEM Tropics campaigns A and B are represented by squares [109].

most probable emission source for these relatively high air concentrations are macro algae. The emission from these organisms has a diurnal variation [30] mainly related to tides (macro algae emit more when they emerge from water) and their metabolism, such as photosynthesis and respiratory cycles. This may explain the high variability of concentrations observed for the values measured in the coastal region (see table 2.4). The concentrations in the open ocean is much more homogeneous in space and time, and shows air concentrations mostly below 4 pptv.

Table 2.4: Percentiles calculated for the air observations compiled by Quack and Wallace, 2003 [92]

CHBr <sub>3</sub> (pptv)	Percentile 50	Percentile 75	Percentile 95
All observations	2.0	3.9	20.4
Coastal region	2.6	6.3	27.8
Open ocean region	1.2	2.0	7.7

Higher values measured in the "open ocean" seem to have substantial input from coastal regions. The measurements reported near the west coast of Africa have a coastal input due to transport by the northeast trade winds from the highly bioactive African coast line related to the upwelling of water [22]; the high values in the Arctic defined as open ocean were measured over the icecap [13]; the high value (6.3 pptv) measured near the Antarctic Peninsula can also be considered as a coastal measurement [98].

The PEM-Tropics campaigns showed an interesting property: the concentrations of natural halocarbons in equatorial regions are enhanced, especially at Phase B (March and April) - see Figure 2.11. This happens not only on the surface, but is detectable in the entire tropical

troposphere [109], which shows the effect of vertical transport and a possible and probable mechanism for the transport of short-lived species into the stratosphere. Besides bromoform, other mainly natural organohalogens showing higher values at the equatorial region are  $\text{CHBr}_2\text{Cl}$ ,  $\text{CHBrCl}_2$ , and  $\text{CH}_2\text{Br}_2$ . The measurements done in the Atlantic, in 1988, on the research vessel FS *Polarstern* had already shown this phenomenon for  $\text{CHBr}_3$  and  $\text{CH}_2\text{Br}_2$ . However, they followed the African coastline, which made it impossible to determine whether the upwelling of water on the open ocean also resulted in an enhancement of the organohalogen air surface concentrations. Furthermore, PEM-Tropics measurements of surface bromoform concentrations show the coast-open ocean contrast only for continental coastlines, but not for islands.

Regarding the seasonality of the emissions, the observations allow the following conclusion: high values will be measured more probably in spring and summer.

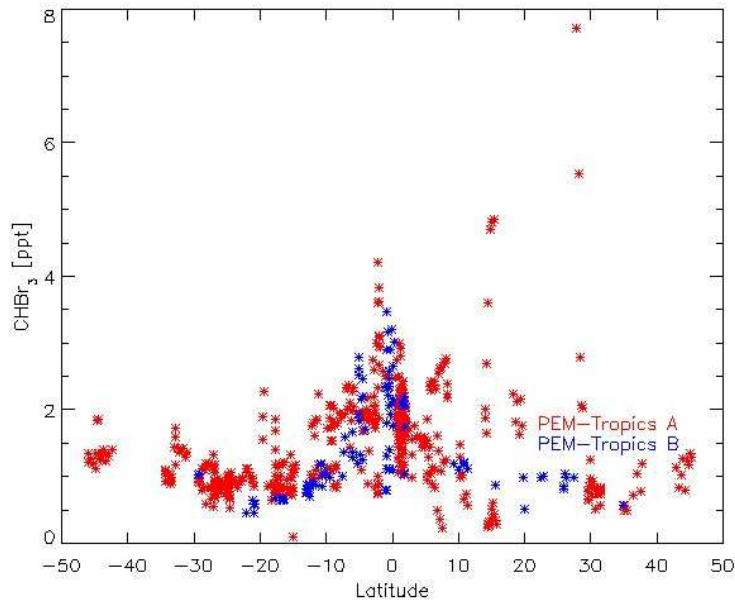


Figure 2.11: Bromoform boundary layer measurements done during the Pacific Exploratory Mission in the Tropical Pacific (PEM-Tropics) in phase A (August and September 1996) and B (March and April 1999) [109].

### 2.3.2 Calculation of emissions

According to estimates in the literature, the global annual emission of  $\text{CHBr}_3$  from sea water is within the range  $2.5 - 20 \text{ Gmol (Br).yr}^{-1}$  [92]. The highest concentrations of bromoform are found in coastal waters. Based on this information and distributing a value of  $10 \text{ Gmol (Br) yr}^{-1}$  over the ocean, three simulations were performed with the model MOZART2:

**simulation A:** We considered a spatially homogeneous distribution of  $\text{CHBr}_3$  in the ocean, leading to a surface flux of  $\text{CHBr}_3$  of  $7.4 \times 10^{-14} \text{ kg.m}^{-2} \cdot \text{s}^{-1}$  over the ocean - Figure 2.12, left panel.

**simulation B:** We considered the same annual global flux, but 2.5 times higher emissions in coastal areas than over the open ocean (coastal:  $14. \times 10^{-14}$   $\text{kg.m}^{-2}.\text{s}^{-1}$ ; open ocean:  $5.7 \times 10^{-14}$   $\text{kg.m}^{-2}.\text{s}^{-1}$  - Figure 2.12, right panel);

**simulation C:** In the last experiment, we used the same spatial emission pattern with 10 times higher emissions in coastal areas than over the ocean ( $27. \times 10^{-14}$  and  $2.7 \times 10^{-14}$   $\text{kg.m}^{-2}.\text{s}^{-1}$  for coastal and open ocean areas, respectively - Figure 2.12, right panel).

Table 2.5 contains the bromoform fluxes for the different regions and simulations.

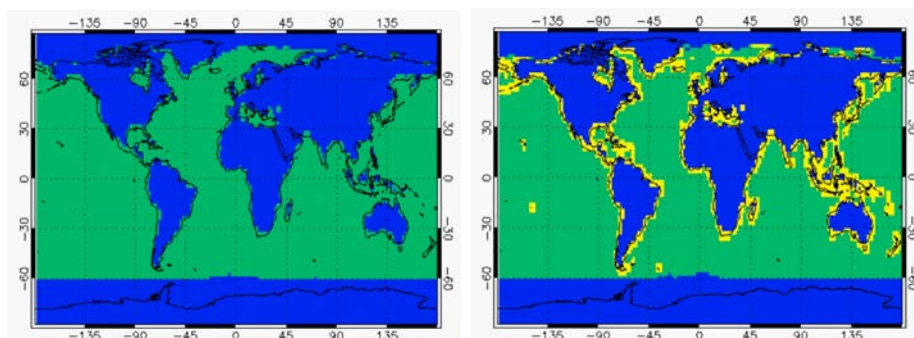


Figure 2.12: Map of the bromoform emission areas used in the simulations: areas with zero surface emissions are in blue; the *left panel* represents simulation A with spatially homogeneous emissions over the ocean (green shaded area); the *right panel* represents simulation B or C in which coastal emissions (yellow shaded areas) are higher than over the open ocean (green shaded area).

Table 2.5: Bromoform fluxes for the different regions for each simulation

$\text{CHBr}_3$ Fluxes ( $\text{kg.m}^{-2}.\text{s}^{-1}$ )	Land	Open ocean	Coastal region
Simulation A	0.	$7.4 \times 10^{-14}$	$7.4 \times 10^{-14}$
Simulation B	0.	$5.7 \times 10^{-14}$	$14. \times 10^{-14}$
Simulation C	0.	$2.7 \times 10^{-14}$	$27. \times 10^{-14}$

The ratio between the coastal and open ocean flux in Simulation C was considered on the basis of a personal communication with Birgit Quack. She suggested a ratio of around 10 between atmospheric surface  $\text{CHBr}_3$  concentrations in coastal and open ocean locations. The assumption in simulation B was made in order to investigate a case with a moderate open ocean - coast contrast in the emission file.

The global annual emission resulting from the simulations A, B and C is 9.1, 9.6, and 9.4 Gmol (Br)/yr, respectively. The differences are due to the sea ice cover that affects the amount of coastal emissions.

The simulations were performed for the years 2001, 2002, and 2003 till July.

We assumed that the 3 bromines are immediately released upon bromoform degradation:





In appendix B the reader can find a chapter regarding the chemistry of bromoform. Our simple chemistry is reasonable as photolysis is the main sink by UV absorption of  $CHBr_3$ . Moreover, bromoform oxidation by OH yields  $CBr_2O$ , which is mainly degraded by photolysis. By these two reaction pathways, and in the low  $NO_x$  environment over the ocean all the Br atoms are released. We ignored the production of CO, which is not important for our purpose.

### 2.3.3 Resulting emission distribution and its evaluation

There is a seasonal variation in the  $CHBr_3$  concentrations in extratropical regions, which is more pronounced in the Southern than in the Northern hemisphere. The maximum concentrations are observed in the winter months of the respective hemisphere (Figure 2.13). The seasonality is related to the temporal variation of the strength of the two chemical sinks of bromoform: photolysis and reaction with OH. This seasonal variation is also present in measurements. Yokouchi *et al.*, 1996, detected a winter/summer ratio of mixing ratios for bromoform of 3 at Alert, Canada [140]. In our case, for the same location, we got ratios of mixing ratios between 2.5 (simulation A) and 3 (simulations B and C). In the simulations, the highest concentrations are in October, and the lowest in May/June. For Yokouchi *et al.*, 1996, the highest mixing ratios are observed in January/February/March, and the lowest are observed in May/June.

The equatorial region does not show any seasonal variation as the radiation source and the OH concentration levels are relatively constant during the year.

From simulation A, to B and C, a progressively higher portion of the emissions are transferred from the open ocean to the coastal regions. The southern hemisphere has a larger open ocean surface area than the northern hemisphere, which translates into progressively higher bromoform mixing ratios in the northern latitudes as it can be seen from Figure 2.13.

In Figure 2.14, we can observe the surface global distribution of the  $CHBr_3$  monthly average concentrations for March 2002 and 2003, and June 2002 and 2003. The main observations from the figures are:

1. the rising concentrations on the coastlines from simulation A to B and C;
2. higher concentrations in the higher northern latitudes in Simulation C (coastal region emissions are the highest in this simulation) and higher concentrations in southern latitudes in Simulation A (open ocean emissions are the highest in this simulation).

Comparing the simulation results with the measurements (Figures 2.9 and 2.10 and table 2.4, respectively) we conclude that all the simulations yield too high concentrations. Overall, 50% of the bromoform measurements are below 2 pptv. Higher concentrations are measured in coastal regions. However, even there the median is 2.6 pptv. Nevertheless, coastal regions are characterized by the detection of very high peaks (maxima of 460 pptv), that leadsto a high standard deviation. The open ocean is the region with the most homogeneous concentrations. All the simulations show averages higher than 3 pptv, and only in simulation C, mainly the southern hemisphere fits to the concentrations observed over the open ocean.

For the coastal regions, the averages are too high in all the simulations. Simulation A compares best with the measurements, simply because the coastal emissions and, consequently, the concentrations are the lowest.

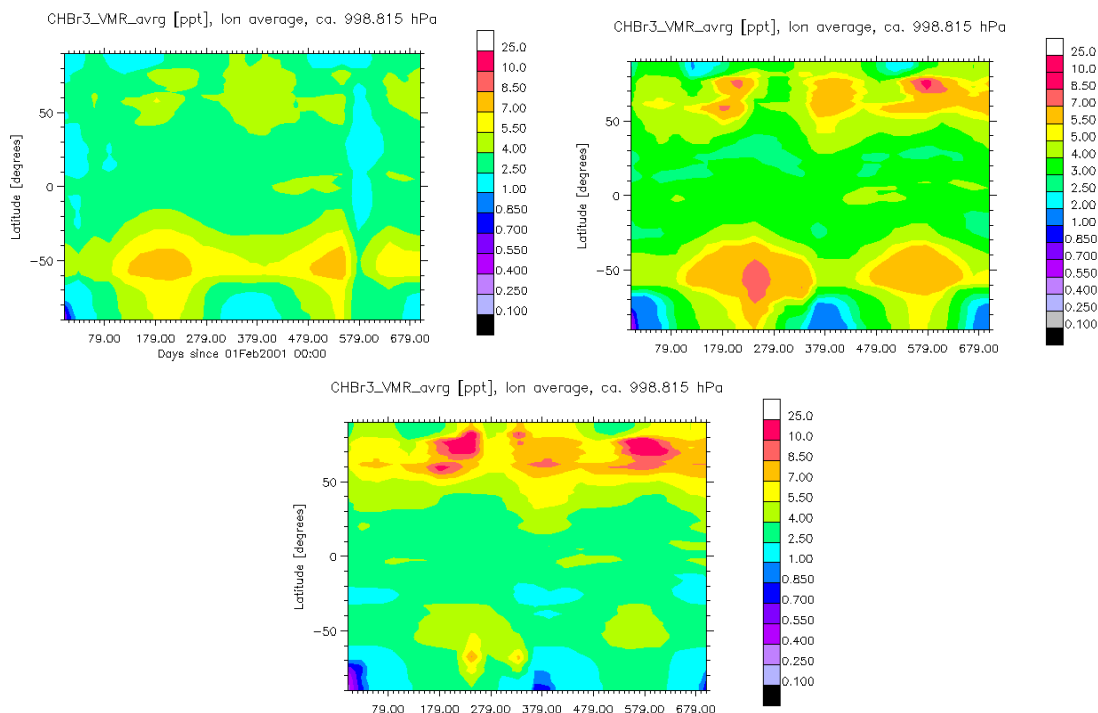


Figure 2.13: Time evolution (1 February 2001 to 31 December 2002) for bromoform atmospheric mixing ratios (pptv), zonal mean at the surface for, from top clockwise: **simulation A** - spatially homogeneous oceanic emission - **simulation B** - coastal regions with 2.5 times higher emissions than open ocean - **simulation C** - coastal regions with 10 times higher emissions than open ocean.

The geographical distribution of bromoform resulting from simulation A (Figure 2.14) seems to indicate an effect of atmosphere dynamics on the open ocean-coastal region contrast. Although there is no difference in the bromoform emission flux between the open ocean and coastal regions, we nevertheless obtain higher concentrations in coastal areas than over the open ocean. The concentrations in coastal regions are higher by a factor of 1.25 in average. Even most of the regions characterized by high primary production (Figure 2.19) are recognizable in the results from simulation A, which indicates a close link between physical processes parameterised in the model and the oceanic regions of high primary production. In this way the west coast of Africa, the Southern ocean productivity belt, areas in the Northern Hemisphere and even upwelling regions in the Pacific and Atlantic Ocean emerge from the background. Moreover, the higher dispersion for spring/summer observed in the observations seems to be also due to physical processes, because it is captured by the simulations (Figure 2.15). The explanation may be the characteristic low photolysis rates in these regions due to cloud coverage.

At first glance, the geographical pattern in the measurements is opposite to the modelled (Figures 2.11 and 2.16), showing the importance of the equatorial enhancement detectable in the PEM-Tropics campaigns.

In Figures 2.17 and 2.18, we plot PEM-Tropics surface measurements versus the medians of the modelled data for March 2002 and 2003 on the left, and September 2002 and 2003 on

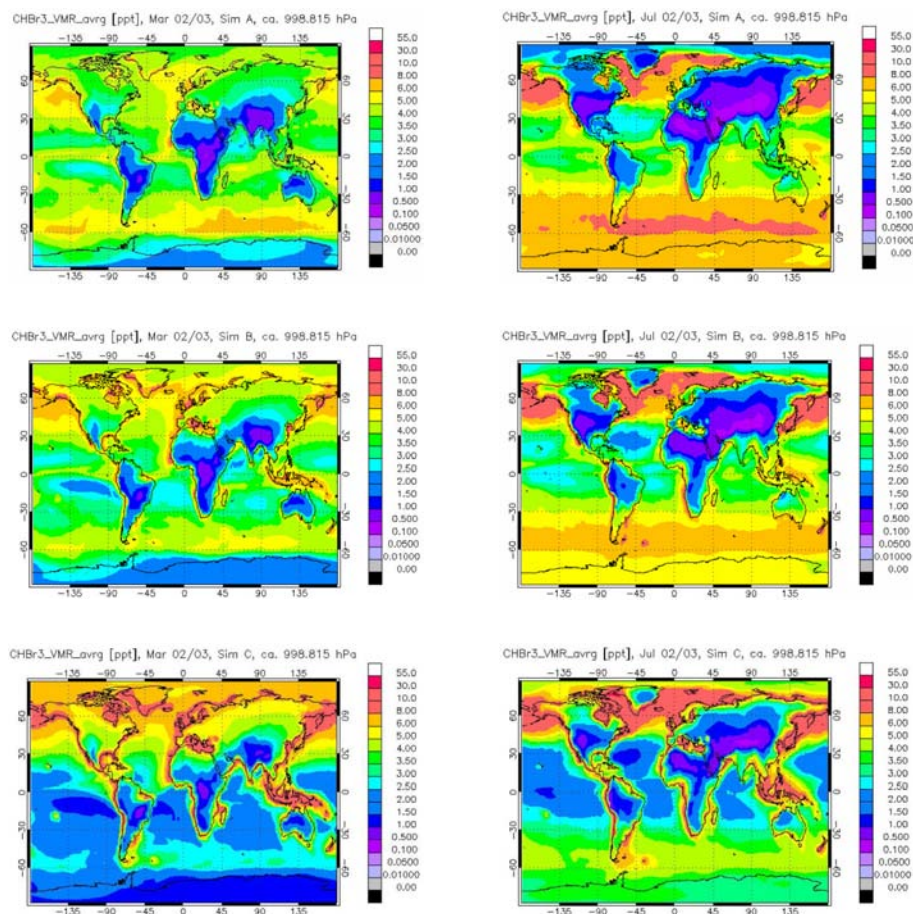


Figure 2.14: Bromoform monthly average atmospheric mixing ratios (pptv) at the surface for March 2002 and 2003 ( $1^{st}$  column) and June 2002 and 2003 ( $2^{nd}$  column) for, top to bottom, **simulation A**, **simulation B**, and **simulation C**.

the right. The modelled data is surface ocean data from the same domain where PEM-Tropics surface data were sampled and the time span was also chosen to be at the same season as for the measurements. From Figures 2.17 and 2.18 it is quite obvious that the simulations are producing too high concentrations. To fit the simulation results outside the equatorial region with the PEM-Tropics measurements it would be necessary to reduce the medians by 65% to 80%.

### 2.3.4 The additional equatorial enhancement study

Realizing the importance of the equatorial enhancement in the bromoform concentration in the measurements (Figure 2.11), we studied environmental variables that could affect the production and ocean emission of  $\text{CHBr}_3$  and explain this concentration maximum.

We analysed the Sea Surface Temperature (SST), the Solar Radiation and the Phytoplankton Pigment Concentration (PPC).

Bromoform saturation in water depends on SST and, consequently, also the flux into the

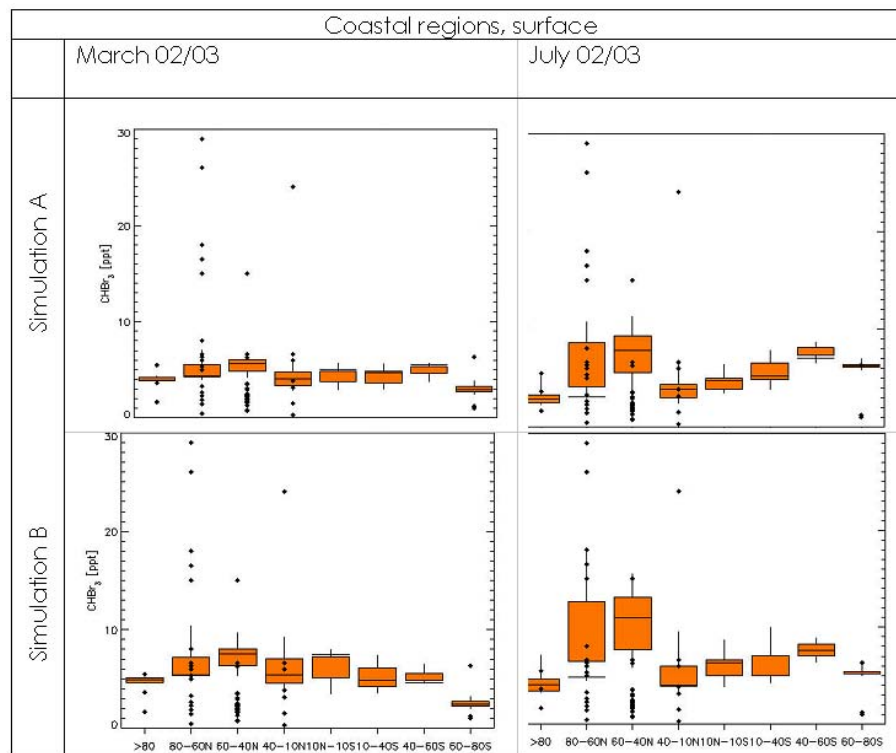


Figure 2.15: Bromoform monthly average atmospheric mixing ratios (pptv) at the surface for March and July 2002 and 2003, for simulations B and C. Modelled data as box plots; observed mean values as individual points from Quack and Wallace, 2003 [92].

atmosphere depends on the SST. Moreover, the SST is associated with the upwelling of water and can be associated with primary biomass production in the ocean. For  $\text{CH}_3\text{Br}$ , the correlation between SST and the surface fluxes was described by King *et al.*, 2002 [62].

The solar radiation affects the production of bromoform by algae and phytoplankton [68, 25]. Finally, the PPC could be a marker for the biogenic production of  $\text{CHBr}_3$  in the Ocean.

The satellite data composites for PPC from the SeaWiFS Project (Figure 2.19) show a strong concentration enhancement in coastal regions (red to yellow), that can be related to the upwelling areas (nutrient transport to the surface), and consequently higher primary production. Bromoform could be produced by macroalgae and also by microalgae. Quack *et al.* (2004) [91] found an association between the deep depth chlorophyll maximum within the tropical thermocline and water bromoform concentrations.

A careful analysis of the atmospheric bromoform surface concentration, SST, solar radiation and PPC showed a better correlation of bromoform surface air concentration with PPC (Figures 2.20 and 2.21). The Pearson Correlation<sup>8</sup> is for the latter 0.5.

The high biological productivity in middle and high latitudes observed in the SeaWiFS data is not related to enhanced  $\text{CHBr}_3$  concentrations. However, the SeaWiFS data do not show the species composition shifts, which probably affects the emissions. Also the

<sup>8</sup>Pearson's correlation is a statistic coefficient that reflects the degree of linear relationship between two variables. It ranges from +1 to -1. A correlation of +1 means that there is a perfect positive linear relationship between the two variables.

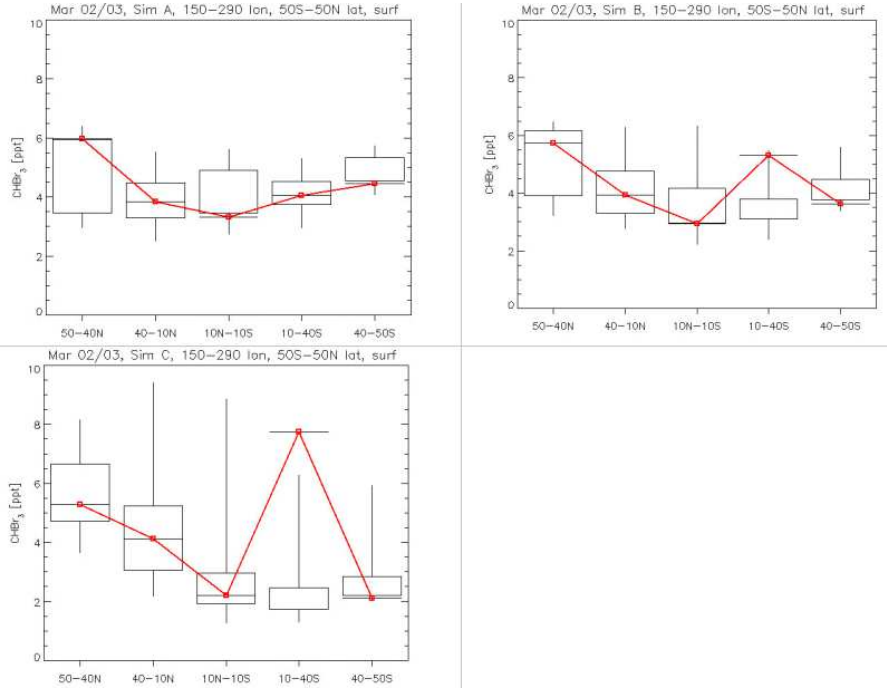


Figure 2.16: Bromoform monthly average atmospheric mixing ratios (pptv) at the surface for March and July 2002 and 2003 from the simulations. The results are for the Pacific Ocean (longitude 150–290°, latitude 50°N – 50°S).

environmental conditions may have an effect [25]. Therefore, the PPC correlation was only used for the reajustment of the bromoform emissions in the latitude strip between 18° S and 18° N, using the equation:

$$E(CHBr_3)_{final} = 15. \times [PPC] \times E(CHBr_3)_{initial}, \quad (2.58)$$

where  $E(CHBr_3)_{final}$  is the bromoform emission after the readjustment of the emission obtained in the simulation B ( $E(CHBr_3)_{initial}$ ).

### 2.3.5 The final run

We made a final run with the following assumptions:

1. the global annual emission flux is around 75% less than the original assumption;
2. the ratio between coastal and open ocean regions would be the one considered for simulation B, i. e. 2.5;
3. reajustment of the bromoform emissions in the latitude strip between 18° S and 18° N using the PPC correlation expressed by equation (2.58). We assume that emissions from the ocean and air concentrations obey a linear relationship.

The simulated bromoform mixing ratios fit well with the measurements (Figures 2.22 and 2.23):

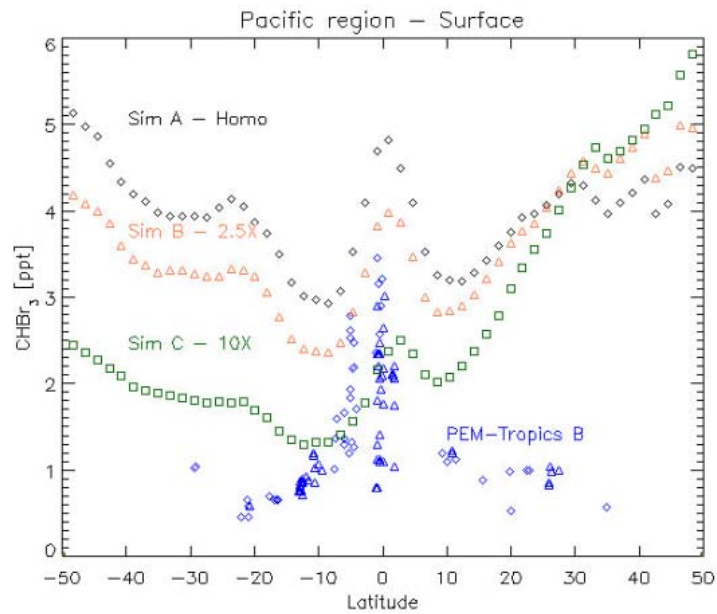


Figure 2.17: Bromoform atmospheric mixing ratios (pptv) at the surface of the ocean: the blue crosses are measurements from the PEM-Tropics campaign phase B (March and April 1999), and the polygons are medians for the results for March 2002 and 2003 for the Pacific Ocean (longitude  $150^{\circ}$ – $290^{\circ}$ , latitude  $50^{\circ}N$  –  $50^{\circ}S$ ) for each of the simulations.

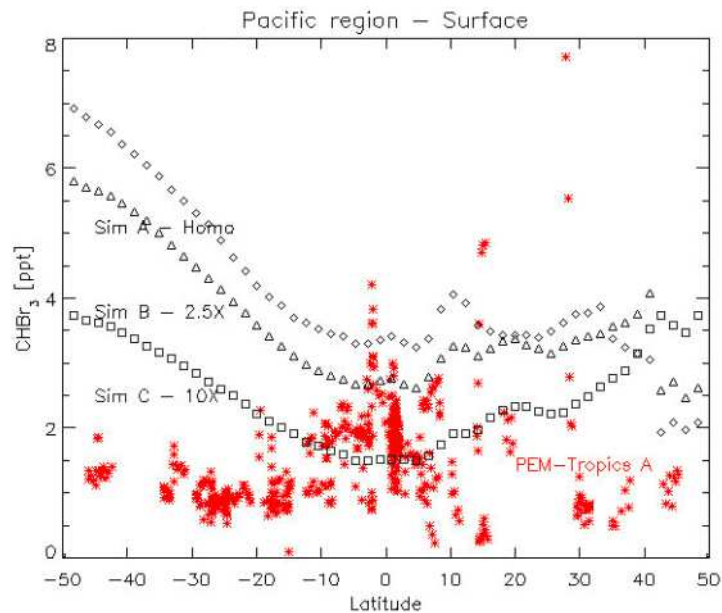


Figure 2.18: Bromoform atmospheric mixing ratios (pptv) at the surface of the ocean: the red crosses are measurements from the PEM-Tropics campaign phase A (August and September 1996), and the polygons are medians for the results for September 2002 and 2003 for the Pacific Ocean (longitude  $150^{\circ}$ – $290^{\circ}$ , latitude  $50^{\circ}N$  –  $50^{\circ}S$ ) for each of the simulations.

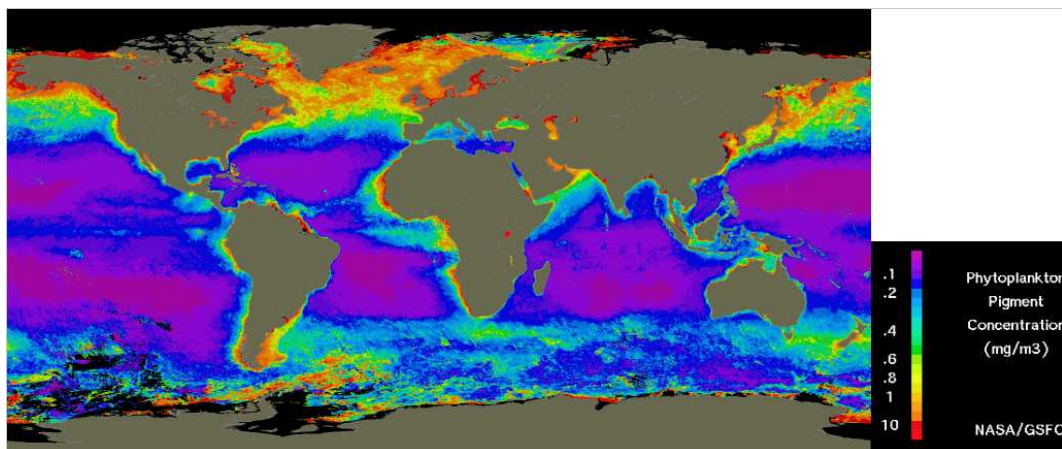


Figure 2.19: Satellite data composites (Nov. 1978–June 1986) for phytoplankton pigment concentration ( $\text{mg}\cdot\text{m}^{-3}$ ) [lower values at the top of the legend bar], SeaWiFS Project, NASA).

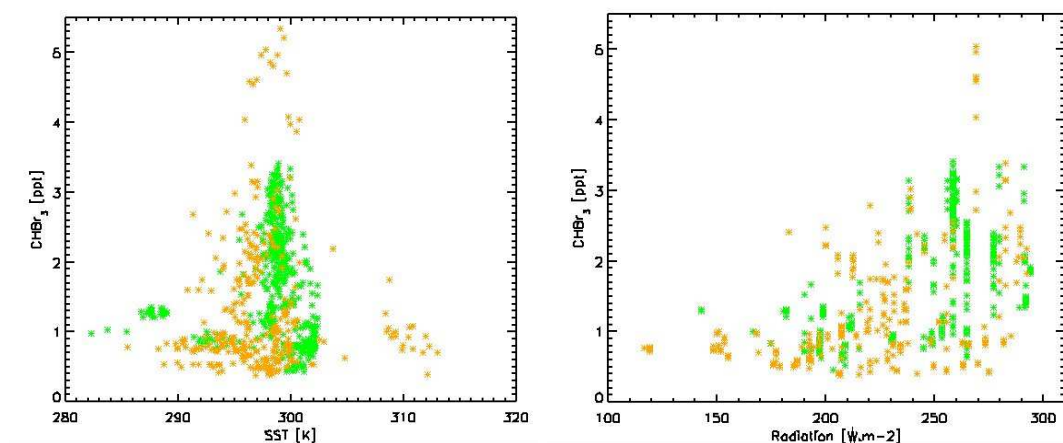


Figure 2.20: Bromoform surface air concentrations versus SST (*left*) and versus Solar radiation (*right*) over the Pacific. The data is from the PEM-Tropics campaign B [109].

1. the equatorial maximum is very well reproduced;
2. the scattering of the measurements at the end of summer is also reproduced by the model. This is related to transport processes and cloud coverage associated with reduced photolysis.

### 2.3.6 The other natural organohalogens

Several studies on the biogenic emissions from the ocean detected concomitantly with bromoform the species:  $\text{CH}_2\text{Br}_2$ ,  $\text{CH}_2\text{BrCl}$ ,  $\text{CHBr}_2\text{Cl}$ , and  $\text{CHBrCl}_2$  (in the Arctic [140], at several locations in the Atlantic [22, 20, 23, 30], in the Tropical Pacific [109], at the coast of Tasmania [21], and Antarctic [98]). Moreover, studies on the emissions of volatile organohalogens from certain species of algae found that the production of the brominated compounds is correlated [4, 81, 24, 68].

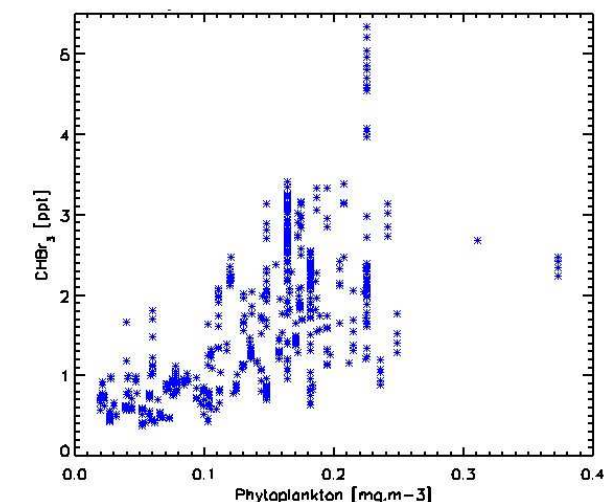


Figure 2.21: Bromoform surface air concentrations versus Phytoplankton Pigment Concentration over the Pacific. The bromoform data is from the PEM-Tropics campaign B [109]. PPC data is from the SeaWIFS project.

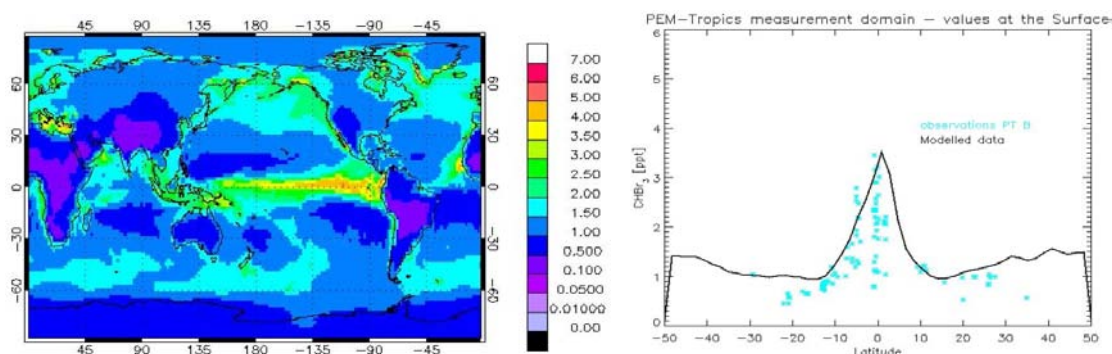


Figure 2.22: Simulated bromoform monthly mixing ratio at the surface (pptv) for March 2001 - *left panel*. Comparison of the median of the simulated bromoform zonal mean concentrations for March 2001 with the PEM-Tropics boundary layer measurements in campaign B (March and April 1999) - *right panel*.

Based on the findings, it is reasonable to correlate the oceanic emissions of other natural organohalogens with the bromoform emissions. We used the work of Carpenter and Liss (2003) [21], in which they define the ratio between the emissions of several halocarbons and bromoform (table 2.6).

More precisely, we used the following emissions of  $\text{CH}_2\text{Br}_2$ ,  $\text{CH}_2\text{BrCl}$ ,  $\text{CHBr}_2\text{Cl}$ , and  $\text{CHBrCl}_2$ :

$$E_{\text{CH}_2\text{Br}_2} = 0.22 \times E_{\text{CHBr}_3} \quad (2.59)$$

$$E_{\text{CHBrCl}_2} = 0.05 \times E_{\text{CHBr}_3} \quad (2.60)$$

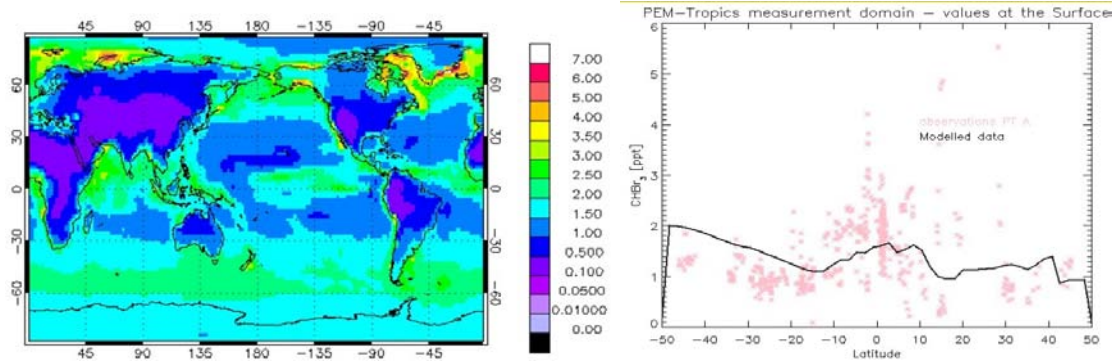


Figure 2.23: Simulated bromoform monthly mixing ratio at the surface (pptv) for September 2001 - *left panel*. Comparison of the median of the simulated bromoform zonal mean concentrations for September 2001 with the PEM-Tropics boundary layer measurements in campaign A (August and September 1996) - *right panel*.

Table 2.6: The emission ratios of several halocarbons to bromoform according to Carpenter and Liss (2003) [21] and the data measured during the PEM-Tropics campaigns A and B [109]

Emission ratio Halocarbons/CHBr <sub>3</sub>	C&L <sup>9</sup>	PEM-Trops A August-September	PEM-Trops B March-April
CH <sub>2</sub> Br <sub>2</sub>	0.15-0.25	0.16	0.34
CHBrCl <sub>2</sub>	0.03-0.06	0.04	0.07
CHBr <sub>2</sub> Cl			0.06
CH <sub>2</sub> BrCl		0.036	0.053

$$E_{CHBr_2Cl} = 0.06 \times E_{CHBr_3} \quad (2.61)$$

$$E_{CH_2BrCl} = 0.44 \times E_{CHBr_3} \quad (2.62)$$

When comparing each of these organohalogens

### 2.3.7 Final global annual emissions

The global annual emissions in Br atoms resulting from our experiment are tabulated in table 2.7

Table 2.7: Global annual emissions of Br for each halocarbon simulated with MOZART2

Halocarbons	Global emissions Mmol(Br).yr <sup>-1</sup>
CHBr <sub>3</sub>	3489
CH <sub>2</sub> Br <sub>2</sub>	524
CHBrCl <sub>2</sub>	518
CHBr <sub>2</sub> Cl	140
CH <sub>2</sub> BrCl	58

Our result for bromoform is in the lower range of the values reported in the literature, which are in the range of 2.5-20 Gmol(Br)/yr. The net oceanic source of short-lived halocarbons is of 4.7 Gmol(Br)/yr, with bromoform representing 75% of this value.

### 2.3.8 Conclusion

The seasonality of simulated bromoform concentrations in the polar regions depends mainly on the chemical reactivity of the atmosphere (radiation and OH), which leads to higher concentrations in the respective winter months. This is a result from field work [140]. At midlatitudes the measurements show the higher values in spring and summer, while this was not reproduced by the model without taking emissions of algae and phytoplankton into account. This discrepancy was a hint that the measured emission maxima were due to a biogenic source that the model did not simulate originally. The highest emissions occur in regions with higher primary biomass production as the coastal areas, and in the open ocean regions with upwelling as in the equatorial region. For the equatorial region, the best agreement with measurements was achieved with the use of a parameterisation of the bromoform emissions according to the Phytoplankton Pigment Concentration. This allowed us to simulate the concentration peak of natural organohalogen observed in measurements. In order to simulate the higher emissions in the coastal regions the emission flux was set to 2.5 times that of the open ocean. CH<sub>2</sub>Br<sub>2</sub>, CH<sub>2</sub>BrCl, CHBr<sub>2</sub>Cl, and CHBrCl<sub>2</sub> emissions seem to be correlated with the emissions of bromoform, probably due to a chemical chain process in the algae metabolism. Based on Carpenter and Liss (2003) [21] and the PEM-Tropics measurements the ratios between the various halocarbon emissions were defined.

## 2.4 Dry Deposition of Halogens

Dry deposition is the absorption of gaseous and particulate species from the atmosphere onto surfaces in the absence of precipitation. Commonly in global models, this process is determined by the dry deposition flux  $F$ :

$$F = -v_d C \quad (2.63)$$

$F$  represents the vertical dry deposition flux, i.e., the amount of the species that deposits per unit surface area per unit time.  $v_d$  represents the deposition velocity.  $C$  is the concentration of the species above the surface. It is considered that the flux is directly proportional to the concentration of the depositing species.

Normally, in global models the deposition velocity is assumed to have a value that varies with the type of surface. The surface types are described by the very broad categories of ocean, desert, vegetation, and ice.

However, besides the surface, other factors affect the deposition velocity e.g. the turbulence in the atmosphere and the chemical properties of the chemical species. The inclusion of these factors can be done as described in [112]. MOZART4 includes this method of calculation, which is called an interactive dry deposition computation.

The deposition velocity for gases is calculated using:

$$v_d = \frac{1}{r_a + r_b + r_c} \quad (2.64)$$

$r_a$  represents the aerodynamic resistance,  $r_b$  is the quasi-laminar resistance, and  $r_c$  is the surface or canopy resistance. The last variable applies only to gases and its accurate quantification is not straightforward. The approach adopted in MOZART4 is the one developed by Wesely, 1989 [136]. It was devised for use in numerical models of atmospheric transport and deposition of pollutants at regional scales. The surface resistances are calculated along three distinct paths of mass transfer to sites of deposition: the upper portions of the canopy or other structures, their lower portions, and the ground or water surfaces. The calculation is done over a range of species, land-use types, and seasons. For the computation, it is necessary to provide the Henry Effective coefficients ( $k_H^*$ ) and the chemical reactivity ( $f_0$ ) of each species.

$k_H^*$  is a measure of the amount of a species that solubilises in the aqueous phase provided a certain partial pressure of the species in the gas phase. It includes the equilibrium between the fraction of the species in the gas phase and in the aqueous phase represented by the Henry coefficient ( $k_H$ ), and the dissociation upon the absorption in water represented by the dissociation equilibrium constant ( $k$ ). To calculate  $k_H$  the following equation is applied [104]:

$$k_H = k_H^\ominus \times \exp\left(\frac{d \ln k_H}{d(1/T)}\left(\frac{1}{T} - \frac{1}{T^\ominus}\right)\right) \quad (2.65)$$

where  $\frac{d \ln k_H}{d(1/T)}$  is the temperature dependence of the Henry coefficient and  $k_H^\ominus$  is the Henry coefficient at standard conditions ( $T^\ominus = 298.15K$ ).

For species that dissociate upon absorption,  $k$  is calculated by a similar expression:

$$k = k^\ominus \times \exp\left(\frac{d \ln k}{d(1/T)}\left(\frac{1}{T} - \frac{1}{T^\ominus}\right)\right) \quad (2.66)$$

Finally,  $k_H^*$  is calculated by:

$$k_H^* = \begin{cases} k_H \times \left(1 + k \times \frac{1}{pH}\right) & \text{if } k_H \neq 0 \\ k \times \frac{1}{pH} & \text{otherwise} \end{cases} \quad (2.67)$$

Note that while  $k_H$  only depends of the temperature,  $k_H^*$  depends on both the temperature and the concentration of  $H^+$  ions in the solution.

To our knowledge measurements of  $v_d$  for halogen species do not exist. Instead, estimates are used based on chemical similarities to other species. Yang *et al.*, 2006 [138] used this approach applying the values of table 2.8 in a non interactive computation procedure.

Table 2.8: Dry deposition velocities of HBr and HOBr (cm/s) used by Yang *et al.*, 2006 [138]

	Forest and Grass	Desert	Oceans	Ice/snow
HBr	1.0	0.5	0.5	0.2
HOBr	0.5	0.2	0.2	0.1

### 2.4.1 Parameters added to MOZART4

The species HBr, HOBr, HCl and HOCl were introduced in the interactive computation of dry deposition velocities in MOZART4. For this purpose, we supplement the tables in `drydep_tables.F90` (table 2.9):

1. the Henry coefficients at standard conditions denoted by  $k_H^\ominus$ ;
2. the temperature dependence of  $k_H$ , denoted by  $\frac{-d \ln k_H}{d(1/T)}$ ;
3. the dissociation equilibrium constant at standard conditions denoted by  $k^\ominus$
4. the temperature dependence of k denoted by  $\frac{-d \ln k}{d(1/T)}$
5. the chemical reactivity of each species denoted by ( $f_0$ ) (estimated by analogy to the other species in `drydep_tables.F90` )

Table 2.9: Parameters introduced for the interactive halogen dry deposition computation

Species	$k_H^\ominus$ <sup>10</sup> [ <i>M.atm</i> <sup>-1</sup> ]	$\frac{-d \ln k_H}{d(1/T)}$ <sup>10</sup> [K]	$k^\ominus$ <sup>11</sup> [M <sup>1-n</sup> /s <sup>12</sup> ]	$\frac{-d \ln k}{d(1/T)}$ <sup>11</sup> [K]	
HBr	0.72	6100.	$1.0 \times 10^{+9}$	0.	$1.0 \times 10^{-36}$
HOBr	1900.	0.	$2.1 \times 10^{-9}$	0.	0.1
HCl	19.	9000.	$1.7 \times 10^{+6}$	6896.	$1.0 \times 10^{-36}$
HOCl	930.	0.	$3.2 \times 10^{-8}$	0.	0.1

### 2.4.2 Deposition velocity results

We present results regarding deposition velocity for the added species. In order to produce comparisons, we also present results for species already present in the original model.

**Ozone:** Figure 2.24 shows the ozone deposition velocity for January 2000 for MOZART4 and MOZECH (RETRO project run). MOZART4 produced generally higher values over the continents compared to the ocean. However, it was expected that land masses would stick out more in the  $v_d$  results. Moreover, the overall maxima and relative higher values were expected over tropical forests compared to higher latitudes, which is not the case, and even seems to be the opposite over Africa. Values higher than 0.5 cm/s over Australia, which is poor in vegetation, is unexpected. In the work of Ganzeveld and Lelieveld, 1995 [39], the values over land are higher with the maxima over South America, which is also the case in the global chemistry transport model MOZECH (see Figure 2.24, right panel). The values of MOZART4 over Ocean and Snow/Ice are comparable to those by Ganzeveld and Lelieveld [39]. MOZECH has lower deposition velocities over the open ocean, but higher values over the polar regions compared to MOZART4.

**Nitrogen dioxide:** The monthly average of the deposition velocity of NO<sub>2</sub> is shown in figure 2.25. The ratio between the O<sub>3</sub> and the NO<sub>2</sub> deposition velocities is in very good agreement with the empirical rule from Ganzeveld and Lelieveld [39] that states: *"The values of  $v_d(NO_2)$  and  $v_d(NO)$  are about 2/3 and 1/10 those of O<sub>3</sub> above vegetation and bare soil, respectively."*

**Nitric acid vapor:** The deposition velocity values for HNO<sub>3</sub> over the ocean are comparable with the results from the MOZECH model and Ganzeveld and Lelieveld [39] (Figure 2.26).

---

<sup>10</sup>(Sander, 1999 [104])

<sup>11</sup>(Sander and Crutzen, 1996 [106])

<sup>12</sup><sub>n</sub> is the chemical reaction order

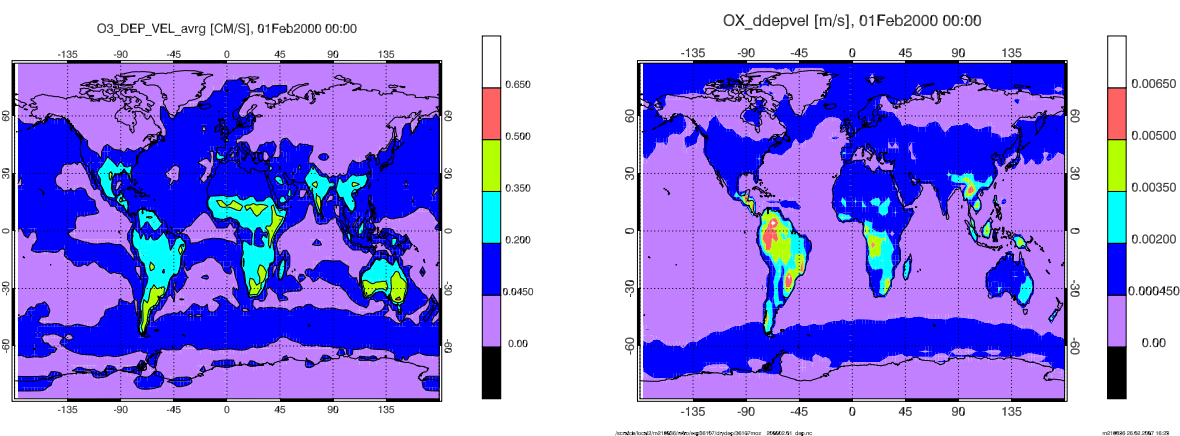


Figure 2.24: MOZART4 result for O<sub>3</sub> dry deposition velocity [cm/s] (left panel). MOZECH result for OX dry deposition velocity [m/s] (right panel). Monthly average for January 2000.

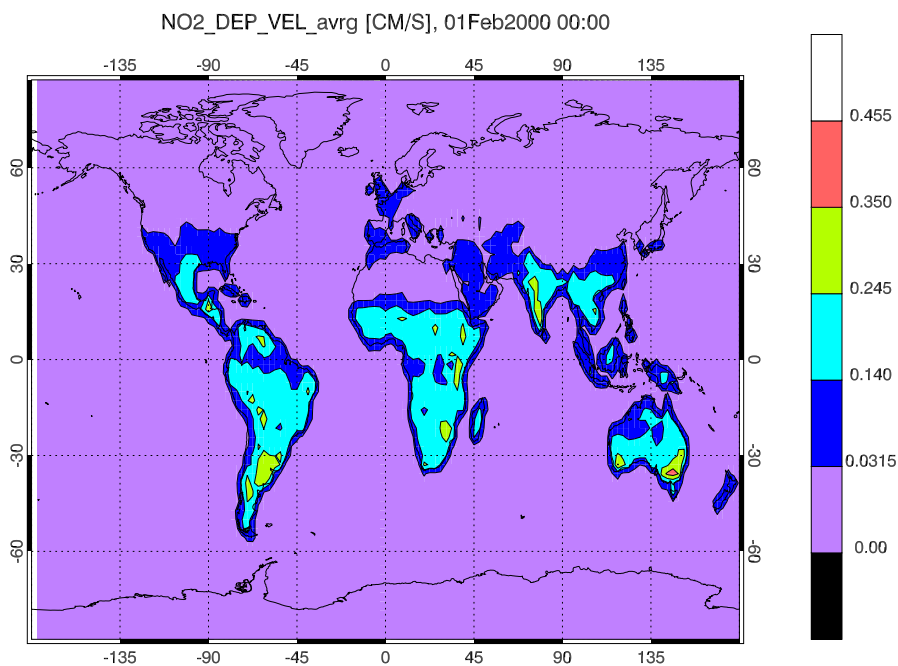


Figure 2.25: MOZART4 result for NO<sub>2</sub> dry deposition velocity [cm/s]. Monthly average for January 2000.

Over land there is a good agreement with MOZECH, except at the North Pole, with differences that can reach a factor of 10. However, comparing with Ganzeveld and Lelieveld [39], the discrepancies are very significant reaching 2 orders of magnitude. This is visible especially at the polar regions, which is worrying as the halogen study will focus on these regions.

**Carbon monoxide:** The deposition velocity for MOZART4 (left panel) and MOZECH (right panel) are presented in figure 2.27. MOZECH shows overall higher values, but as this

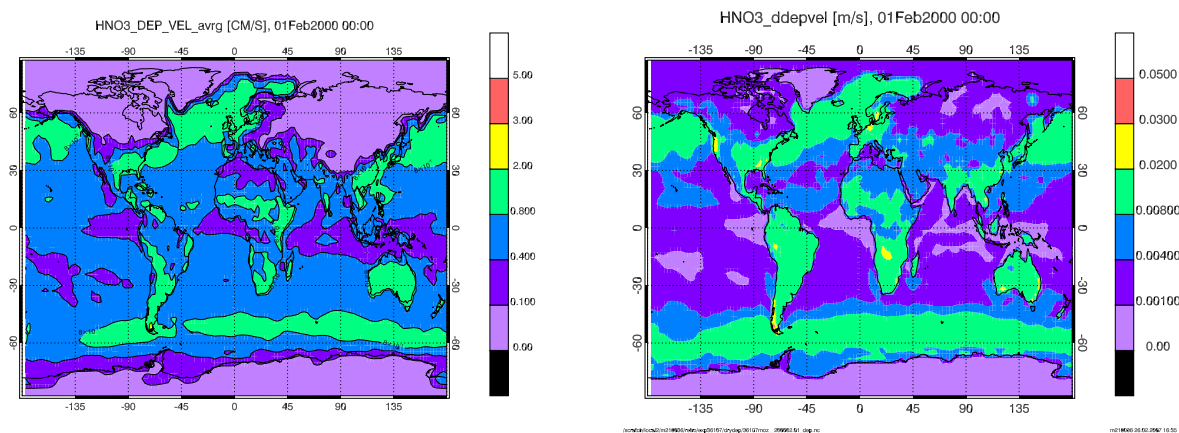


Figure 2.26: MOZART4 result for  $\text{HNO}_3$  dry deposition velocity [cm/s] (left panel). MOZECH result for  $\text{HNO}_3$  dry deposition velocity [m/s] (right panel) Monthly average for January 2000.

model has lower atmospheric concentrations of CO compared with other models it may be that the dry deposition for this species is somewhat too high. However, the spatial patterns are reasonably similar in both models MOZART4 and MOZECH.

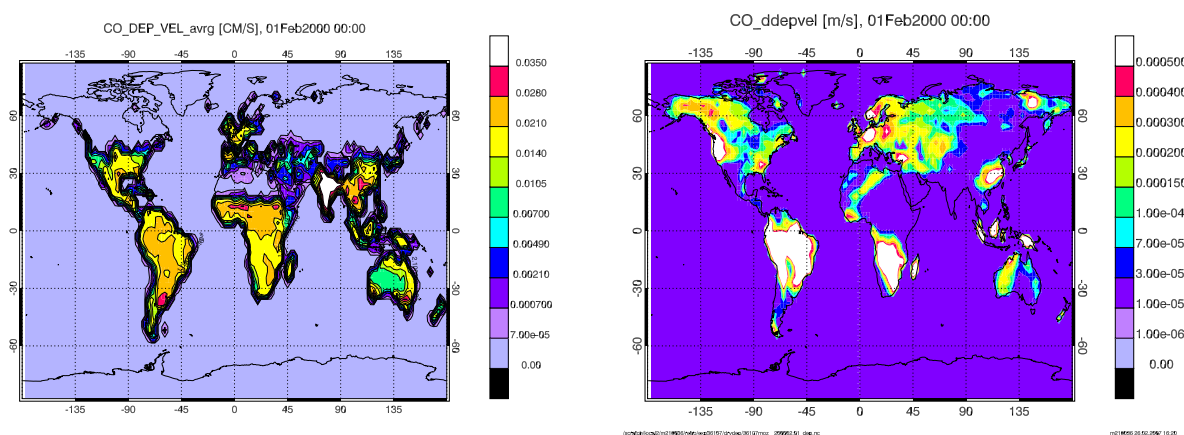


Figure 2.27: MOZART4 result for CO dry deposition velocity [cm/s] (left panel). MOZECH result for CO dry deposition velocity [m/s] (right panel). Monthly average for January 2000.

**The halogen species:** HBr, HCl, HOBr and HOCl deposition velocities from MOZART4 are shown in Figure 2.28. When the values of the figures are compared with the values used by Yang *et al.*, 2006 (table 2.8) the values seem to be generally similar, except in regions with ice/snow cover. In table 2.10 we present mean dry deposition velocities from MOZART4. We note that also the deserts show low  $v_d$  when compared with Yang *et al.*, 2006. It seems that the dry deposition velocities calculated in MOZART4 for snow, ice, and desert are very small when compared with other available sources. The same is true for HOBr and HOCl. Even if wet deposition is a stronger sink for halogens, the polar regions play such a fundamental role in halogen tropospheric chemistry so that it may be important not to have a deviation of the order of  $10^2$  as is the ratio between the model results and the values used by Yang *et*

*al.*, 2006.

According to Xin Yang, the reasoning for the determination of the dry deposition velocity values on ice and snow is the following: *"The basic rule we used is assuming the dry deposition on snow/ice is half of the value over water, like  $\text{HNO}_3/\text{H}_2\text{O}_2/\text{HNO}_4$  etc used in our model. Since for  $\text{HBr}$  0.5cm/s is given over ocean, so 0.2cm/s over ice is obtained."* Over the ocean and land, Yang *et al.*[138] they took the values from Sander and Crutzen, 1996 [106].

The parameterization used in MOZART4 takes the higher surface resistance into account when the temperature decreases. We do not know if halogen species may be an exception to this rule, as it is suggested for  $\text{H}_2\text{O}_2$  in Wesely, 1989 [136]. They report that for the resistance to uptake on leafs and ground, lower temperatures are expected to increase it, but he remarks that this effect that holds for  $\text{HNO}_3$  and  $\text{NO}_2$ , may have exceptions, like for  $\text{H}_2\text{O}_2$ . In our particular case, there is no evidence (theoretical or experimental) to change our values, therefore we are going to use the values derived by the model.

Deserts are a small fraction of land, where halogen concentrations are insignificant. Therefore, underestimation over deserts is probably not important. Regarding  $\text{HOBr}$  and  $\text{HOCl}$  the forest does not imprint a "signature" on the results.

Another striking feature in the results is the similarity between the plots for  $v_d(\text{HBr})$  and  $v_d(\text{HCl})$ , but the apparent differences over the ocean between  $v_d(\text{HOBr})$  and  $v_d(\text{HOCl})$ . From the parameters included in the model (table 2.9) it is not clear why this should be the case.

Table 2.10: Average dry deposition velocities of  $\text{HBr}$  and  $\text{HOBr}$  (cm/s) resulting from MOZART4

	Land <sup>13</sup>	Desert	Oceans	Sea ice
$\text{HBr}$	0.5	0.01	0.3	0.008
$\text{HOBr}$	0.1	0.002	0.2	0.005

### 2.4.3 Conclusions

The differences in the dry deposition velocity between the rare literature sources and the results may lead to inaccuracies and uncertainties especially in the polar regions. These uncertainties limit the validity of our conclusions since tropospheric chemistry for halogens is particularly important in these regions. In addition, there may be deposition and subsequent desorption under certain meteorological conditions that are not taken into account.

In other regions of the globe wet deposition plays a much more important role, so that the inaccuracies in the dry deposition do not play an important role.

## 2.5 Wet Deposition of Halogens

Wet deposition is the scavenging of gaseous species by condensed water in the atmosphere with the eventual deposition on the Earth's surface. This process is difficult to parameterize due to its dependence on multiple and composite processes (chemical reactions, dissolution, evaporation, etc.). Furthermore, it involves different physical phases (gas, aqueous, solid), and is influenced by phenomena on a wide range of physical scales (from the microscale to

<sup>13</sup>Includes all the grid points that are not ocean.

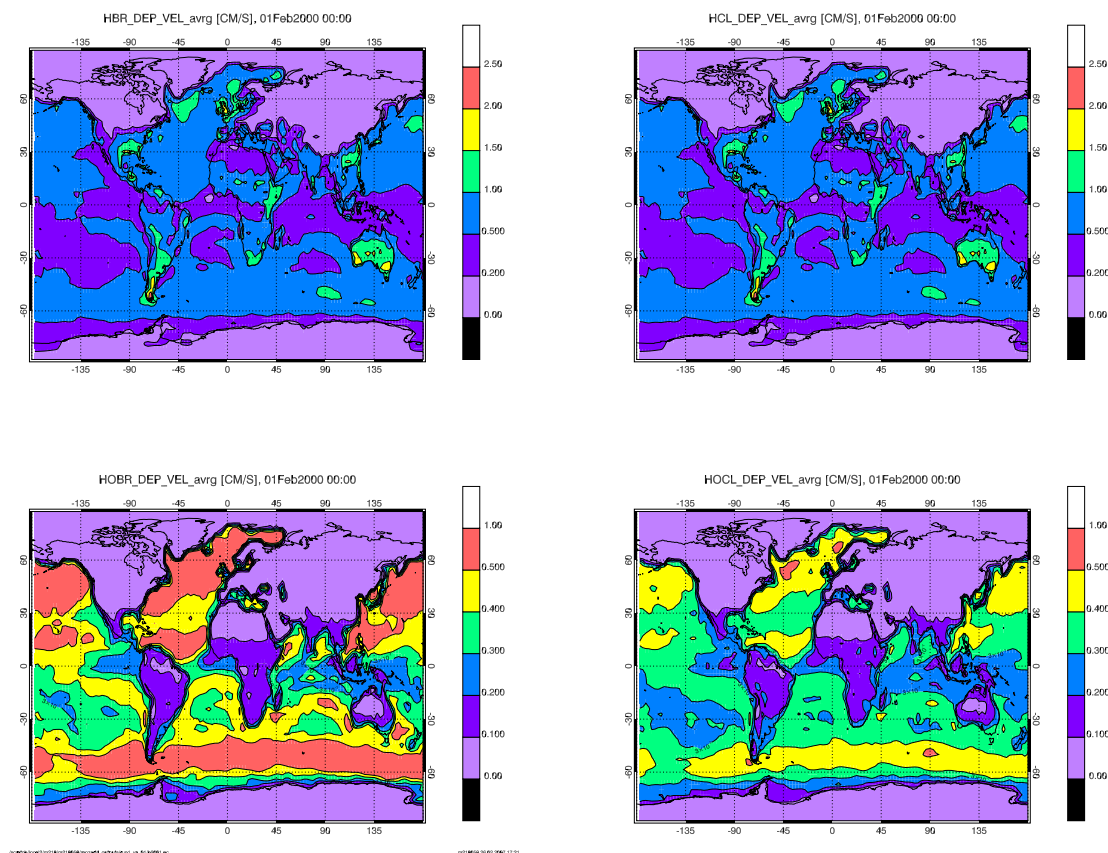


Figure 2.28: MOZART4 result for the dry deposition [cm/s] of (from the top left clockwise): HBr, HCl, HOBr, and HOCl. Monthly average for January 2000.

the macroscale). We define "wet deposition processes" as the scavenging by cloudwater, rain, snow, ice crystals, sleet, hail, etc.

Wet deposition is effective inside a cloud and in the precipitation below it. In MOZART4, the scavenging only happens in rainy clouds and it is irreversible. For very soluble species both processes take place, while the less soluble species are only involved in below-cloud scavenging.

The solubility of gases is described by Henry's law coefficient that is defined as:

$$k_H = \frac{C_{eq}^{(l)}}{p^{(g)}} \quad (2.68)$$

where  $C_{eq}^{(l)}$  is the concentration of a species in the aqueous phase and  $p^{(g)}$  is the partial pressure of that species in the gas phase.

After the dissolution in water, some species dissociate into ions, a reversible reaction that reaches equilibrium rapidly. In this case, we can define a second Henry's law coefficient incorporating the dissociation process, called Effective Henry coefficient (already discussed in

section 2.4). The Effective Henry coefficient ( $k_H^*$ ) always exceeds the Henry's law coefficient, which means that the total amount that dissolves is higher than predicted by  $k_H$ .

It is important to note that  $k_H$  refers to gases which physically dissolve, but do not undergo a chemical reaction. So, it includes solvation, but does not include hydration or hydrolysis. Hydrolysis is effective for the species  $\text{BrONO}_2$  and  $\text{ClONO}_2$ , which have a very high uptake coefficient. These species are very efficiently dissolved in water. However, it cannot be considered that the uptake is a wet deposition process as described by the Henry law coefficient.

The species  $\text{HBr}$ ,  $\text{HOBr}$ ,  $\text{HCl}$ , and  $\text{HOCl}$  are inorganic acids or polar molecules which are therefore soluble in water. Consequently, we have to account for the wet deposition of these species in our model.

### 2.5.1 Below-cloud scavenging in MOZART4

Inside a cloud, rain drops are formed. During this process interactions between the drops and aerosols and the drops and trace gases take place. In order to estimate the amount of the gas that is removed from the atmosphere by diffusion into a drop, it is necessary to take the physico-chemical properties of the gaseous species, the rain drop size and its descending velocity into account. The scheme used in this study considers solubilisation as an irreversible process.

To calculate the rate at which chemical compounds are scavenged, the strategy in MOZART4 is to count at each level how much water passes through and how much of the substance the water removes from the gas phase. The computation starts at the top of the highest cloud and descends to the surface.

In more detail, let  $n_{eq}^{(l)}$  be the number of molecules going into the water phase so that an equilibrium with the gas phase is reached:

$$n_{eq}^{(l)} = n_{bs}^{(g)} - n_{eq}^{(g)} \quad (2.69)$$

Here,  $n_{bs}^{(g)}$  is the number of molecules in the gas phase before scavenging (bs), and  $n_{eq}^{(g)}$  is the number of molecules in the gas phase that are in equilibrium with the water phase. Dividing by the total number of molecules in the gas phase we have:

$$x_{eq}^{(g \rightarrow l)} = x_{bs}^{(g)} - x_{eq}^{(g)} \quad (2.70)$$

$x_{eq}^{(g \rightarrow l)}$  is the volume mixing ratio (x) in the gas phase that would potentially be transferred from the gas phase to the water phase, provided that equilibrium is reached and that the water phase is not yet "contaminated" with the gas phase species. For our parameterization, we determine  $x_{eq}^{(g \rightarrow l)}$ .

According to the ideal gas law, we have

$$p^{(g)} V^{(g)} = n_{eq}^{(g)} RT \quad (2.71)$$

$p^{(g)}$  is the pressure of the gas phase,  $V^{(g)}$  is the volume of the gas phase,  $R$  is the molar gas constant, and  $T$  is the temperature of the gas phase medium. Substituting this into equation (2.69), we obtain

$$n_{eq}^{(l)} = n_{bs}^{(g)} - \frac{p^{(g)}V^{(g)}}{RT} \quad (2.72)$$

From equation (2.68), we know that

$$\begin{aligned} p^{(g)} &= \frac{C_{eq}^{(l)}}{k_H^*} \\ &= \frac{n_{eq}^{(l)}}{k_H^* V^{(l)}} \end{aligned} \quad (2.73)$$

Considering (2.72) and (2.73), we find

$$n_{eq}^{(l)} = n_{bs}^{(g)} - \frac{n_{eq}^{(l)}V^{(g)}}{k_H^* RTV^{(l)}}$$

With  $\chi = \frac{V^{(l)}}{V^{(g)}}$ :

$$\begin{aligned} n_{eq}^{(l)} &= \frac{n_{bs}^{(g)}}{1 + \frac{1}{k_H^* RT\chi}} \\ &= \frac{n_{bs}^{(g)}}{\chi + \frac{1}{k_H^* RT}} \chi \end{aligned} \quad (2.74)$$

Dividing both sides by the total number of molecules in the gas phase:

$$x_{eq}^{(g \rightarrow l)} = \frac{x_{bs}^{(g)}}{\chi + \frac{1}{k_H^* RT}} \chi \quad (2.75)$$

In table 2.11, we put the correspondence between the symbols used in the present document and the one used in the model-code.

Table 2.11: Correspondence between the symbology in this report and the one in the model

Report	Units	MOZART4	Units
$x_{eq}^{(g \rightarrow l)}$	mol (i) <sup>14</sup> /mol (air)	<code>xeqca</code>	mol (i)/mol (air)
$x_{bs}^{(g)}$	mol (i)/mol (air)	<code>xgas</code>	mol (i)/mol (air)
$x_{eq}^{(l)}$	mol (i)/mol (air)	<code>xca</code>	(mol (i)/mol (air))(cm <sup>3</sup> (H <sub>2</sub> O))
$\chi$	m <sup>3</sup> (H <sub>2</sub> O)/m <sup>3</sup> (air)	<code>xliq</code>	g (H <sub>2</sub> O)/m <sup>3</sup> (air)
$k_H^*$	M (i)/atm (air)	<code>xhen</code>	M (i)/atm (air)
R	J (i)/mol (i)/K (air)	<code>const0</code>	atm (air)/K (air)/cm <sup>3</sup> (i)
T	K (air)	<code>tfld</code>	K (air)
M	g (i)/mol (i)	<code>m<sub>H2O</sub></code>	g (i)/mol (i)

Let's now consider that the top of the highest cloud is level  $j$ . In the computation of the amount scavenged, we descend from  $j$  and check at each level if there is rain. Let the

<sup>14</sup> $i$  for chemical species

first level with rain be level  $j+n$ . We follow the rain generated in this level  $j+n$  down to the surface, and account for the amount of the species that remains after scavenging at each level  $j+m \geq j+n$ . Going down through the column, there may exist additional levels in which rain is generated, and then there are several scavenging computations at each level  $m$ . We count these different scavenging computations by an extra index  $r=0,1,2,\dots$ , and call it a "rain episode".  $r$  is closely linked to the level where the rain was generated ( $j+n$ ). Introducing the indices in equation (2.75), we have

$$x_{eq,j+m}^{(g \rightarrow l),r} = \frac{x_{bs,j+m}^{(g),r}}{\chi_{j+n} + \frac{1}{k_{H,j+m}^* R T_{j+m}}} \chi_{j+n} \quad (2.76)$$

At the first rain episode found in the column,  $r=0$ , and  $x_{bs,j+m}^{(g),0} = x_{initial,j+m}^{(g)}$ . The latter is the gas volume mixing ratio at the beginning of the time step.

The gas concentration in the aqueous phase is calculated using an expression similar to equation 20.20 from Seinfeld and Pandis [112]:

$$x_{eq,j+m}^{(l),r} = \text{geo\_fac} \times \text{xkgm} \times \frac{x_{bs,j+m}^{(g),r-1}}{x_{rm} \times x_{um}} \times \Delta z_{j+m} \times \chi_{j+n} \quad (2.77)$$

$\text{geo\_fac}$  is the droplet geometry factor. The droplet geometry factor is:

$$\text{geo\_fac} = \frac{A_{surf} \times d}{V} \quad (2.78)$$

$A_{surf}$ ,  $d$ , and  $V$  are the surface area, the diameter, and the volume of the rain drop, respectively.  $\Delta z$  is the height of the level  $j+m$ .

$\text{xkgm}$  is the mass flux onto the rain drop, and is calculated by an empirical equation (according to a communication from Horowitz):

$$\text{xkgm} = \frac{\text{xdg}}{\text{xrm}} \times 2. + \frac{\text{xdg}}{\text{xrm}} \times 0.6 \times \sqrt{\frac{\text{xrm} \times \text{xum}}{\text{xvv}}} \times \sqrt[3]{\frac{\text{xvv}}{\text{xdg}}} \quad (2.79)$$

In MOZART4, the information regarding the droplet characteristics are mean quantities that are maintained constant during the simulation. Their values are given in table 2.12. Nevertheless, we should keep in mind that according to Seinfeld and Pandis [112]: *The simplification of an average droplet diameter can easily lead to significant errors.* In general, it is important to consider the number of droplets and the size of the droplets.

Table 2.12: Constant values in the wet deposition parameterization in MOZART4

$\text{xrm}$	mean diameter of rain drop	0.189	cm
$\text{xum}$	mean rain drop terminal velocity	748.	cm/s
$\text{xvv}$	kinetic viscosity of water	0.0618	cm <sup>2</sup> /s
$\text{xdg}$	mass transport coefficient	0.112	cm/s
$\text{geo\_fac}$	droplet geometry factor	6.	-
$\text{xkgm}$	mass flux onto the rain drop	15.1	cm/s <sup>(15)</sup>

We also follow the content of the droplet in its downward path. In each rain episode  $\mathbf{r}$  and level  $\mathbf{m} \geq \mathbf{n}$ , the amount of species is accumulated in the drop:

$$\sum_{i=j}^m x_{eq,i}^{(l),r} \quad (2.80)$$

In this way,

$$x_{bs,j+m}^{(g),r} = \begin{cases} x_{eq,j+m}^{(g),r} - x_{eq,j+m}^{(l),r} & \text{if } x_{eq,j+m}^{(g),r} > \sum_{i=j}^m x_{eq,i}^{(l),r} \\ 0 & \text{otherwise} \end{cases} \quad (2.81)$$

This means that the scavenging only takes place if the droplet is not saturated with the chemical species, according to its solubility properties.

Summing up all rain episodes at each level  $\mathbf{j+m}$ , we have  $x_{final,j+m}^{(g)}$  that will be:

$$0 \leq x_{final,j+m}^{(g)} \leq x_{initial,j+m}^{(g)} \quad (2.82)$$

For each level and grid box, the maximum time it will take for the gas species to be totally scavenged from the atmosphere with respect to wet deposition is given by

$$\tau_{j+m} = \frac{x_{initial,j+m}^{(g)}}{x_{initial,j+m}^{(g)} - x_{final,j+m}^{(g)}} \times xdtm \quad (2.83)$$

$xdtm$  is the descend travelling time of the rain drop in the grid ( $\Delta z$ ), calculated through the multiplication of the height of the grid and the mean rain drop terminal velocity ( $xum$ ).

Finally, the rate of removal of a gaseous species by wet deposition is defined by

$$k_{w,j+m} = \frac{1}{\tau_{j+m}} \times stay_{j+n} \quad (2.84)$$

where  $stay$  is the fraction of the distance between the cloud and the surface that is traversed by the falling drop in the timestep. This expression provides a way to calculate the water column scavenging without having to actually follow the droplets.

### 2.5.2 In-cloud scavenging in MOZART4

In this case the amount of water in the cloud is taken into account in the calculation of the wet deposition rate:

$$k_w = \frac{\mathbf{rain}}{M \times \left( \chi + \frac{1}{k_H^* \times R \times T} \right)} \times \mathbf{satcoeff} \quad (2.85)$$

The variable  $\mathbf{rain}$  expresses the conversion rate of water vapor into rain water (molecules/cm<sup>3</sup>/s);  $M$  is the molecular weight of water (g/mol); and  $\mathbf{satcoeff}$  is the saturation factor in clouds, defined empirically for the species HNO<sub>3</sub> (0.016), H<sub>2</sub>O<sub>2</sub> (0.016),

<sup>15</sup>The units of the mass flux onto the rain drop should be cm/s. The units on the right and left handside of equation (2.79) are not equal because the equation is empirical.

and CH<sub>2</sub>O (0.1)(Horowitz personal communication). These factors are used also for other chemical species.

This expression is similar to the one deduced by Giorgi and Chameides [41], however they have below-cloud scavenging in mind, and the variable `rain` in their formula does not express the water content, but the water that was removed.

### 2.5.3 Simulations performed to test the reliability of the wet deposition rates for halogen species

Three simulations were performed:

1. Simulation 1 - We attribute the volume mixing ratio of HNO<sub>3</sub>, a very soluble species, to the halogen species. HNO<sub>3</sub> has higher wet deposition rates in the tropics and below and in-cloud scavenging is included in the computation.
2. Simulation 2 - We attribute to the halogen species the volume mixing ratio of a less soluble species, CH<sub>3</sub>OOH, which only includes in-cloud scavenging, the higher wet deposition rates being in the polar regions.
3. Simulation 3 - In the third experiment, the volume mixing ratio of all halogen species is equal to  $1. \times 10^{-14}$ , but we apply the original specific wet deposition.

The parameters for the wet deposition of HNO<sub>3</sub> and CH<sub>3</sub>OOH are defined in table 2.13:

1. the Henry coefficients at standard conditions are denoted by  $k_H^\ominus$ ;
2. the temperature dependence of  $k_H$  are denoted by  $\frac{-d \ln k_H}{d(1/T)}$ ;
3. the dissociation equilibrium constant at standard conditions is denoted by  $k^\ominus$
4. the temperature dependence of k is denoted by  $\frac{-d \ln k}{d(1/T)}$

Table 2.13: Parameters for the computation of gas uptake by rain water

	$k_H^\ominus$ <sup>16</sup> [ <i>M.atm</i> <sup>-1</sup> ]	$\frac{-d \ln k_H}{d(1/T)}$ <sup>16</sup> [K]	$k^\ominus$ <sup>17</sup> [ <i>M</i> <sup>1-n</sup> /s <sup>18</sup> ]	$\frac{-d \ln k}{d(1/T)}$ <sup>17</sup> [K]
Established species used in this report as reference				
HNO <sub>3</sub>	$2.1 \times 10^{+5}$	8700.	$1.54 \times 10^{+1}$	0.
CH <sub>3</sub> OOH	$2.27 \times 10^{+2}$	5610.	-	-
Species added				
HBr	0.72	6100.	$1.0 \times 10^{+9}$	0.
HOBr	1900.	0.	$2.1 \times 10^{-9}$	0.
HCl	19.	9000.	$1.7 \times 10^{+6}$	6896.
HOCl	930.	0.	$3.2 \times 10^{-8}$	0.

<sup>16</sup>Sander, 1999 [104]

<sup>17</sup>Sander and Crutzen, 1996 [106]

<sup>18</sup>n is the chemical reaction order

We assume that the wet deposition rates for  $\text{HNO}_3$  and  $\text{CH}_3\text{OOH}$  are correct, and we analyse wet deposition rates of the halogen species on the basis of this assumption. Moreover, all species were introduced in the below and in-cloud scavenging, even the ones with low effective Henry coefficients (HOBr and HOCl). For the calculation of  $k_H^*$  the parameters in table 2.13 were used.

#### 2.5.4 Analysis of the wet deposition simulation results

Wet deposition was added in MOZART4 in the treatment of HBr, HOBr, HCl and HOCl (in-cloud (rainy clouds) and below-cloud wet deposition).

The new wet deposition rates of the halogenated species are first compared with those already established: nitric acid ( $\text{HNO}_3$ ), a very soluble species, and  $\text{CH}_3\text{OOH}$ , a moderately soluble one.

$\text{HNO}_3$  is one of the most water-soluble atmospheric gases. This is due to a high Henry constant and concomitantly high dissociation constant in water, which results in a very high Effective Henry coefficient (Figure 2.29, black curve). This means that  $\text{HNO}_3$  dissolves readily in clouds in the form of nitrate ions:



The highest  $\text{HNO}_3$  wet deposition rates ( $\geq 5 \times 10^{-5} \text{ s}^{-1}$ ) are located in the tropics (Figure 2.30), which can be attributed to the high convective precipitation in these regions (Figure 2.31, left panel). However, there are apparently more variables that influence the wet deposition rate. The indirect connection between deposition and precipitation becomes clear from the observation. These observations show that the maximum for  $\text{HNO}_3$  wet deposition rates (Figure 2.30), for example over the Indonesian islands or over the Pacific Ocean are not at all related to local maxima for the precipitation or even the cloud water content (Figures 2.31 and 2.32). In certain cases, the opposite can be observed, e.g. maxima in cloud water content over North Australia going along with relatively low wet deposition rates.

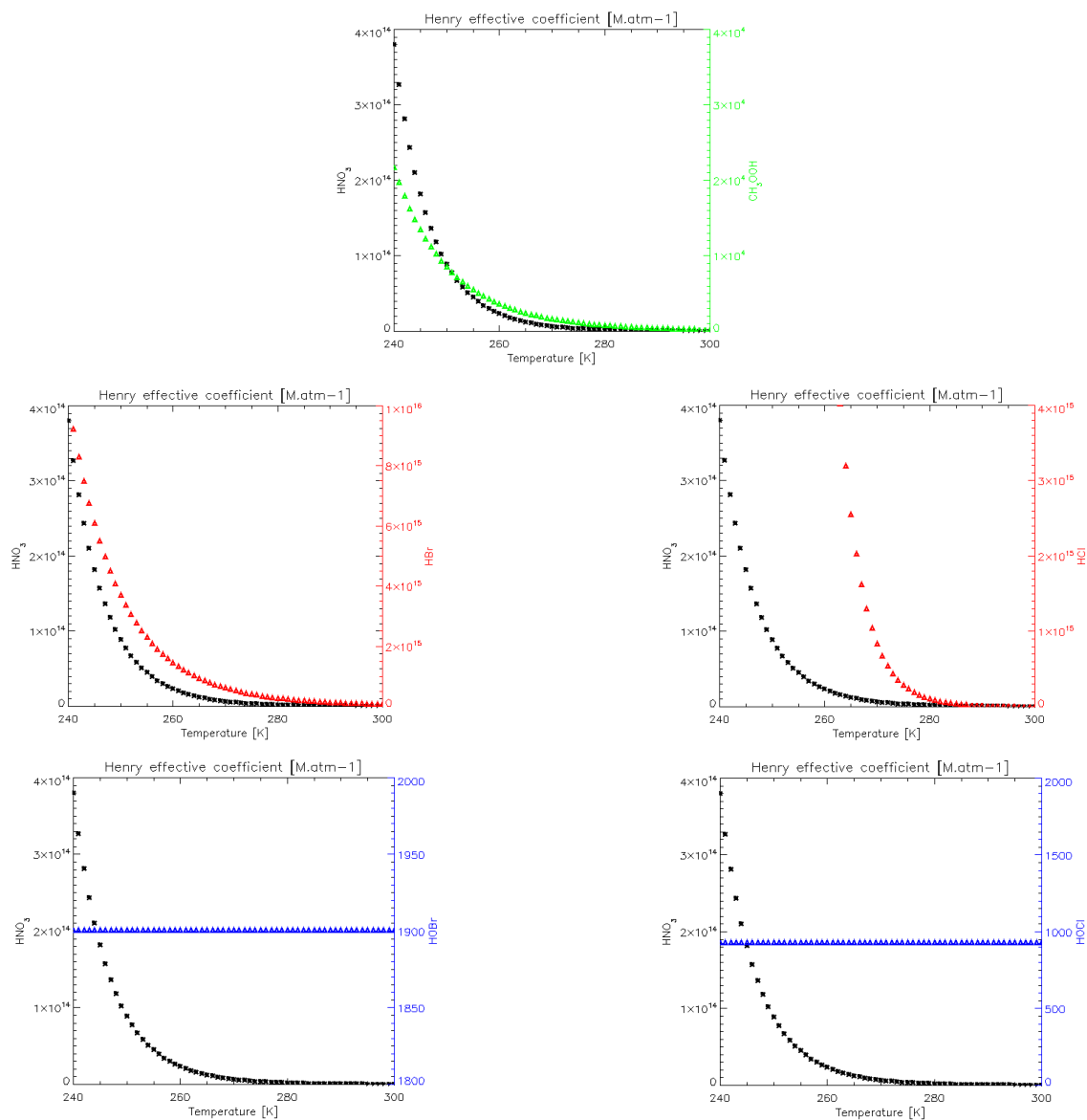


Figure 2.29: Henry Effective Coefficient ( $k_H^*$ ) for  $\text{HNO}_3$  (black) and other species ( $\text{CH}_3\text{COOH}$ , HBr, HOBr, HCl, and HOCl) considered in this report  $[\text{M}/\text{atm}]$ . Note different scales.

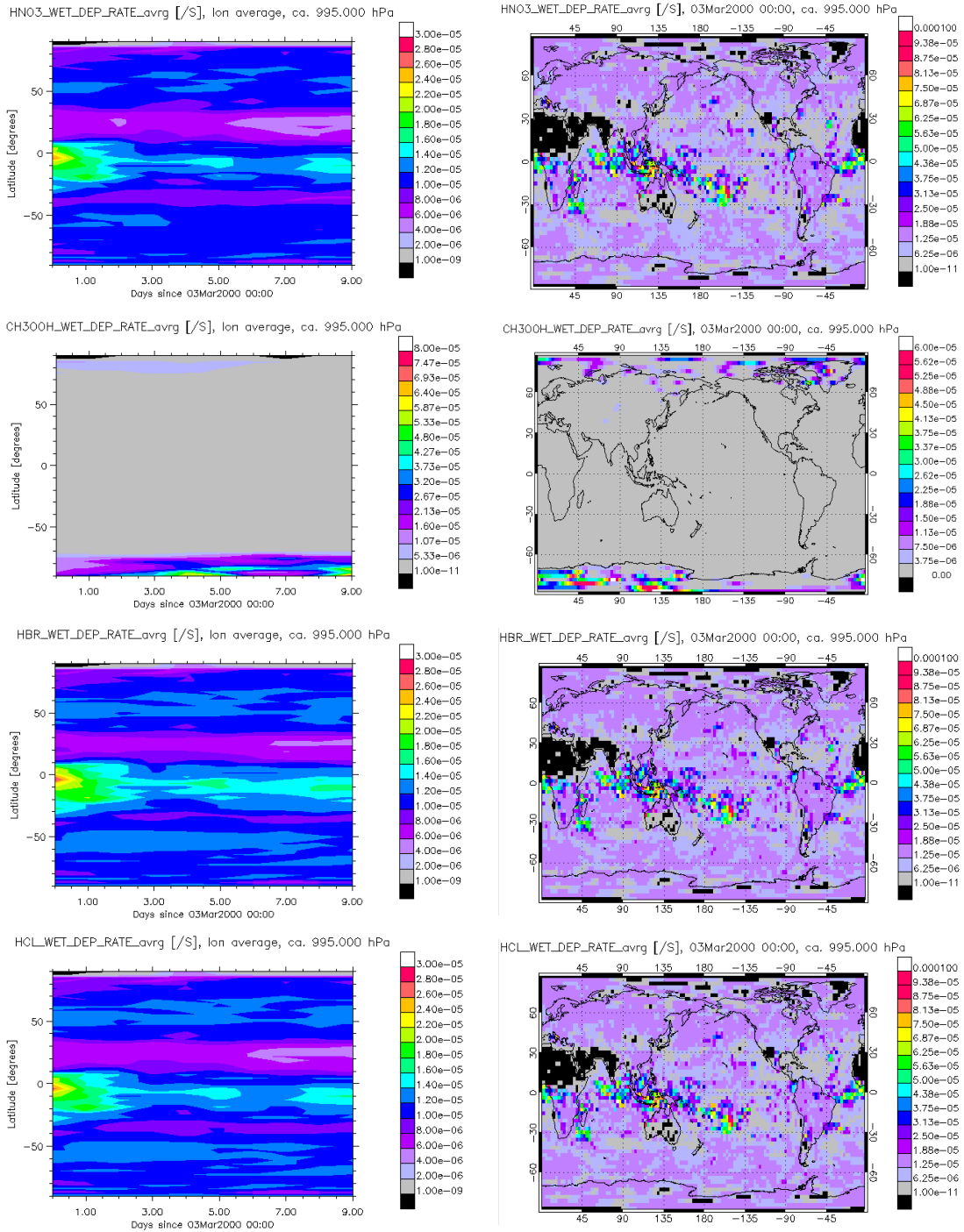


Figure 2.30: MOZART4 results for the wet deposition rates on the surface for  $\text{HNO}_3$ ,  $\text{CH}_3\text{OOH}$ ,  $\text{HBr}$ , and  $\text{HCl}$  [ $\text{s}^{-1}$ ]: time evolution of the longitudinal average from 3<sup>rd</sup> to 13<sup>th</sup> March 2000 (left side), and global distribution for  $\text{HCl}$  for the first day of the simulation (right side).

It would be important to know which kind of clouds or precipitation is active (for example: convective or stratiform systems) in a certain grid cell due to the connection of wet deposition

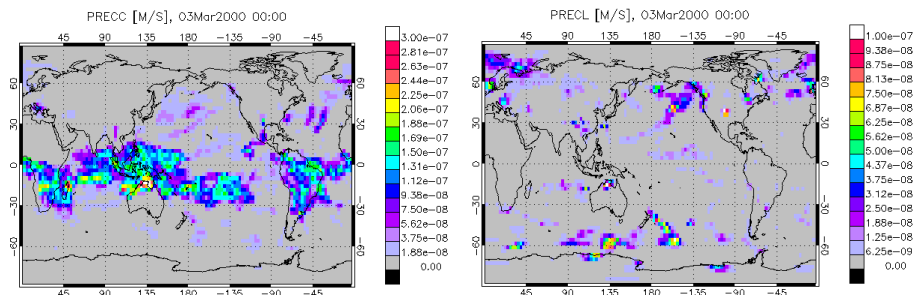


Figure 2.31: Diurnal average for the precipitation [m/s]: convective (left panel) and stratiform (right panel).

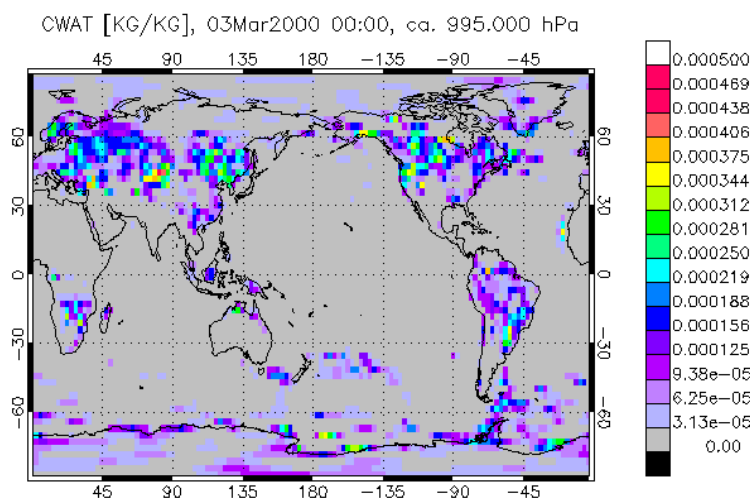


Figure 2.32: Global surface cloud water content distribution for the 3<sup>rd</sup> of March of 2000 [kg/kg] (diurnal average).

with the size and number distribution of the droplets. However, this information is not directly available in MOZART4. Generally, we observe that the wet deposition rates are higher at locations with convective rain (Figure 2.31). This can be explained by the high water content in tropical convective systems, with a very high rate of water condensation and rainfall.

The volume mixing ratio of a chemical species should determine to a large extent the wet removal rate. In the case of  $\text{HNO}_3$ , we notice that the locations with higher volume mixing ratios nevertheless have wet deposition rates in the lower range of the scale (Figure 2.33). Actually, when analysing the other gas species in this report, we realized that the volume mixing ratio has no visible influence on the wet deposition rate for species with high  $k_H^*$ . The volume mixing ratio has only importance as a tipping point, that works on the conditional statement that defines the calculation of  $x_{final,j+m}^{(g)}$  (equation (2.82)). This means that the levels of the volume mixing ratio are essential in defining  $x_{final,j+m}^{(g)}$  as zero or as a calculated value.

On the surface,  $\text{CH}_3\text{OOH}$  has its highest wet deposition rates in the polar regions, especially in the Southern Hemisphere (Figure 2.30). The highest volume mixing ratio for this species is in the tropical latitudes as shown in Figure 2.37, right panel. This anticorrela-

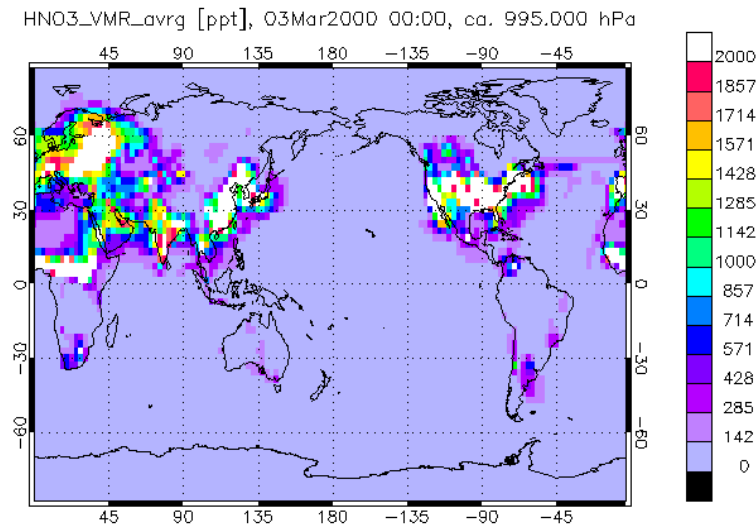


Figure 2.33: Volume mixing ratio for  $\text{HNO}_3$  at the surface on the 3<sup>rd</sup> of March 2000 [ppt] (diurnal average).

tion between wet deposition rates and volume mixing ratios could be related to its solubility.  $\text{CH}_3\text{OOH}$  is only lost by in-cloud scavenging, because it is considered to be not soluble enough to enter a falling droplet. In Figure 2.34, we show that the conversion rate of cloud water into rain water in the lowest model level is responsible for the  $\text{CH}_3\text{OOH}$  deposition. Keeping in mind that the solubility is higher at lower temperatures (confer Figure 2.35), we can understand the wet deposition rate distribution for  $\text{CH}_3\text{OOH}$  at the surface. In the tropics, for the 3<sup>rd</sup> of March, there are raining clouds between 8-16 km altitude, with correspondent wet deposition rates of  $\text{CH}_3\text{OOH}$  in the order of  $10^{-5} \text{ s}^{-1}$ .

$\text{HNO}_3$  has in-cloud and below-cloud deposition. The polar latitudes exhibit high values of scavenging in terms of absolute values, even if it is 5 times lower than in the tropics. So, we conclude that below-cloud scavenging is more efficient than in-cloud scavenging for soluble species.

HBr has a very high wet deposition rate (Figure 2.30). It is generally higher or equal to that of  $\text{HNO}_3$ , which we expect because the effective uptake is much higher for HBr than for  $\text{HNO}_3$ , as it can be seen from Figure 2.29. There are six grid boxes over desert areas that are an exception ( $k_w(\text{HNO}_3)$  is  $> 100\%$  higher than  $k_w(\text{HBr})$ ), as it can be seen in Figure 2.36. However, the wet deposition rates are very low at these locations.

The three experiments, in which the HBr volume mixing ratios are high - Figure 2.37 - ( $0.2$  to  $1.4 \times 10^4$  ppt in simulation 1 and  $18$  to  $1.6 \times 10^3$  ppt in simulation 2) and low ( $1. \times 10^{-14}$  ppt), and with different surface distributions, produce exactly the same wet deposition rate values of Figure 2.30. This shows that the gas phase concentration of HBr was not important for the determination of the wet deposition rate. This is due to the relation between concentrations in both phases, which are dependent on the air-water equilibrium.

For HCl, we obtain similar to HBr (Figure 2.30). The grid points at which the highest wet deposition rates are reached have almost the same wet deposition values as the corresponding grid points for HBr. For the other grid points the wet deposition rate of HCl is lower than that of HBr. This can be understood from the fact that HBr tends to have lower effective Henry constants than HCl in the temperature range of the troposphere (compare Figure 2.29 and

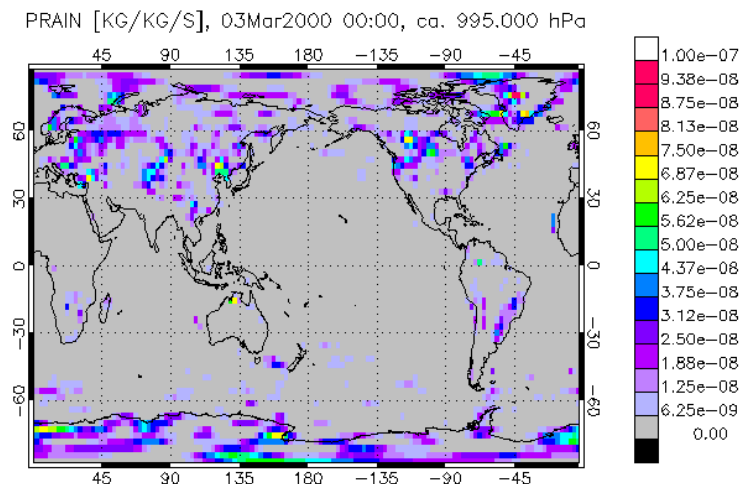


Figure 2.34: Global surface distribution of the rate of conversion of condensate to precipitation for the 3<sup>rd</sup> of March of 2000 [K] (diurnal average).

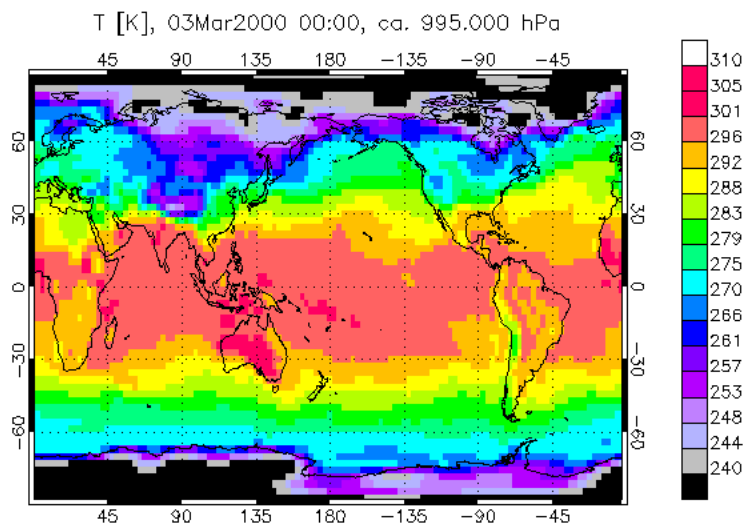


Figure 2.35: Global surface temperature distribution for the 3<sup>rd</sup> of March of 2000 [K] (diurnal average).

table 2.13). However, taking into account the steep slope below 275K for the  $k_H^*$  (Figure 2.29), we would expect higher wet deposition rates for HCl in the polar regions.

HOBr is a species with a relatively low solubility having an effective Henry coefficient of 1900 M/atm (Figure 2.29). Its wet deposition rate depends on the initial concentration prescribed in each simulation as it can be seen from Figure 2.38. Looking into simulation 3, where the volume mixing ratio is relatively constant throughout the atmosphere, and comparing the wet deposition rate with the cloud water content (Figure 2.32), we can see the correlation between the cloud water content and the deposition rate.

The results of simulation 1 show the highest wet deposition rates of all simulations. The maxima are located over the Indian Ocean and east of Indonesia. These local maxima in the deposition rate cannot be explained solely by the effect of the volume mixing ratios, but

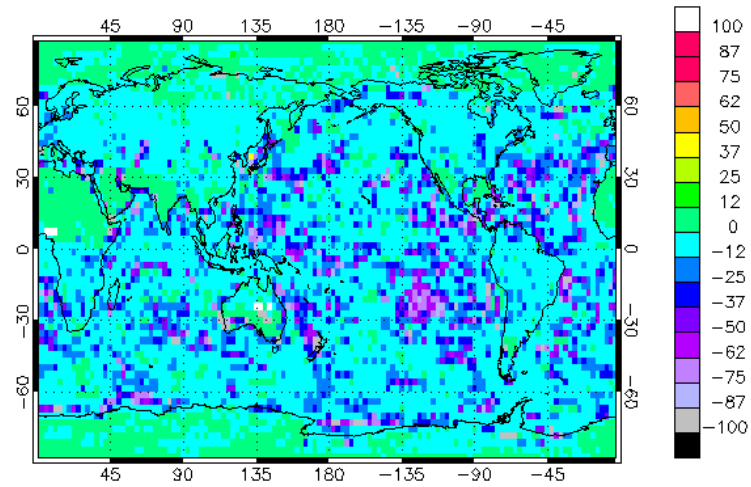


Figure 2.36: The difference in percent of the wet deposition rates of  $\text{HNO}_3$  and HBr.

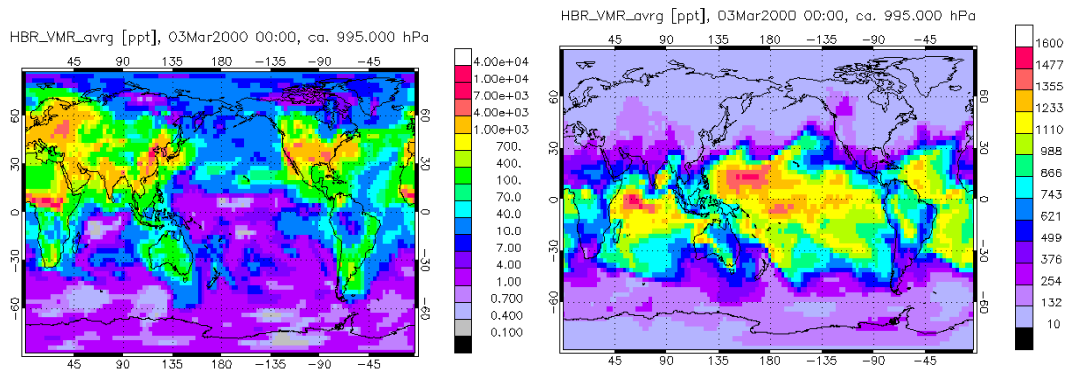


Figure 2.37: Diurnal average on the surface for the HBr volume mixing ratio [ppt] used in simulation 1 (equal to the volume mixing ratio of  $\text{HNO}_3$ ) - left panel - and simulation 2 (equal to the volume mixing ratio of  $\text{CH}_3\text{COOH}$ ) - right panel).

also by the solubility. In the case of a species with high solubility, saturation of the droplets is normally not reached and scavenging is effective along the column. This is true even in low altitudes in the case that high concentrations are found in higher levels. However, for species with low solubility as HOBr, the droplet may saturate during its path downwards. This can be observed in Figure 2.39 that presents a vertical section at the  $90^\circ$  meridian for simulation 1 and 2. E.g. around  $0^\circ$  latitude, the volume mixing ratio is low in simulation 1 while it is high in simulation 2. At this location, the wet deposition rate  $k_w$  is equal for both simulations above 900 hPa, but it is higher for simulation 1 below 900 hPa. This is a consequence of the droplets not being saturated below 900 hPa for simulation 1 due to the 1000 times lower volume mixing ratios at high altitudes in this simulation compared with simulation 2.

The lower wet deposition rates of HOCl compared to HOBr are a consequence of the lower effective Henry constant of HOCl. The effect of saturation is observable in both cases.

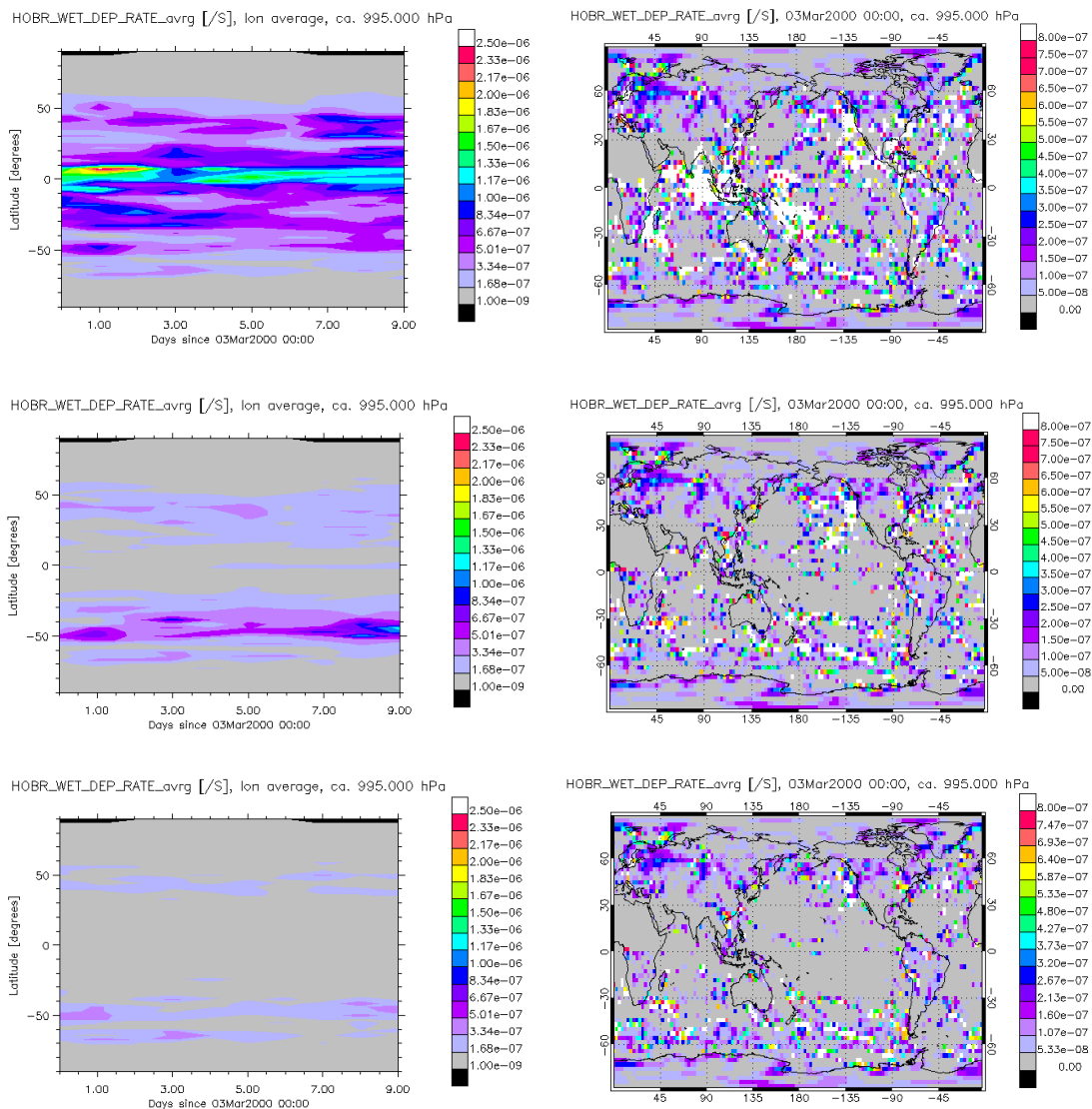


Figure 2.38: MOZART4 results for the wet deposition rates on the surface for HOBr in each of the experiments (simulation 1 at the top, simulation 2 middle row, and simulation 3 at the bottom): time evolution of the longitudinal average from 3<sup>rd</sup> to 13<sup>th</sup> March 2000 (left side), and global distribution for the first day of the simulation (right side).

### 2.5.5 Conclusion

For highly soluble species, we observed that below-cloud scavenging is more efficient than in-cloud scavenging. Therefore, the highest wet deposition rates are observed at the locations where convective precipitation is present. For species of low solubility, water content and in-cloud scavenging are dominant. Moreover, the volume mixing ratio has an observable effect in the wet deposition rate  $k_w$  results for species with low solubility, while for highly soluble species the volume mixing ratios tested ( $0.01$  to  $1. \times 10^4$  ppt) do not show an effect on  $k_w$ .

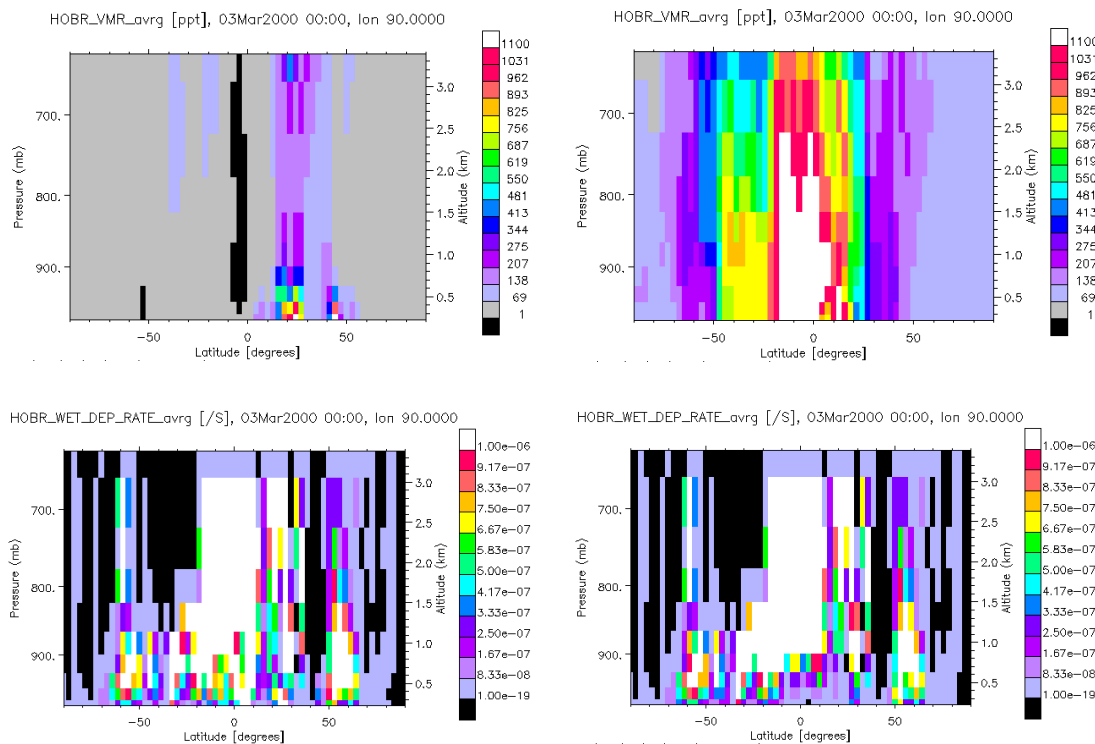


Figure 2.39: Diurnal averages of volume mixing ratios (up) and wet deposition rates (bottom) for HOBr in simulation 1 (left side) and 2 (right side), on the 3<sup>rd</sup> of March 2000, at meridian 90°.

This is explained by the saturation of water droplets in the case of low solubility.

Finally, we like to note that the dissociation of H<sub>2</sub>O<sub>2</sub> in water droplets is not taken into account in MOZART4. The value that is reported in Sander and Crutzen [106] for the dissociation equilibrium constant of H<sub>2</sub>O<sub>2</sub> at standard conditions is  $2.7 \times 10^7 \text{ s}^{-1}$ . This is a higher value than for the dissociation equilibrium constant of HNO<sub>3</sub>, which is included in the model and has a significant loss through washout.

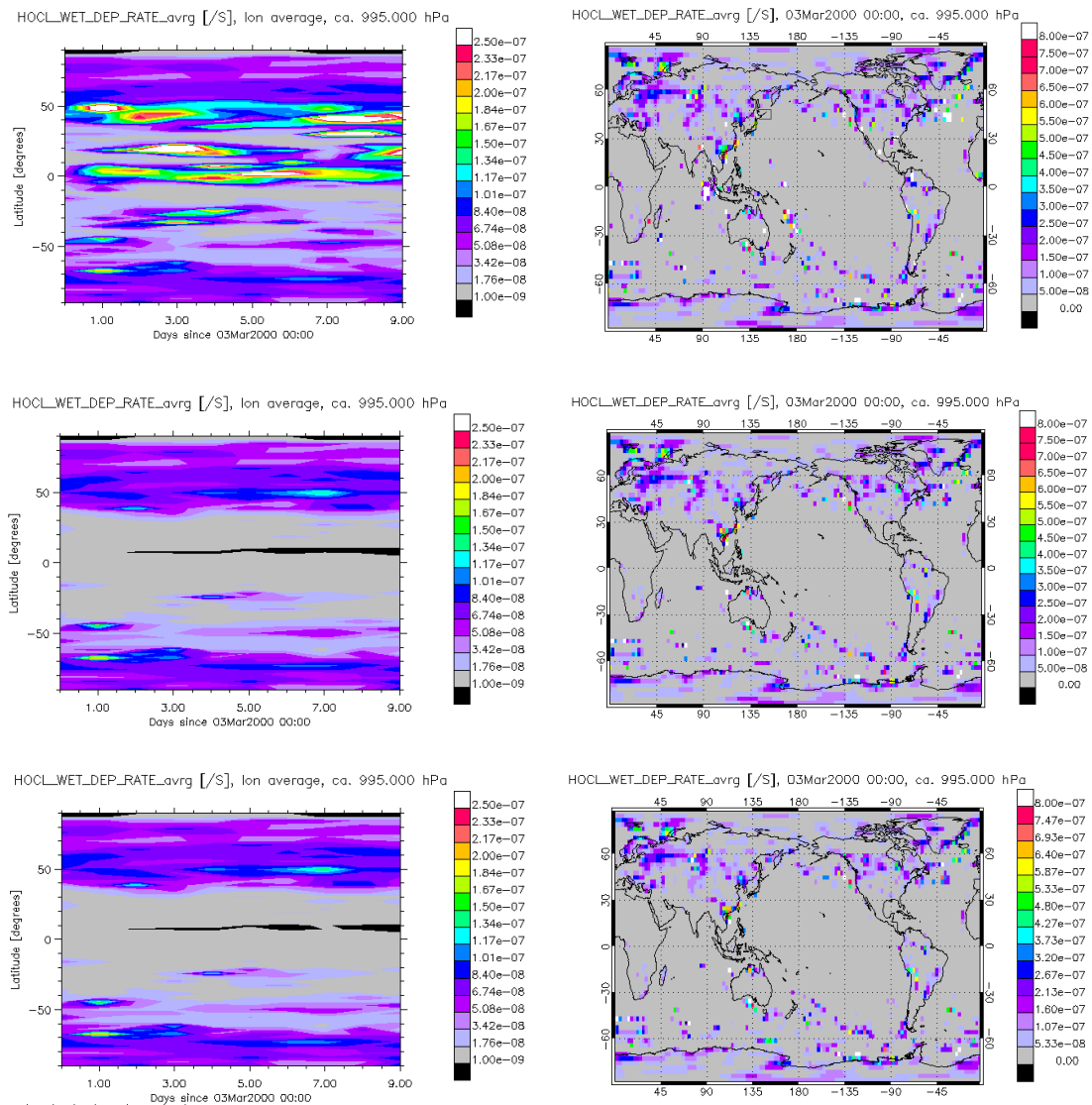


Figure 2.40: MOZART4 results for the wet deposition rates on the surface for HOCl in each of the experiments (simulation 1 at the top, simulation 2 middle row, and simulation 3 at the bottom): time evolution of the longitudinal average from 3<sup>rd</sup> to 13<sup>th</sup> March 2000 (left side), and global distribution for the first day of the simulation (right side).

## Chapter 3

# The Effect of Bromine on Tropospheric Chemistry

In this chapter, we assess the impact of bromine species on the tropospheric chemistry in two steps. First, we characterise and evaluate the atmospheric concentrations of bromine species from the model (especially BrO) using the available observations or other modelling experiments. Second, we analyse the impact of bromine species on O<sub>3</sub> and related species as OH, HO<sub>2</sub>, H<sub>2</sub>O<sub>2</sub>, NO<sub>x</sub>, CO, and others.

The measurements of bromine in the troposphere are mostly obtained from the detection of BrO, the product of the reaction between Br and O<sub>3</sub>. The most commonly used technique is the Differential Optical Absorption Spectroscopy (DOAS). This technique uses the absorption of radiation by molecules, typically using simultaneous intensity measurements at several wavelengths, which makes it a specific and versatile technique. It is possible to use the sun as a light source, and in this way, the method is used in remote sensing by satellites.

### 3.1 Simulations

We describe the seven main simulations which are summarised in table 3.1. The simulation *Base run* uses the standard MOZART4. All the other simulations include the same gas phase and photolysis reactions listed in appendix A. Furthermore, the bromine species are included into the dry deposition and wet deposition schemes, as described in chapter 2. In all the simulations, except the *base run*, the very-short lived halocarbon species–VSLs–(chapter 2.3) and CH<sub>3</sub>Br are taken into account. This last compound has a homogeneous tropospheric volume mixing ratio of 9 ppt.

Two reactions on sulphate are included (see appendix A) and described in subsection 2.2.4. The emission from sea salt over the open ocean is parameterised by a net bromine production through heterogeneous reactions. In subsection 2.2.5, we explain how the values for the total reactive uptake and yield were chosen from the published literature. For all simulations with bromine chemistry on sea salt, we used a total reactive uptake  $\Gamma$  of 0.02 for BrONO<sub>2</sub> and 0.1 for HOBr. For simulations *SS1* and *SSIce* we used the yield of 0.9 for the production of Br<sub>2</sub> and of 0.1 for the production of BrCl. From an analysis of the results of the two last simulations mentioned, we conclude that the production of bromine adopted is too high in the Southern hemisphere. In addition, we conclude, based on the literature about the acidity of sea salt particles in the atmosphere, that our assumption that the acidifying agents in the

Table 3.1: Main experiments performed with MOZART4 for this study

Simulation	Description
<i>Base run</i>	the standard MOZART4, without bromine chemistry.
<i>G1</i>	Bromine chemistry, including the gas phase and photolysis reactions. Emissions from short-lived halocarbons.
<i>S1</i>	<i>G1</i> + heterogeneous chemistry on sulphate and other background particles.
<i>SS1</i>	<i>S1</i> + heterogeneous chemistry on sea salt over open ocean (no limitation of pH).
<i>SS1ice</i>	<i>SS1</i> + parameterised emissions from sea ice in the polar regions (proxy for all sea salt sources in those regions including frost flowers).
<i>SS2ice</i>	<i>SS1ice</i> + heterogeneous reactions on sea salt over open ocean with pH limitation.
<i>SS3ice</i>	<i>SS2ice</i> + heterogeneous reaction rates on sea ice $100 \times$ higher than in <i>SS2ice</i> .

atmosphere exist in sufficient quantities all over the globe may be incorrect. Consequently, we decided to perform experiment *SS2ice*, in which we choose the yield obtained in the experiment of Fickert and co-workers for newly formed sea salt particles [33] (see Figure 2.8 in subsection 2.2.5), which is 0.2 for  $\text{Br}_2$  and 0.8 for  $\text{BrCl}$  for both reactions of one molecule of  $\text{HOBr}$  or one molecule of  $\text{BrONO}_2$  reacting on a sea salt particle .

The results of simulation *SS1*, in which potential effects of the sea ice on the bromine cycle are ignored, showed that the distribution of  $\text{BrO}$  observed in satellite retrievals was not captured by the model. The emissions from the polar regions are therefore essential for a good global agreement of the  $\text{BrO}$  distribution with satellite retrievals, although the information from satellite retrievals is currently more qualitative than quantitative. For the parameterisation of the emissions from the sea ice, we use the fractional sea ice map  $f_{ice}$  of MOZART4. We introduce on the surface of the ice sheet two additional reactions similar to the ones occurring on sea salt over the open ocean:



The production of  $\text{Br}_2$  from sea ice is calculated by the equation:

$$\frac{dC_{\text{Br}_2}}{dt} = 2 \times (k_{max}^a \cdot C_{\text{BrONO}_2} + k_{max}^b \cdot C_{\text{HOBr}}) \times f_{ice} \quad (3.3)$$

where  $k_{max}^a$  and  $k_{max}^b$  are the maximum values obtained in simulation *SS1* for the reactions on sea salt over open ocean, which are  $4.0 \times 10^{-5} \text{s}^{-1}$  and  $2.5 \times 10^{-4} \text{s}^{-1}$ , respectively. Our objective is to estimate the maximum possible effect of emissions from sea ice. To this end, we assume that for each reactant molecule ( $\text{BrONO}_2$  or  $\text{HOBr}$  containing one  $\text{Br}$ ) the reaction product is  $\text{Br}_2$ .

The analysis of the *SS2ice* results show that this case does not represent a maximum scenario as intended. Thus, we performed an additional simulation *SS3ice* where  $k_{max}^a$  and  $k_{max}^b$  are chosen to be  $4.0 \times 10^{-3} \text{s}^{-1}$  and  $2.5 \times 10^{-2} \text{s}^{-1}$ , respectively.

We note that in our discussions we focus on the simulations most relevant in the particular context. E.g., in simulations *S1* and *G1*, the volume mixing ratios of the bromine species are low and not relevant to compare with observations. However, as we will see, it is relevant to take them into consideration when discussing effects.

## 3.2 Bromine emissions from the simulations

We first derive the total annual emissions of bromine for the MOZART4 simulations from the various sources included in the model for the year 2000. The result is presented in Table 3.2. The emissions from the halocarbons are constant in all the simulations at 7.3 Gmol Br/yr. In simulation *G1*, in which the source of bromine in the model is provided only by halocarbons, the resulting tropospheric average of the volume mixing ratio of BrO is in the order of  $10^{-3}$  ppt (the same is true for simulation *S1*). This value is very low compared to the estimated global BrO concentration of 1-2 ppt derived from observations. Moreover, the maxima are found in the equatorial region, which is understandable as most of VLSL emissions are located there. However, the explanation of the observed BrO levels is left unanswered in terms of quantity and global distribution. Therefore, the addition of inorganic sources in the model is essential to study bromine in the troposphere.

Table 3.2: The global emissions obtained in MOZART4 simulations for the year 2000

Sources (Gmol Br/yr 2000)	<i>Base run</i>	<i>G1</i>	<i>S1</i>	<i>SS1</i>	<i>SS1ice</i>	<i>SS2ice</i>	<i>SS3ice</i>
Natural halocarbons + CH <sub>3</sub> Br	-	7.3	7.3	7.3	7.3	7.3	7.3
Sea salt over open ocean	-	-	-	5	8.4	1.3	2.6
Sea salt over sea ice	-	-	-	-	0.8	0.5	18

The emissions of bromine from sea salt vary between simulations. Between simulations *SS1* and *SS1ice* the emission from sea salt increases by 68%. This is due to the additional bromine source in *SS1ice*. The emission from sea ice is 0.8 Gmol Br/yr, which raises the atmospheric concentration of BrONO<sub>2</sub> and HOBr available to react on the sea salt particles over the open ocean. When we introduce a pH limitation on the emission from sea salt particles in the Southern hemisphere, the emissions from sea salt over the open ocean diminish by 84% from simulation *SS1ice* to *SS2ice*. Correspondingly, the emissions from sea ice diminish by 38% as the feedback between Br in the gas phase and on sea salt is weakened. The impact of the change in the yield is extreme, and gives an impressive idea of the importance of the pH in the description of the chemical release of bromine from sea salt particles. The same is probably true for frost flowers, even if the process is somewhat different. Sander and colleagues give the following explanation on how the acidification of frost flowers may occur: they propose that there is a precipitation of calcium carbonate in freezing sea water, lowering the buffer capacity of the liquid and acidifying the solution [105]. Both processes involve intricate aqueous phase chemistry. Between simulations *SS2ice* and *SS3ice* the emissions from sea ice increase by a factor of 36 due to the increase of the heterogeneous reaction rates on this substrate by a factor of 100. The emissions from sea salt over open ocean concomitantly double.

### 3.3 Evaluation of BrO

**Satellite observations of BrO.** Satellite retrieval allows to track the vertical tropospheric column density (VTCD) of BrO globally along the year<sup>1</sup>. The comparison of the model results with GOME retrievals can not be achieved on a quantitative level, because of the uncertainties in the BrO VTCD in the troposphere (personal communication by Andreas Richter). These uncertainties arise, within other reasons, from a lack of the exact knowledge of the BrO concentration in the stratosphere and the albedo. More precisely, we have to take into account that three height regimes contribute to the BrO VTCD retrieved by the satellite: the BrO concentration profile in: 1) the stratosphere; 2) the free troposphere; and 3) the boundary layer. All three regimes contribute with different weights to the measurements. Over dark surfaces (open water) the satellite is more sensitive to BrO at location 1) and 2). In these regions the atmospheric BrO is overestimated and, consequently, the satellite retrievals are poor tools to evaluate BrO emitted through heterogeneous reactions on sea salt over the open ocean. This is due to the fact that the satellite is less sensitive to boundary layer BrO over water. Over bright surfaces (ice), the sensitivity is higher for surface BrO and this one is therefore overestimated. Moreover, clouds have to be carefully monitored, as they block retrievals below the clouds and enhance the satellite sensitivity above them due to their brightness. For example, in the Northern hemispheric winter (Figure 3.1), it is possible to detect enhancements over inland areas of Russia and Europe. This is probably due to changes in sensitivity to BrO in the free troposphere in the presence of snow/ice or low clouds.

The observed annual cycle of the BrO distribution over the globe shows a strong seasonal cycle at the poles. During polar spring the chemical activation gives rise to VTCD of  $> 6 \times 10^{13}$  molecules/cm<sup>2</sup>. From February to May high column densities are retrieved at the North Pole, and similarly over the South Pole during September-December. This is due to the unique one-day/one-night light regime and to the fact that BrO chemistry is driven by sunlight.

**Vertical Tropospheric Column Densities (VTCD) of BrO.** In Figures 3.2, 3.3, 3.4, and 3.5 we show the BrO VTCD obtained from MOZART4 simulations *SS1*, *SS1ice*, *SS2ice*, and *SS3ice*, respectively. In the North Polar region, the model results exhibit the minimum VTCD during polar night, also in the simulation that does not incorporate emissions from sea ice (*SS1*), showing that this seasonality depends mainly on the sunlight driven chemistry. The results from simulation *SS1* are characterised by a belt of high BrO VTCD located around 58°S. This belt forms during the Southern hemispheric winter months, because of high sea salt emissions and concentrations in the boundary layer due to heavy storms. The consequent release of bromine into the atmosphere is very high since more bromine in the atmosphere can activate more bromine from the sea salt particles. Due to the circumpolar pattern of the winds, there is no region where this feedback may break down. Some of the BrO is even transported into regions where there is polar night. Nonetheless, we still observe a strong gradient in the BrO VTCD results at the transition from day to polar night.

Although we do not observe high BrO VTCD in the Northern hemisphere in simulation *SS1*, the bromine production rates from sea salt in the Northern hemisphere are similar to the production rates in the Southern hemispheric regions where the same quantity of sea salt

---

<sup>1</sup>Satellites GOME and SCHIAMACHY products that can be visualised at <http://www.oma.be/BIRA-IASB/Molecules/BrO/level3.php> or <http://www.iup.uni-bremen.de/doas/gome.htm>. Last accessed April 24, 2008.

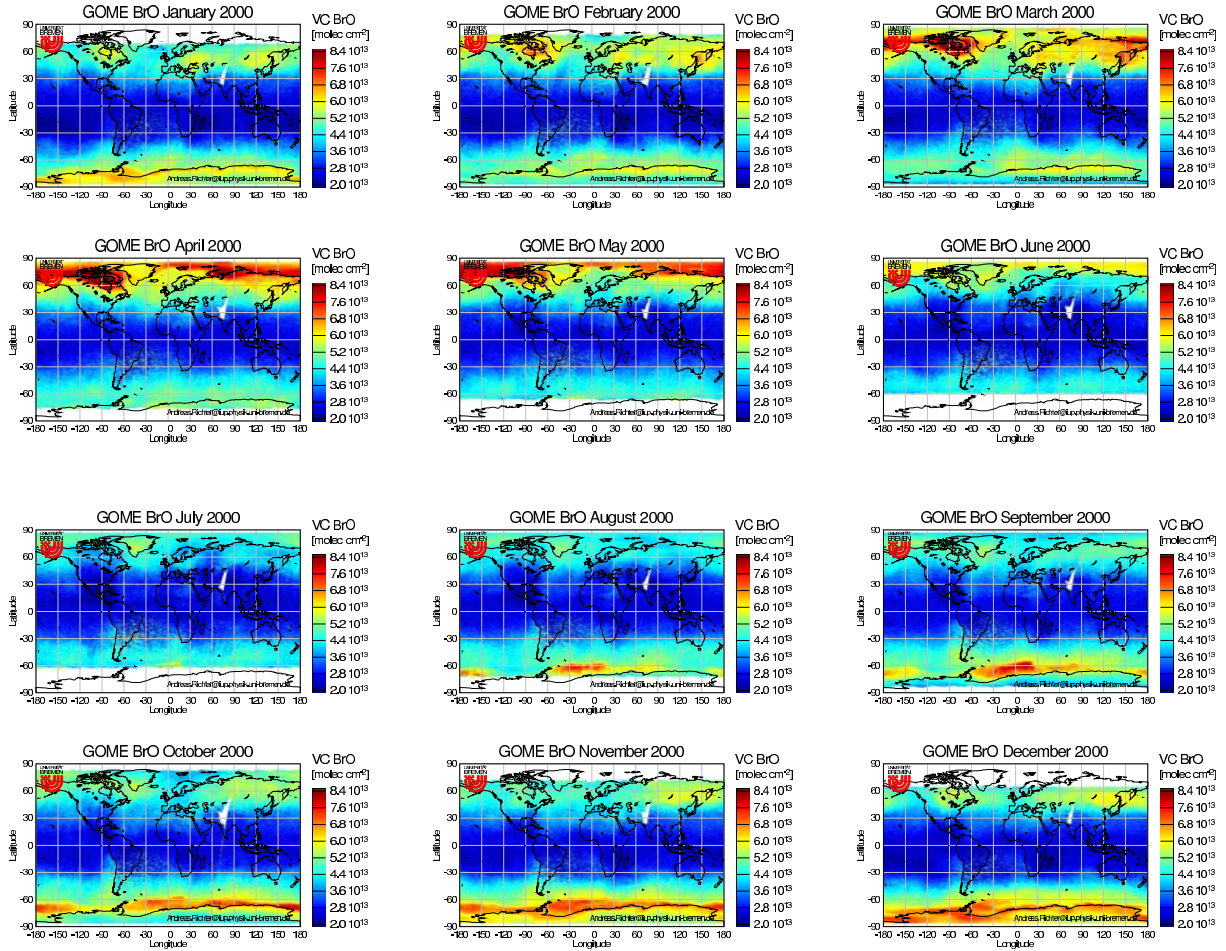


Figure 3.1: BrO vertical column density [molecules/cm<sup>2</sup>] retrieved by GOME.

is available, as it can be concluded comparing Figures 3.6 and 3.7. In Figure 3.6 we show the atmospheric surface density of sea salt particles in MOZART4 for four months of the year 2000, and in Figure 3.7 we show the bromine production rates from sea salt for the model surface level and for the same months. The similar production rates in both hemispheres do not result in similar levels of atmospheric BrO in the boundary layer (Figure 3.8) or tropospheric column densities (Figure 3.2). The calculated BrO VTCD for SS1 in the Northern hemisphere are 10 to 100 times lower compared with the results in the Southern hemispheric regions .

In order to corroborate the similarity of chemical processes in the Northern and Southern hemispheres, we chose two regions with similar sea salt surface area densities in each hemisphere for March and compared variables that are linked to the BrO VTCD, between these two regions. In Figure 3.9 we show the surface area density (SAD) of sea salt for the region in the Northern hemisphere (grid points between 32<sup>0</sup>-46<sup>0</sup>N and 156<sup>0</sup>E-176<sup>0</sup>E) as black symbols and the region in the Southern hemisphere (grids between 46<sup>0</sup>-60<sup>0</sup>S and 156<sup>0</sup>W-176<sup>0</sup>W) as red symbols, for March, June, September, and December 2000. Each symbol in the plots represents a value of a model grid point. In March, the SAD values in these two regions are similar. In December, the grid points with highest SAD are located in the Northern

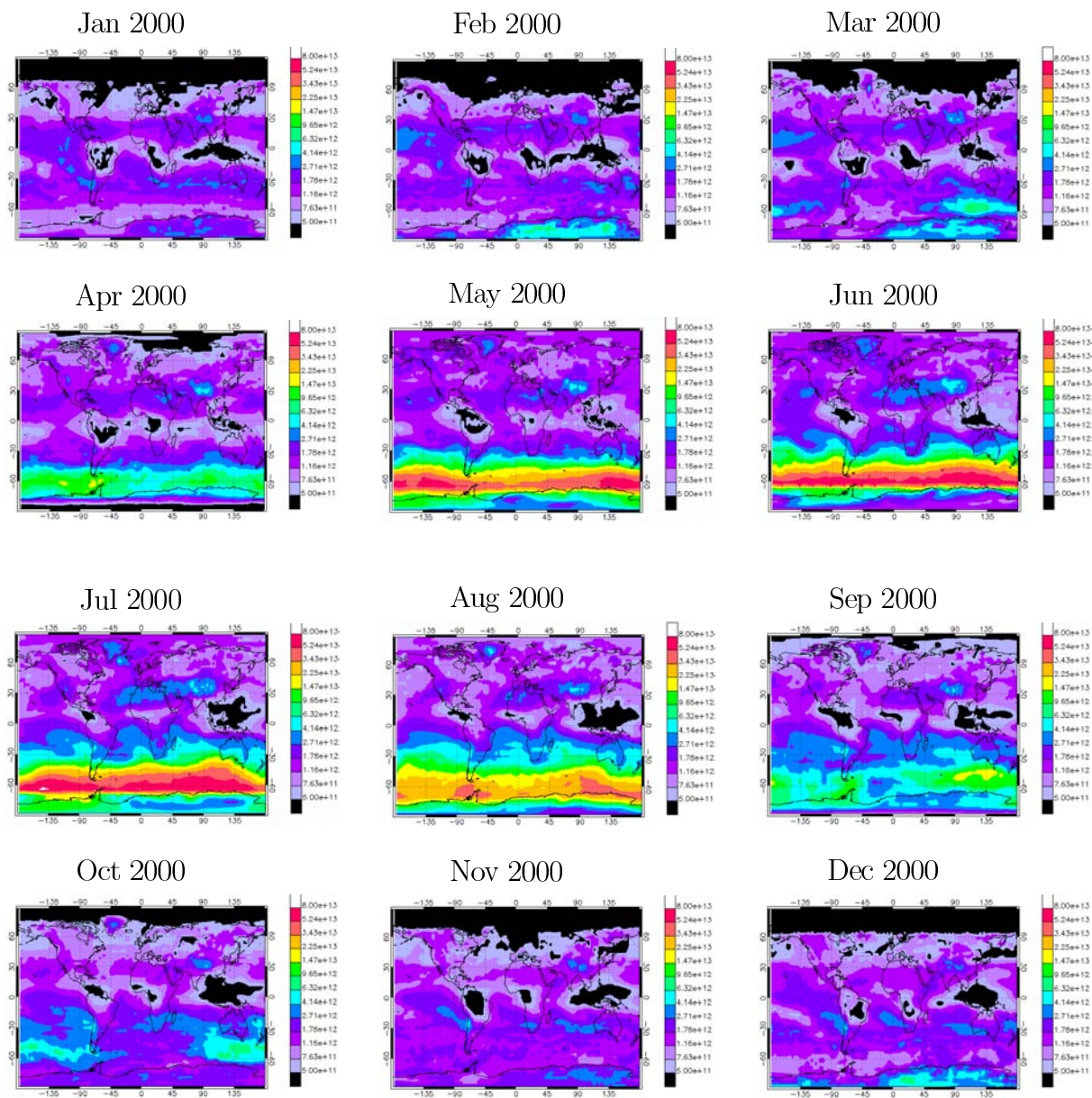


Figure 3.2: BrO vertical column density [molecules/cm<sup>2</sup>] in the troposphere from the MOZART4 simulation *SS1*. Monthly averages of daily instantaneous results at 10h30 local time.

hemisphere, and in June and September it is the opposite, the differences being in the order of a factor 2 to 3. The difference in SAD is related to the 10 m wind speed in the respective hemispheres.

Observing in Figure 3.10 the VMR of BrO for the same grid points, we observe that with the exception of December, the values in the Southern hemisphere are 10 to 100 times higher. The temperature values are very similar, and therefore also the heterogeneous reaction rates on both hemispheres are similar (see equation 2.22 in chapter 2.2). However, looking at the VMR of BrONO<sub>2</sub> and HOBr we can infer that the explanation for the differences lies in the

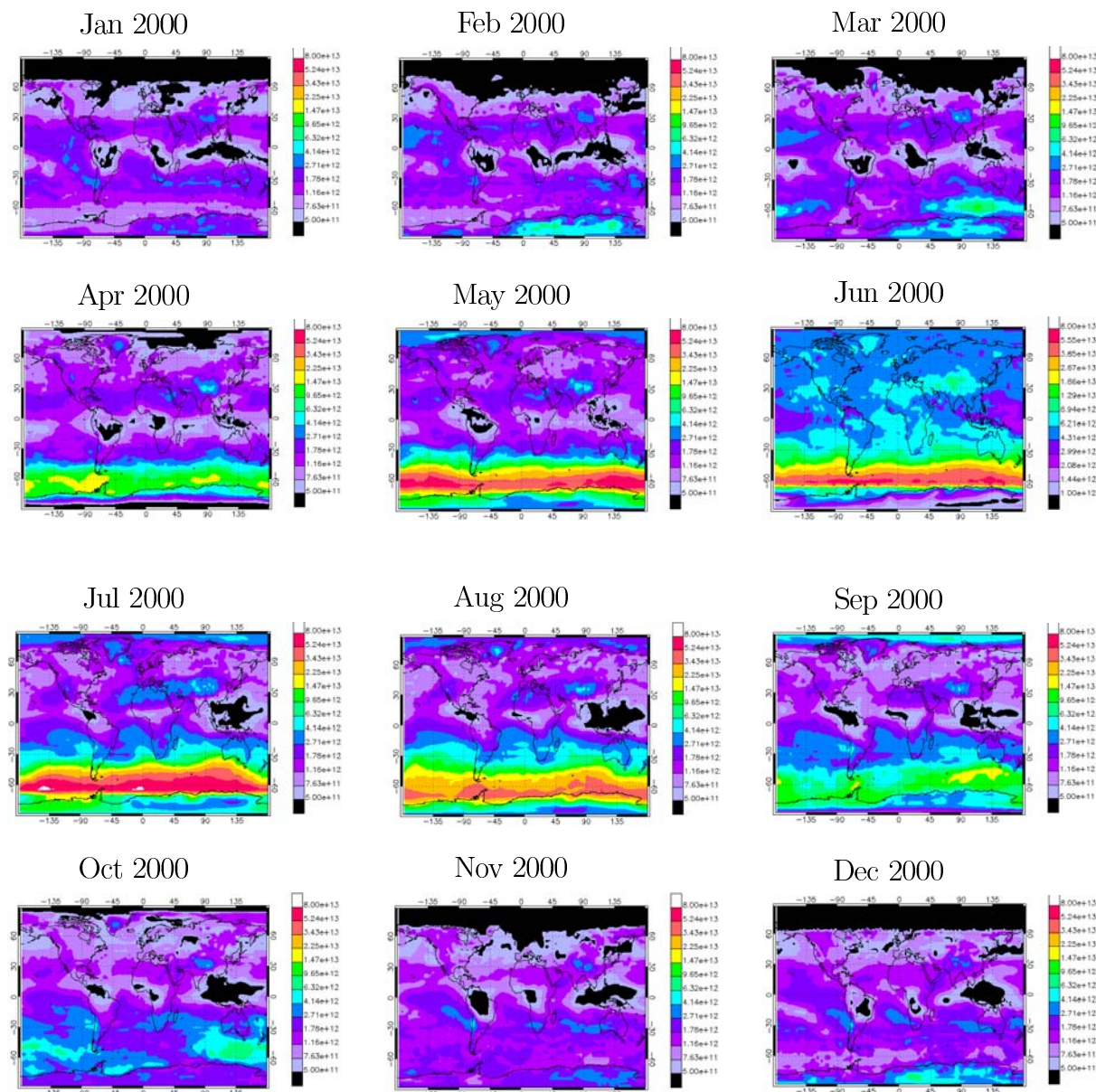


Figure 3.3: BrO vertical column density [ $\text{molecules}/\text{cm}^2$ ] in the troposphere from the MOZART4 simulation *SSlice*. Monthly averages of daily instantaneous results at 10h30 local time.

concentrations of the species involved in the reactions on sea salt. In Figures 3.11 and 3.12 we observe that the VMR of HOBr and BrONO<sub>2</sub> in the Southern hemisphere are 10 to 100 times higher in June and 10 times higher in September. We concluded that the differences in the BrO concentrations between hemispheres is due to lower atmospheric concentrations of the reactants involved in the heterogeneous chemistry in the Northern hemispheric region. The fewer BrONO<sub>2</sub> and HOBr are molecules available (as shown in Figures 3.11 and 3.12) the lower is the resulting volume mixing ratio of BrO (Figure 3.10), even if the available SAD is similar (Figure 3.9). In the Southern hemisphere, the dynamic conditions around 58°S trap the bromine molecules in this region and promote a strong chemical feedback that explains

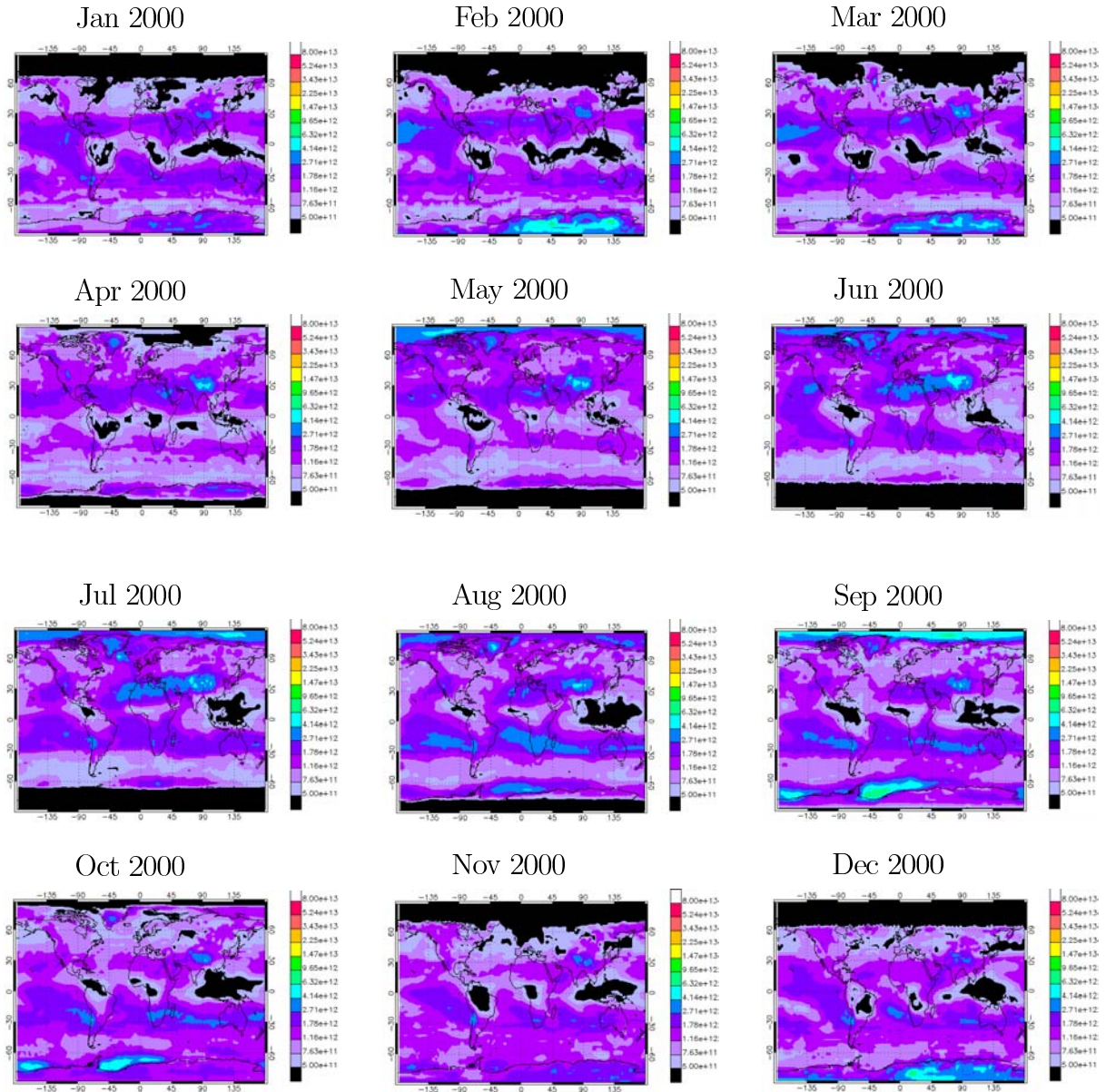


Figure 3.4: BrO vertical column density [molecules/cm<sup>2</sup>] in the troposphere from the MOZART4 simulation *SS2ice*. Monthly averages of daily instantaneous results at 10h30 local time.

such high VMR in the model results.

From the comparison of simulation *SS1* and GOME retrievals (Figure 3.1), we see that the main discrepancies between the model and the observations are: 1) the absence of emissions in the polar regions, which obviously are essential to explain the observations; 2) high BrO concentrations due to the sea salt belt around 58°S. GOME never observes such belt. High levels of BrO are always detected over or near areas with frozen salt water [132, 131]. Measurements on the ground corroborate this: BrO observations performed on board of a ship that travelled near the Antarctic coast in the winter of 2006 [130], show that enhanced concentrations of BrO are found in areas of young sea ice, but outside these areas BrO con-

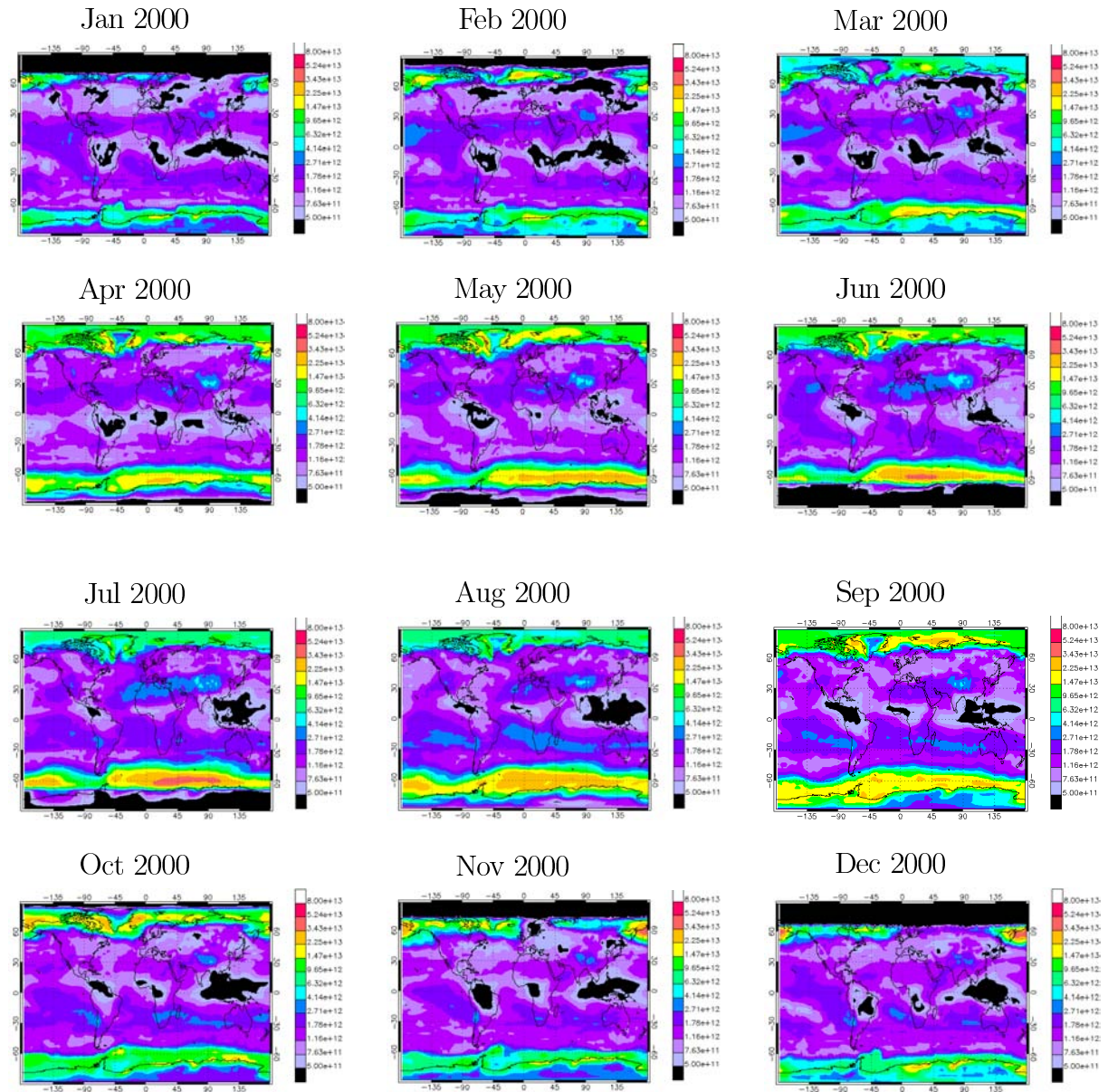


Figure 3.5: BrO vertical column density [molecules/cm<sup>2</sup>] in the troposphere from the MOZART4 simulation *SS3ice*. Monthly averages of daily instantaneous results at 10h30 local time.

centrations are below 3.7 ppt. Consequently, we suppose that the monthly mean VMR of more than 7 ppt BrO for simulations *SS1* and *SS1ice* for the months of May, June, and July, over the open ocean are not realistic.

**Seasonality in BrO VTCD.** Normally, the seasonal cycle in the Northern high latitudes exhibits high values detected by satellite in February until mid May. Our model results diverge in that the enhancement starts only in March. This discrepancy is due to the fact that we still have polar night in the model during February, even if in reality some light is already available triggering the photochemical reactions. Looking into the results of the simulations that include emissions from sea ice (*SS1ice*, *SS2ice* and *SS3ice*), we observe that high BrO

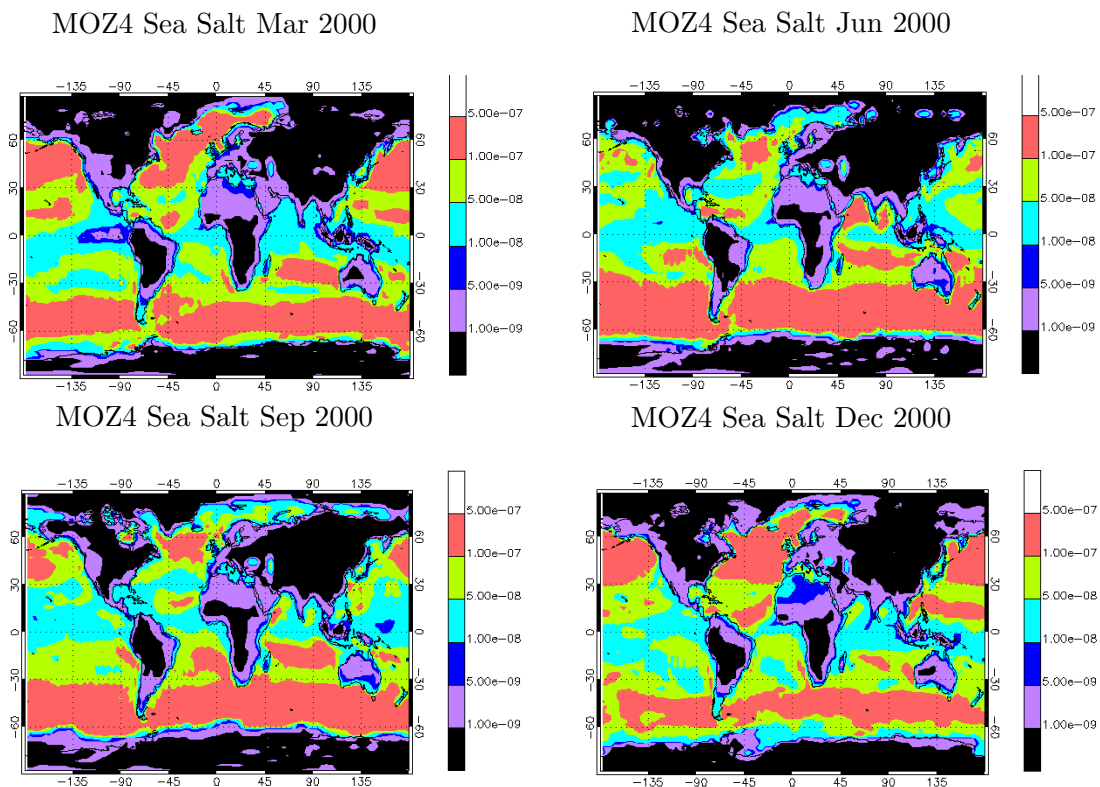


Figure 3.6: Surface area density of sea salt particles in MOZART4 [ $\text{cm}^2/\text{cm}^3$ ] in the simulation year 2000.

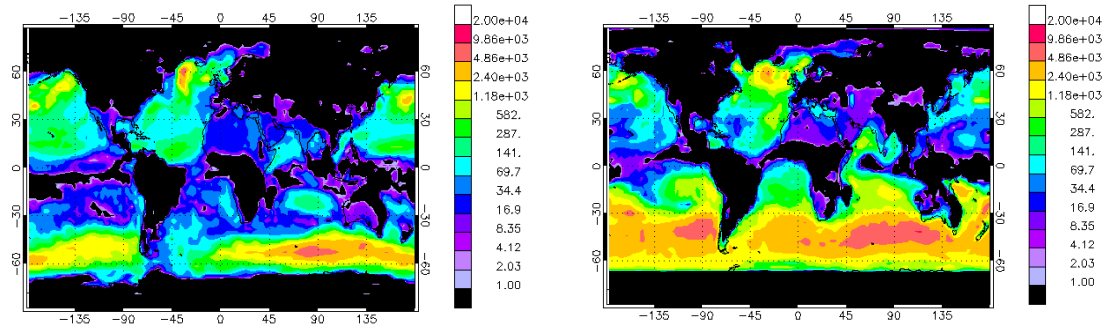
VTCD are observed also from July to September. This is mainly due to the sea ice cover in the model in the Arctic, which has a too large extension for the summer months<sup>2</sup>. This is even truer for the more recent years, as observations show a rapid decline in Arctic sea-ice extent, especially in the summer months [50].

For 1997, Richter and co-workers [99] describe BrO enhancements over the Hudson Bay from February to May. Similar events were also observed by the same working group for the year 2000 [100]. Our model can not reproduce such an increase in BrO as there is no sea ice cover at the Hudson Bay in the model.

In the Southern hemisphere, GOME observations show the BrO enhancement in the months from September to January. The emissions from sea ice we have in simulations *SS1ice* and *SS2ice* are too low to lead to the same pattern of BrO VTCD as in the satellite observations. In simulation *SS1ice*, bromine emissions from sea salt over open ocean are too large producing the highest values of BrO VTCD over the open ocean instead of the coastal regions. In simulation *SS2ice* the emissions from sea salt decreased, but emissions from sea ice are too low. This leads to simulated BrO VTCD which are about 10 times lower than the observed ones. Moreover, because the total emissions at the Antarctic coast are low compared to the emissions from sea salt over the open ocean in the simulation, the coastal

<sup>2</sup>Check internet site <http://arctic.atmos.uiuc.edu/cryosphere/>. Last accessed April 30, 2008.

Bromine production from Sea Salt Mar 2000 Bromine production from Sea Salt Jun 2000



Bromine production from Sea Salt Sep 2000 Bromine production from Sea Salt Dec 2000

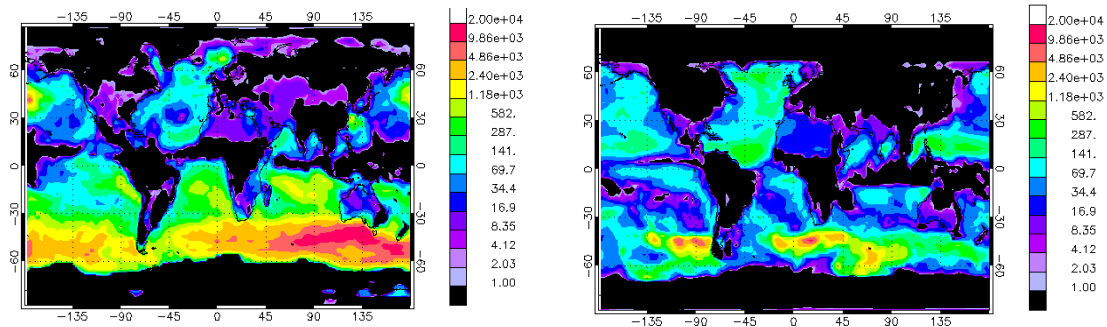


Figure 3.7: Bromine production from sea salt in MOZART4 simulations *SS1* [molecules/cm<sup>3</sup>/s] at the surface level. Monthly averages.

BrO levels are noticeably affected by the transport from the sea salt emissions of bromine farther in the North. This is obvious in simulation *SS1ice*, as the bromine emissions from sea salt over open ocean are not pH-limited and therefore are very high. In simulation *SS3ice* we increased the emissions from sea ice and obtain as a result the maximum BrO VTCD values over sea ice, as expected. However, the yearly maximum value is  $4.5 \times 10^{13}$  molecules/cm<sup>2</sup>, which is compared to GOME retrievals still low (simulation *SS3ice*). However, taking the uncertainty of the retrievals into account this is a fairly good agreement. The uncertainty in the retrievals can be demonstrated by the fact that two scientific groups obtain different values: The IASB-BIRA product provides higher BrO VTCD than the product of Bremen's group. Furthermore, positioning the tropopause in the model with 4 km difference corresponds to a difference of 20% in BrO VTCD at high latitudes. Therefore, we think that a quantitative comparison of absolute values is only possible with more ground-based measurements.

In Figure 3.13, we compare the simulated maxima at the Antarctic coast of simulations *SS2ice* and *SS3ice* to the sea ice cover in the months of September and October. In the same figure, we can compare the results of the simulations with GOME retrievals for the same months (last row). We observe that the sea ice map of MOZART4 allows a reasonable description of the BrO pattern around the Antarctic coast. Simulation *SS2ice* results are obviously too low compared to the observations; also the ratio between the VTCD values calculated within and out the region covered with sea ice are around 2. Wagner and co-

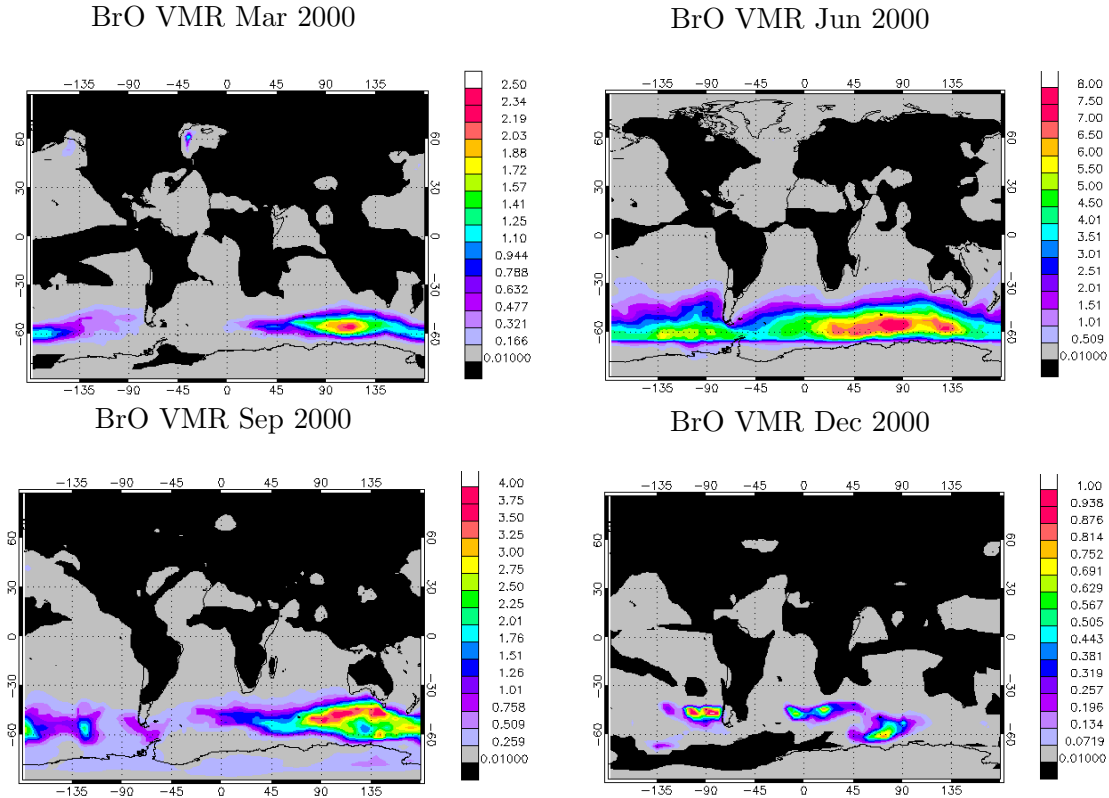


Figure 3.8: BrO volume mixing ratio [ppt] at MOZART4 surface level for simulation *SS1*. Monthly averages. Beware different scales.

workers [130] found a ratio in their measurements of 5. The results of simulation *SS3ice* are better, with maxima in the order of  $10^{13}$  molecules/cm<sup>2</sup>. The ratios between BrO column densities within and without the sea ice covered region are circa 4.

The observation of the simulations results (Figures 3.2, 3.3 and 3.4 shows that there is transport and accumulation over the Antarctic continent in February and December. This is corroborated by GOME observations (for example [100]).

**Comparison with ground-based measurements.** There are few ground-based measurements of BrO in the atmosphere. We discuss next the observations that can be compared with our simulation experiments.

Schofield *et al.*[110] retrieved tropospheric columns of BrO at Arrival Height, Antarctica ( $77.8^{\circ}\text{S}$ ,  $166.7^{\circ}\text{E}$ ) from 7 September to 27 October, 2002. Most of their retrievals form an approximately normal distribution about a mean of  $0.3 \pm 0.3 \times 10^{13}$  molecules/cm<sup>2</sup>. They measured higher values on the 21<sup>st</sup>, 24<sup>th</sup>, and 25<sup>th</sup> October. At these dates, the distribution was statistically different from the background days, with a mean tropospheric column of  $1.8 \pm 0.1 \times 10^{13}$  molecules/cm<sup>2</sup>. We obtain mean values of  $1.4 \times 10^{13}$  and  $1 \times 10^{13}$  molecules/cm<sup>2</sup> at this location, for September and October 2000 in simulation *SS3ice*. These values lie between both distributions found by Schofield *et al.*, that is, between the values characteristic of background days and the days with high-BrO columns. In simulation

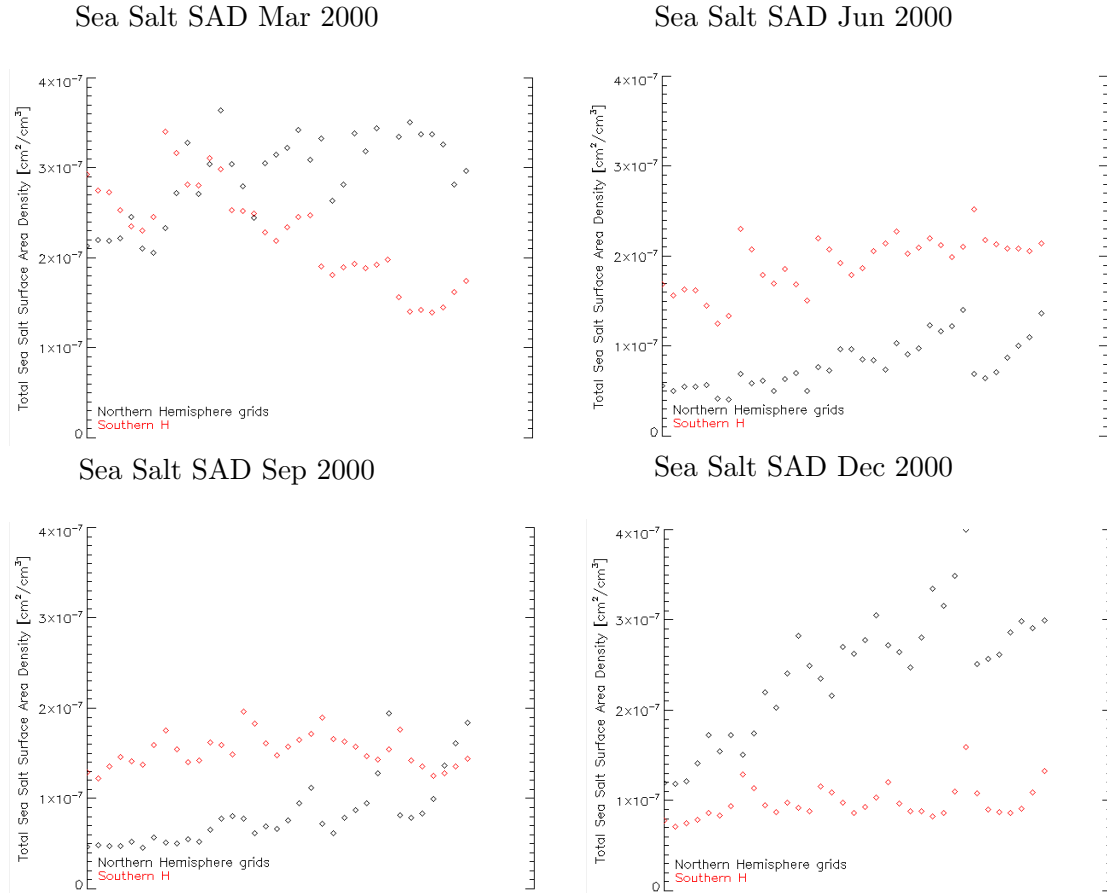


Figure 3.9: Surface Area Density (SAD) of sea salt [ $\text{cm}^2/\text{cm}^3$ ] in MOZART4, simulation *SS1* at the surface. Each symbol represents a value at a certain grid point. The Northern hemispheric grid points are located between  $32^{\circ}\text{N}$ - $46^{\circ}\text{N}$  and  $156^{\circ}\text{E}$ - $176^{\circ}\text{E}$ . The Southern hemispheric grid points are located between  $46^{\circ}\text{S}$ - $60^{\circ}\text{S}$  and  $184^{\circ}\text{E}$ - $204^{\circ}\text{E}$ .

*SS2ice*, with lower emissions of BrO from sea ice, we obtain a mean value of  $0.14 \times 10^{13}$  and  $0.24 \times 10^{13}$  molecules/ $\text{cm}^2$  in September and October, respectively. These values are consistent with the retrieval of Schofield *et al.* for background days.

Schofield and co-workers [111] gathered observations at Lauder, New Zealand ( $45.0^{\circ}\text{S}$ ,  $169.7^{\circ}\text{E}$ ), obtaining a variance weighted mean of  $0.2 \times 10^{13} \pm 0.4 \times 10^{13}$  molecules/ $\text{cm}^2$  for a group of 72 discrete tropospheric column observations done between March 2001 and April 2003. The mean values we obtain for the gridbox containing the location of the measurements for the modelled year 2000 is  $0.5 \times 10^{13}$  molecules/ $\text{cm}^2$  for simulation *SS1* and for simulation *SS1ice*. For simulation *SS2ice* the value is  $0.1 \times 10^{13}$  molecules/ $\text{cm}^2$  and for *SS3ice* it is  $0.2 \times 10^{13}$  molecules/ $\text{cm}^2$ . Given the high variability of the BrO VTCD, we have a good agreement of the order of magnitude of the measurements and the simulations.

Still in the Southern hemisphere but closer to the Equator, Theys and colleagues [123] reported measurements of tropospheric BrO vertical columns over Reunion Island ( $20.9^{\circ}\text{S}$ ,  $55.5^{\circ}\text{E}$ ), during the period of August 2004-June 2005. For the entire observation period,

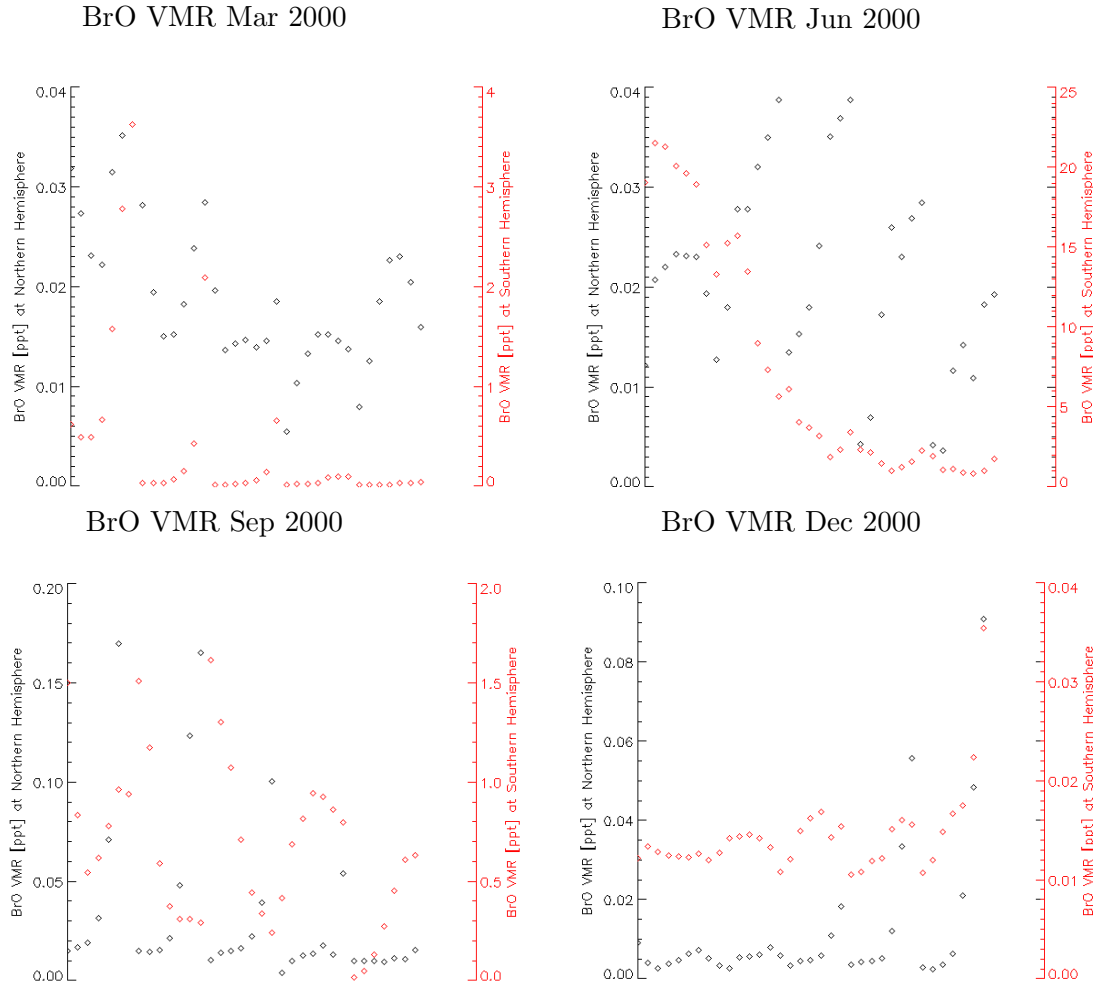


Figure 3.10: BrO volume mixing ratio [ppt] at the model surface level in simulation *SS1*. Each symbol represents a value at a certain grid point. The Northern hemispheric grid points are located between  $32^{\circ}$ - $46^{\circ}$ N and  $156^{\circ}$ - $176^{\circ}$ E. The Southern hemispheric grid points are located between  $46^{\circ}$ - $60^{\circ}$ S and  $184^{\circ}$ - $204^{\circ}$ E.

they derived a mean value of  $1.1 \pm 0.45 \times 10^{13}$  molecules/cm<sup>2</sup>. We obtain a mean value of  $0.18 \times 10^{13}$  molecules/cm<sup>2</sup> for the 12 months of 2000, in both simulations *SS2ice* and *SS3ice*. In simulations *SS1* and *SS1ice*, with higher bromine emissions from sea salt in the Southern hemisphere, the annual average at Reunion Island is  $0.25 \times 10^{13}$  molecules/cm<sup>2</sup>, which is still more than 2 times lower than the observations.

Measurements of BrO vertical column densities were performed during a ship cruise from Bremerhaven, Germany, to Cape Code, South Africa, in October 2000 [70]. Most of their measurements were below the estimated detection limits, with the exception of two days when the ship was passing near the Canary Islands. On these days, they obtained a mean BrO vertical column density of  $0.17 \pm 0.06 \times 10^{13}$  molecules/cm<sup>2</sup> (maximum of  $0.59 \pm 0.53 \times 10^{13}$  molecules/cm<sup>2</sup>). In our model simulations, we obtained at that location

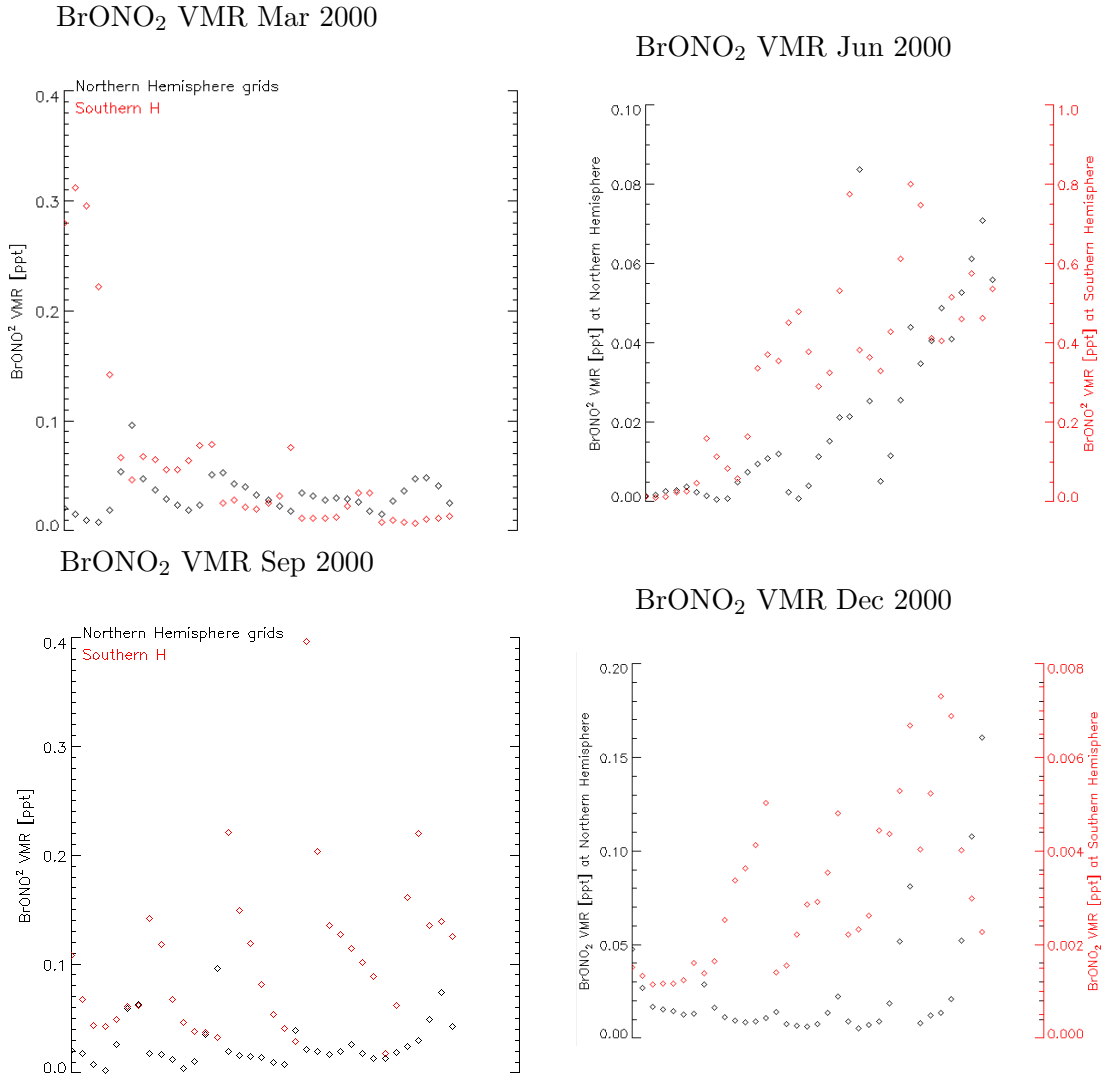


Figure 3.11: BrONO<sub>2</sub> volume mixing ratio [ppt] at the model surface level in simulation *SS1*. Each symbol represents a value at a certain grid point. The Northern hemispheric grid points are located between 32<sup>o</sup>-46<sup>o</sup>N and 156<sup>o</sup>-176<sup>o</sup>E. The Southern hemispheric grid points are located between 46<sup>o</sup>-60<sup>o</sup>S and 184<sup>o</sup>-204<sup>o</sup>E.

a monthly mean value of  $0.15 \times 10^{13}$  molecules/cm<sup>2</sup> in October 2000. This study and table 4 of the review of Sander *et al.* [107], show that in several campaigns the observations of BrO were below the rather high detection limits. In the referred table 4, the lowest detection limit is 0.3 ppt. Therefore, one has to be careful, because we may compare relatively high episodic values from observations with background (averaged) values provided by the model. In this particular case, our result fits well with the measurement. However, looking the values we have from the model along the ship path it is interesting that Leser and co-workers did not obtain statistically significant observations in the other days.

Hendrick *et al.* [53] measured tropospheric BrO columns at Harestua, Southern Norway

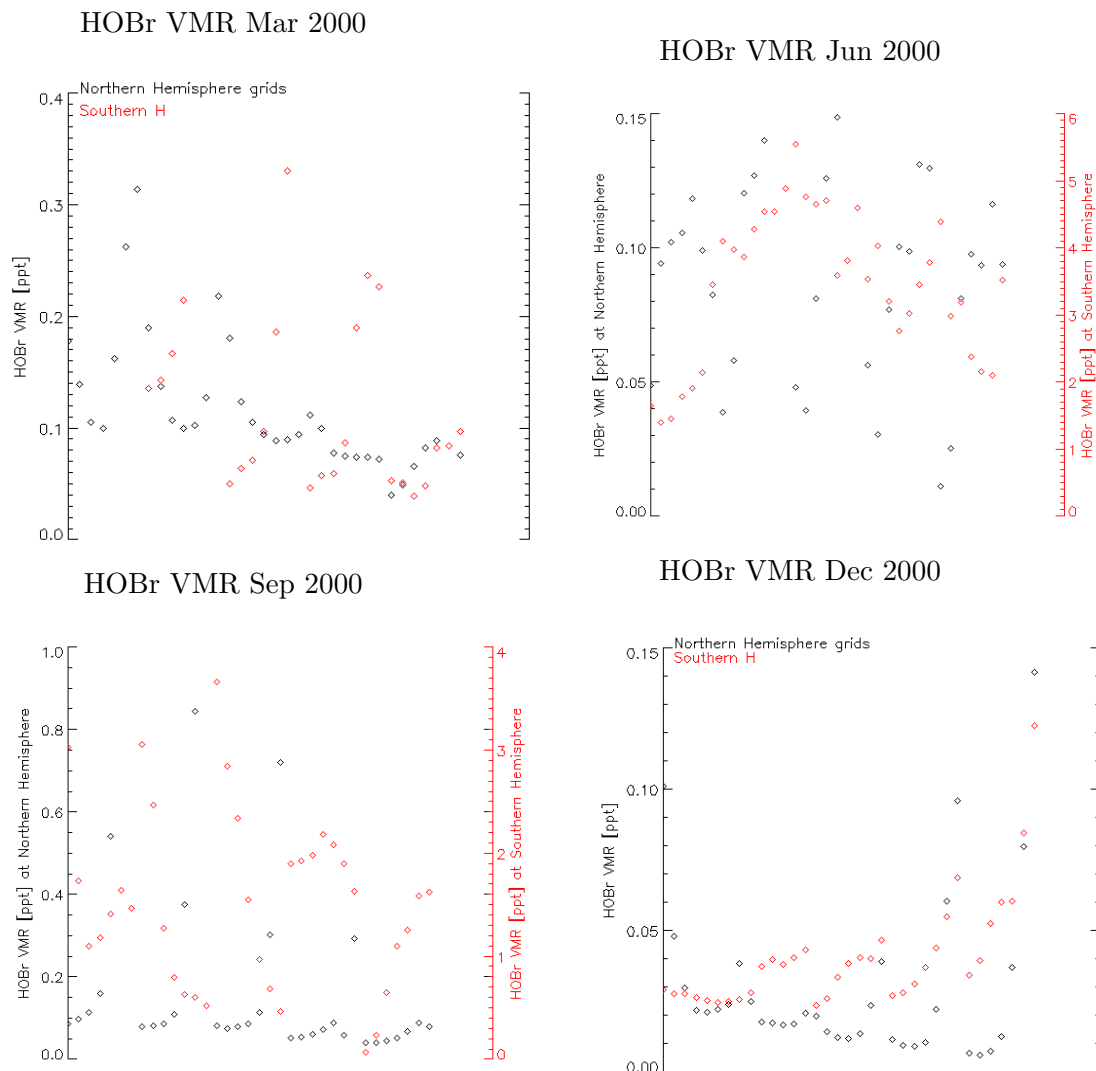


Figure 3.12: HOBBr volume mixing ratio [ppt] at the model surface level in simulation SS1. Each symbol represents a value at a certain grid point. The Northern hemispheric grid points are located between  $32^{\circ}$ - $46^{\circ}$ N and  $156^{\circ}$ - $176^{\circ}$ E. The Southern hemispheric grid points are located between  $46^{\circ}$ - $60^{\circ}$ S and  $184^{\circ}$ - $204^{\circ}$ E.

( $60^{\circ}$ N,  $11^{\circ}$ E) for the 2000-2006 period. Their observations show a marked seasonality with the highest values in the beginning of the year and the lowest at the end of the summer. From all our simulations, only SS3ice results, with the highest bromine emissions from sea ice, show a seasonality that resembles the data of Hendrick *et al.* Nevertheless, our maximum (in April) and minimum (in November) are later than in the observations. Hendrick and colleagues observations range from a mean value of  $0.92 \pm 0.38 \times 10^{13}$  to  $1.52 \pm 0.62 \times 10^{13}$  molecules/cm<sup>2</sup>. The mean values of BrO VTCD for simulation SS3ice are in the range  $0.05$ - $0.26 \times 10^{13}$  molecules/cm<sup>2</sup>. The other simulations show even lower values of BrO VTCD.

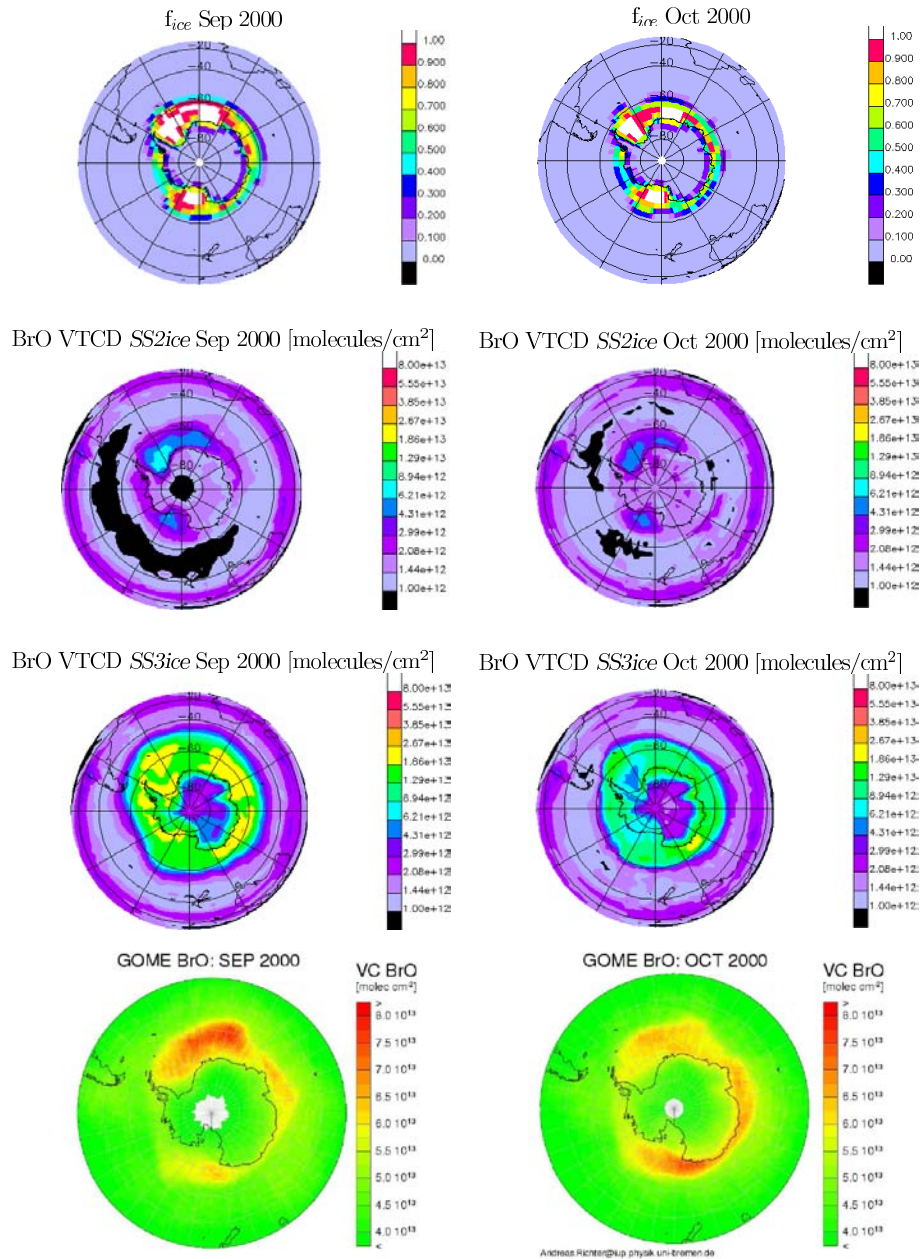


Figure 3.13: Southern hemispheric view for September and October 2000 of the sea ice cover fraction in MOZART4, VTCD of BrO [molecules/cm<sup>2</sup>] for simulations *SS2ice* and *SS3ice*, and GOME retrievals.

We also have altitudinal profiles measured in the Northern hemisphere at Kiruna (67.1°N, 22.5°E) [35]. In Figure 3.14, we compare the profiles obtained by Fitzenberger and co-workers (circles), and the ones resulting from simulations *SS2ice* (squares) and *SS3ice* (triangles). We show in the Figure two profiles of observations, one taken in February 1999 and another in August 1998. For the simulations, we calculated two profiles for the gridbox where Kiruna is located for February and August 2000.

The profiles for February show that the values from simulation *SS2ice* are lower than the

measurements (by almost two orders of magnitude), meaning that our concentration results are too low, which corroborates the conclusion that our emissions from sea ice are too low in this simulation. The results from simulation *SS3ice* have a reasonable agreement in the boundary layer. Above 10 km altitude the BrO concentration is the same for both simulations showing no effect from the bromine boundary layer emissions. Also, above 10 km, the results are lower than the measurements, maybe due to the lack of long-lived halocarbon emissions in the model simulations. We observe a striking agreement in the shape of the curves for February. The profiles show an S shape, with maxima at around 2 km altitude and minima in the range of 6-7.5 km. The differences at the altitude of the minima are probably due to the description of the boundary layer in the model, which restricts transport to the free troposphere. This agreement is observed although we compare different years. The excellent agreement of the profiles in February, gives us some confidence in the chemistry introduced in the model and the capability to reproduce the correct seasonality.

Regarding the profiles in August, we see that around 2 km of altitude the measurements go from very low values to values of the order of  $10^7$ . We suppose that at the time of the measurements transport processes increased the values above 2 km. The results from both simulations do not agree with the measurements in magnitude or pattern there.

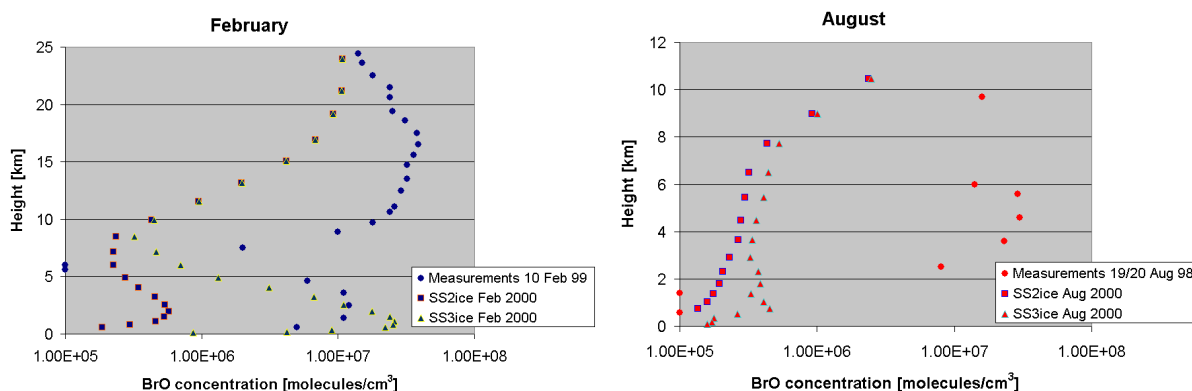


Figure 3.14: BrO concentration profiles [molecules/cm<sup>3</sup>] resulting from measurements [35] (circles) and from Mozart4 simulations *SS2ice* (squares) and *SS3ice* (triangles) at Kiruna (model grid: 67.1<sup>0</sup>N, 22.5<sup>0</sup>E); monthly averages of daily instantaneous outputs at 10h30 local time. Symbols on the Y-axis represent small values below  $1 \times 10^5$ . The standard deviation of the measurements is roughly 30%.

The comparisons between observations and model results show that the model is capable of reproducing at least qualitatively some of the observed seasonality. However, it also suggests that the emissions from sea ice may be too high in simulation *SS3ice*, and the total bromine emissions at lower latitudes may be too low.

### 3.4 Total inorganic bromine, partitions and the chemistry of the bromine species

In this section, we give an overview of the spatial and temporal distribution of the inorganic bromine species for various simulation experiments. We analyse the total amount of inorganic bromine in the atmosphere: Br<sub>x</sub>, which is the sum of the concentrations of Br, BrO, HOBr, HBr, BrONO<sub>2</sub>, BrCl, and 2 × Br<sub>2</sub>. We also analyse their partitions and their reaction pathways at selected locations in order to obtain some insight into the relative importance of those reactions depending on the local conditions.

We show in Figure 3.15 the zonal averages of Br<sub>x</sub> volume mixing ratios for *SS1* (bromine chemistry with heterogeneous chemistry on sea salt; no pH limitation in the Southern hemisphere; no emission from polar sea ice) for all simulated months of 2000. In all months, we observe a strong interhemispheric gradient in the volume mixing ratios of Br<sub>x</sub>, like for BrO. Again, this is a consequence of the high production rate of bromine species in the belt of high sea salt aerosol concentrations around the Antarctic continent. The high Br<sub>x</sub> concentrations are especially pronounced from May to September, which are the Southern hemisphere winter months with the highest surface wind speed. We obtained very low Br<sub>x</sub> VMR near the North pole, especially from September to March during the Northern hemispheric winter months under polar night conditions.

We present selected monthly zonal averages of Br<sub>x</sub> volume mixing ratios for simulation *S1* in Figure 3.16. This simulation has only VLSL as a source of bromine in the troposphere. Comparing these results with those of *SS1*, gives us an idea how important is the sea salt source of bromine over open ocean in the global troposphere. For simulation *S1*, the highest values of Br<sub>x</sub> are always located in the upper troposphere and the lower stratosphere.

In Figure 3.17, we show selected monthly zonal averages of Br<sub>x</sub> volume mixing ratios for simulation *SS1ice*. This simulation has compared to *SS1* the additional bromine source of sea ice in the polar regions. This leads to a significant increase of Br<sub>x</sub> VMR, which can be seen from the extension of the regions with Br<sub>x</sub> VMR above 13 ppt in the Southern hemisphere for *SS1ice*. In the North polar region, we now find Br<sub>x</sub> VMR in the range of 0.1–44 ppt, while it varied from 0.04 to only 3.7 ppt in *SS1*. Considering now (Figure 3.18), the simulation *SS2ice*, which includes a pH limitation on bromine production from sea salt over open ocean, we observe a strong decrease in the Br<sub>x</sub> VMR below 500 hPa in the Southern hemisphere. The Br<sub>x</sub> concentrations in the Northern hemisphere are unaffected.

Simulation *SS3ice* has higher bromine emissions from sea ice than *SS2ice*. This is visible in the monthly zonal averages of Br<sub>x</sub> volume mixing ratios (Figure 3.19) in both hemispheres at high latitudes. However, the values reach 90 ppt in the Northern hemisphere, which is extremely high and not correct. According to Li *et al.* [71], the average Br<sub>x</sub> during spring in Alert is 17 pptv. Our very high values are due to continuous emissions from sea ice and too low dry deposition velocities of HBr over snow and ice in MOZART4.

Regarding the lower latitudes, William T. Sturges [117] reports measurements of gaseous Br with a mean density of 28 ng(Br)/m<sup>3</sup> on the Isle of Harris, off the Northwest of Scotland, during the period of 26<sup>th</sup> April to 5<sup>th</sup> May 1983. Considering standard atmospheric conditions this value translates into a volume mixing ratio of 8 ppt. We obtain for the gridbox 57<sup>o</sup>-60<sup>o</sup>N and 4<sup>o</sup>-7<sup>o</sup>W where the measurement stations are located, values below 4.2 pptv in simulation *SS3ice*, and even lower values in the other MOZART4 simulations.

Pszenny and co-workers [90] reported for Oahu, Hawaii, values in the range of < 1.5 to

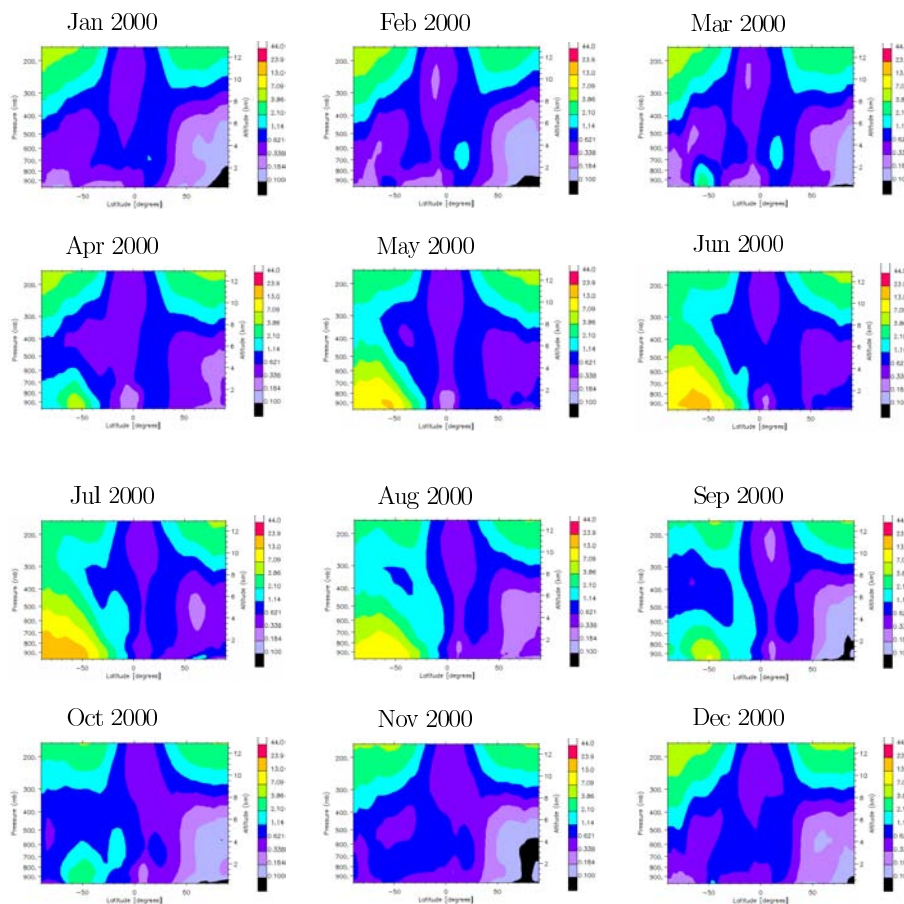


Figure 3.15: Monthly zonal averages of the total gas phase inorganic bromine  $Br_x$  VMR [ppt] for simulation *SS1*.

9 pptv during September 1999. For the gridbox that contains that location we obtain for all our simulations that include bromine emissions from sea salt the average volume mixing ratio of 0.4 pptv.

The two last observations in the literature suggest that we probably have too low bromine emissions at low latitudes.

From the partition of BrO bromine species for simulations *SS1ice* and *SS2ice*, presented in Figures 3.21 and 3.22, left column, 2<sup>nd</sup> line, we see that BrO is indeed one of the main constituents of  $Br_x$  near the sources of bromine at the surface and in the upper troposphere. At surface locations with very active bromine chemistry, BrO represents 20 to 40% of  $Br_x$ .

The contribution of the species Br,  $Br_2$ , BrCl, BrONO<sub>2</sub>, and HOBr to  $Br_x$  is generally low. However, there is a shift in the partition of Br and BrONO<sub>2</sub> towards higher values (20–40%) in the upper troposphere due to higher photolysis rates. Near the surface, HOBr and BrONO<sub>2</sub> represent an important part of  $Br_x$  in regions with very active bromine chemistry. BrONO<sub>2</sub> occurs in comparatively important amounts only where NO<sub>x</sub> is available, e.g., near 40°N–50°N.

HBr contributes to a large extent to  $Br_x$  all over the troposphere. The areas with the lowest values of HBr/ $Br_x$  are at high altitudes and where heterogeneous chemistry is very active. Otherwise, we have very high values for HBr/ $Br_x$  reaching 100% in the high latitudes.

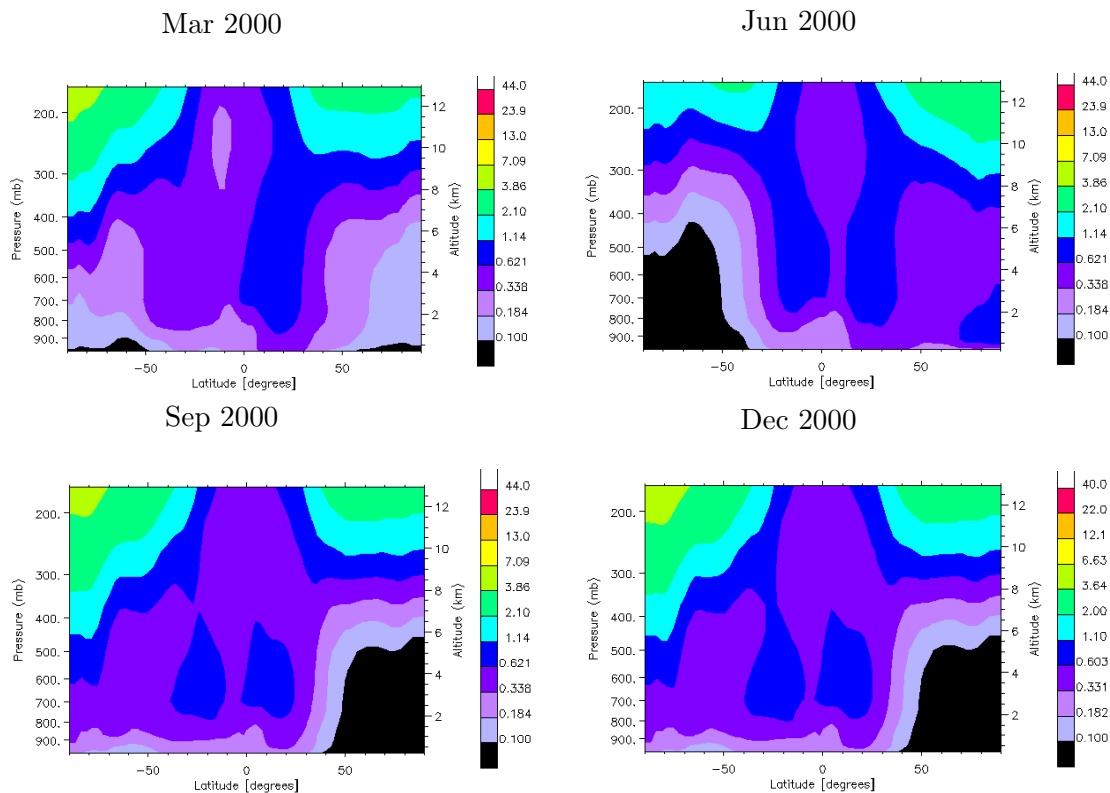


Figure 3.16: Monthly zonal averages of the total gas phase inorganic bromine Br<sub>x</sub> [ppt] for simulation *S1*.

This contribution is too high and it is most likely a consequence of our very low dry deposition velocities of about 0.008 cm/s for HBr over ice and of too low wet deposition. Nevertheless, these high HBr concentrations do not affect the bromine chemistry since the conversion of HBr into chemically active bromine species (in this case Br) is not significant, as we will see later. This means that the bromine atoms forming HBr are lost for the atmospheric bromine chemistry.

In order to investigate the effects of low dry deposition velocities on HBr concentrations we present a meridional slice of Br<sub>x</sub> instantaneous VMR at longitude 180° at UTC 00:00h for the 1<sup>st</sup> of March and the 1<sup>st</sup> of September 2000 in Figure 3.20. In the 1<sup>st</sup> of March the polar-day period is starting in the Northern hemisphere, so that the high emissions from sea ice are still not visible in the HBr volume mixing ratios. However, in the figure showing the 1<sup>st</sup> of September, five months of high sea ice emissions over a large area are visible over the regions covered with sea ice. We obtain very high values of HBr VMR going up to 50 ppt. In the Southern hemisphere, a similar accumulation does not occur, because the area covered by sea ice is smaller and the transport to areas over the ocean allows a faster loss of HBr from the atmosphere by wet scavenging and dry deposition.

In Figure 3.23, we present the concentrations of bromine species and the most important chemical fluxes in a chemically very active area for simulation *SS1*. The calculations were done for selected boxes on the surface located in the Southern hemisphere in the belt of

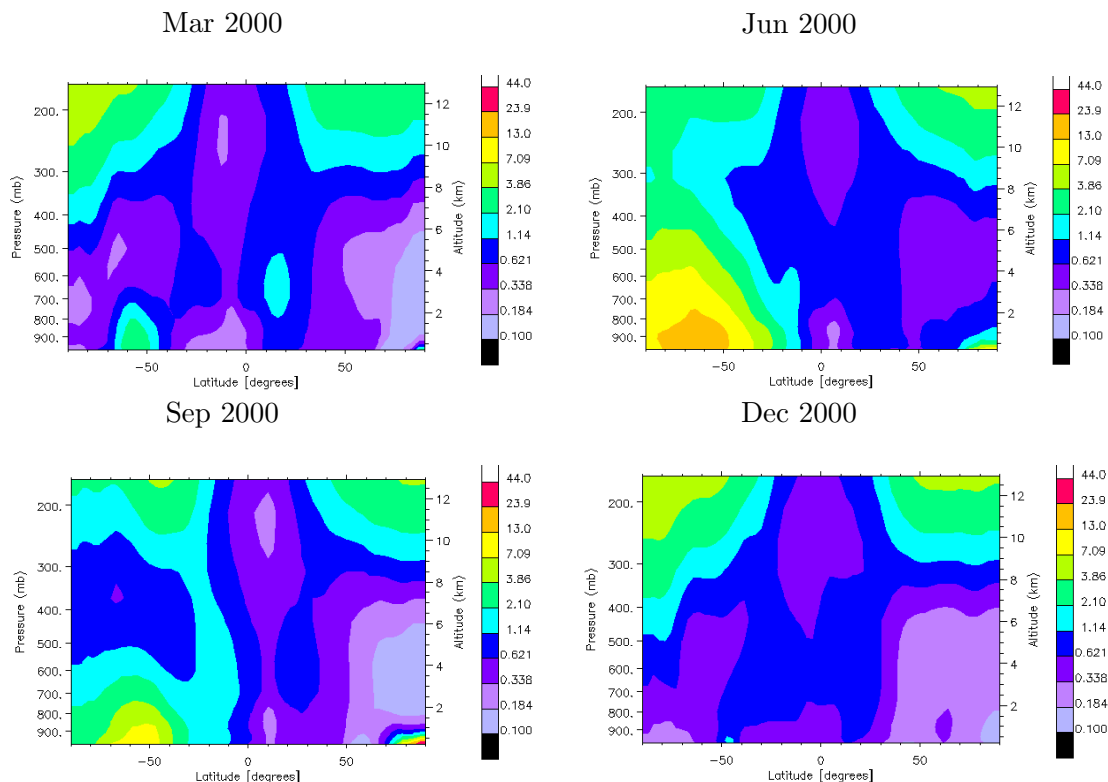


Figure 3.17: Monthly zonal averages of the total gas phase inorganic bromine  $\text{Br}_x$  [ppt] for simulation *SSlice*.

high bromine production from sea salt at local noon. Br and BrO are the central species in the bromine chemical cycle. The main reactions are the direct interconversion of BrO and Br. A second cycle between BrO and Br involves HOBr. The magnitude of the chemical fluxes varies with the location on the globe, but these fluxes remain the most important ones under daylight conditions. The termolecular reaction of BrO and  $\text{NO}_2$  is the main production pathway of  $\text{BrONO}_2$ .

In this particular example in Figure 3.23, the heterogeneous chemistry on sea salt is introducing large amounts of bromine into the gas phase. At the equator, where heterogeneous chemistry plays a minor role compared to the emissions of VSLs, the effective chemical cycle reduces to the gas phase cycle  $\text{BrO}-(\text{HOBr})-\text{Br}$  and the production and deposition of HBr. Further in the North, where sulphate and  $\text{NO}_x$  occur in higher concentrations, the importance of the chemical cycle  $\text{BrO}-\text{BrONO}_2-\text{HOBr}-\text{Br}-\text{BrO}$  increases significantly.

From Figure 3.23 we can also observe that photolysis is a fundamental part of the cycles. At the beginning of the night, the pathways leading to the reservoir species  $\text{BrONO}_2$  and HOBr are dominant. During the night, the main processes are the washout of HBr and the heterogeneous chemistry, that continues consuming HOBr and  $\text{BrONO}_2$  producing  $\text{Br}_2$  and BrCl, which accumulate until the morning.

Under the conditions of Figure 3.23, the lifetime of BrO is 41 seconds. In regions with lower BrO concentrations, the lifetime decreases to a minimum of 10 seconds. In polluted

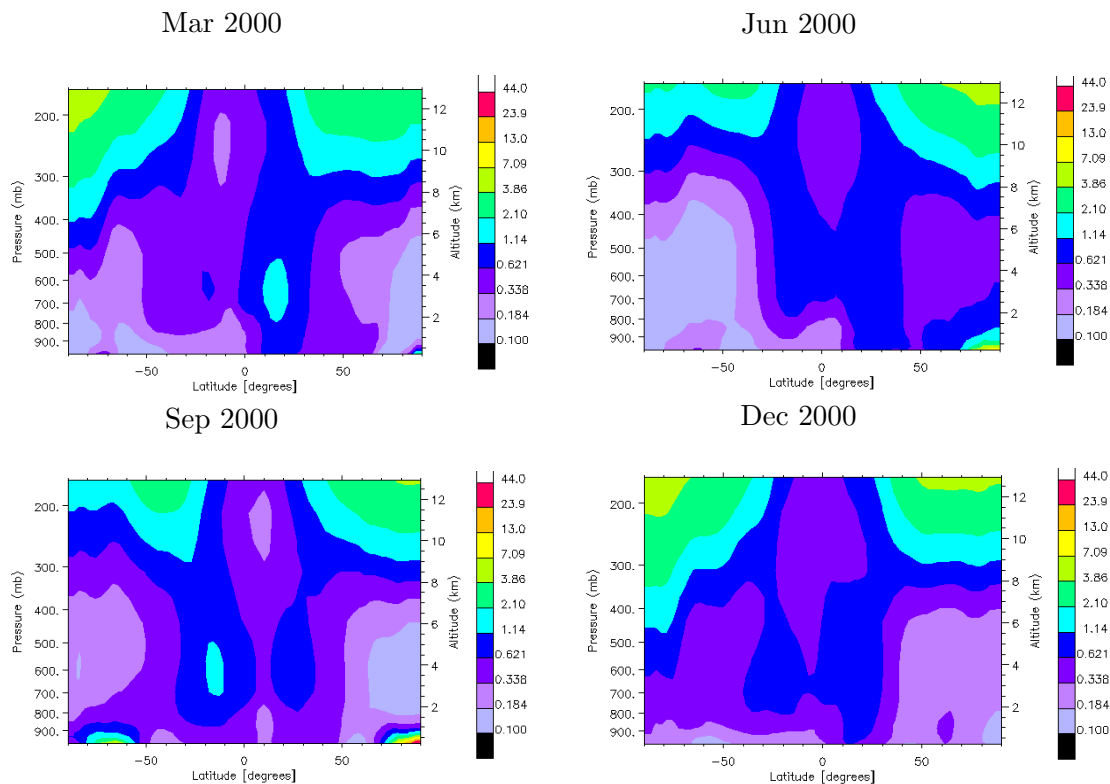


Figure 3.18: Monthly zonal averages of the total gas phase inorganic bromine Br<sub>x</sub> [ppt] for simulation SS2ice.

regions or in the upper troposphere, the reaction of BrO with NO<sub>X</sub> is more important than the reaction with HO<sub>2</sub>.

HBr is the main reservoir species. The partition in the troposphere is in the range of 50 to 100%, during day and night. It has the longest lifetime of all inorganic bromine species. Under the conditions of Figure 3.23, the lifetime is around 17 hours, while other inorganic bromine species do not have lifetimes exceeding 1 hour. HBr is produced by the reaction of Br with HO<sub>2</sub> and several aldehydes, the most important being CH<sub>2</sub>O. According to Larichev and co-workers [66], HBr can also be produced by the reaction of HO<sub>2</sub> with BrO, however this reaction has an estimated maximum contribution to the HBr yield of 1.5% at low temperatures. At temperatures above 200 K this contribution is even lower (< 0.01 %) [78]. As this contribution is very low, we decided not to include this reaction into the bromine chemistry scheme. The main loss of HBr is wet and dry deposition and represents the main loss of bromine from the atmosphere.

HOBr is another reservoir species with partition values in the troposphere that reach 45% in regions that are inorganic sources of bromine through heterogeneous chemistry involving HOBr. E.g., we observe in Figure 3.22 the highest HOBr/Br<sub>x</sub> at locations with high atmospheric sea salt and sulphate concentrations. However, HOBr is consumed and not produced by reactions on sea salt particles, nevertheless it represents an important fraction of Br<sub>x</sub> at these locations. This is because of the high emission of bromine and the role of HOBr in

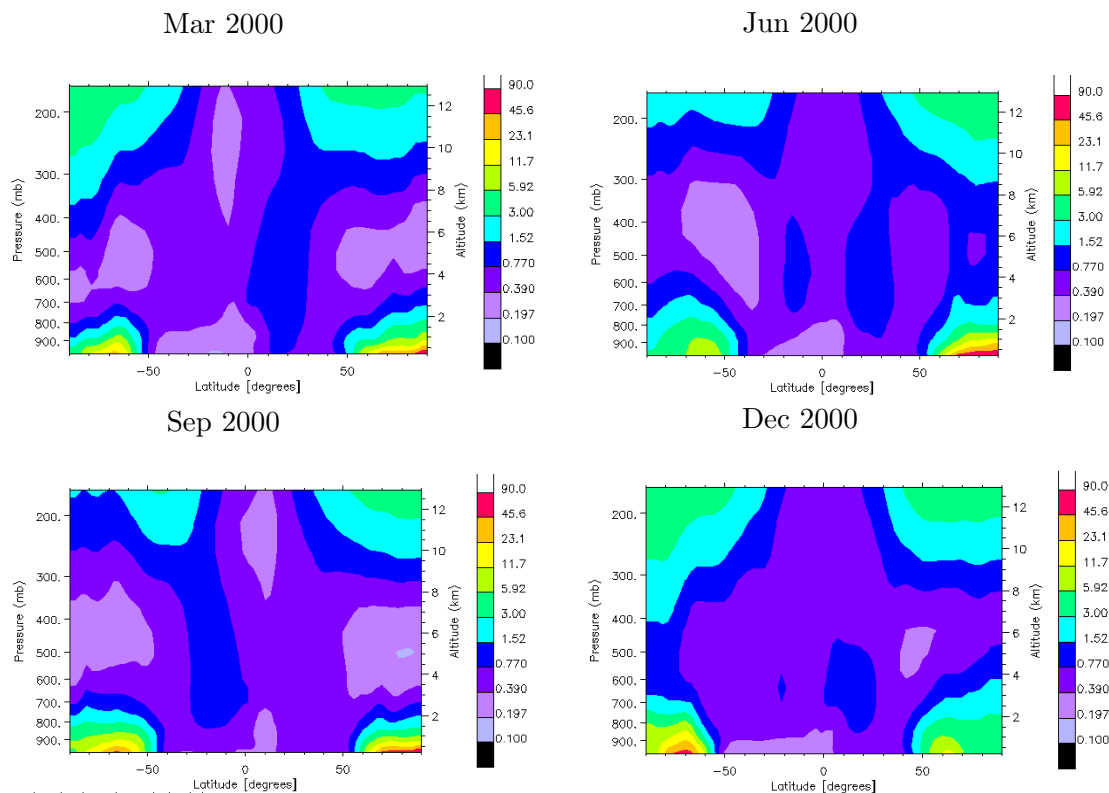


Figure 3.19: Monthly zonal averages of the total gas phase inorganic bromine  $Br_x$  [ppt] for simulation *SS3ice*.

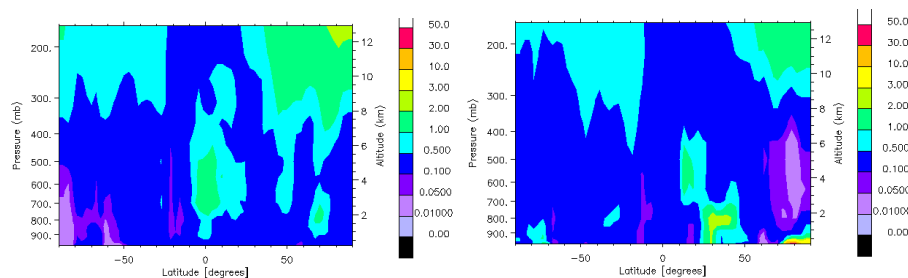


Figure 3.20: Meridional slice at longitude  $180^{\circ}$  of HBr instantaneous VMR at the  $1^{st}$  of March and the  $1^{st}$  of September 2000 for simulation *SS2ice*

the gas phase bromine cycle, with a lifetime higher than that of BrO and Br. Dry and wet deposition of HOBr represent a bromine loss from the atmosphere. It has a lifetime of around 12 minutes at the surface under sunlit conditions. The main production pathway is through the reactions of BrO with  $HO_2$  and  $CH_3O_2$  and the main loss is by photolysis. HOBr has a small partition in the stratosphere, because at this altitude the reaction of HOBr with molecular O represents an additional loss towards the production of BrO.

In addition to HOBr, also  $BrONO_2$  reacts on sulphate and sea salt. The highest partition of 20% is found in the Northern hemisphere midlatitudes as its production by the termolecular

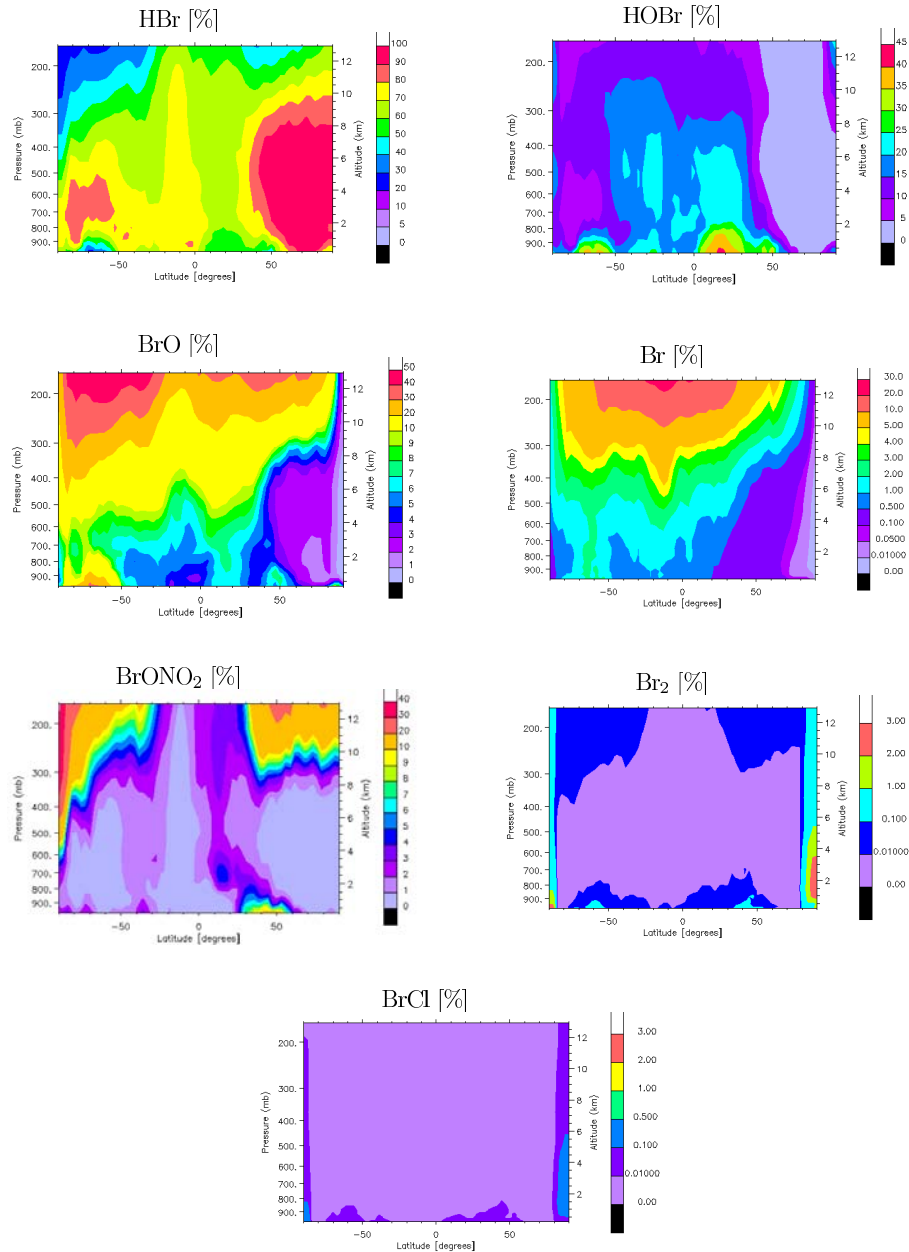


Figure 3.21: Vertical distribution of the partitioning of the seven inorganic bromine species in the gas phase at longitude  $180^{\circ}$ . Monthly average of the daily instantaneous outputs at 00:00 UCT in March 2000 for simulation *SSlice*.

reaction of  $\text{NO}_2$  with  $\text{BrO}$  is favoured under high  $\text{NO}_x$  conditions. In other tropospheric regions the partition is normally lower than 3%. In the stratosphere, the partition values increase because its loss in this region is lower compared to the other species. The lifetime in the troposphere is around 12 minutes. The photolysis of  $\text{BrONO}_2$  produces  $\text{BrO}$  or  $\text{Br}$ . The photolysis of  $\text{BrONO}_2$  to  $\text{BrO}$  represents the mere reversion of the  $\text{BrONO}_2$  formation, while the photolysis to  $\text{Br}$  leads to the subsequent catalytic destruction of ozone. However, the photolysis of  $\text{BrONO}_2$  to  $\text{BrO}$  is dominant.

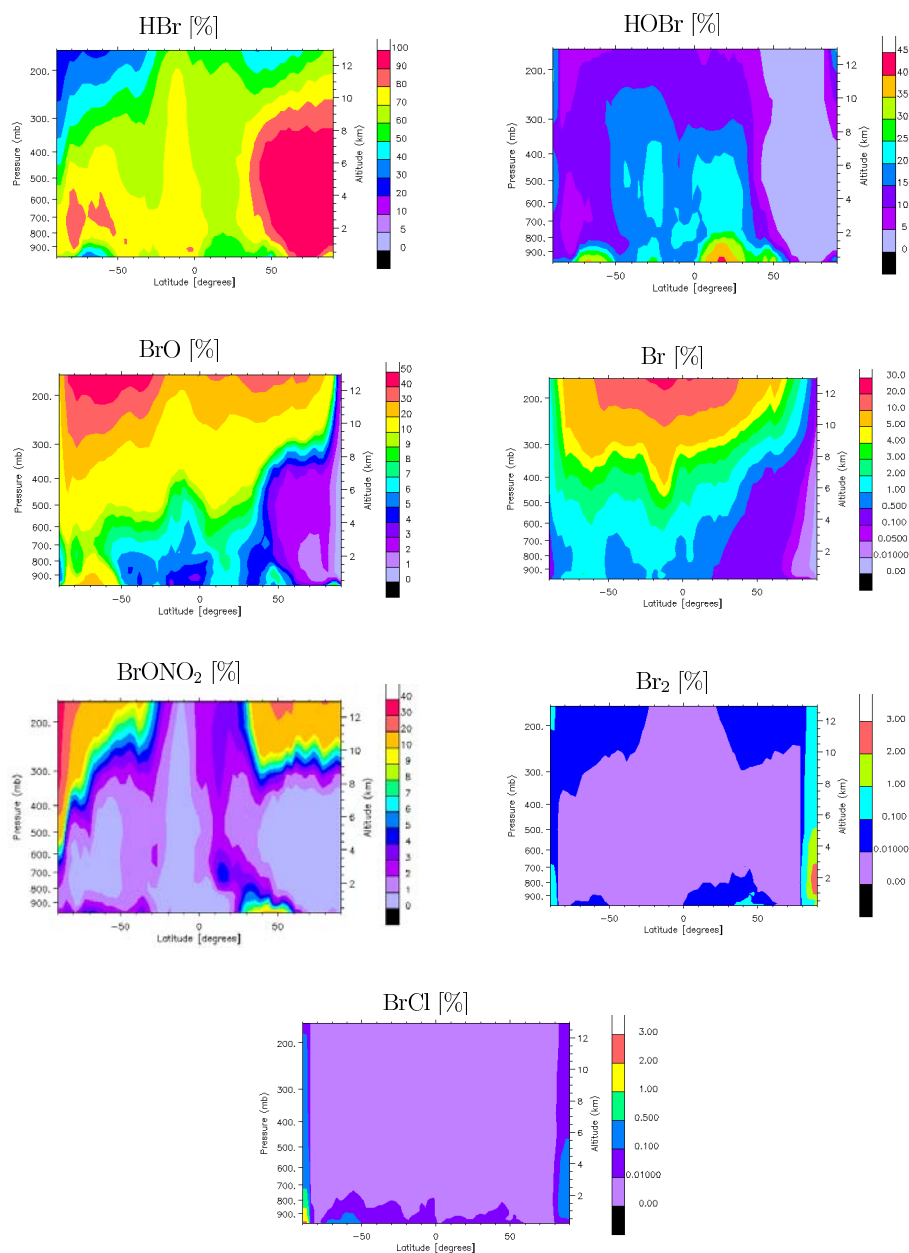


Figure 3.22: Vertical distribution of the partitioning of the seven inorganic bromine species in the gas phase at longitude 180°. Monthly average of the daily instantaneous outputs at 00:00 UCT in March 2000 for simulation *SS2ice*.

Br is the inorganic bromine species with the lowest lifetime (around 1 second) and therefore represents a small part of Br<sub>x</sub> in the troposphere. This radical is the key in the initiation of the gas-phase bromine chemistry after being produced by the decomposition of organic halocarbons. It rapidly reacts with ozone producing BrO. Under sunlight conditions its regeneration is also very fast mainly through photolysis of different species.

Br<sub>2</sub> and BrCl are the products of the heterogeneous reactions on sulphate and sea salt and they are quickly destroyed by photolysis. The partition values are rather low during the day

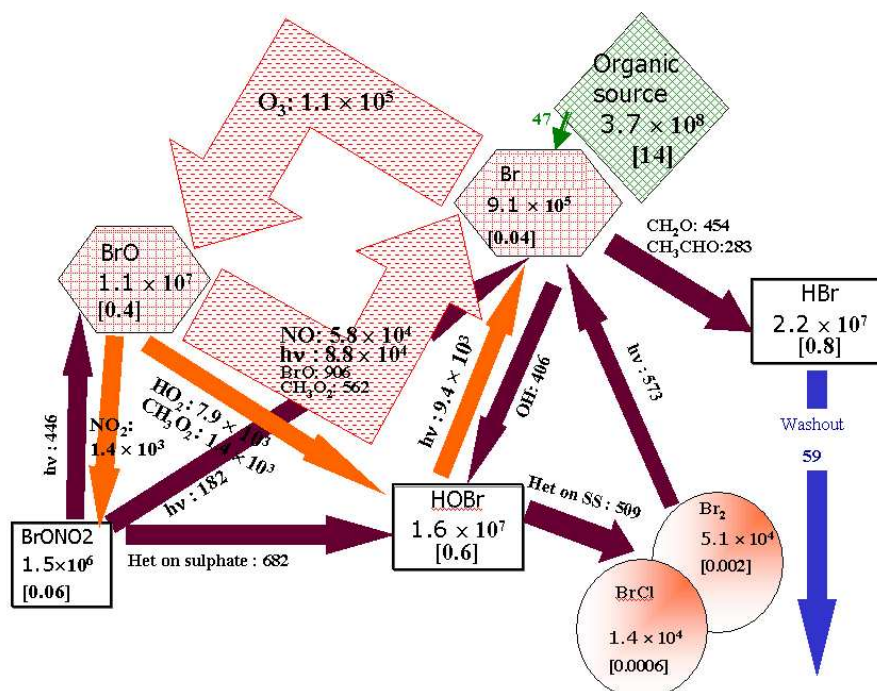


Figure 3.23: Concentrations of the bromine species [molecules/cm<sup>3</sup>, ppt in square brackets] and highest chemical fluxes [molecules/cm<sup>3</sup>/s] calculated for some gridboxes in the region of high bromine production rates from sea salt in the Southern Pacific at the surface. Instantaneous output at the 1<sup>st</sup> of April, 00:00 UTC (corresponding to local noon).

(<3%) and increase during the night. This is due to the interruption of their destruction by photolysis and their continued production while BrONO<sub>2</sub> and HOBr still exist. Consequently, during the night, partition values at the surface for these two species go up to 30% of Br<sub>x</sub>.

### 3.5 Comparison with other modelling experiments

Yang and co-workers [138] performed simulations including bromine chemistry using the chemical transport model *p*-TOMCAT. The horizontal resolution was approximately  $5.6^0 \times 5.6^0$  (T21) on 31 levels from the surface to 10 hPa. They included organic bromine sources as very short-lived bromocarbons (VSLs) + CH<sub>3</sub>Br and inorganic sources corresponding to the emission from sea salt over open ocean. The sea salt bromine source is dependent on the sea salt production rate and on a factor taking into account the bromine depletion on the sea salt particles. The heterogeneous reactions include the hydrolysis of BrONO<sub>2</sub> and N<sub>2</sub>O<sub>5</sub> on what they call background particles. The halocarbons comprise, as in our experiments with MOZART4, CH<sub>3</sub>Br, CHBr<sub>3</sub>, CH<sub>2</sub>Br<sub>2</sub>, CH<sub>2</sub>BrCl, CHBr<sub>2</sub>Cl, and CHBrCl<sub>2</sub>. These species contribute with a total of 7.8 Gmol(Br)/yr to the bromine emissions. This is a higher value than in our study (see table 3.3). Yang and co-workers report an inorganic emission of 14 or 26 Gmol Br/yr, depending on which expression they use, from two alternatives, to calculate the production rate of sea salt.

For a comparison with the *p*-TOMCAT simulations, we used the results from experiments *SS1*, *SS2ice*, and *SS3ice*. Simulations *SS1* and *SS2ice* provide lower emissions than

Table 3.3: The global emissions obtained from various MOZART4 simulations for the year 2000 and for the *p*-TOMCAT simulation of Yang and co-workers[138]

Sources (Gmol Br/yr)	<i>SS1</i>	<i>SS2ice</i>	<i>SS3ice</i>	<i>p</i> -TOMCAT
Natural halocarbons + CH <sub>3</sub> Br	7.3	7.3	7.3	7.8
Sea salt over open ocean	5	1.3	2.6	14 or 26
Sea salt over sea ice	-	0.5	18	-
Total inorganic source	5	1.8	20.6	14 or 26

the simulations with *p*-TOMCAT, while *SS3ice* has emissions which lie between the two emission values reported by Yang *et al.* [138]. Nevertheless, there are important differences between these studies, in terms of the magnitude of the atmospheric concentrations of various bromine species and their distribution on the globe. The analysis of these differences allows a better understanding of our own results, the limitations of our study and possible future improvements. In the following, we mainly compare *SS2ice* to Yang and colleagues simulation, because it may be the most similar one. *SS3ice* has very high HBr concentrations over the poles, because of the low deposition rates in MOZART4, which may be uncertain. On the other hand, the partition between the species in *SS2ice* and *SS3ice* is rather similar.

In Figure 3.24, we show the volume mixing ratios of Br<sub>x</sub> at the surface that Yang and co-workers obtained for March, June, September, and December from the simulation with bromine emission of 14 Gmol(Br)/yr. In the Northern hemisphere, they obtain a weaker seasonal cycle than in the Southern hemisphere. Moreover, the lowest values in the Southern hemisphere appear in June, with one region having a maximum of 3 pptv, and the highest VMR are obtained in December, with a maximum of 12 pptv. This is the opposite seasonal cycle observed in the results from our simulation *SS1*, where the inorganic bromine source is only sea salt over the open ocean like in the work of Yang *et al.*[138]. We obtain the highest Br<sub>x</sub> values in June and the lowest in December, because the strongest surface winds over the Southern ocean occur in June and the weakest in December.

In Figure 3.25, we show the near surface distribution of Br<sub>x</sub> from simulation *SS2ice* for March, June, September, and December 2000. For this simulation we have an inorganic emission of 1.8 Gmol(Br)/yr. In terms of volume mixing ratios, we found lower values than Yang *et al.* almost everywhere on the globe, except at high latitudes. In areas with sea ice, we have very high Br<sub>x</sub> VMR due to high emissions of bromine from the sea ice and low dry deposition rates. In contrast to the *p*-TOMCAT model, we have an average dry deposition velocity of HBr on sea ice of 0.008 cm/s, compared to 0.2 cm/s of Yang *et al.* [138]. In simulation *SS3ice*, with an emission of 20.6 Gmol Br/yr, the difference in the high latitudes is even more pronounced, but for the rest of the globe the VMR of *SS3ice* are not higher than those from *SS2ice*. It seems that the near surface Br<sub>x</sub> fields obtained from MOZART4 can show an accumulation of Br<sub>x</sub> in regions with high emissions with at most a slight increase in other regions. Consequently, we get rather sharp gradients in the horizontal distribution of Br<sub>x</sub> which can not be observed in the results of Yang *et al.* From this we conclude, that there is less long range transport of bromine in MOZART4 than in *p*-TOMCAT. One possible reason is that the simulations with *p*-TOMCAT were performed in the T21 horizontal resolution, while ours were performed at a higher resolution (T42). Sharp gradients are difficult to represent in a coarse model and therefore disappear rather rapidly due to higher numerical diffusion. Another possible reason may be a different overall Br<sub>x</sub> lifetime.

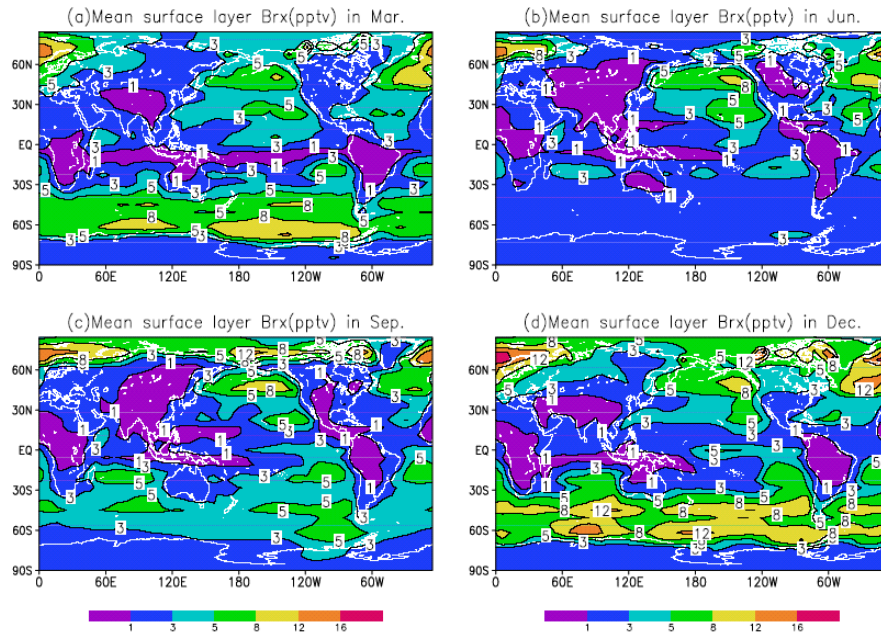


Figure 3.24: Distribution of monthly mean  $Br_x$  [pptv] obtained by Yang *et al.* [138] near the surface in the simulation with an annual  $Br$  production from sea salt of 14 Gmol/yr. The model surface layer has an average height of about 65m over the surface.

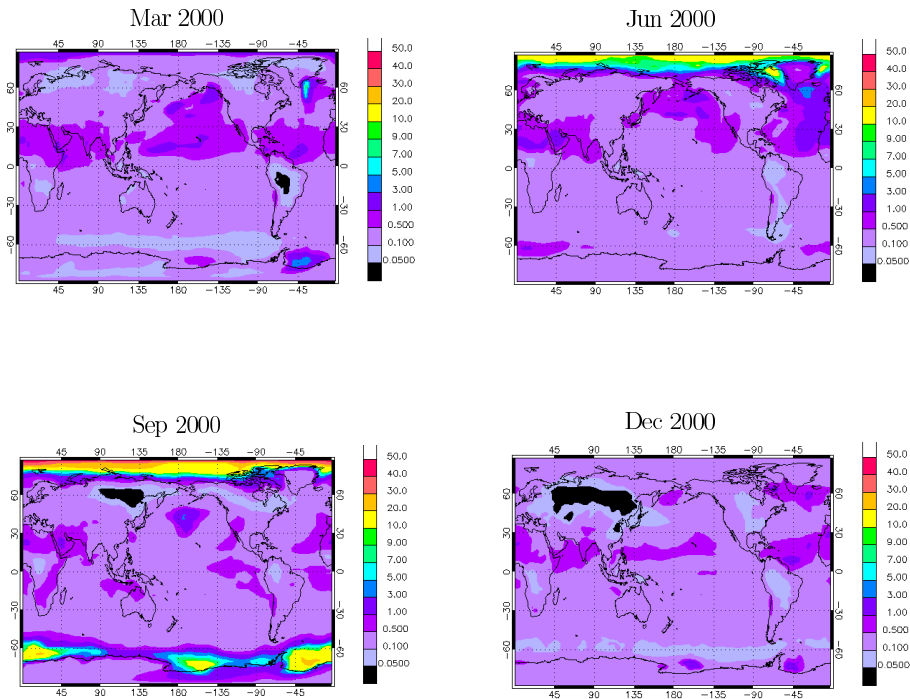


Figure 3.25: Simulation *SS2ice*: Distribution of monthly mean  $Br_x$  [pptv] at about 94m altitude above the surface for March, June, September, and December 2000.

For simulation *SS2ice*, we observe a maximum  $\text{Br}_x$  VMR of 7 pptv in the Northern hemisphere for March 2000 (Figure 3.25). This local maximum occurs in an area of high sea salt aerosol concentration over the open ocean. In the Southern hemisphere, we find a maximum of 5 pptv in an area of high bromine emission from sea ice. The *p*-TOMCAT simulation results in much larger areas with VMR above 5 pptv (Figure 3.24) and an overall higher bromine VMR near the surface, that is, more than ten times higher than our results in large regions. This is similar to simulation *SS3ice*, as the increase of volume mixing ratios compared to *SS2ice* is restricted to the high latitude regions. The region with high (around 8 pptv)  $\text{Br}_x$  VMR around  $60^\circ\text{S}$  in Figure 3.24 for March is not present in simulations *SS2ice* or *SS3ice*, but it is observed in simulation *SS1* (see Figure 3.26). This shows that the pattern observed in the Southern hemisphere for the *p*-TOMCAT results in March is a consequence of bromine emissions from sea salt over the open ocean but not from emissions in the polar region itself. When both sources are introduced and the pH in the sea salt particles is taken into account, the region around  $60^\circ\text{S}$  does not show a maximum, but a minimum as observed for simulation *SS2ice* (Figure 3.25).

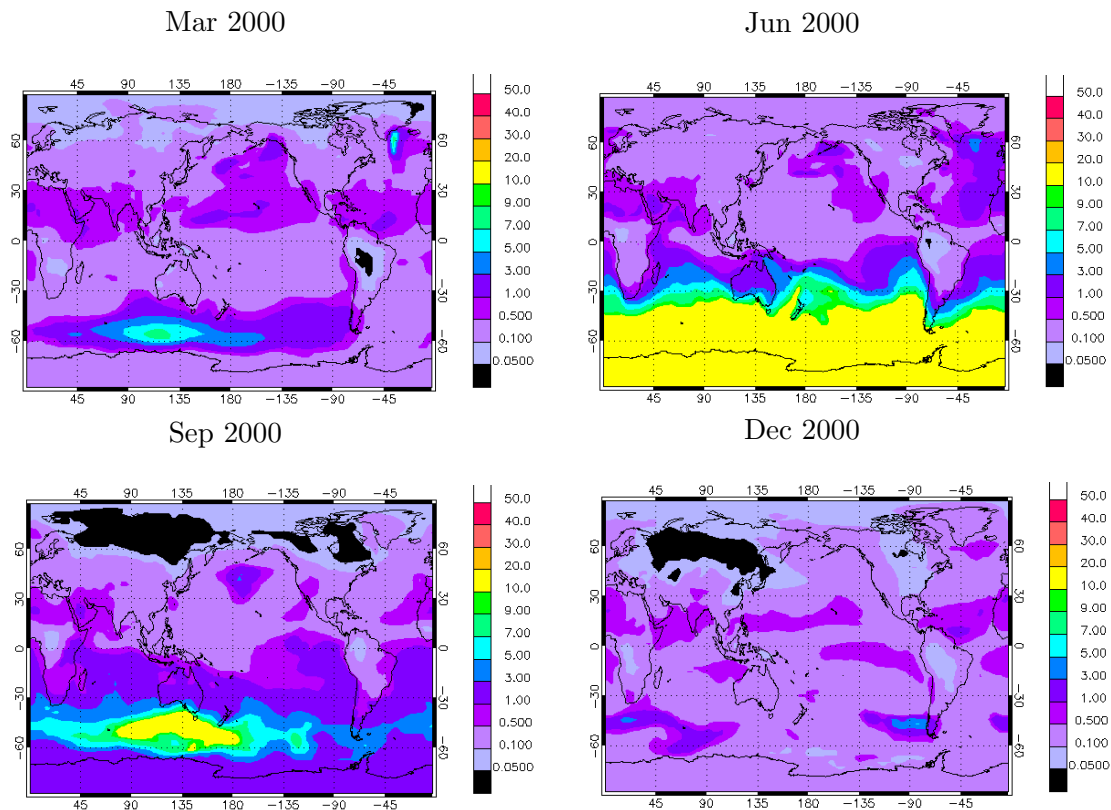


Figure 3.26: Simulation *SS1* results: horizontal distribution of monthly mean  $\text{Br}_x$  [ppt] at 982hPa (94m altitude) for March, June, September, and December 2000.

Yang *et al.* find low values (1–3 pptv) in most regions of the Southern hemisphere in June, whereas the  $\text{Br}_x$  VMR is at over 10 pptv in our *SS1* simulation, because no pH limitation is effective and wind speeds are high in this region in June leading to high sea salt aerosol

content in the air. Much lower VMR are found for  $\text{Br}_x$  in the *SS2ice* simulation because of the pH limitation. We find VMR between 0.1 and 1 pptv which are still higher than in March (mostly below 0.1 pptv). Yang and colleagues use an emission efficiency factor which they call sea salt aerosol bromine depletion factor in their study for the region south of  $30^\circ$ . This factor limits the bromine emission from sea salt. It has a seasonal variation with the maximum in December and the minimum in June. We think that the low concentrations found by Yang *et al.* in June are due to the application of the bromine emission efficiency factor. Indeed, the higher sea salt atmospheric concentrations in June are counteracted in their simulation by a weaker bromine emission from sea salt particles with respect to March. In contrast, our strategy of limiting the bromine emission from sea salt particles in simulations *SS2ice* and *SS3ice* does not take into account seasonality. A similar discussion applies for the December results. During this month the emission efficiency has its highest value, and therefore the bromine emission for the simulations of Yang *et al.* experience the weakest limitation. Therefore, *p*-TOMCAT results are comparatively high for this month, while the MOZART4 results provide low  $\text{Br}_x$  concentrations, because of their mere dependence on the available sea salt aerosol concentration that directly depends on wind speed.

The concentrations for the reactive bromine species in MOZART4 simulations (Figure 3.28 for the results of simulation *SS2ice*) are lower than for *p*-TOMCAT, with the exception of HBr on sea ice in the polar regions during periods with high emissions from sea salt. In terms of the partitions, the differences in the values and patterns observed between Figures 3.27 and 3.22 (*SS2ice*) are due to:

1. the much lower dry deposition velocities of HBr on sea ice in MOZART4 compared to *p*-TOMCAT;
2. the different formulation of the inorganic bromine emissions from sea salt and sea ice: in MOZART4, HOBr and  $\text{BrONO}_2$  are consumed in heterogeneous reactions, but Yang and co-workers introduce a simple emission flux;
3. The higher horizontal and vertical resolution of MOZART4 .

Concerning simulation *SS2ice*, Yang *et al.* have 5 to 10 times higher emissions of bromine from sea salt over open ocean (table 3.3). This may account for the lower background values of BrO VTCD in the mid-latitudes in our results, as we have minima below  $5 \times 10^{11}$  molecules/cm<sup>2</sup>, while the *p*-TOMCAT simulation (Figure 3.29) provides BrO VTCD results which go up to  $1 \times 10^{12}$  molecules/cm<sup>2</sup>. The emission of bromine from sea ice in *SS3ice* increases the values generally so that they came close to the values obtained by Yang and co-workers. Nevertheless, the maxima are not necessarily at the same locations. In December, e.g., we observe that our maxima are located near the poles, where the sea ice emissions are highest and Yang's maxima are over the open ocean, where the sea salt source is located. This is a consequence of the high emission over sea ice in our simulation which represent 90% of the inorganic bromine emissions, whereas the emission of Yang and colleagues mostly occur over the open ocean. We believe that the geographical distribution of our emissions is more realistic, because we can reproduce the shape and the magnitude of the measurements at Kiruna in February in the *SS3ice* simulation whereas Yang *et al.* obtained too high values there (Figures 3.14 and 3.30). In addition, the shape of their curve is quite different. In order to discuss the spatio-temporal distribution of inorganic bromine emissions further, we urgently need more ground-based measurements.

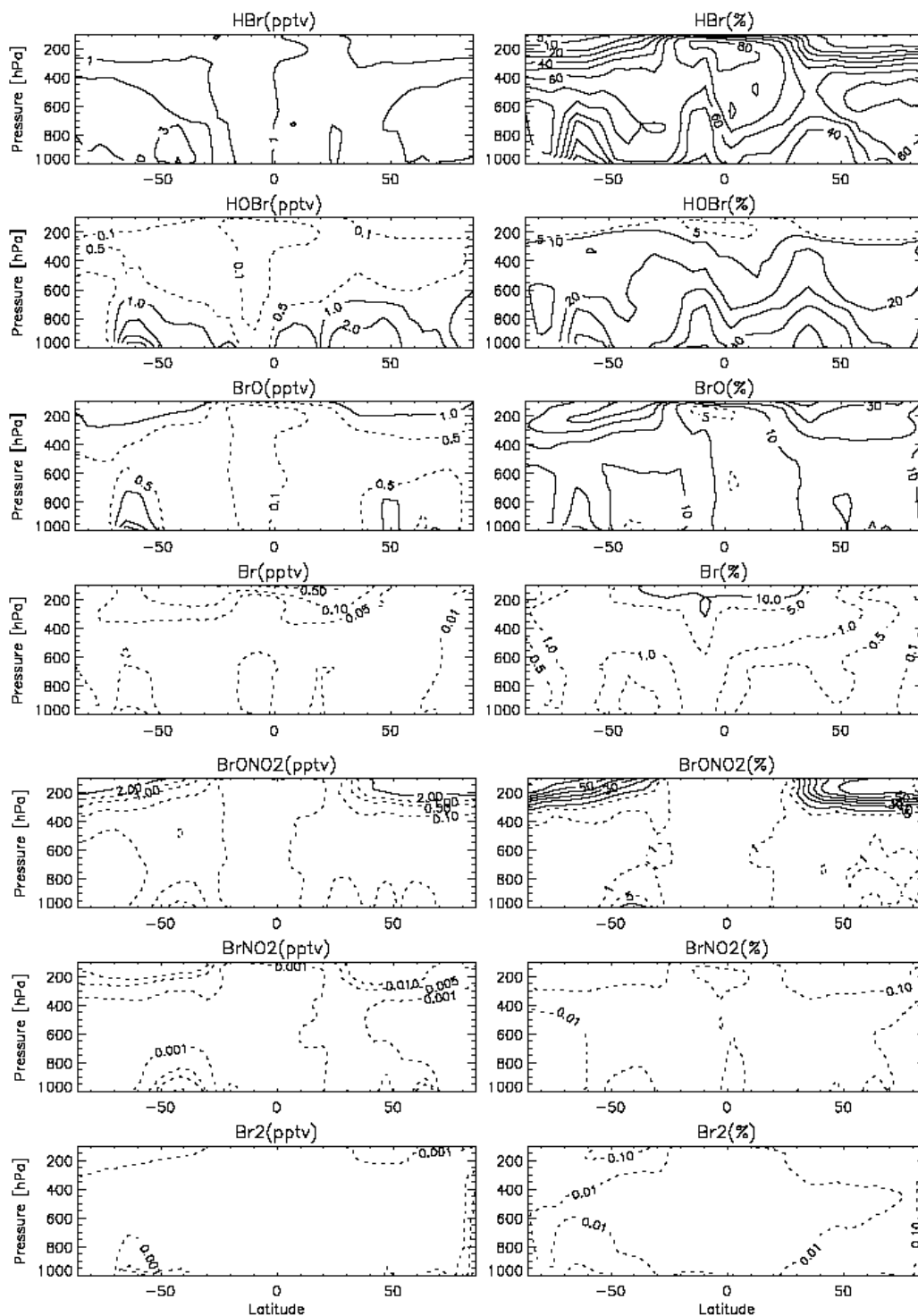


Figure 3.27: Vertical distribution of the monthly mean of the seven inorganic bromine species at 00:00h UTC in March for the simulation of Yang and co-workers [138]. The left panels are for concentrations (pptv), and the right panels are for percentages of total Br<sub>x</sub>. For the left panels, the minimum value for the various solid lines is 1 pptv increasing in steps of 1 pptv; for the right panels, the minimum value of the solid line is 10% increasing in steps of 10%.

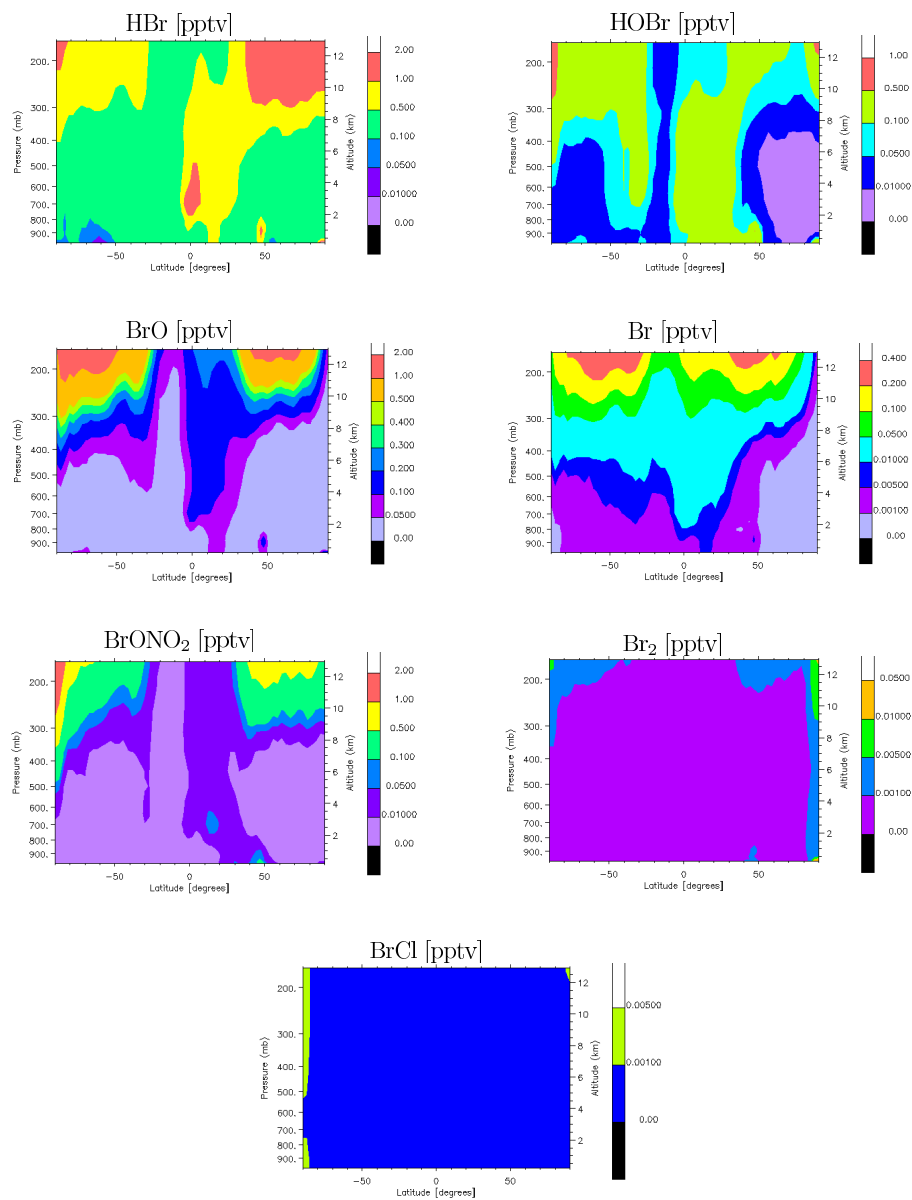


Figure 3.28: Vertical distribution of monthly mean concentrations [pptv] of the seven inorganic bromine species at 00:00 UTC in March in simulation *SS2ice*.

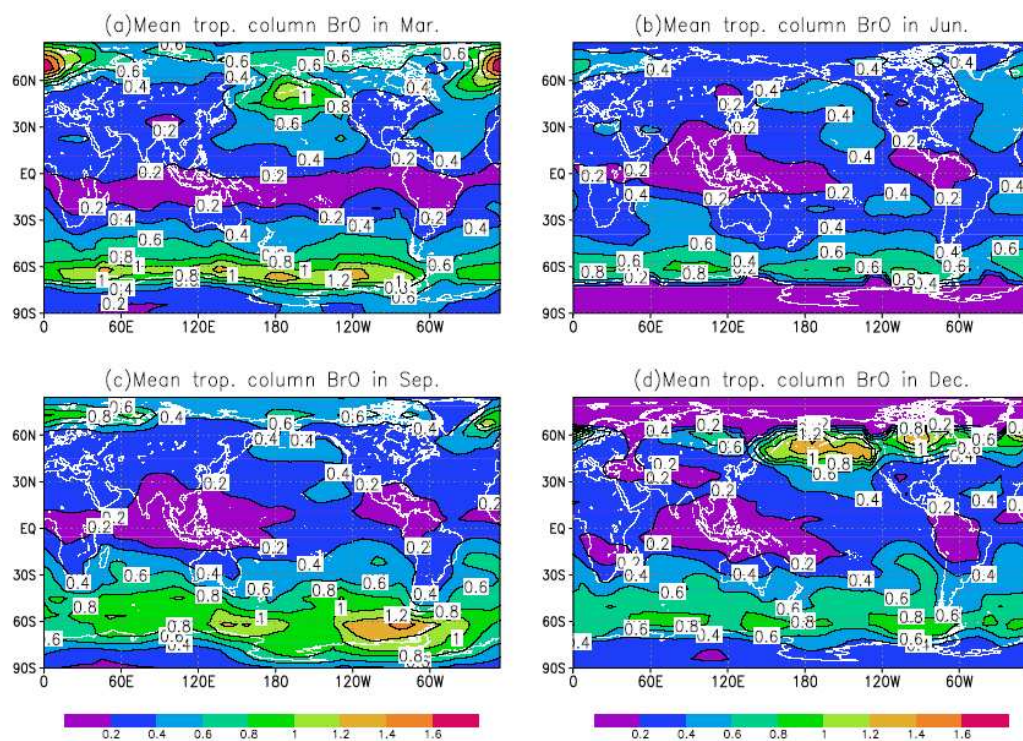


Figure 3.29: Distribution of monthly mean tropospheric column BrO [ $\times 10^{13}$  molecules/cm<sup>2</sup>] in daytime (09:00-15:00 LT) in *p*-TOMCAT [138].

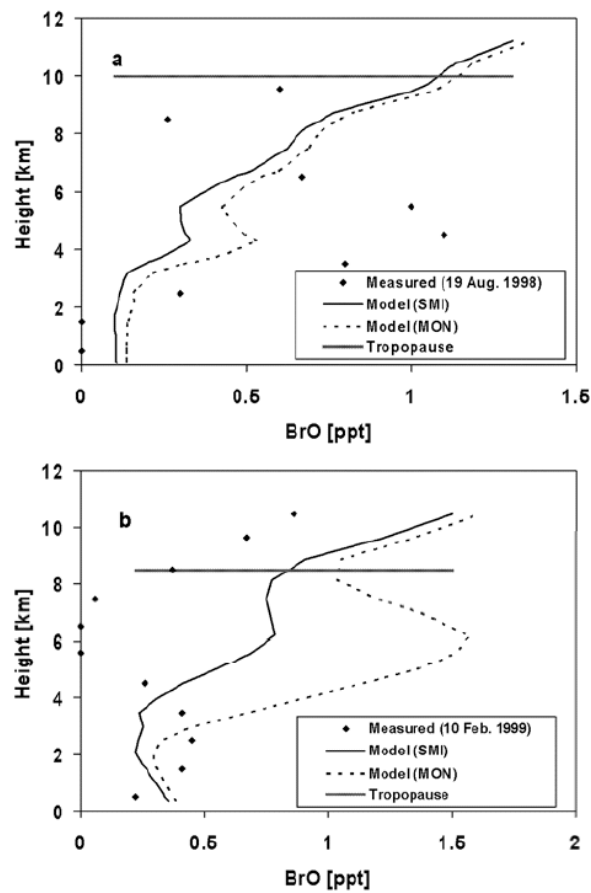


Figure 3.30: BrO profiles [pptv] resulting from measurements [35] and by Yang *et al.* [138] (*p*-TOMCAT) at Kiruna ( $68^{\circ}\text{N}$ ,  $21^{\circ}\text{E}$ ). The curve "Model(SMI)" represents the simulation including an equation for the sea salt droplet production rate that produces a bromine emission of 14 Gmol/yr; curve "Model(MON)" is the simulation with the bromine emission of 26 Gmol/yr.

### 3.6 Evaluation of ozone

Ozone is catalytically destroyed by the reactive species Br forming BrO as already mentioned in the introduction. Therefore, the occurrence of BrO in the atmosphere is considered as a sign for ozone destruction processes.

We observe in simulations *G1* and *S1*, in which the only source of bromine are VSLs and  $\text{CHBr}_3$  and bromine species atmospheric concentrations are low, that the destruction or production of ozone lead to a change in the ozone volume mixing ratio that is lower than 6% when compared with the *Base run* (Figure 3.31). This is a low value, which shows a limited importance of halocarbon emissions to the ozone concentrations in the troposphere. As we will see next, ozone is mostly affected when bromine emissions from sea ice are taken into account.

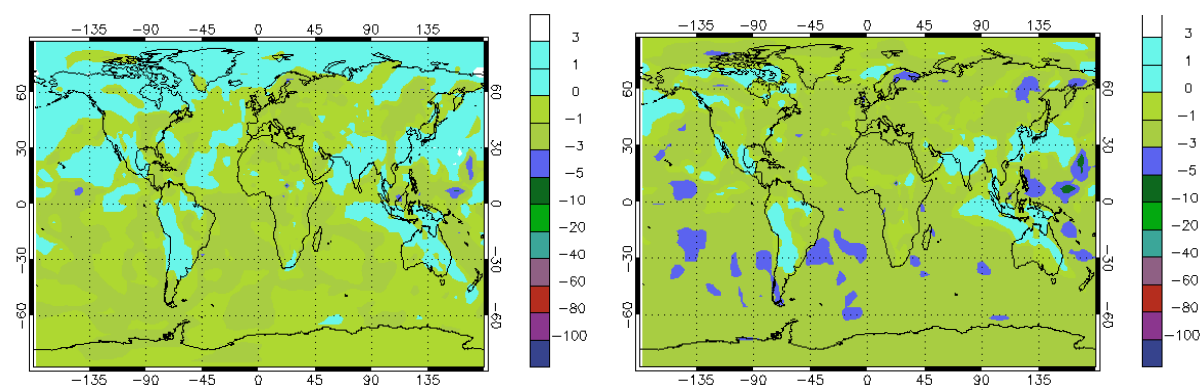


Figure 3.31: The percent difference in ozone [%] between the simulations *G1* and the *Base run* (left) and *S1* and the *Base run* (right). Monthly average for September 2000.

In Figures 3.32 to 3.35, we show distributions of BrO and ozone and the effect of the introduction of bromine chemistry into the model for the month of September, when we have important bromine emissions in both polar regions. For this purpose, we compare the *Base run* that does not contain any bromine chemistry with the simulation *SS3ice* that contains bromine chemistry combined with a scenario of high bromine emissions from the polar regions.

For September 2000, we observe in Figure 3.32 that we have regions at both poles with a BrO column density of 1.5 to 3.4 molecules/cm<sup>2</sup>, which are also the regions with the highest surface VMR, up to 17 pptv. From the graph at the top of Figure 3.33, it is confirmed that the high VTCD are due to surface BrO. These high BrO levels are correlated with ozone decreases in the order of 60 to nearly 100% relative to the *Base run* (graph at bottom right in Figures 3.32, 3.34, and 3.35).

In Figures 3.34 and 3.35, we present the polar views of BrO and ozone distributions in the North and South, and the impact on ozone VMR in these regions. The strong O<sub>3</sub> decrease of 60% to nearly 100% occurs in the regions of high Br emissions over sea ice. Since the calculated vertical column of BrO has a magnitude that is close to the column derived from space observations, we conclude that in the "real atmosphere", the high BrO concentrations are susceptible of destroying considerable amounts of ozone at high latitudes. This confirms the possible formation of a tropospheric "ozone hole". Nevertheless, the geographical sea ice distribution used in MOZART4 and the spatio-temporal variation of the bromine emissions is not necessarily realistic. In particular, the release of bromine from sea ice, as shown by

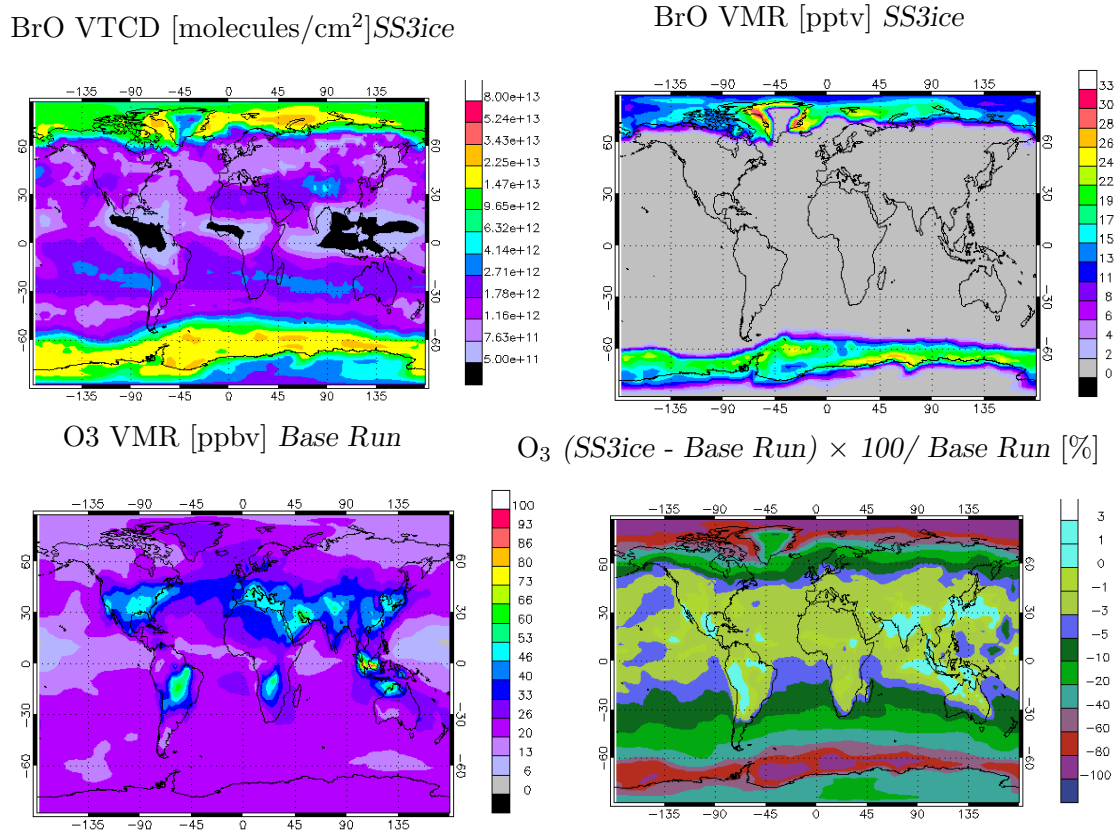


Figure 3.32: Top: vertical tropospheric column density of BrO [molecules/cm<sup>2</sup>] (left) and volume mixing ratio [pptv] of BrO at the surface (right). Bottom: volume mixing ratio [ppbv] of ozone at the surface and the percent difference in ozone between the simulations *SS3ice* and the *Base run*. Monthly average for September 2000.

ground-based measurements, is not as uniform and continuous as produced by the model, so that the high ozone depletion appear as episodic events. Therefore, the results should be considered to be more a study of the general effects of the bromine chemistry than a case study of a specific year or season.

Although our simulation is not a study of the specific year 2000, we show comparisons between time series of the ozone VMR resulting from the simulations and from observations for the year 2000 (Figure 3.36). This comparison is not straightforward, because MOZART4, like other chemical transport models, does not represent accurately the transport of chemical compounds (including ozone) in the polar regions. Simulations *SS1*, *SS1ice*, and *SS2ice* result in a small decrease of O<sub>3</sub> compared to the MOZART4 *Base run*. For simulation *SS3ice*, we observe a strong decrease in the O<sub>3</sub> VMR for the stations presented in Figure 3.36. For the stations located in Iceland, Greenland, and at the South Pole, this reduction in the O<sub>3</sub> VMR does not represent an improvement of the model results towards a better agreement with the measurements since even the *Base run* provides too low O<sub>3</sub> VMR. On the other hand, at Barrow, one of the stations where the "Polar Ozone Depletion Events" were observed first, the simulation *SS3ice* results in an ozone reduction during spring time that brings the

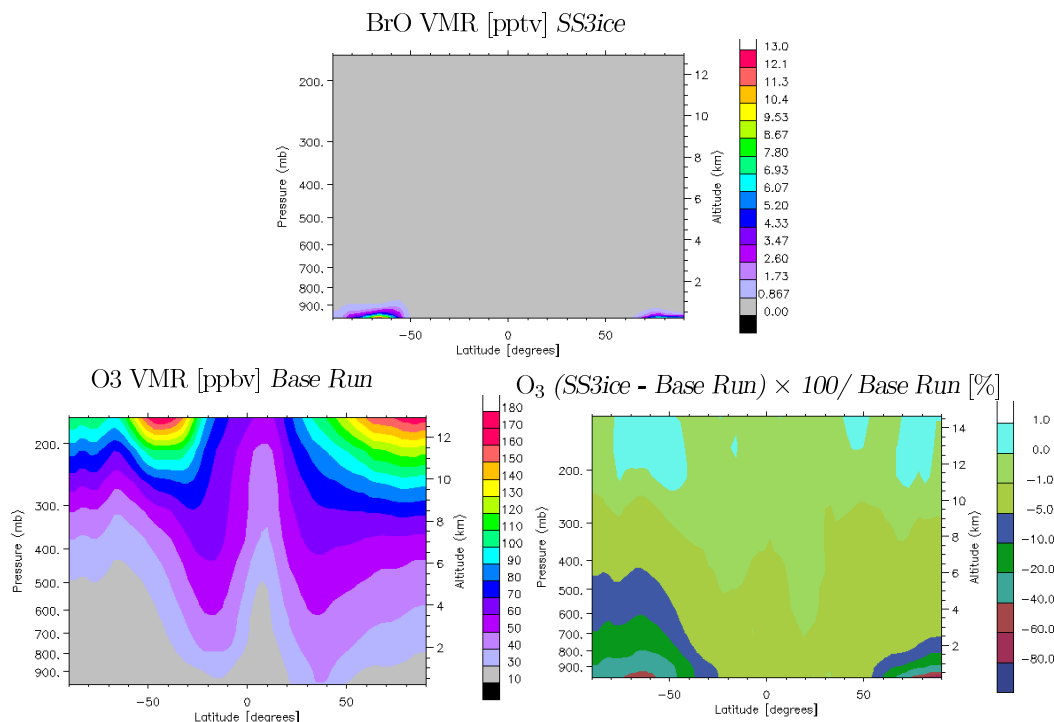


Figure 3.33: Top: zonal average of the volume mixing ratio [pptv] of BrO. Bottom: volume mixing ratio [ppbv] of ozone at the surface and the percent difference in ozone between the simulations *SS3ice* and the *Base run*. Monthly average for September 2000.

simulated  $O_3$  VMR closer to the measurements. In the simulation these low values persist during the whole summer season because of the continuous high bromine emissions from sea ice in the model. A better spatio-temporal representation of the bromine emissions would certainly lead to a better agreement of the seasonal ozone cycle at these stations and it is a subject of future research projects.

The differences in the seasonal cycle of the  $O_3$  VMR at the South Pole between the various simulations merit some further analysis. In simulations *SS1* and *SS1ice*, the Southern hemispheric winter ozone recovery from March to July does not take place to the same degree as in the observations. This is a combined effect of the overestimated bromine emissions from sea salt over open ocean in winter and of the atmospheric transport. *SS3ice* shows a better seasonal cycle compared to the observations. However, the ozone concentrations are again too low.

The impact on ozone values of the sea ice emissions is regional, as it is observed from Figure 3.37. In this figure we have the percent ozone difference between simulations *SS3ice* and *SS2ice* for September 2000. From simulation *SS2ice* to *SS3ice* the emissions from sea ice increased 36 times, from 0.5 to 18 Gmol(Br)/yr. This results in very high ozone decreases between these simulations in the regions with sea ice emissions. This effect decreases rapidly towards lower latitudes, reaching negligible values around the equator of a maximum of 1%.

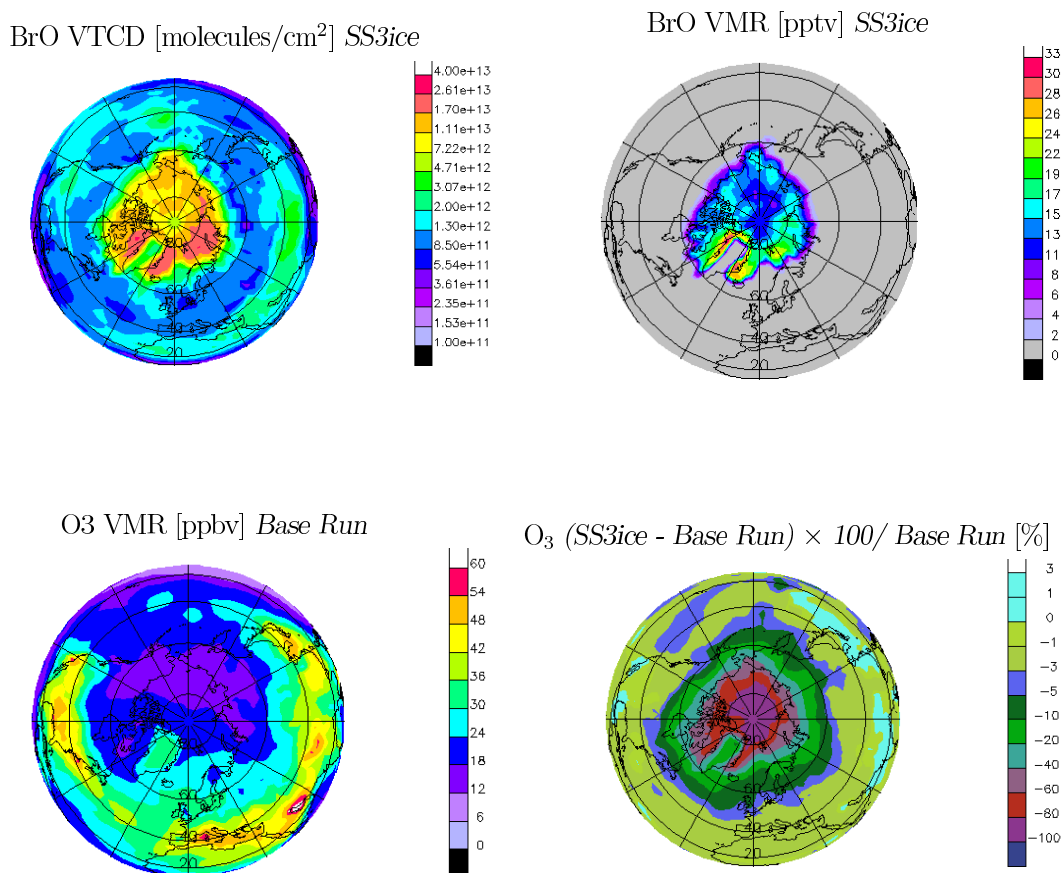


Figure 3.34: Top: vertical tropospheric column density of BrO [molecules/cm<sup>2</sup>] (left) and volume mixing ratio [pptv] of BrO at the surface (right). Bottom: volume mixing ratio [ppbv] of ozone at the surface and the percent difference in ozone between the simulations *SS3ice* and the *Base run*. Monthly average for September 2000.

### 3.7 Evaluation of $\text{NO}_x$ and $\text{HO}_x$

The bromine chemistry introduced in MOZART4 has also substantial effects on other species besides ozone. In Figure 3.38, we show the changes in the  $\text{HO}_2/\text{OH}$  and in the Leighton ratio ( $\text{NO}_2/\text{NO}$ ) between simulations *SS3ice* (high bromine emissions in the polar regions) and the *Base run* (no bromine chemistry) for the month of September 2000. In Figure 3.39, we show the sea ice mask used in the model for September, and for the same month the BrO volume mixing ratio on the surface, which is directly correlated with the catalytic ozone destruction.

We see that the  $\text{HO}_2/\text{OH}$  ratio decreases in areas with high values of BrO, except in those where heterogeneous chemistry on sea ice is most active, that is, where the sea ice fraction ( $f_{ice}$ ) is 1. Everywhere,  $\text{HO}_2$  and OH VMR decrease by around 70% compared to the *Base run*. Odd hydrogen (OH and  $\text{HO}_2$ ) decreases mainly due to the reaction:



which is a net loss for these radicals if HOBr is then destroyed by heterogeneous reactions. The heterogeneous reaction on sea ice

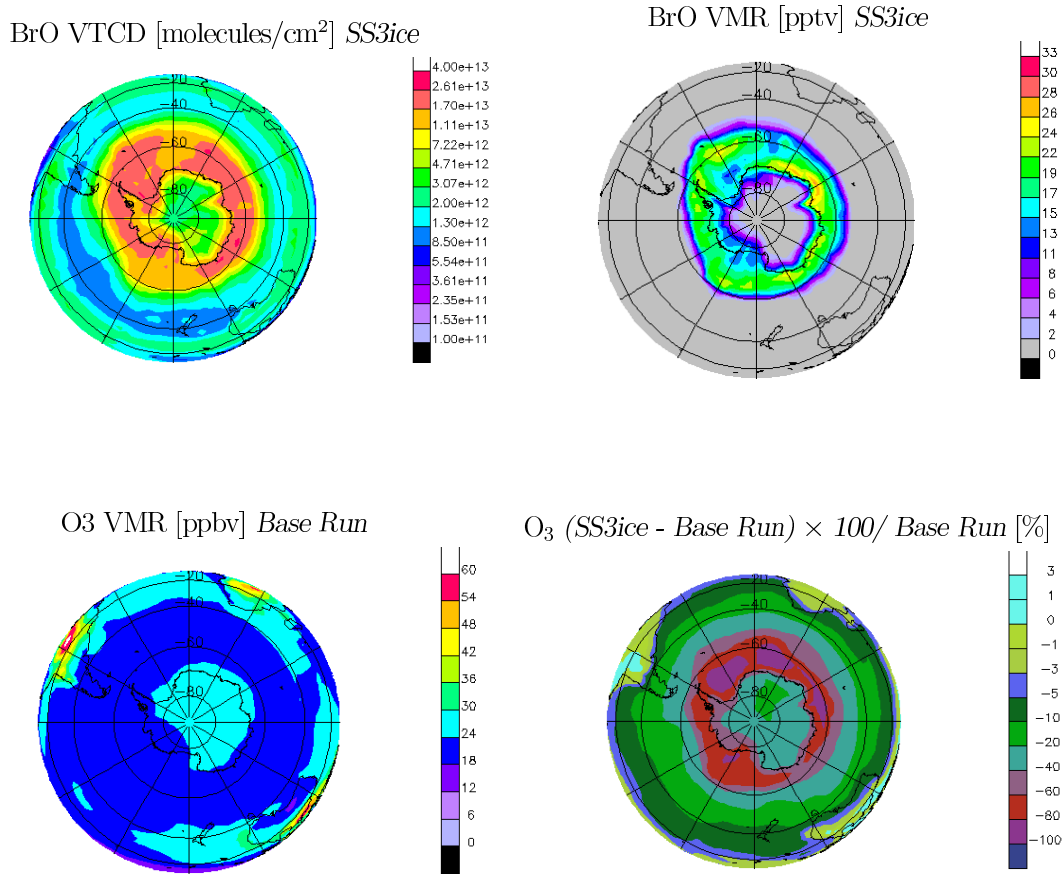


Figure 3.35: Top: vertical tropospheric column density of BrO [molecules/cm<sup>2</sup>] (left) and volume mixing ratio [pptv] of BrO at the surface over the South pole (right). Bottom: volume mixing ratio [ppbv] of ozone at the surface level and the percent difference in ozone between the simulations *SS3ice* and the *Base run*. Monthly average for September 2000.



has a high rate, especially in areas with  $f_{ice}=1$ . Also, in this reaction the OH remains in the substrate, and does not return into the atmosphere. This cycle has a positive feedback, because more production of Br<sub>2</sub> implies higher atmospheric concentrations of BrO and HOBr. The latter then reacts on the sea ice, and removes additional quantities of odd hydrogen.

In areas where equation (3.5) is less important, photolysis is the main loss of HOBr, which returns OH to the atmosphere. Therefore, the HO<sub>2</sub>/OH concentration ratio decreases in these areas.

The Leighton ratio shows the opposite tendency between simulations *SS3ice* and the *Base run*. In this case, the determining process is the heterogeneous reaction of BrONO<sub>2</sub> on sea ice. In regions where this heterogeneous reaction is more important than photolysis, the Leighton ratio decreases, because NO<sub>2</sub> is removed from the atmosphere when BrONO<sub>2</sub> reacts on sea ice. For regions where the photolysis of BrONO<sub>2</sub> is the main loss, the Leighton ratio increases. Furthermore, NO<sub>x</sub> decreases by more than 60% in regions with high ozone destruction. The connection between NO<sub>x</sub> removal by heterogeneous BrONO<sub>2</sub> and ClONO<sub>2</sub> chemistry and O<sub>3</sub> destruction was already reported by Pszenny *et al.* [90].

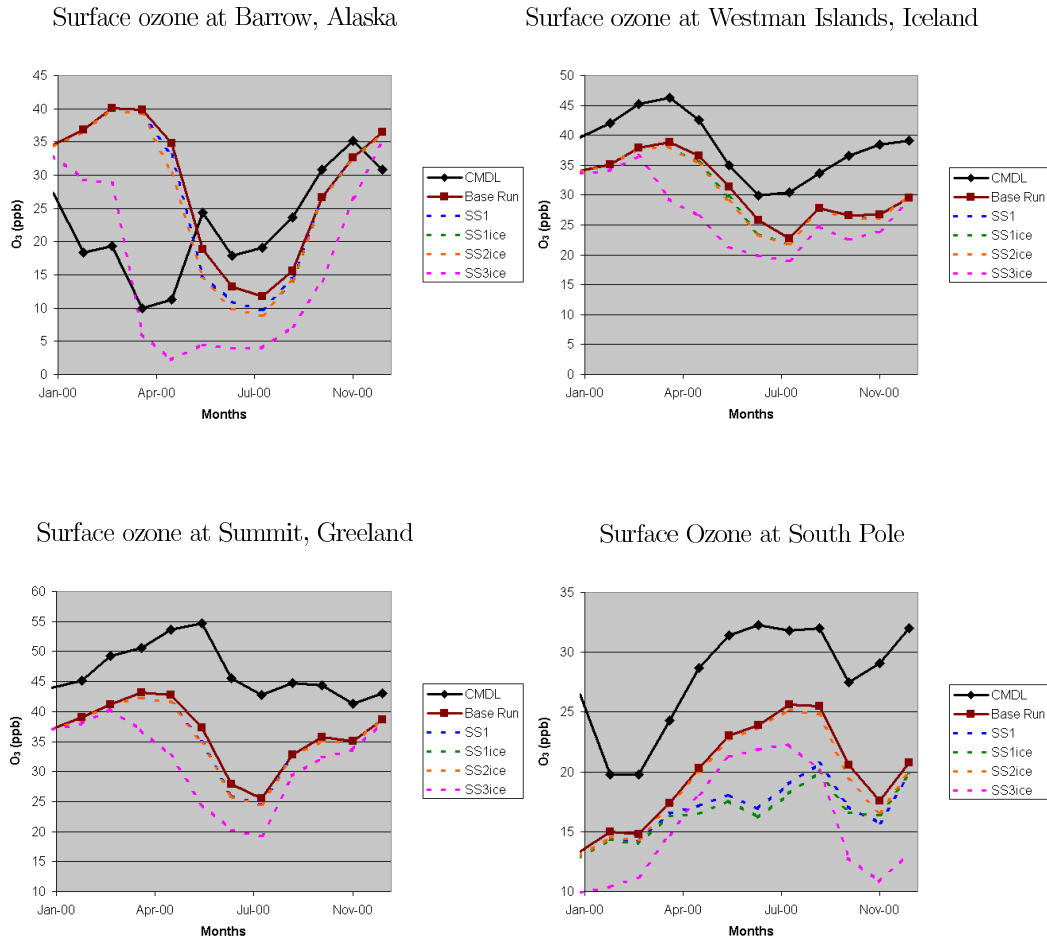


Figure 3.36: Ozone monthly averages [ppb] at four stations of the CMDL group in the year 2000, and corresponding values for MOZART4 simulations.

Platt *et al.* [88], discuss the effects of tropospheric bromine chemistry on the  $\text{HO}_2/\text{OH}$  and the Leighton ratio. They expect a decrease of the  $\text{HO}_2/\text{OH}$  and an increase of the  $\text{NO}_2/\text{NO}$ . Wernberg *et al.* [135] observed such changes in the upper troposphere. In our simulation this predicted effect occurs in regions where the heterogeneous chemistry is not dominant. This also holds for the free troposphere (see Figure 3.38).

### 3.8 Comparison with data composites

We compared the results of simulation *G1* and *Base run* with the data composites of chemical species provided by Emmons *et al.*, 2000. The first version of the data base is described in [31] and we use an updated version, in which the observations of the TOPSE, TRACE-P, and SONEX campaigns are added.

We select the TOPSE campaign for the comparison since it took place in 2000, the year corresponding to our simulation. TOPSE provided measurements from flights between Colorado (USA) and Greenland. To investigate the impacts in the tropical region we adopted the observations made during the PEM-Tropics A campaign, which is generally characterised

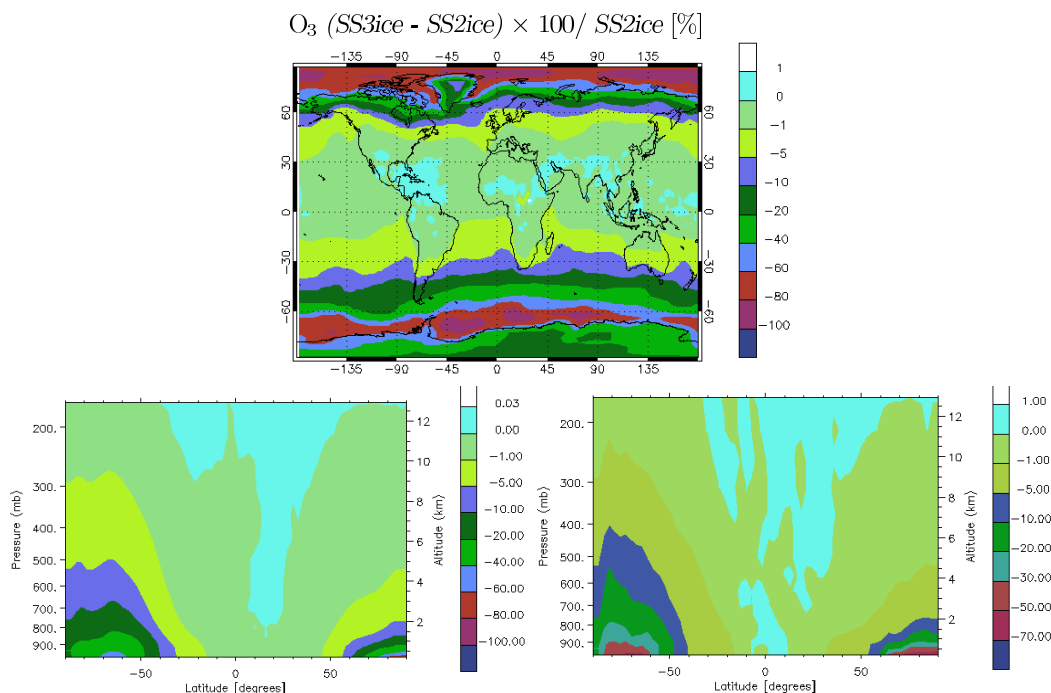


Figure 3.37: Percent ozone difference between simulations *SS3ice* and *SS2ice* in September 2000. Clockwise we have the horizontal distribution, the zonal average, and a zonal slice at  $180^\circ$

by climatological airflow patterns [31]. PEM-Tropics B is a follow-up of PEM-Tropics A, which showed similar results in the comparison. However, it might have taken place under special atmospheric conditions [95]. The SONEX campaign took place in the North Atlantic in 1997. We do not show the comparison, because in most cases the measurements are in the upper troposphere/lower stratosphere, while most of the effects we are investigating are below this altitude. Three campaigns, whose data were available, took place in East Asia. However, normally they are designed to study the Asian outflow. It would be advantageous for us to have a campaign with airflow mainly from the ocean. That is the case for PEM-West A, however it seems that the circulation patterns during this campaign were considered to be not representative of climatological values [31]. Moreover, this campaign is rather old (it took place in 1991), therefore it is expectable that the emissions prescribed in the model are not appropriate.

In simulation *G1* the only bromine source are halocarbons (VSLs+CHBr<sub>3</sub>). However, generally speaking, the comparison with TOPSE observations shows that the inclusion of the bromine chemistry into MOZART4 improves the performance of the model with respect to several ozone precursors. For the TOPSE campaign, we show the VMR profiles of several species at three locations (Figure 3.40 to 3.43): Thule in Greenland as an Arctic station, Boulder (USA) a continental station in the midlatitudes, and Churchill at the Hudson Bay in the higher midlatitudes, for February and May.

In particular, we observe that the species associated with the oxidation capacity of the atmosphere (CH<sub>3</sub>OOH, PAN, H<sub>2</sub>O<sub>2</sub>) sometimes have calculated VMR which considerably exceed the measured ones in the *Base run*, e.g., 80% for CH<sub>3</sub>OOH at Churchill in May, 130% at Thule in February, and 160% for H<sub>2</sub>O<sub>2</sub> at Boulder in February. These overpredictions are

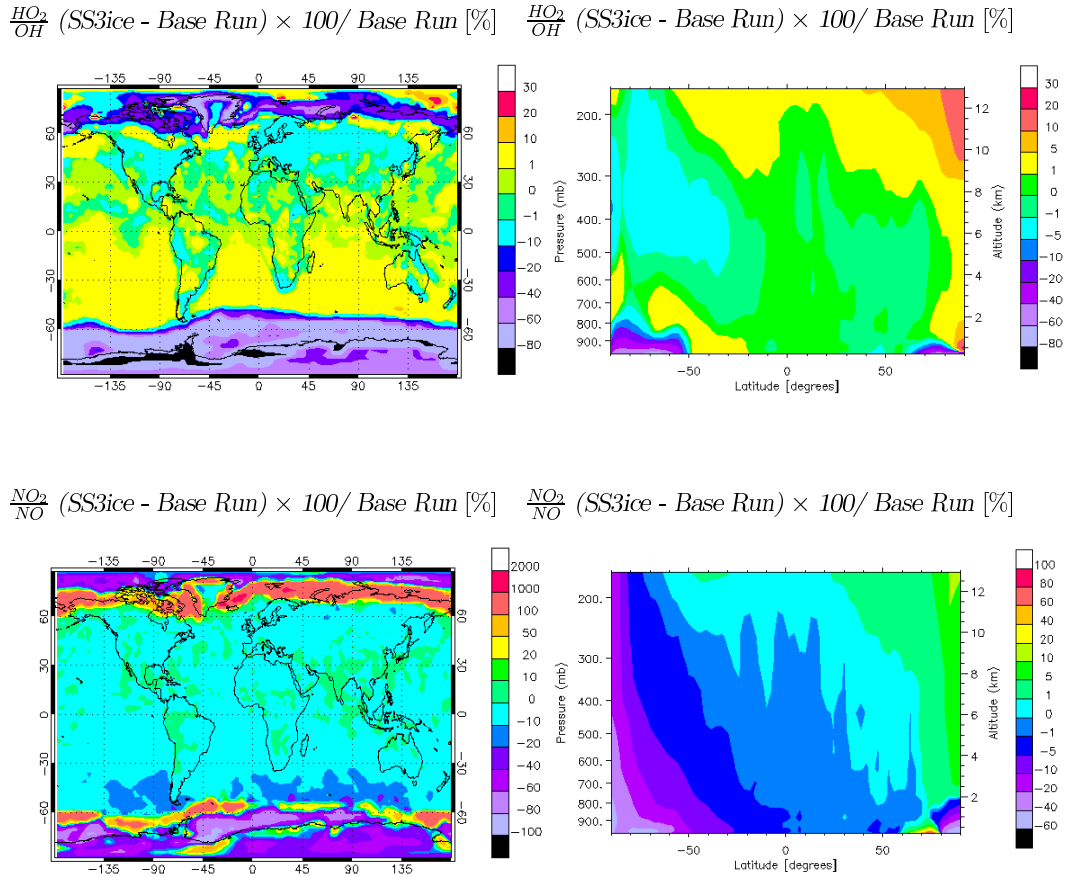


Figure 3.38: Horizontal distribution and zonal average of the percentage difference [%] between simulations *SS3ice* and *Base run* of the ratios  $NO_2/NO$  and  $HO_2/OH$  for September 2000.

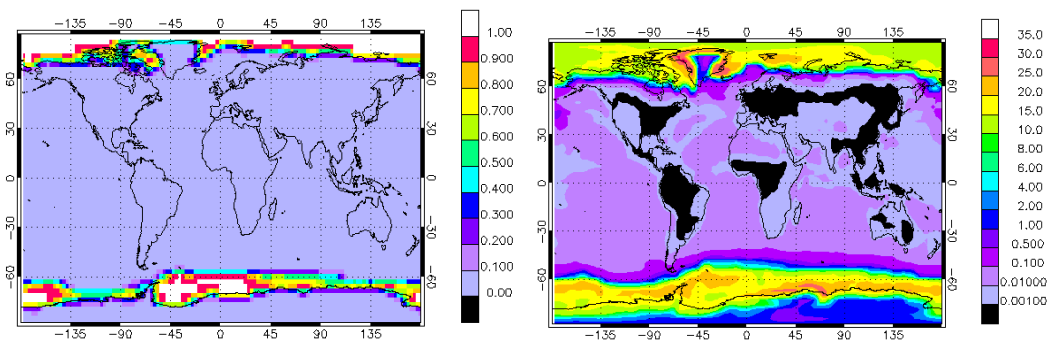


Figure 3.39: Sea ice fraction in MOZART4 [0 to 1] and the distribution of BrO VMR [pptv] in simulation *SS3ice* at the surface for September 2000.

reduced to 40%, 70%, and 8% in the aforementioned cases in the simulations with bromine chemistry and bromine emissions from VLS (*G1*). Species which become oxidized in the atmosphere are normally underpredicted in the *Base run*, in particular ethane, propane and CO. Ethane and CO VMR are 50% too low at Thule in May. This underprediction is reduced to almost zero and roughly 20% by the inclusion of the bromine chemistry although

deficiencies in the form of the profiles remain. At some locations, the *Base run* provides too low VMR for PAN (by 50% at Churchill in May) or too high formaldehyde VMR (by 50% at Thule in May). These deviations are reduced to almost zero by the inclusion of bromine chemistry in the model.

PEM-Tropics A provides measurements near several Pacific islands, where halocarbon emissions are stronger. In Figures 3.44 and 3.45, we show the VMR profiles for the PEM-Tropics A campaign. The measurements were performed from August-September 1996. We selected the profiles at the Easter Island, Fiji, and Hawaii, which are all three islands in the Pacific Ocean.

We observe that when bromine chemistry influences the concentration of other chemical species, they usually improve the performance of the model. That is the case for  $C_2H_6$  and CO at all three locations,  $C_3H_8$  at Fiji and especially Hawaii, and for PAN in the upper troposphere, at Easter Island and Fiji. The percentage differences between the results of the simulation *G1* and the *Base run* are lower than for TOPSE, but still important. Maybe the effects observed are lower, because the measurements were performed in 1996 and the simulations were done for 2000.

We conclude that VSLs have a substantial effect on several precursors of ozone and on the oxidising capacity of the troposphere, even if their impact on ozone itself is limited (less than 6% compared with the *Base run*).

When comparing the measurements with the other simulations, we observe that the introduction of heterogeneous chemistry on sulphate (simulation *S1*) results in slight effects, mainly observable in the TOPSE campaign. The highest effects are on  $H_2O_2$  (17% in April),  $C_3H_8$  (14% in summer), and  $CH_3OOH$  (4% in April)<sup>3</sup>. However, the inclusion of sulphate chemistry leads usually to a worse agreement with the observations. When the sea ice emissions are introduced the tendency between *G1* and *S1* is reversed.

The introduction of sea salt emissions does not produce any observable effect on the chemical species analysed. The introduction of sea ice emissions produces strong effects in the boundary layer for PAN and  $CH_2O$ , with decreases up to 70% compared with *G1*. Also ozone is affected by a 120% decrease (relative to the measurement) down to a VMR close to zero), which represents a substantial improvement with respect to measurements. The effect increases from the beginning of the campaign in February to the end in May. This matches well with the fact that February is the beginning of the polar day period in the Northern hemisphere and consequently the beginning of the emissions from sea ice, while we can see the cumulative effect of three months of continued emissions on the chemistry in May.

We note that an important impact on ozone is only observed when very high emissions exist, like the ones from sea ice. This impact is regional as are the emissions. However, VSLs has an important global impact on the oxidation capacity of the troposphere, which has the tendency to decrease when the bromine chemistry is included.

---

<sup>3</sup>The difference is between simulation *S1* and *G1*, but normed by the observed volume mixing ratio, so that the percentage is a relative difference with respect to the observation.

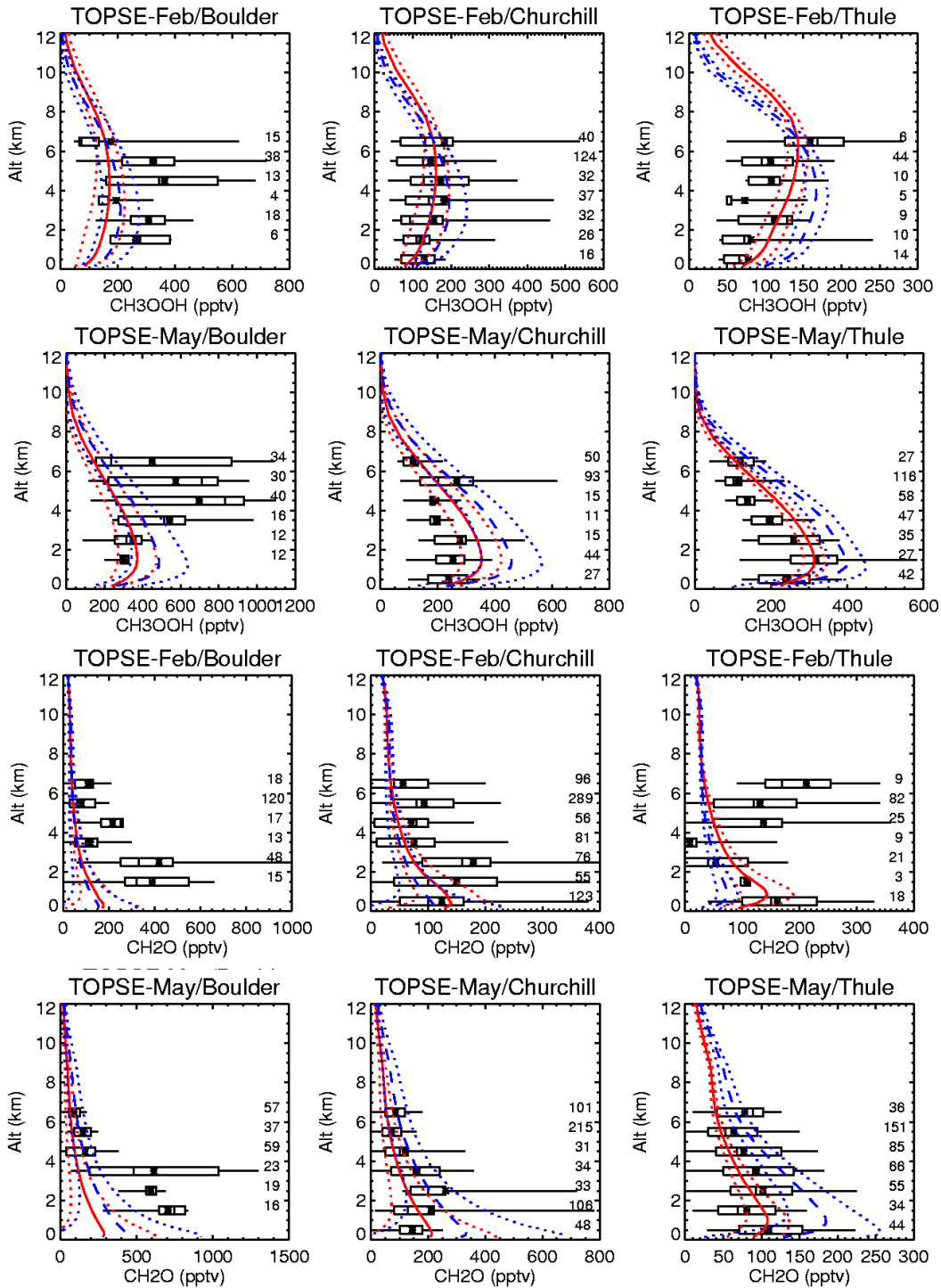


Figure 3.40: Comparison of methyl hydroperoxide (six upper panels) and formaldehyde (six lower panels) VMR profiles for the simulation *G1* (red) and the *Base run* (blue) with measurements from the TOPSE campaign (black). We present the profiles obtained at Boulder (left), Churchill (middle), and Thule (right) for the months of February and May. Boxes and whiskers indicate the central 50% and 90% of the observations, the vertical bar representing the median, the star indicating the mean. The dotted lines represent the standard deviation in time for the simulations.

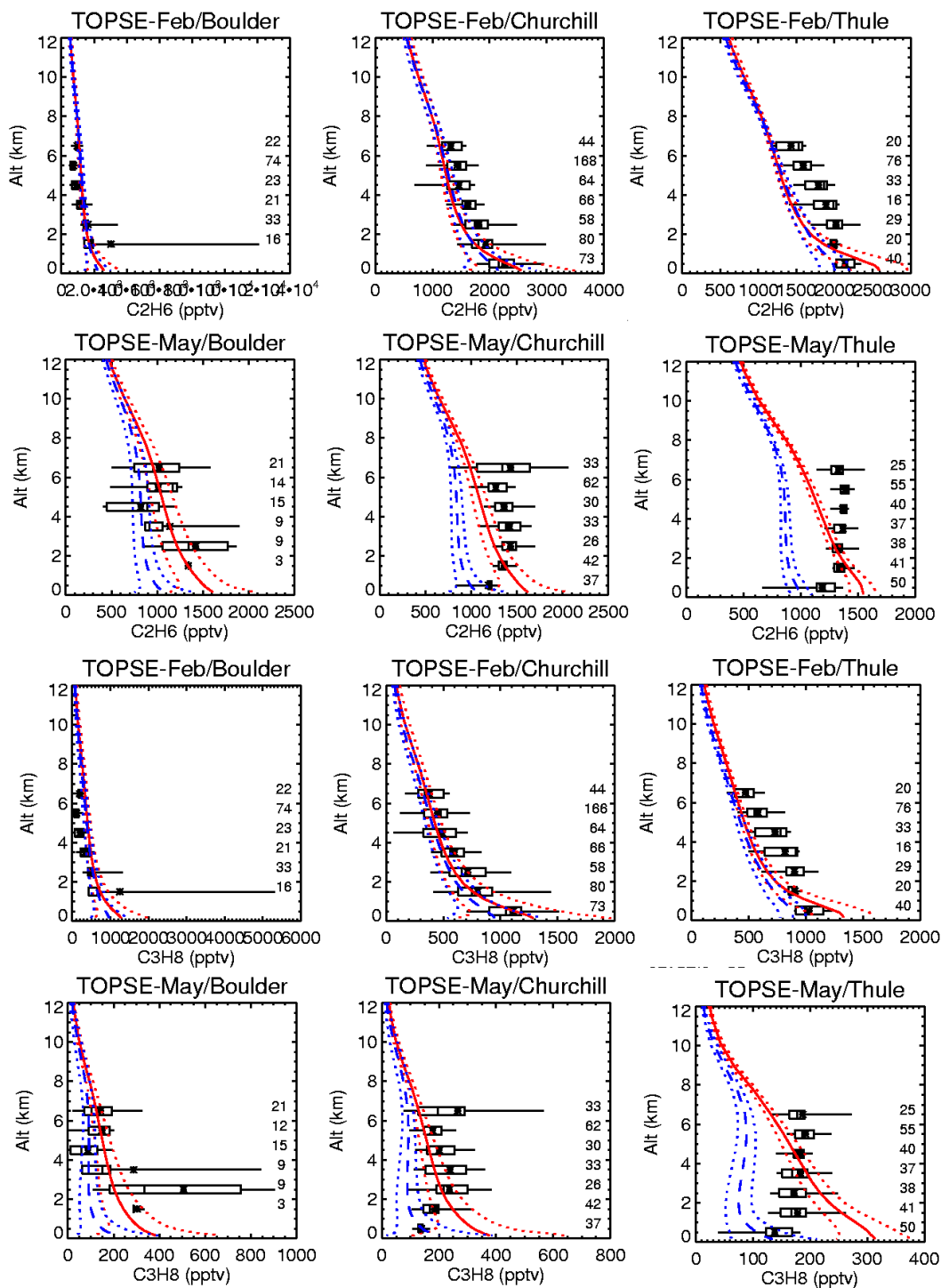


Figure 3.41: Comparison of ethane (six upper panels) and propane (six lower panels) VMR profiles for the simulation *G1* (red) and the *Base run* (blue) with measurements from the TOPSE campaign (black). We present the profiles obtained at Boulder (left), Churchill (middle), and Thule (right) for the months of February and May. For further explanations, see Fig. 3.40.

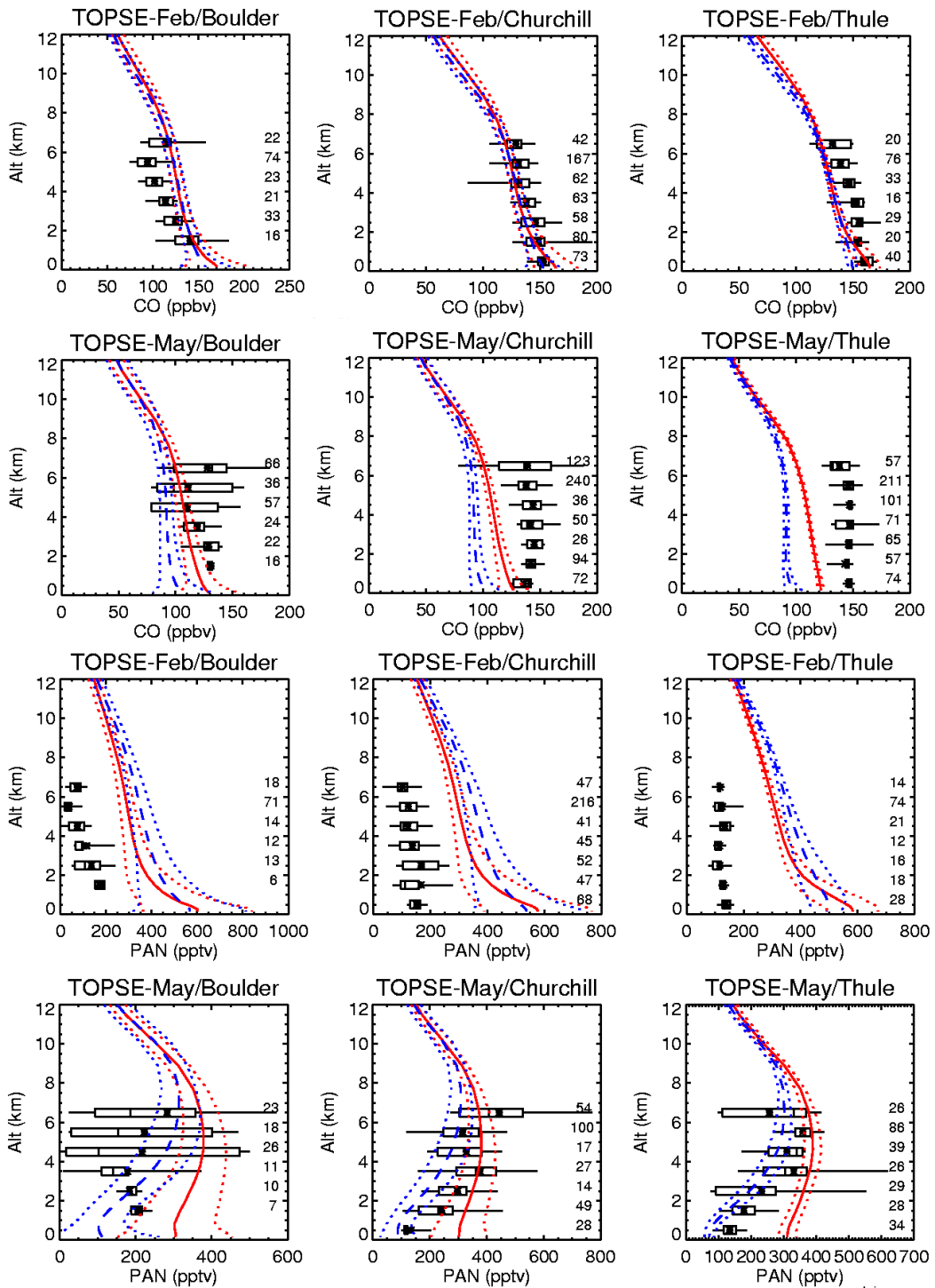


Figure 3.42: Comparison of carbon monoxide (six upper panels) and PAN (six lower panels) VMR profiles for the simulation *G1* (red) and the *Base run* (blue) with measurements from the TOPSE campaign (black). We present the profiles obtained at Boulder (left), Churchill (middle), and Thule (right) for the months of February and May. For further explanations, see Fig. 3.40.

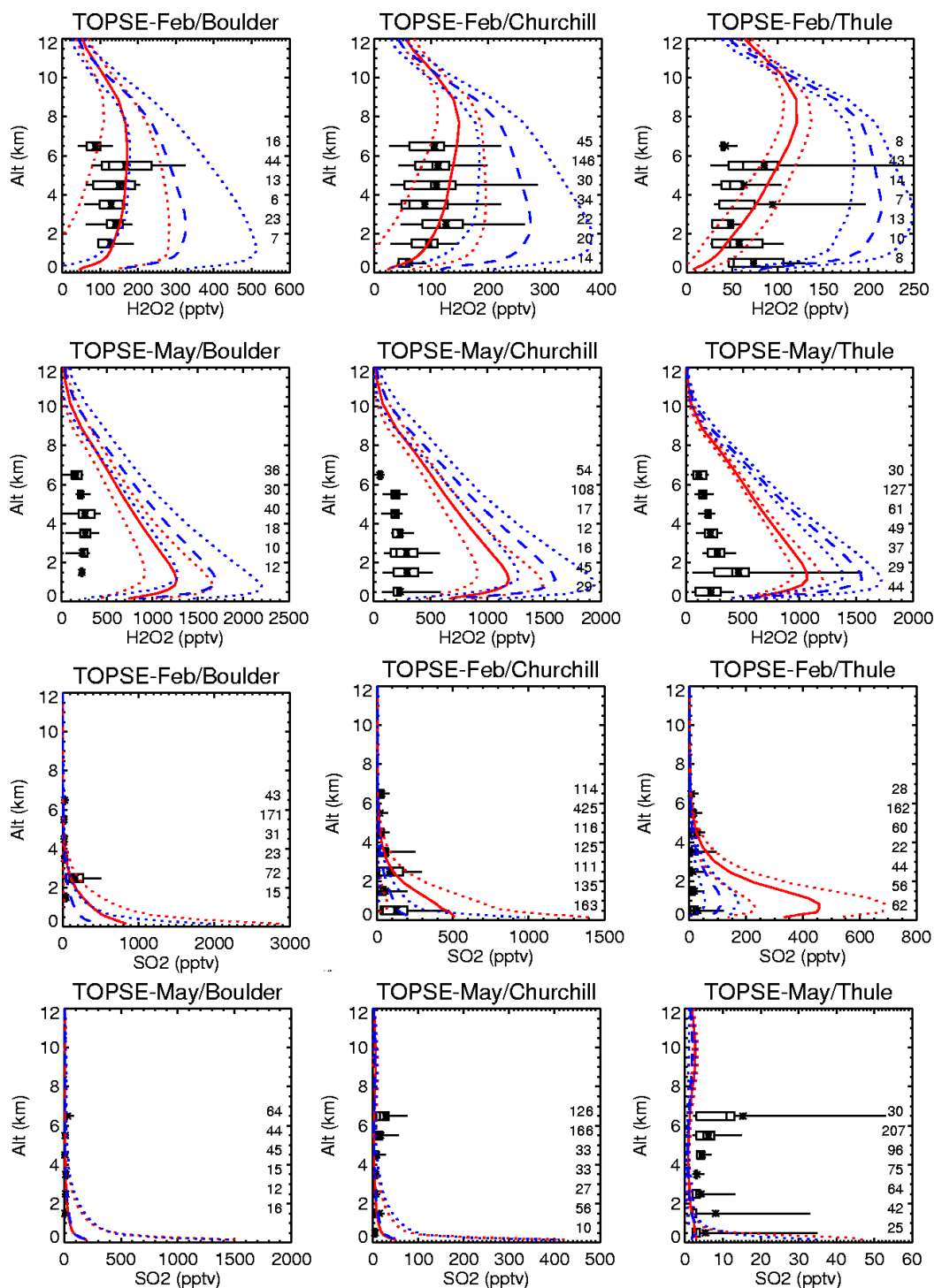


Figure 3.43: Comparison of  $\text{H}_2\text{O}_2$  (six upper panels) and  $\text{SO}_2$  (six lower panels) VMR profiles for the simulation *G1* (red) and the *Base run* (blue) with measurements from the TOPSE campaign (black). We present the profiles obtained at Boulder (left), Churchill (middle), and Thule (right) for the months of February and May. For further explanations, see Fig. 3.40.

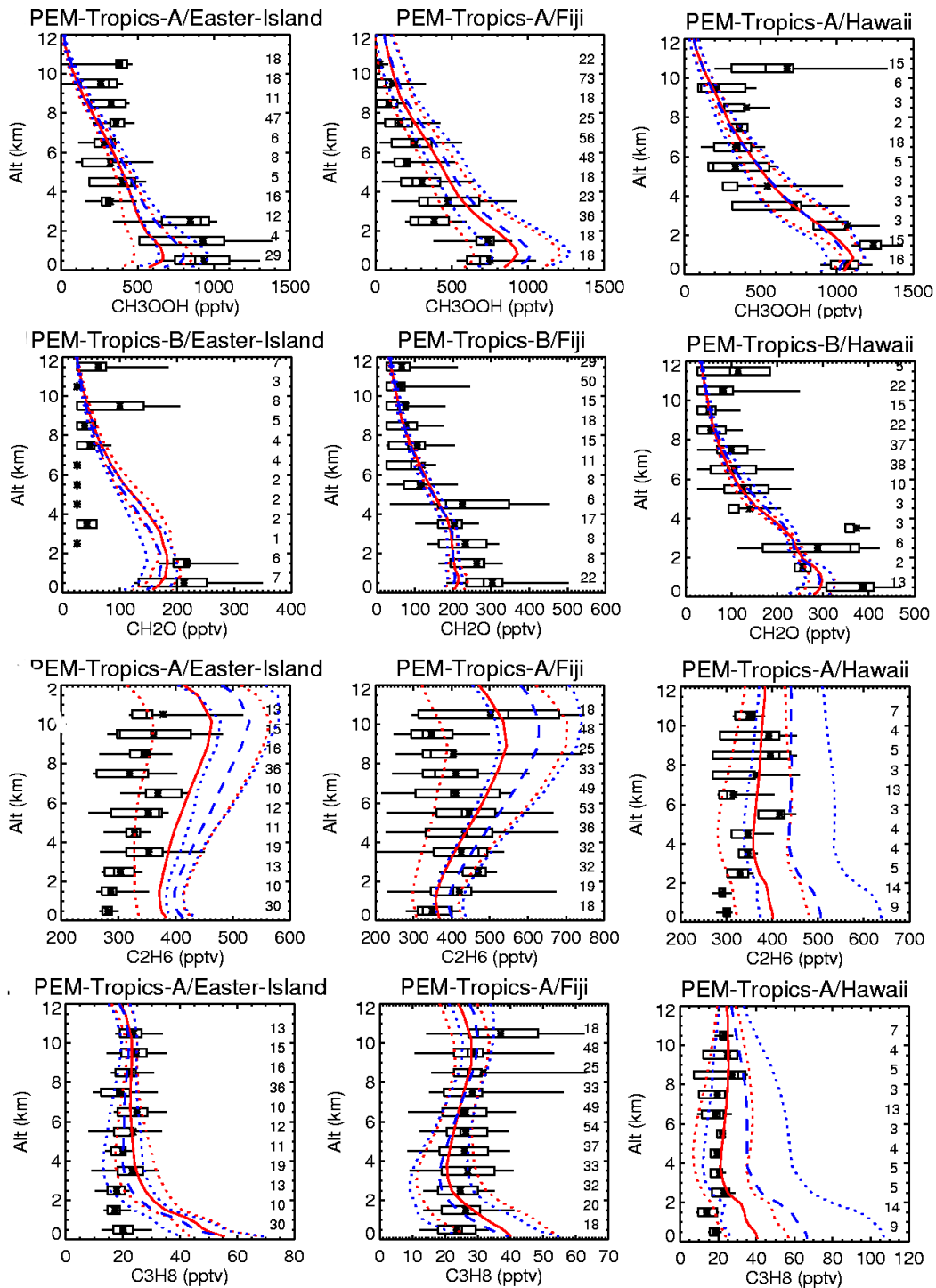


Figure 3.44: Comparison of (from top to bottom) methyl hydroperoxide, formaldehyde, ethane, and propane VMR profiles for the simulation *G1* (red) and the *Base run* (blue) with measurements from the PEM-Tropics A campaign (black), with the exception of formaldehyde, where we only have data from PEM-Tropics B. We present the profiles obtained at Easter Island (left), Fiji (middle), and Hawaii (right). For further explanations, see Fig. 3.40.

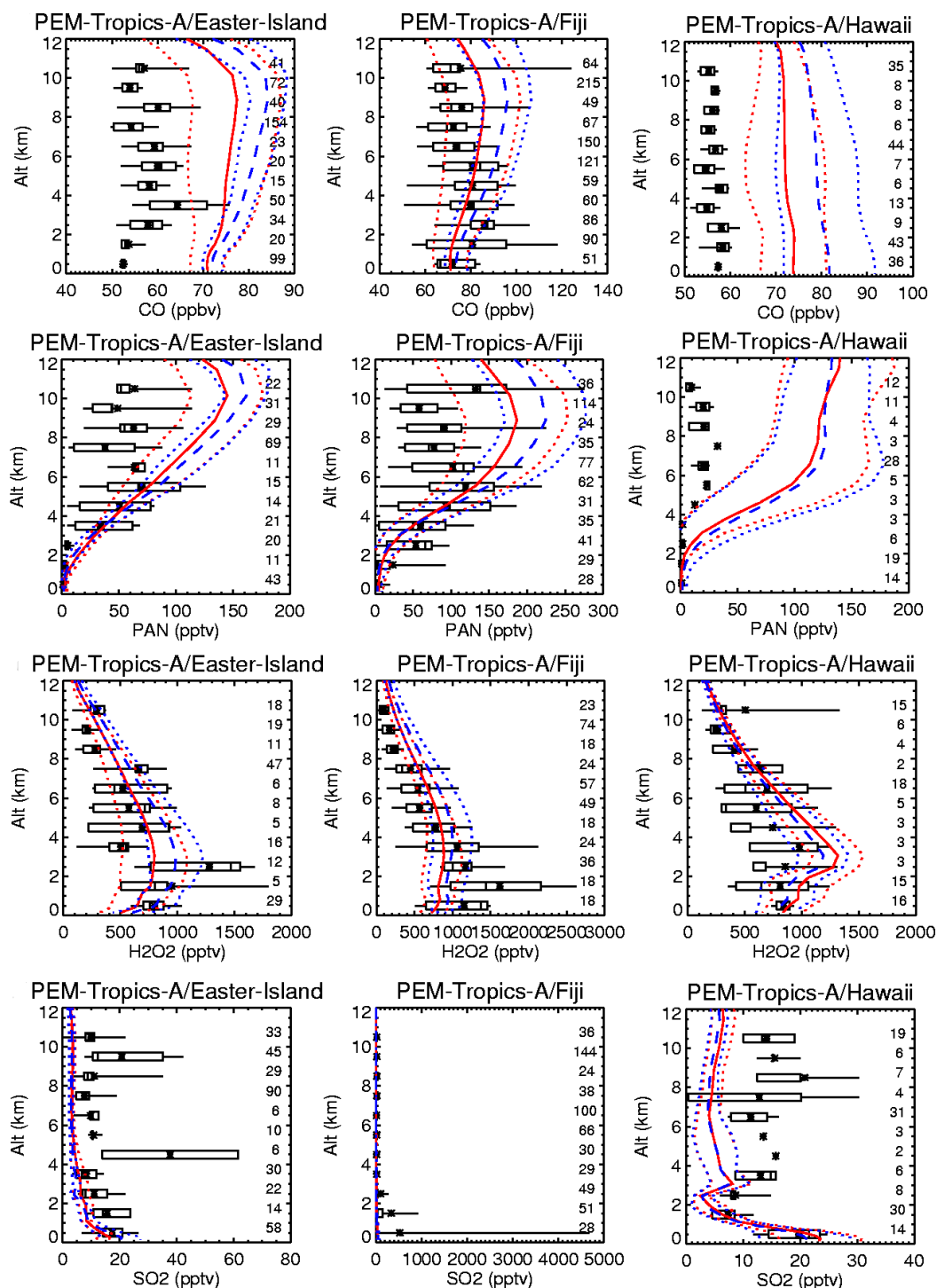


Figure 3.45: Comparison of (from top to bottom) monoxide carbon, PAN, H<sub>2</sub>O<sub>2</sub>, and SO<sub>2</sub> VMR profiles for the simulation *G1* (red) and the *Base run* (blue) with measurements from the PEM-Tropics A campaign (black). We present the profiles obtained at Easter Island (left), Fiji (middle), and Hawaii (right). For further explanations, see Fig. 3.40.

## Chapter 4

# Summary

The aim of this work was to describe the global impact of halogenated species on tropospheric ozone ( $O_3$ ). Halogenated species are the focus of this study, because they are involved in the ozone destruction in the atmosphere. Despite the relatively small concentration of halogenated species in the atmosphere, their ozone destruction potential is high, because of the catalytic mechanism of ozone depletion that regenerates halogenated species making them available for further reactions with ozone.

Numerical models that simulate tropospheric ozone show important discrepancies with observations. It has been postulated that one of the reasons for these discrepancies is the absence of halogen chemistry in those models [67, 128, 138, 97].

The halogens chlorine (Cl), bromine (Br), and iodine (I) are potentially important for the ozone depletion in the troposphere. In our study, we decided to focus on bromine chemistry, because it has an efficiency for ozone depletion in the troposphere, which is 40% higher than that of chlorine, and compared to iodine the global sources of bromine are considerably larger. Therefore, the global impact of this compound is expected to be higher.

The most important sources of bromine in the troposphere are bromocarbons, sea salt aerosols, and frost flowers. Bromocarbons are important contributors to the bromine burden in the troposphere. They are mainly produced in the oceans, in locations with high primary biological productivity. Bromine production from sea salt is, obviously, limited to the ocean. Moreover, due to its fast removal by sedimentation and wet scavenging, its impact is limited to the marine boundary layer. Frost flowers are ice crystals formed from sea water, that grow over young sea ice, on frozen leads and polynyas. They usually last some days, and are a very important source of bromine in the polar atmosphere, because of their very high content in bromide. This global study has the advantage to allow the assessment of the relative importance of the various sources. From our work, we found that the bromine sources are the highest in the polar regions. Their effect on ozone is regional. The emissions from bromocarbons have an important effect on other chemical species, ozone precursors, PAN,  $H_2O_2$ , etc., with a much wider geographical influence. Furthermore, the bromine of organic origin is an initiator of inorganic bromine emissions. Sea salt bromine emissions have very small effects on the tropospheric composition in our simulations. However, sea salt emissions are probably too low in our simulations. All the sources are essential to explain the tropospheric background BrO concentrations of 1-2 ppt derived from observations [49, 74, 103]. The inclusion of the bromine chemistry in MOZART4 improved clearly its ability to produce realistic distributions of several chemical compounds.

To address the aim of this work, we use the three-dimensional global chemistry trans-

port model MOZART4 designed to simulate tropospheric ozone and its precursors. We had to develop a new version of MOZART4 that is expanded by bromine chemistry comprising photolysis, gas-phase reactions, and reactions on aerosol surfaces of sulphate,  $\text{NH}_4\text{NO}_3$ , organic carbon, and sea salt. Dry and wet deposition are also included. In terms of emissions, maps with the oceanic emissions of very short lived species (VSLs) of bromocarbons were developed and inserted in the list of files read by the model during a simulation. Inorganic bromine emissions are calculated interactively as far as possible. A first approach was made to parameterise the emissions from sea salt and sea ice resulting from heterogeneous reactions of the gas-phase species  $\text{BrONO}_2$  and  $\text{HOBr}$  on the surface substrates, which lead to the production of  $\text{Br}_2$  and  $\text{BrCl}$ . The yield of these two products depends on the pH of the reaction site. A calculation of the pH is difficult, but the implementation is such that it is possible to introduce a geographically varying yield. Each single process was evaluated as described in chapter 2 of this document.

The expanded version of MOZART4 is stable and can be used for long term runs. We performed 2.5 year simulations and used one year for the analysis, because bromine chemistry is a fast process. In the T42 resolution, a simulation of one year was normally executed in one real day on the bluevista machine<sup>1</sup> at NCAR.

In the following table, we summarise the simulations performed with MOZART4, the results of which are analysed in this study.

Simulation	Description
<i>Base run</i>	the standard MOZART4, without bromine chemistry.
<i>G1</i>	Bromine chemistry, including the gas phase and photolysis reactions. Emissions from short-lived halocarbons.
<i>S1</i>	<i>G1</i> + heterogeneous chemistry on sulphate and other background particles.
<i>SS1</i>	<i>S1</i> + heterogeneous chemistry on sea salt over open ocean (no limitation of pH).
<i>SS1ice</i>	<i>SS1</i> + parameterised emissions from sea ice in the polar regions (proxy for all sea salt sources in those regions including frost flowers).
<i>SS2ice</i>	<i>SS1ice</i> + heterogeneous reactions on sea salt over open ocean with pH limitation.
<i>SS3ice</i>	<i>SS2ice</i> + heterogeneous reaction rates on sea ice $100 \times$ higher than in <i>SS2ice</i> .

The simulations showed that the bromine production from the VSLs (7.3 Gmol (Br)/yr) results in  $\text{BrO}$  vertical tropospheric column density (VTCD) in the order of  $10^{10}$  molecules/cm<sup>2</sup> at the equatorial region. Further away, the concentrations are lower, resulting in a global tropospheric mean mixing ratio of  $10^{-3}$  pptv of  $\text{BrO}$ . This translates into ozone changes up to 6% (relative to a simulation without bromine chemistry).

The introduction of the production of bromine from airborne sea salt increases the  $\text{BrO}$  VTCD up to the order of  $10^{13}$  molecules/cm<sup>2</sup>. Such values have been observed in the troposphere using the DOAS technique. However, these high calculated values are located in a belt around 58°S, which is not consistent with the observations. Instead, the  $\text{BrO}$  VTCD of  $10^{13}$  molecules/cm<sup>2</sup> detected by satellites are located in the polar regions. In simulations

<sup>1</sup>Bluevista is a supercomputer with an IBM clustered Symmetric MultiProcessing system based on the POWER5 processor.

*SS1* and *SS1ice* (see table before), we assumed that the sea salt particles are slightly acid all over the globe, even in the clean Southern hemisphere, where less acidifying agents occur. The acid pH means that the bromide in the aqueous phase is available for oxidation and forms bromine species that will be released from the particle into the gas phase. In simulation *SS2ice*, we assumed that the particles maintained their original pH in the Southern hemisphere and changed the reaction yields accordingly. The high values in the 58°S belt decreased to values in the order of  $10^{12}$  molecules/cm<sup>2</sup>. The change in this sensitivity simulation is probably too drastic. However, we would need to know the exact pH of the particles to improve the parameterisation of bromine emission from sea salt over the open ocean.

In order to capture the highest BrO VTCD in the polar regions as shown in the satellite retrievals, we implemented a parameterization of bromine emission from sea ice in the polar regions. It was intended as a proxy for all sea salt sources in those regions: sea salt deposited on the snowpack or included in it and sea ice, including frost flowers. We used the original sea ice distribution of MOZART4 in the simulations. *SS1ice*, as already mentioned, shows too high emissions from the sea salt over open ocean, which results in wrong BrO VTCD distribution globally. Simulation *SS2ice* results are generally 10 times lower than the satellite retrievals in the regions where a comparison is possible. In simulation *SS3ice*, we increased the production rates of bromine from sea ice 100 times compared to *SS2ice*. The results showed a distribution of BrO VTCD that resembles GOME retrievals and the highest values are in the order of  $10^{13}$  molecules/cm<sup>2</sup>. In the set of simulations performed for this work, we think that simulation *SS3ice* has the results that are closest to the observed reality. To improve the performance of the model, we need more ground-based measurements.

In simulation *SS3ice*, the impact on ozone in the regions with BrO VTCDs of  $10^{13}$  molecules/cm<sup>2</sup> was a decrease in VMRs relatively to the *Base run* in the range of 40-100%. Thus, we would expect that over the polar regions where the satellites "detect" the high VTCD, the ozone loss would be of the same magnitude.

The total amount of bromine produced from sea salt over the open ocean in each simulation differed extremely. In simulation *SS1*, the emission was 5 Gmol (Br)/yr. In simulation *SS1ice*, in which we added the sea ice bromine production to *SS1*, the emissions rose to 8.4 Gmol (Br)/yr. This is because the added source results in a higher atmospheric concentration of HOBr and BrONO<sub>2</sub> and, therefore, a higher production of bromine on airborne sea salt. In simulation *SS2ice*, the production of bromine from sea salt is curtailed in the Southern hemisphere, resulting in an emission of 1.3 Gmol Br/yr. Interestingly, the decrease from *SS1ice* to *SS2ice* is extreme due to feedback processes and shows the sensitivity of the emissions to pH and correspondingly to the yield of the heterogeneous reactions. In *SS3ice* the emission from sea salt doubled compared to *SS2ice* due to the increase of the emission from sea ice. The emissions from sea ice in the polar regions in simulations *SS1ice* and *SS2ice* are 0.8 Gmol (Br)/yr and 0.5 Gmol (Br)/yr, respectively. These values are found to be too low, because the resulting BrO VTCD did not have their maxima in the polar regions, as is observed in the satellite retrievals. In simulation *SS3ice* the emission was 18 Gmol (Br)/yr and the resulting BrO VTCD in the polar regions is satisfactory. However, the comparison of our model results with Schofield *et al.* [110] ground-based measurements in Antarctica indicates that the results of BrO VTCD from *SS2ice* are characteristic of background conditions, while the BrO VTCD from simulation *SS3ice* are between values characteristic of background and "bromine explosion" conditions.

Our simple parameterisation of bromine emissions from sea ice depends only on the light conditions. This means that there is a continuous emission of bromine from sea ice, with,

consequently, a too high impact on ozone. To better understand the impact of bromine chemistry on ozone chemistry, it is necessary to better represent the spatio-temporal variation of the emissions. Consequently, the insertion of frost flowers and their dependence on physical variables as temperature in water, would improve our analysis and understanding.

The losses of bromine species over snow/ice are believed to be too low, as highlighted by the high HBr volume mixing ratios and, consequently, the values of  $\text{Br}_x$  (total inorganic bromine) in the polar regions. Fortunately, in the bromine chemistry scheme, the bromine in HBr is actually lost for the atmospheric bromine chemistry, because the conversion rate of HBr to other forms of bromine is low. The literature does not provide much information on parameters for the dry deposition and wet deposition of bromine compounds on snow and ice surfaces. Thus, we need laboratory experiments that determine dry and wet deposition parameters of bromine species.

---

## Chapter 5

# Outlook

Concerning the field of bromine chemistry in the troposphere, the most exciting challenge at the moment is to define the location and timing of bromine emissions in the polar regions. Interactions between the scientists in the field and in the laboratories, and atmospheric modellers and satellite specialists are required to make significant progress. The contribution of the global modeller is to investigate the global effects and explain observations.

It is quite certain that most of the bromine in the troposphere is emitted in the polar regions. In our study, we determined that the polar fraction of the tropospheric bromine emissions is roughly 65%. Thus, it is very important to improve the accuracy of polar emissions in global models. Moreover, model simulations have to be tested against observations. At the moment, the satellite retrievals from GOME allowed an approximative analysis of the relative emission fluxes of bromine from the different sources, which are important for the troposphere. The next step must be a comparison of the model simulations against ground-based measurements. The observations that exist show that bromine sources are very variable in space and time. Therefore, the comparisons of the model results with ground-based measurements can lead to a better description of the spatio-temporal variability of the emissions. The translation of the results of such an intercomparison into a detailed knowledge of emissions is a non-trivial task and will involve regional models, e.g. the frost flower detection model of Kaleschke and co-workers [61]. These authors constructed a one dimensional thermodynamic model that defines the regions potentially covered with frost flowers, using as input parameters the ice concentration and the surface air temperature. Their predictions and the regions with observed BrO enhancements are in good agreement. The snowpack is also a source of bromine<sup>1</sup>. The surface area of snow in the snowpack is very large. However, Rankin and colleagues [94] argue that the concentration of bromide in snow is small (they calculated a value of 3.29 ng/g, while the value for frost flowers measured by them is  $5 \times 10^4$  times higher). Thus, the focus on frost flowers in the next development steps seems to be more promising.

In our study, we concluded that the losses of bromine species in the polar regions derived in the model are too low. The dry deposition velocities on ice/snow are of the magnitude of  $10^{-3}$  cm/s. The values are calculated interactively in the model MOZART4. Based on the literature it is not possible to determine accurate values of dry deposition velocities on ice/snow. There may also be inaccuracies in the wet deposition, particularly in the polar regions, in which the wet deposition scheme is used to account for the scavenging of bromine species by snow and ice. For a further improvement of the simulations of these processes,

---

<sup>1</sup>The snowpack incorporates salt, by deposition or by wicking brine [57].

we need laboratory studies that determine dry and wet deposition parameters of bromine species.

The bromine emission from the inorganic sources, salt and ice, is dependent on complex aqueous chemistry. Probably, it is not necessary to include these in detail into a global model like MOZART4. However, it is essential to have a better parameterisation of the conditions on the substrates that determine the efficiency of bromine emission. This is the case for the acidity of a particle [107]. The comparison between model results and ground-based measurements hints to too low bromine emissions from sea salt in the model. Another evidence of the inaccuracy in the emissions from sea salt are the results reported in a very recent article of Read *et al.* [97]. They performed measurements of several chemical species such as ozone, its precursors, BrO, IO, etc., and of dynamical variables, like wind speed, at Cape Verde archipelago (17°N, 25°W) in the Atlantic Ocean, from October 2006 to October 2007. Their BrO measurements were around 2 pptv all the year long. The results from the MOZART4 simulations *SS1* and *SS1ice*, which have the highest bromine emissions from sea salt over open ocean in our study, were 100 times lower at the gridbox where Cape Verde is located. Read *et al.* argue that the site where the ground-based measurements were performed is representative of the surrounding open ocean marine boundary layer. Under the conditions of our model, this location is representative of open ocean conditions near the Equator<sup>2</sup>. In MOZART4, this region is characterised by low sea salt aerosol production as expected in these low latitudes with low wind speed.

The bromine production from sea salt is less well established than the production from very short-lived species. The atmospheric concentrations of the latter to measurements and their chemical degradation are less uncertain than the bromine flux from sea salt particles. If the pH in the sea salt particle is not considered, the estimated direct bromine production is 77.5 Gmol(Br)/yr [107]. Yang *et al.* [138] obtained a flux of 14/26 Gmol(Br)/yr. We obtained a maximum of 8.4 Gmol(Br)/yr in simulation *SS1ice*. Thus, there is much space for improvement. However, this can only be accomplished with more ground-based measurements. At lower latitudes, we especially need long-term measurements, in order to establish the background concentration with higher accuracy. The work of Read and co-workers and the prospective results from the OASIS campaign<sup>3</sup> are a valuable source of information that will allow a substantial improvement of the knowledge of bromine emissions into the troposphere.

---

<sup>2</sup>We increased 15 times the emissions of VLSL within 18°N-18°S compared to higher latitudes, because the observations show an equatorial enhancement in VLSL concentrations (see chapter 2.3).

<sup>3</sup>Plan of the OASIS campaign at [http://www.oasishome.net/oasis\[underscore\]science.php](http://www.oasishome.net/oasis[underscore]science.php). Last accessed July 22, 2008.

## Appendix A

# Additional Chemistry in MOZART4

Table A.1: Halogenated species and processes in which they interact

Species	Wet deposition	Dry deposition	Surf emissions	Fix lower bound conds	Heterog reactions	Photolysis
Halocarbons						
Short-lived						
CH <sub>3</sub> Br	<i>no</i>	<i>no</i>	<i>no</i>	<i>yes</i>	<i>no</i>	<i>yes</i>
CHBr <sub>3</sub>	<i>no</i>	<i>no</i>	<i>yes</i>	<i>no</i>	<i>no</i>	<i>yes</i>
CH <sub>2</sub> Br <sub>2</sub>	<i>no</i>	<i>no</i>	<i>yes</i>	<i>no</i>	<i>no</i>	<i>yes</i>
CH <sub>2</sub> BrCl	<i>no</i>	<i>no</i>	<i>yes</i>	<i>no</i>	<i>no</i>	<i>yes</i>
CHBr <sub>2</sub> Cl	<i>no</i>	<i>no</i>	<i>yes</i>	<i>no</i>	<i>no</i>	<i>yes</i>
CHBrCl <sub>2</sub>	<i>no</i>	<i>no</i>	<i>yes</i>	<i>no</i>	<i>no</i>	<i>yes</i>
Inorganic bromine						
Br	<i>no</i>	<i>no</i>	<i>no</i>	<i>no</i>	<i>no</i>	<i>no</i>
BrO	<i>no</i>	<i>no</i>	<i>no</i>	<i>no</i>	<i>no</i>	<i>yes</i>
HBr	<i>yes</i>	<i>yes</i>	<i>no</i>	<i>no</i>	<i>no</i>	<i>no</i>
HOBr	<i>yes</i>	<i>yes</i>	<i>no</i>	<i>no</i>	<i>yes</i>	<i>yes</i>
BrONO <sub>2</sub>	<i>no</i>	<i>no</i>	<i>no</i>	<i>no</i>	<i>yes</i>	<i>yes</i>
Br <sub>2</sub>	<i>no</i>	<i>no</i>	<i>no</i>	<i>no</i>	<i>yes</i> <sup>1</sup>	<i>yes</i>
BrCl	<i>no</i>	<i>no</i>	<i>no</i>	<i>no</i>	<i>yes</i> <sup>1</sup>	<i>yes</i>
Inorganic chlorine						
Cl	<i>no</i>	<i>no</i>	<i>no</i>	<i>no</i>	<i>no</i>	<i>no</i>
ClO	<i>no</i>	<i>no</i>	<i>no</i>	<i>no</i>	<i>no</i>	<i>no</i>
HCl	<i>yes</i>	<i>yes</i>	<i>no</i>	<i>no</i>	<i>no</i>	<i>yes</i>
HOCl	<i>yes</i>	<i>yes</i>	<i>no</i>	<i>no</i>	<i>no</i>	<i>yes</i>
ClONO <sub>2</sub>	<i>no</i>	<i>no</i>	<i>no</i>	<i>no</i>	<i>no</i>	<i>yes</i>
Cl <sub>2</sub>	<i>no</i>	<i>no</i>	<i>no</i>	<i>no</i>	<i>no</i>	<i>yes</i>
OCIO	<i>no</i>	<i>no</i>	<i>no</i>	<i>no</i>	<i>no</i>	<i>yes</i>
Cl <sub>2</sub> O <sub>2</sub>	<i>no</i>	<i>no</i>	<i>no</i>	<i>no</i>	<i>no</i>	<i>yes</i>

<sup>1</sup>as a product

Table A.2: Gaseous reactions

	Arrhenius A-factor A	Temperature dependence $-E/T$
$\text{CH}_3\text{Br} + \text{OH} \rightarrow \text{Br} + \text{H}_2\text{O} + \text{HO}_2$	$2.35 \times 10^{-12}$	-1300.
$\text{CHBr}_3 + \text{OH} \rightarrow 3^*\text{Br} + \text{H}_2\text{O}$	$1.35 \times 10^{-12}$	-600.
$\text{CH}_2\text{Br}_2 + \text{OH} \rightarrow 2^*\text{Br}$	$2.0 \times 10^{-12}$	-840.
$\text{CH}_2\text{BrCl} + \text{OH} \rightarrow \text{Br} + \text{Cl}$	$2.4 \times 10^{-12}$	-920.
$\text{CHBr}_2\text{Cl} + \text{OH} \rightarrow 2^*\text{Br} + \text{Cl}$	$2.4 \times 10^{-12}$	-920.
$\text{CHBrCl}_2 + \text{OH} \rightarrow \text{Br} + 2^*\text{Cl}$	$2.4 \times 10^{-12}$	-920.
$\text{Br} + \text{O}_3 \rightarrow \text{BrO} + \text{O}_2$	$1.70 \times 10^{-11}$	-800.
$\text{Br} + \text{HO}_2 \rightarrow \text{HBr} + \text{O}_2$	$4.80 \times 10^{-12}$	-310.
$\text{Br} + \text{CH}_2\text{O} \rightarrow \text{HBr} + \text{HO}_2 + \text{CO}$	$1.70 \times 10^{-11}$	-800.
$\text{Br} + \text{NO}_3 \rightarrow \text{BrO} + \text{NO}_2$	$1.6 \times 10^{-11}$	
$\text{Br} + \text{OH} \rightarrow \text{HOBr}$	$4.2 \times 10^{-11}$	
$\text{Br} + \text{CH}_3\text{CHO} \rightarrow \text{CH}_3\text{CO}_3 + \text{HBr}$	$1.30 \times 10^{-11}$	-360.
$\text{BrO} + \text{O} \rightarrow \text{Br} + \text{O}_2$	$1.90 \times 10^{-11}$	230.
$\text{BrO} + \text{OH} \rightarrow \text{Br} + \text{HO}_2$	$1.7 \times 10^{-11}$	250.
$\text{BrO} + \text{HO}_2 \rightarrow \text{HOBr} + \text{O}_2$	$4.5 \times 10^{-12}$	460.
$\text{BrO} + \text{NO} \rightarrow \text{Br} + \text{NO}_2$	$8.80 \times 10^{-12}$	260.
$\text{BrO} + \text{NO}_2 + \text{M} \rightarrow \text{BrONO}_2 + \text{M}$	$5.2 \times 10^{-31}$	$3.2, 6.9 \times 10^{-12}, 2.9, .6$
$\text{BrO} + \text{ClO} \rightarrow \text{Br} + \text{OCIO}$	$9.50 \times 10^{-13}$	550.
$\text{BrO} + \text{ClO} \rightarrow \text{Br} + \text{Cl} + \text{O}_2$	$2.30 \times 10^{-12}$	260.
$\text{BrO} + \text{ClO} \rightarrow \text{BrCl} + \text{O}_2$	$4.10 \times 10^{-13}$	290.
$\text{BrO} + \text{BrO} \rightarrow 2^*\text{Br} + \text{O}_2$	$1.5 \times 10^{-12}$	230.
$\text{BrO} + \text{CH}_3\text{O}_2 \rightarrow \text{Br} + \text{CH}_2\text{O} + \text{HO}_2$	$1.6 \times 10^{-12}$	
$\text{BrO} + \text{CH}_3\text{O}_2 \rightarrow \text{HOBr} + \text{CH}_2\text{O}$	$4.10 \times 10^{-12}$	
$\text{BrO} + \text{CH}_3\text{CO}_3 \rightarrow \text{Br} + \text{CH}_3\text{O}_2$	$1.7 \times 10^{-12}$	
$\text{HBr} + \text{OH} \rightarrow \text{Br} + \text{H}_2$	$5.5 \times 10^{-12}$	200.
$\text{HBr} + \text{O} \rightarrow \text{OH} + \text{Br}$	$5.8 \times 10^{-12}$	-1500.
$\text{HOBr} + \text{O} \rightarrow \text{OH} + \text{BrO}$	$1.2 \times 10^{-10}$	-430.
$\text{Br}_2 + \text{OH} \rightarrow \text{HOBr} + \text{Br}$	$2.1 \times 10^{-11}$	240.
$\text{BrONO}_2 + \text{O} \rightarrow \text{BrO} + \text{NO}_3$	$1.91 \times 10^{-11}$	215.
$\text{BrONO}_2 + \text{Br} \rightarrow \text{Br}_2 + \text{NO}_3$	$1.78 \times 10^{-11}$	365.
$\text{BrONO}_2 + \text{Cl} \rightarrow \text{BrCl} + \text{NO}_3$	$6.28 \times 10^{-11}$	215.
$\text{Cl} + \text{O}_3 \rightarrow \text{ClO} + \text{O}_2$	$2.30 \times 10^{-11}$	-200.
$\text{Cl} + \text{H}_2 \rightarrow \text{HCl} + \text{H}$	$3.70 \times 10^{-11}$	-2300.
$\text{Cl} + \text{H}_2\text{O}_2 \rightarrow \text{HCl} + \text{HO}_2$	$1.10 \times 10^{-11}$	-980.
$\text{Cl} + \text{HO}_2 \rightarrow \text{HCl} + \text{O}_2$	$1.80 \times 10^{-11}$	+170.
$\text{Cl} + \text{HO}_2 \rightarrow \text{OH} + \text{ClO}$	$4.10 \times 10^{-11}$	-450.
$\text{Cl} + \text{CH}_2\text{O} \rightarrow \text{HCl} + \text{HO}_2 + \text{CO}$	$8.10 \times 10^{-11}$	-30.
$\text{Cl} + \text{CH}_4 \rightarrow \text{CH}_3\text{O}_2 + \text{HCl}$	$9.60 \times 10^{-12}$	-1360.
$\text{ClO} + \text{O} \rightarrow \text{Cl} + \text{O}_2$	$3.00 \times 10^{-11}$	+70.
$\text{ClO} + \text{OH} \rightarrow \text{Cl} + \text{HO}_2$	$7.40 \times 10^{-12}$	+270.
$\text{ClO} + \text{OH} \rightarrow \text{HCl} + \text{O}_2$	$6.0 \times 10^{-13}$	230
$\text{ClO} + \text{HO}_2 \rightarrow \text{O}_2 + \text{HOCl}$	$2.7 \times 10^{-12}$	+220.
$\text{ClO} + \text{NO} \rightarrow \text{NO}_2 + \text{Cl}$	$6.40 \times 10^{-12}$	+290.
$\text{ClO} + \text{NO}_2 + \text{M} \rightarrow \text{ClONO}_2 + \text{M}$	$1.8 \times 10^{-31}$	$3.4, 1.5 \times 10^{-11}, 1.9, 0.6$
$\text{ClO} + \text{ClO} \rightarrow 2^*\text{Cl} + \text{O}_2$	$3.00 \times 10^{-11}$	-2450.
$\text{ClO} + \text{ClO} \rightarrow \text{Cl}_2 + \text{O}_2$	$1.00 \times 10^{-12}$	-1590.
$\text{ClO} + \text{ClO} \rightarrow \text{Cl} + \text{OCIO}$	$3.50 \times 10^{-13}$	-1370.

*table continued on next page*

Table A.2: Gaseous reactions — continued

$\text{ClO} + \text{ClO} + \text{M} \rightarrow \text{Cl}_2\text{O}_2 + \text{M}$	$1.6 \times 10^{-32}$	$4.5, 2.0 \times 10^{-12}, 2.4, 0.6$
$\text{Cl}_2\text{O}_2 + \text{M} \rightarrow 2^*\text{ClO} + \text{M}$		
$\text{HCl} + \text{OH} \rightarrow \text{H}_2\text{O} + \text{Cl}$	$2.60 \times 10^{-12}$	-350.
$\text{HCl} + \text{O} \rightarrow \text{Cl} + \text{OH}$	$1.00 \times 10^{-11}$	-3300.
$\text{HOCl} + \text{O} \rightarrow \text{ClO} + \text{OH}$	$1.70 \times 10^{-13}$	
$\text{HOCl} + \text{Cl} \rightarrow \text{HCl} + \text{ClO}$	$2.50 \times 10^{-12}$	-130.
$\text{HOCl} + \text{OH} \rightarrow \text{H}_2\text{O} + \text{ClO}$	$3.00 \times 10^{-12}$	-500.
$\text{ClONO}_2 + \text{O} \rightarrow \text{ClO} + \text{NO}_3$	$2.90 \times 10^{-12}$	-800.
$\text{ClONO}_2 + \text{OH} \rightarrow \text{HOCl} + \text{NO}_3$	$6.5 \times 10^{-12}$	-135.
$\text{ClONO}_2 + \text{Cl} \rightarrow \text{Cl}_2 + \text{NO}_3$	$6.50 \times 10^{-12}$	135.
$\text{Cl}_2 + \text{OH} \rightarrow \text{HOCl} + \text{Cl}$	$1.4 \times 10^{-12}$	-900.

Table A.3: Photolysis reactions

$\text{CH}_3\text{Br} + h\nu \rightarrow \text{Br} + \text{CH}_3\text{O}_2$
$\text{CHBr}_3 + h\nu \rightarrow 3^*\text{Br}$
$\text{CH}_2\text{Br}_2 + h\nu \rightarrow 2^*\text{Br}$
$\text{CH}_2\text{BrCl} + h\nu \rightarrow \text{Br} + \text{Cl}$
$\text{CHBr}_2\text{Cl} + h\nu \rightarrow 2^*\text{Br} + \text{Cl}$
$\text{CHBrCl}_2 + h\nu \rightarrow \text{Br} + 2^*\text{Cl}$
$\text{BrO} + h\nu \rightarrow \text{Br} + \text{O}$
$\text{HOBr} + h\nu \rightarrow \text{Br} + \text{OH}$
$\text{BrONO}_2 + h\nu \rightarrow \text{Br} + \text{NO}_3$
$\text{BrONO}_2 + h\nu \rightarrow \text{BrO} + \text{NO}_2$
$\text{Br}_2 + h\nu \rightarrow 2^*\text{Br}$
$\text{BrCl} + h\nu \rightarrow \text{Br} + \text{Cl}$
$\text{HCl} + h\nu \rightarrow \text{H} + \text{Cl}$
$\text{HOCl} + h\nu \rightarrow \text{OH} + \text{Cl}$
$\text{ClONO}_2 + h\nu \rightarrow \text{Cl} + \text{NO}_3$
$\text{ClONO}_2 + h\nu \rightarrow \text{ClO} + \text{NO}_2$
$\text{Cl}_2 + h\nu \rightarrow 2^*\text{Cl}$
$\text{OCIO} + h\nu \rightarrow \text{O} + \text{ClO}$
$\text{Cl}_2\text{O}_2 + h\nu \rightarrow 2^*\text{Cl}$

Table A.4: Heterogeneous reactions

---

$\text{BrONO}_2(\text{g}) + \text{H}_2\text{SO}_4 \cdot \text{H}_2\text{O}(\text{particle}) \rightarrow \text{HOBr}(\text{g})$ + $\text{HNO}_3(\text{g})$	$\Gamma = f(y_{\text{H}_2\text{SO}_4})$
$\text{BrONO}_2(\text{g}) + \text{H}_2\text{O}(\text{NH}_4\text{NO}_3 \text{ or organic carbon})$ $\rightarrow \text{HOBr}(\text{g}) + \text{HNO}_3(\text{g})$	$\Gamma = 0.032$
$\text{HOBr}(\text{g}) + \text{H}_2\text{SO}_4 \cdot \text{HCl}(\text{wet particle}) \rightarrow \text{BrCl}(\text{g})$ + $\text{H}_2\text{SO}_4 \cdot \text{H}_2\text{O}(\text{particle})$	$\Gamma = f(y_{\text{H}_2\text{SO}_4}, T, p, y_{\text{HCl}}, y_{\text{HOBr}}, y_{\text{H}_2\text{O}}, a)$
$\text{HOBr}(\text{g}) + \text{H}_2\text{SO}_4 \cdot \text{HBr}(\text{wet particle}) \rightarrow \text{Br}_2(\text{g}) +$ $\text{H}_2\text{SO}_4 \cdot \text{H}_2\text{O}(\text{particle})$	$\Gamma = f(y_{\text{H}_2\text{SO}_4}, T, p, y_{\text{HBr}}, y_{\text{HOBr}}, y_{\text{H}_2\text{O}}, a)$
$\text{BrONO}_2(\text{g}) + \text{deliquescent sea salt} \rightarrow n_1$	$\Gamma = 0.02$
$\text{Br}_2(\text{g}) + n_2 \text{BrCl}(\text{g})$	
$\text{HOBr}(\text{g}) + \text{deliquescent sea salt} \rightarrow n_3 \text{Br}_2(\text{g})$ + $n_4 \text{BrCl}(\text{g})$	$\Gamma = 0.1$

---

$y_s$  - weight percent of species  $s$

$a$  - radius of the particle

$n_1, n_2, n_3, n_4$  - yields

## Appendix B

# The Atmospheric Chemistry of Bromoform

The atmospheric removal of bromoform is dominated by photolysis (lifetime 36 days) and by reaction with OH (lifetime 100 days). Both lead to an estimate for the local lifetime of 26 days [85]. The photolysis leads to the direct elimination of a halogen atom and the formation of a formyl halide:



According to several studies, the quantum yield of reaction (B.1) is near unity (personal communication from John Orlando). The  $\text{CHBr}_2$  has sufficient internal energy to undergo a subsequent dissociation with two possible pathways: the production of  $\text{CHBr} + \text{Br}$  or of  $\text{CBr} + \text{HBr}$  [77] with quantum yields of 0.3 and 0.4, respectively. HBr is very soluble and rapidly removed from the gas into the aqueous phase.

The reaction with OH is followed by several steps (Figure B.1), and in sunlit oceanic conditions will promptly release the 3 Br atoms. The rate of the reaction of  $\text{CHBr}_3$  with OH is  $1.8 \times 10^{-13} \text{ cm}^3\text{s}^{-1}$  at standard conditions [6], yielding the tribromomethyl radical ( $\text{CBr}_3$ ), which rapidly reacts with  $\text{O}_2$  to form the tribromomethyl peroxy radical ( $\text{CBr}_3\text{O}_2$ ). The reaction of  $\text{CBr}_3\text{O}_2$  with NO results in an activated peroxy nitrite molecule ( $\text{CBr}_3\text{OONO}^*$ ). In a low NO environment the reaction with  $\text{HO}_2$  will be more important forming the molecule  $\text{CBr}_3\text{OOH}$  and subsequently the  $\text{CBr}_3\text{O}$  radical, due to the weakness of the O-O bond.  $\text{CBr}_3\text{O}$  rapidly degrades into  $\text{CBr}_2\text{O}$ , which also has an ephemeral atmospheric lifetime.  $\text{CBr}_2\text{O}$  releases the remaining 2 Br atoms after an initial photolysis step [76].  $\text{CBr}_2\text{O}$  may also react with water vapour in an endothermic reaction which leads to a net formation of  $2\text{HBr} + \text{CO}_2$  [37].

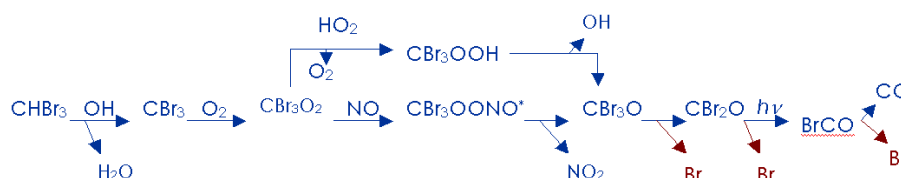


Figure B.1: Schematic oxidation path for bromoform till it releases all its bromine atoms.

# Acknowledgements

I thank Guy Brasseur and Sebastian Rast especially, without whom this work would never have come to light. Their patience and guidance were essential.

In the process of developing the emission fields of bromocarbons, I thank the valuable input of Birgit Quack; for welcoming me at NCAR (National Center of Atmospheric Research, Boulder, USA) and introducing me to the model MOZART4, I thank Louisa Emmons; for support at NCAR, for suggestions and comments, I give my gratitude to Jean-François Lamarque and John Orlando; for technical help at NCAR, I thank Stacy Walters and Garth D'Attilo.

In the difficult subject of satellite retrievals and how to interpret and use the information to evaluate model results, I send my gratitude to Andreas Richter, who opened warmly the channels for discussion. The same is true for Lars Kaleschke in disclosing the interesting world of frost flowers.

I thank the Max Planck Institute for Meteorology in Hamburg, the German Climate Computing Centre (DKRZ) and CIS (Central IT Services) for giving me all the conditions to pursue this work. I also thank the University of Hamburg for granting me the PhD.

Finally, thanks to Antje Weitz for her kindness and constant support.

For the economical support I acknowledge the following institutions: Ebelin and Gerd Bucerius ZEIT-Stiftung, Fundação Calouste Gulbenkian, and the Max Planck Institute for Meteorology. Without them, I could not afford the energy to feed my brain.

---

# Bibliography

- [1] J.P.D. Abbatt. Interactions of HBr, HCl, and HOBr with supercooled sulfuric acid solutions of stratospheric composition. *J. Geophysical Research*, 100:14,009–14,017, 1995.
- [2] J.P.D. Abbatt and J.B. Nowak. Heterogeneous interactions of HBr and HOCl with cold sulfuric acid solutions: implications for Arctic boundary layer bromine chemistry. *J. Phys. Chem A*, 101:2131–2137, 1997.
- [3] J.P.D. Abbatt and G.C.G. Waschewsky. Heterogeneous interactions of HOBr, HNO<sub>3</sub>, O<sub>3</sub>, and NO<sub>2</sub> with deliquescent NaCl aerosols at room temperature. *J. Phys. Chem A*, 102:3719–3725, 1998.
- [4] K. Abrahamsson, K.-S. Choo, M. Pedersén, G. Johansson, and P. Snoeijs. The seasonal variation of selected natural and anthropogenic halocarbons in the Arctic troposphere. *Atmospheric Environment*, 30(10/11):1723–1727, 1996.
- [5] J.W. Adams, N.S. Holmes, and J.N. Crowley. Uptake and reaction of HOBr on frozen and dry NaCl/NaBr surfaces between 253 and 233 K. *Atmos. Chem. Phys.*, 2:79–91, 2002.
- [6] National Aeronautics and Space Administration (NASA). Chemical kinetics and photochemical data for use in atmospheric studies. In S.P. Sander, R.R. Friedl, A.R. Ravishankara, D.M. Golden, C.E. Kolb, M.J. Kurylo, R.E. Huie, V.L. Orkin, M.J. Molina, G.K. Moortgat, H. Rudek, P.H. Wine, and B.J. Finlayson-Pitts, editors, *Jet Propulsion Laboratory - JPL Publication 06-02*. California Institute of Technology, Pasadena, 2006.
- [7] O.T. Afe, A. Richter, B. Sierk, F. Wittrock, and J.P. Burrows. BrO emission from volcanoes: A survey using GOME and SCIAMACHY measurements. *Geophys. Res. Lett.*, 31:L24113, doi:10.1029/2004GL020994, 2004.
- [8] A. Aguzzi and M. Rossi. The kinetics of the heterogeneous reaction of BrONO<sub>2</sub> with solid alkali halides at ambient temperature. A comparison with the interaction of ClONO<sub>2</sub> on NaCl and KBr. *Phys. Chem. Chem. Phys.*, 106(1):4337–4346, 1999.
- [9] E.L. Atlas, W. Pollock, J. Greenberg, and L. Heidt. Alkyl nitrates, nonmethane hydrocarbons, and halocarbon gases over the equatorial Pacific ocean during SAGA 3. *J. Geophysical Research*, 98:16,933–16,947, 1993.
- [10] G.P. Ayers, R.W. Gillett, J.M. Caine, and A.L. Dick. Chloride and bromide loss from sea-salt particles in southern ocean air. *J. Atmos. Chem.*, 33:299–319, 1999.

- [11] L. Barrie and U. Platt. Arctic tropospheric chemistry: An overview. *Tellus*, 49B:450–454, 1997.
- [12] L.A. Barrie. Features of the atmospheric cycle of aerosol trace elements and sulphur dioxide revealed by baseline observations in Canada. *J. Atmos. Chem.*, 3:139–152, 1985.
- [13] L.A. Barrie, J.W. Bottenheim, R.C. Schnell, P.J. Crutzen, and R.A. Rasmussen. Ozone destruction and photochemical reactions at polar sunrise in the lower Arctic atmosphere. *Nature*, 334:138–141, 1988.
- [14] N. Bobrowski, R. von Glasow, A. Aiuppa, S. Inguaggiato, I. Louban, O.W. Ibrahim, and U. Platt. Reactive halogen chemistry in volcanic plumes. *J. Geophysical Research*, 112:D06311, doi:10.1029/2006JD007206, 2007.
- [15] L.P. Bobylev, K.Ya. Kondratyev, and O.M. Johannessen. *Arctic environment variability in the context of global change*. Springer, 2003.
- [16] J.W. Bottenheim, L.A. Barrie, E. Atlas, L.E. Heidt, H. Niki, R.A. Rasmussen, and P.B. Shepson. Depletion of lower tropospheric ozone during Arctic spring: The Polar Sunrise Experiment 1988. *J. Geophysical Research*, 95:18,555–18,568, 1990.
- [17] J.W. Bottenheim, A.G. Gallant, and K.A. Brice. Measurements of NO<sub>y</sub> species and O<sub>3</sub> at 82°N latitude. *Geophys. Res. Lett.*, 13(113-116), 1986.
- [18] G.P. Brasseur, R.G. Prinn, and A.P. Pszenny, editors. *Atmospheric chemistry in a changing world: An integration and synthesis of a decade of tropospheric chemistry research*. Global Change - The IGBP Series. Springer, 2003.
- [19] L.J. Carpenter. Iodine in the marine boundary layer. *Chem. Rev.*, 103:4953–4962, 2003.
- [20] L.J. Carpenter and P.S. Liss. On temperate sources of bromoform and other reactive organic bromine gases. *J. Geophysical Research*, 105(D16):20,539–20,547, 2000.
- [21] L.J. Carpenter, P.S. Liss, and S.A. Penkett. Marine organohalogenes in the atmosphere over the Atlantic and Southern oceans. *J. Geophysical Research*, 108(D9):4256, doi:10.1029/2002JD002769, 2003.
- [22] T. Class and K. Ballschmiter. Chemistry of organic traces in air, VIII: sources and distribution of bromo- and bromochloromethanes in marine air and surface water of the Atlantic Ocean. *J. Atmos. Chem.*, 6:35–46, 1988.
- [23] T. Class, R. Kohnle, and K. Ballschmiter. Chemistry of organic traces in air, VII: bromo- and bromochloromethanes in air over the Atlantic Ocean. *Chemosphere*, 15(4):429–436, 1986.
- [24] J. Collén, A. Ekdahl, K. Abrahamsson, and M. Pedersén. The involvement of hydrogen peroxide in the production of volatile halogenated compounds by *meristiella gelidium*. *Phytochemistry*, 36(5):1197–1202, 1994.
- [25] G.F. Cota and W.T. Sturges. Biogenic bromine production in the Arctic. *Marine Chemistry*, 56:181–192, 1997.

- [26] P.V. Danckwerts. Absorption by simultaneous diffusion and chemical reaction into particles of various shapes and into falling droplets. *Trans. Faraday Soc.*, 47:1014, 1951.
- [27] P.V. Danckwerts. *Gas-Liquid Reactions*. McGraw-Hill, New York, 1970.
- [28] G. Deiber, Ch. George, S. Le Calvé, F. Schweitzer, and Ph. Mirabel. Uptake study of ClONO<sub>2</sub> and BrONO<sub>2</sub> by halide containing droplets. *Atmos. Chem. Phys.*, 4:1291–1299, 2004.
- [29] V.L. Dvortsov, M.A. Geller, S. Solomon, S.M. Schauffler, E.L. Atlas, and D.R. Blake. Rethinking reactive halogen budgets in the midlatitude lower stratosphere. *Geophys. Res. Lett.*, 26:1699–1702, 1999.
- [30] A. Ekdahl, M. Pedersén, and K. Abrahamsson. A study of the diurnal variation of biogenic volatile halocarbons. *Marine Chemistry*, 63:1–8, 1998.
- [31] L.K. Emmons, D.A. Hauglustaine, J.-F. Müller, M.A. Carroll, G.P. Brasseur, D. Brunner, J. Staehelin, V. Thouret, and A. Marenco. Data composites of airborne observations of tropospheric ozone and its precursors. *J. Geophysical Research*, 105(D16):20,497–20,538, 2000.
- [32] S. Enami, C.D. Vecitis, J. Cheng, M.R. Hoffmann, and A.J. Colussi. Global inorganic source of atmospheric bromine. *J. Phys. Chem A*, 111:8749–8752, 2007.
- [33] S. Fickert, J.W. Adams, and J.N. Crowley. Activation of Br<sub>2</sub> and BrCl via uptake of HOBr onto aqueous salt solutions. *J. Geophysical Research*, 104(D19):23,719–23,727, 1999.
- [34] B.J. Finlayson-Pitts. The tropospheric chemistry of sea salt: A molecular-level view of the chemistry of NaCl and NaBr. *Chem. Rev.*, 103:4801–4822, 2003.
- [35] R. Fitzenberger, H. Bösch, C. Camy-Peyret, M.P. Chipperfield, H. Harder, U. Platt, B.-M. Sinnhuber, T. Wagner, and K. Pfeilsticker. First profile measurements of tropospheric BrO. *J. Geophysical Research Letters*, 27(18):2921–2924, 2000.
- [36] National Center for Atmospheric Research (NCAR). In G.P. Brasseur, J.J. Orlando, and G.S. Tyndall, editors, *Atmospheric Chemistry and Global Change*. Oxford University Press, New York, 1999.
- [37] J. Francisco. Energetics of the reaction of CBr<sub>2</sub>O with water. *Chemical Physics Letters*, 363:275–282, 2002.
- [38] U. Friess, J. Hollwedel, G. Koenig-Langlo, T. Wagner, and U. Platt. Dynamics and chemistry of tropospheric explosion events in the Arctic coastal region. *J. Geophysical Research*, 109:D06305, doi:10.1029/2003JD004133, 2004.
- [39] L. Ganzeveld and J. Lelieveld. Dry deposition parameterization in a chemistry general circulation model and its influence on the distribution of reactive trace gases. *J. Geophysical Research*, 100(D10):20999–21012, 1995.
- [40] T.M. Gerlach. Volcanic sources of tropospheric ozone-depleting trace gases. *Geochemistry Geophysics Geosystems*, 5:Q09007, doi:10.1029/2004GC000747, 2004.

- [41] F. Giorgi and W.L. Chameides. The rainout parameterization in a photochemical model. *J. Geophysical Research*, 90(D5):7872–7880, 1985.
- [42] C. Granier, J.-F. Lamarque, A. Mieville, J.F. Muller, J. Olivier, J. Orlando, J. Peters, G. Petron, G. Tyndall, and S. Wallens. POET, a database of surface emissions of ozone precursors. Available on internet at <http://www.aero.jussieu.fr/projet/ACCENT/POET.php> (last accessed January 18, 2008), 2005.
- [43] W.G. Gribble. The natural production of organobromine compounds. *Environ. Sci. and Pollut. Res.*, 7(1):37–49, 2000.
- [44] D.R. Hanson. Reactivity of BrONO<sub>2</sub> and HOBr on sulfuric acid solutions at low temperatures. *J. Geophysical Research*, 108(D8):doi:10.1029/2002JD002519, 2003.
- [45] D.R. Hanson and A.R. Ravishankara. Heterogeneous chemistry of bromine species in sulfuric acid under stratospheric conditions. *Geophys. Res. Lett.*, 22(4):385–388, 1995.
- [46] D.R. Hanson, A.R. Ravishankara, and E.R. Lovejoy. Reaction of BrONO<sub>2</sub> with H<sub>2</sub>O on submicron sulfuric acid aerosol and the implications for the lower stratosphere. *J. Geophysical Research*, 101(D4):9063–9069, 1996.
- [47] D.R. Hanson, A.R. Ravishankara, and S. Solomon. Heterogeneous reactions in sulfuric acid aerosols: A framework for model calculations. *J. Geophysical Research*, 99(D2):3615–3629, 1994.
- [48] K. Hara, K. Osada, M. Kido, M. Hayashi, K. Matsunaga, Y. Iwasaka, T. Yamanouchi, G. Hashida, and T. Fukatsu. Chemistry of sea-salt particles and inorganic halogen species in Antarctic regions: compositional differences between coastal and inland stations. *J. Geophysical Research*, 109(D20208):doi:10.1029/2004JD004713, 2004.
- [49] H. Harder, C. Camy-Peyret, F. Ferlemann, R. Fitzenberger, T. Hawat, H. Osterkamp, M. Schneider, D. Perner, U. Platt, P. Vradelis, and K. Pfeilsticker. Stratospheric BrO profiles measured at different latitudes and seasons: Atmospheric observations. *Geophys. Res. Lett.*, 25:3843–3846, 1998.
- [50] Susan Joy Hassol. *Impacts of a warming Arctic*. International Geophysics Series. Arctic Climate Impact Assessment, Cambridge University Press, 2004.
- [51] K. Hebestreit, J. Stutz, D. Rosen, V. Matveev, M. Peleg, and M. Luria and U. Platt. DOAS measurements of tropospheric bromine oxide in mid-latitudes. *Science*, 283:55–57, 1999.
- [52] D. Helmig, S.J. Oltmans, D. Carlson, J.-F. Lamarque, A. Jones, C. Labuschagne, K. Anlauf, and K. Hayden. A review of surface ozone in the polar regions. *Atmospheric Environment*, 41:5138–5161, 2007.
- [53] F. Hendrick, M. Van Roozendaal, M.P. Chipperfield, M. Dorf, F. Goutail, X. Yang, C. Fayt, C. Hermans, K. Pfeilsticker, J.-P. Pommereau, J.A. Pyle, N. Theys, and M. De Mazière. Retrieval of stratospheric and tropospheric BrO profiles and columns using ground-based zenith-sky DOAS observations at Harestua, 60°N. *Atmos. Chem. Phys.*, 7:4869–4885, 2007.

- [54] J. Hollwedel, M. Wenig, S. Beirle, S. Kraus, S. Kühl, W. Wilms-Grabe, U. Platt, and T. Wagner. Year-to-year variations of spring time polar tropospheric BrO as seen by GOME. *Adv. Space Res.*, 34(4):804–808, 2004.
- [55] L.W. Horowitz, S. Walters, D.L. Mauzerall, L.K. Emmons, P.J. Rasch, C. Granier, X. Tie, J.-F. Lamarque, M.G. Schultz, G.S. Tyndall, J.J. Orlando, and G.P. Brasseur. A global simulation of tropospheric ozone and related tracers: Description and evaluation of MOZART, version 2. *J. Geophysical Research*, 108(D24, 4784):doi:10.1029/2002JD002853, 2003.
- [56] A.K. Huff and J.P.D. Abbatt. Kinetics and product yields in the heterogeneous reactions of HOBr with ice surfaces containing NaBr and NaCl. *J. Phys. Chem A*, 106:5279–5287, 2002.
- [57] M.A. Hutterli, T. Huthwelker, M.M. Miedaner, F. Enzmann, M. Ammann, M. Schneebeli, S. Maus, M. Stamparoni, A.E. Jones, and E.W. Wolff. A 3D X-ray micro computer tomography perspective of sea ice, frost flowers and snow as sources of reactive halogens. In *EGU General Assembly 2008*, number EGU2008-A-04181 in Geophysical Research Abstracts. European Geosciences Union, April 2008.
- [58] L.T. Iraci, R.R. Michelsen, S.F.M. Ashbourn, T.A. Rammer, and D.M. Golden. Uptake of hypobromous acid (HOBr) by aqueous sulfuric acid solutions: low-temperature solubility and reaction. *Atmos. Chem. Phys.*, 5:1577–1587, 2005.
- [59] P. Jungwirth and D.J. Tobias. Molecular structure of salt solutions: A new view of the interface implications for heterogeneous atmospheric chemistry. *J. Phys. Chem A*, pages 10468–10472, 2001.
- [60] P. Jungwirth and D.J. Tobias. Ions at the air/water interface. *J. Phys. Chem A*, pages 6361–6373, 2002.
- [61] L. Kaleschke, A. Richter, J. Burrows, O. Afe, G. Heygster, J. Notholt, A. M. Rankin, H. K. Roscoe, J. Hollwedel, T. Wagner, and H.-W. Jacobi. Frost flowers on sea ice as a source of sea salt and their influence on tropospheric halogen chemistry. *Geophys. Res. Lett.*, 31:L16114, doi:10.1029/2004GL020655, 2004.
- [62] D.B. King, J.H. Butler, S.A. Yvon-Lewis, and S.A. Cotton. Predicting oceanic methyl bromide saturation from SST. *Geophys. Res. Lett.*, 29(24):2199, doi:10.1029/2002GL016091, 2002.
- [63] R. Kistler, E. Kalnay, W. Collins, S. Saha, G. White, J. Woollen, M. Chelliah, W. Ebisuzaki, M. Kanamitsu, V. Kousky, H. van den Dool, R. Jenne, and M. Fiorinono. The NCEP/NCAR 50-Year reanalysis: Monthly means CD-ROM and documentation. *Bull. Am. Meteorol. Soc.*, 82:247–268, 2001.
- [64] M.K.W. Ko, N.-D. Sze, C.J. Scott, and D.K. Weisenstein. On the relation between stratospheric chlorine/bromine loading and short-lived tropospheric source gases. *J. Geophysical Research*, 102:25,507–25,517, 1997.
- [65] T. Koop, A. Kapilashrami, L.T. Molina, and M.J. Molina. Phase transitions of sea-salt/water mixtures at low temperatures: Implications for ozone chemistry in the polar marine boundary layer. *J. Geophysical Research*, 105:26,393–26,402, 2000.

- [66] M. Larichev, F. Le Bras, and G. Poulet. Kinetics and mechanism of the  $\text{BrO} + \text{HO}_2$  reaction. *J. Phys. Chem.*, 99:15911–15918, 1995.
- [67] D.J. Lary. Halogens and the chemistry of the free troposphere. *Atmos. Chem. Phys.*, 5:227–237, 2005.
- [68] F. Laturus. Release of volatile halogenated organic compounds by unialgal cultures of polar macroalgae. *Chemosphere*, 31(6):3387–3395, 1995.
- [69] C. Lee, Y.J. Kim, H. Tanimoto, N. Bobrowski, U. Platt, T. Mori, K. Yamamoto, and C.S. Hong. High ClO and ozone depletion observed in the plume of Sakurajima volcano, Japan. *Geophys. Res. Lett.*, 32:L21809, doi:10.1029/2005GL023785, 2005.
- [70] H. Leser, G. Hönninger, and U. Platt. MAX-DOAS measurements of BrO and  $\text{NO}_2$  in the marine boundary layer. *Geophys. Res. Lett.*, 30(10):doi:10.1029/2002GL015811, 2003.
- [71] S.-M. Li, Y. Yokouchi, L.A. Barrie, K. Muthuramu, P.B. Shepson, J.W. Bottenheim, W.T. Sturges, and S. Landsberger. Organic and inorganic bromine compounds and their composition in the Arctic troposphere during polar sunrise. *J. Geophysical Research*, 99(D12):25,415–25,428, 1994.
- [72] S. Madronich. Photodissociation in the atmosphere 1. actinic flux and the effects of ground reflections and clouds. *J. Geophysical Research*, 92:9740–9752, 1987.
- [73] V. Matveev, M. Peleg, D. Rosen, D.S. Tov-Alper, J. Stutz, K. Hebestreit, U. Platt, D. Blake, and M. Luria. Bromine oxide-ozone interaction over the Dead Sea. *J. Geophysical Research*, 106:10,375–10,378, 2001.
- [74] C.T. McElroy, C.A. McLinden, and J.C. McConnell. Evidence for bromine monoxide in the free troposphere during the Arctic polar sunrise. *Nature*, 397:338–341, 1999.
- [75] G. McFiggans, J.M.C. Plane, B.J. Allan, L.J. Carpenter, H. Coe, and C. O’Dowd. A modeling study of iodine chemistry in the marine boundary layer. *J. Geophysical Research*, 105(D11):14,371–14,385, 2000.
- [76] W.S. McGivern, J.S. Francisco, and S.W. North. Investigation of the atmospheric oxidation pathways of bromoform: initiation via OH/Cl reactions. *J. Phys. Chem*, 106:6,395–6,400, 2002.
- [77] W.S. McGivern, O. Sorkhabi, A.G. Suits, A. Derecskei-Kovacs, and S.W. North. Primary and secondary processes in the photodissociation of  $\text{CHBr}_3$ . *J. Phys. Chem*, 104:10,085–10,091, 2000.
- [78] A. Mellouki, R.K. Talukdar, and C.J. Howard. Kinetics of the reactions of HBr with  $\text{O}_3$  and  $\text{HO}_2$ : The yield of HBr from  $\text{HO}_2 + \text{BrO}$ . *J. Geophysical Research*, 99(D11):22,949–22,954, 1994.
- [79] S.A. Miller. *Chemical Oceanography*. CRC press, 1996.
- [80] S.A. Montzka, J.H. Butler, B.D. Hall, D.J. Mondeel, and J.W. Elkins. A decline in tropospheric organic bromine. *J. Geophysical Research*, 30(15):1826, doi:10.1029/2003GL017745 2003.

- [81] R.M. Moore, M. Webb, R. Tokarczyk, and R. Wever. Bromoperoxidase and iodoperoxidase enzymes and production of halogenated methanes in marine diatom cultures. *J. Geophysical Research*, 101(C9):20,899–20,908, 1996.
- [82] G.K. Moortgat, R. Meller, and W. Schneider. Temperature dependence (256–296 K) of the absorption cross sections of bromoform in the wavelength range 285–360 nm. In H. Niki and K.H. Becker, editors, *The Tropospheric chemistry of ozone in the polar regions*, volume 7 of *NATO ASI Series I: Global environmental change*. Springer, 1993.
- [83] S.J. Oltmans and W.D. Komhyr. Surface ozone distributions and variations from 1973–1984 measurements at the NOAA Geophysical Monitoring for Climate Change baseline observatories. *J. Geophysical Research*, 91(D4):5229–5236, 1986.
- [84] World Health Organization. *Health Aspects of Air Pollution with Particulate Matter, Ozone and Nitrogen Dioxide*. Report on a WHO Working Group, <http://www.euro.who.int/document/e79097.pdf> (last accessed December 5, 2007), 13–15 January 2003.
- [85] World Meteorological Organization. *Scientific Assessment of Ozone Depletion: 2002, Global Ozone Research and Monitoring Project - Report n. 47*. WMO, Geneva, 2003.
- [86] L.L. Pan, J.C. Wei, D.E. Kinnison, R.R. Garcia, D.J. Wuebbles, and G.P. Brasseur. A set of diagnostics for evaluating chemistry-climate models in the extratropical tropopause region. *J. Geophysical Research*, 112(D9):D09316, 2007.
- [87] D.K. Perovich and J.A. Richter-Menge. Surface characteristics of lead ice. *J. Geophysical Research*, 99:16,341–16,350, 1994.
- [88] U. Platt and G. Hoenninger. The role of halogen species in the troposphere. *Chemosphere*, 52:325–338, 2003.
- [89] P. Pratte and M.J. Rossi. The heterogeneous kinetics of HOBr and HOCl on acidified sea salt and model aerosol at 40–90% relative humidity and ambient temperature. *Phys. Chem. Chem. Phys.*, 8:3988–4001, 2006.
- [90] A.A.P. Pszenny, J. Moldanová, W.C. Keene, R. Sander, J.R. Maben, M. Martinez, P.J. Crutzen, D. Perner, and R.G. Prinn. Halogen cycling and aerosol pH in the Hawaiian marine boundary layer. *Atmos. Chem. Phys.*, 4:147–168, 2004.
- [91] B. Quack, E. Atlas, G. Petrick, V. Stroud, S. Schauffler, and D.W.R. Wallace. Oceanic bromoform sources for the tropical atmosphere. *Geophys. Res. Lett.*, 31:doi:10.1029/2004GL020597, 2004.
- [92] B. Quack and D.W.R. Wallace. Air-sea flux of bromoform: Controls, rates and implications. *Global Biogeochemical Cycles*, 17(1):doi:10.1029/2002GB001890, 2003.
- [93] B. Ramacher, J. Rudolph, and R. Koppmann. Hydrocarbon measurements during tropospheric ozone depletion events: Evidence for halogen atom chemistry. *J. Geophysical Research*, 104:3633, 1999.
- [94] A.M. Rankin, E.W. Wolff, and S. Martin. Frost flowers: Implications for tropospheric chemistry and ice core interpretation. *J. Geophysical Research*, 107:4683, doi:10.1029/2002JD002492, 2002.

- [95] J.L. Raper, M.M. Kleb, D.J. Jacob, D.D. Davis, R.E. Newell, H.E. Fuelberg, R.J. Bendura, J.M. Hoell, and R.J. McNeal. Pacific Exploratory Mission in the Tropical Pacific: PEM-Tropics B, March-April 1999. *J. Geophysical Research*, 106(D23):32,401–32,425, 2001.
- [96] A.R. Ravishankara. Heterogeneous and multiphase chemistry in the troposphere. *Science*, 276:1058–1065, 1997.
- [97] K.A. Read, A.S. Mahajan, L.J. Carpenter, M.J. Evans, B.V.E. Faria, D.E. Heard, J.R. Hopkins, J.D. Lee, S.J. Moller, A.C. Lewis, L. Mendes, J.B. McQuaid, H. Oetjen, A. Saiz-Lopez, M.J. Pilling, and J.M.C. Plane. Extensive halogen-mediated ozone destruction over the tropic Atlantic ocean. *Nature*, 453(doi:10.1038/nature07035):1232–1235, 2008.
- [98] W. Reifenhäuser and K.G. Heumann. Bromo- and bromochloromethanes in the Antarctic atmosphere and the south polar sea. *Chemosphere*, 24(9):1293–1300, 1992.
- [99] A. Richter, F. Wittrock, M. Eisinger, and J.P. Burrows. GOME observations of tropospheric BrO in Northern hemispheric spring and summer 1997. *Geophys. Res. Lett.*, 25(14):2683–2686, 1998.
- [100] A. Richter, F. Wittrock, A. Ladstätter-Weissenmayer, and J.P. Burrows. GOME measurements of stratospheric and tropospheric BrO. *Adv. Space Res.*, 29(11):1667–1672, 2002.
- [101] B.A. Ridley, E.L. Atlas, D.D. Montzka, E.V. Browell, C.A. Cantrell, D.R. Blake, N.J. Blake, L. Cinquini, M.T. Coffey, L.K. Emmons, R.C. Cohen, R.J. DeYoung, J.E. Dibb, F.L. Eisele, F.M. Flocke, A. Fried, F.E. Grahek, W.B. Grant, J.W. Hair, J.W. Hannigan, B.J. Heikes, B.L. Lefer, R.L. Mauldin, J.L. Moody, R.E. Shetter, J.A. Snow, R.W. Talbot, J.A. Thornton, J.G. Walega, A.J. Weinheimer, B.P. Wert, and A.J. Wimmers. Ozone depletion events observed in the high latitude surface layer during the TOPSE aircraft program. *J. Geophysical Research*, 108:doi:10.1029/2001JD001507, 2003.
- [102] B.A. Ridley, T. Zeng, Y. Wang, E.L. Atlas, E.V. Browell, P.G. Hess, J.J. Orlando, K. Chance, and A. Richter. An ozone depletion event in the sub-arctic surface layer over Hudson Bay, Canada. *J. Atmos. Chem.*, 57:255–280, 2007.
- [103] M. Van Roozendaal, T. Wagner, A. Richter, I. Pundt, D.W. Arlander, J.P. Burrows, M. Chipperfield, C. Fayt, P.V. Johnston, J.-C. Lambert, K. Kreher, K. Pfeilsticker, U. Platt, J.-P. Pommereau, B.-M. Sinnhuber, K.K. Tornkvist, and F. Wittrock. Intercomparison of BrO measurements from ERS-2 GOME, ground-based and balloon platforms. *Adv. Space Res.*, 11:1661–1666, 2002.
- [104] R. Sander. *Compilation of Henry's Law Constants for inorganic and organic species of potential importance in environmental chemistry (version 3)*. Max Planck Institute of Chemistry, Mainz, {<http://www.henrys-law.org>} (last accessed December 5, 2007), 1999.
- [105] R. Sander, J. Burrows, and L. Kaleschke. Carbonate precipitation in brine - the trigger for tropospheric ozone depletion events. *Atmos. Chem. Phys.*, 6:4653–4658, 2006.

- [106] R. Sander and P.J. Crutzen. Model study indicating halogen activation and ozone destruction in polluted air masses transported to the sea. *J. Geophysical Research*, 101(D4):9121–9138, 1996.
- [107] R. Sander, W.C. Keene, A.A.P. Pszenny, R. Arimoto, G.P. Ayers, E. Baboukas, J.M. Cainey, P.J. Crutzen, R.A. Duce, G. Hoenninger, B.J. Huebert, W. Maenhaut, N. Mihalopoulos, V.C. Turekian, and R. van Dingenen. Inorganic bromine in the boundary layer: A critical review. *Atmos. Chem. Phys.*, 3:1301–1336, 2003.
- [108] J.L. Sarmiento, R. Slater, R. Barber, L. Bopp, S.C. Doney, A.C. Hirst, J. Kleypas, R. Matear, U. Mikolajewicz, P. Monfray, V. Soldatov, S.A. Spall, and R. Stouffer. Response of ocean ecosystems to climate warming. *Global Biogeochemical Cycles*, 18(GB3003), doi: 10.1029/2003GB002134 2004.
- [109] S.M. Schauffler, E.L. Atlas, D.R. Blake, F. Flocke, R.A. Lueb, J.M. Lee-Taylor, V. Stroud, and W. Travnicek. Distributions of brominated organic compounds in the troposphere and lower stratosphere. *J. Geophysical Research*, 104(D17):21,513–21,535, 1999.
- [110] R. Schofield, P.V. Johnston, A. Thomas, K. Kreher, B.J. Connor, S. Wood, D. Shooter, M.P. Chipperfield, A. Richter, and R. von Glasow C.D. Rodgers. Tropospheric and stratospheric BrO columns over Arrival Heights, Antarctica, 2002. *J. Geophysical Research*, 111(D22310):doi:10.1029/2005JD007022, 2006.
- [111] R. Schofield, K. Kreher, B.J. Connor, P.V. Johnston, A. Thomas, D. Shooter, M.P. Chipperfield, C.D. Rodgers, and G.H. Mount. Retrieved tropospheric and stratospheric BrO columns over Lauder, New Zealand. *J. Geophysical Research*, 109(D14304):doi:10.1029/2003JD004463, 2004.
- [112] J.H. Seinfeld and S.N. Pandis. *Atmospheric chemistry and physics. From air pollution to climate change*. Wiley, New York, 1998.
- [113] B.-M. Sinnhuber and I. Folkins. Estimating the contribution of bromoform to stratospheric bromine and its relation to dehydration in the tropical tropopause layer. *Atmos. Chem. Phys.*, 6(4755-4761), 2006.
- [114] S. Solberg, N. Schmidbauer, A. Semb, F. Stordal, and O. Hov. Boundary-layer ozone depletion as seen in the Norwegian Arctic in spring. *J. Atmos. Chem.*, 23(3):301–332, 1996.
- [115] S. Solomon. Stratospheric ozone depletion: A review of concepts and history. *Rev. Geophys.*, 37:275–316, 1999.
- [116] W.T. Sturges. The reaction of NO<sub>2</sub> with NaBr: Possible source of BrNO in polluted marine atmospheres. *Atmospheric Environment*, 23:1167–1168, 1989.
- [117] W.T. Sturges. Excess particulate and gaseous bromine at a remote coastal location. *Atmospheric Environment*, 24A(1):167–171, 1990.
- [118] W.T. Sturges, D.E. Oram, L.J. Carpenter, S.A. Penkett, and A. Engel. Bromoform as a source of stratospheric bromine. *Geophys. Res. Lett.*, 27:2081–2084, 2000.

- [119] J. Stutz, R. Ackermann, J.D. Fast, and L. Barrie. Atmospheric reactive chlorine and bromine at the Great Salt Lake, Utah. *Geophys. Res. Lett.*, 29(10):10.1029/2002GL014812, 2002.
- [120] A. Tabazadeh, O.B. Toon, S.L. Clegg, and P. Hamill. A new parameterization of H<sub>2</sub>SO<sub>4</sub>/H<sub>2</sub>O aerosol composition: Atmospheric implications. *Geophys. Res. Lett.*, 24(15):1931–1934, 1997.
- [121] T. Tang and J.C. McConnell. Autocatalytic release of bromine from arctic snow pack during polar sunrise. *Geophys. Res. Lett.*, 23:2633–2636, 1996.
- [122] D.W. Tarasick and J.W. Bottenheim. Surface ozone depletion episodes in the Arctic and Antarctic from historical ozonesonde records. *Atmos. Chem. Phys.*, 2:197–205, 2002.
- [123] N. Theys, M. Van Roozendael, F. Hendrick, C. Fayt, C. Hermans, J.-L. Baray, F. Goutail, J.-P. Pommereau, and M. De Mazière. Retrieval of stratospheric and tropospheric BrO columns from multi-axis DOAS measurements at Reunion Island (21°S, 56°E). *Atmos. Chem. Phys.*, 7:4733–4749, 2007.
- [124] X. Tie, G. Brasseur, L. Emmons, L. Horowitz, and D. Kinnison. Effects of aerosols on tropospheric oxidants: A global model study. *J. Geophysical Research*, 106:2931–2964, 2001.
- [125] X. Tie, S. Madronich, S. Walters, D.P. Edwards, P. Ginoux, N. Mahowald, R. Zhang, C. Lou, and G. Brasseur. Assessment of the global impact of aerosols on tropospheric oxidants. *J. Geophysical Research*, 110(D03204):doi:10.1029/2004JD005359, 2005.
- [126] M. Tuckermann, R. Ackermann, C. Gölz, H. Lorenzen-Schmidt, T. Senne, J. Stutz, B. Trost, W. Unold, and U. Platt. DOAS-observation of halogen radical-catalysed Arctic boundary layer ozone destruction during the ARCTOC-campaigns 1995 and 1996 in Ny-Alesund, Spitsbergen. *Tellus*, 49B:533–555, 1997.
- [127] R. Vogt, P.J. Crutzen, and R. Sander. A mechanism for halogen release from sea-salt aerosol in the remote marine boundary layer. *Nature*, 383:327–330, doi:10.1038/383327a0 1996.
- [128] R. von Glasow, R. von Kuhlmann, M.G. Lawrence, U. Platt, and P.J. Crutzen. Impact of reactive bromine chemistry in the troposphere. *Atmos. Chem. Phys.*, 4:2481–2497, 2004.
- [129] M. Wachsmuth, H.W. Gäggeler, R. von Glasow, and M. Ammann. Accommodation coefficient of HOBr on deliquescent sodium bromine aerosol particles. *Atmos. Chem. Phys.*, 2:121–131, 2002.
- [130] T. Wagner, O. Ibrahim, R. Sinreich, U. Friess, R. von Glasow, and U. Platt. Enhanced tropospheric BrO over Antarctic sea ice in mid winter observed by MAX-DOAS on board the research vessel Polarstern. *Atmos. Chem. Phys.*, 7:3129–3142, 2007.
- [131] T. Wagner, C. Leue, M. Wenig, K. Pfeilsticker, and U. Platt. Spatial and temporal distribution of enhanced boundary layer BrO concentrations measured by the GOME instrument aboard ERS-2. *J. Geophysical Research*, 106(D20):24,225–24,235, 2001.

- [132] T. Wagner and U. Platt. Observation of tropospheric BrO from GOME satellite. *Nature*, 395:486–490, 1998.
- [133] Peter Warneck. *Chemistry of the natural atmosphere*, volume 71 of *International Geophysics Series*. Academic press, 1999.
- [134] G.C.G. Waschewsky and J.P.D. Abbatt. HOBr in sulfuric acid solutions: Solubility and reaction with HCl as a function of temperature and concentration. *J. Phys. Chem A*, 103:5312–5320, 1999.
- [135] P.O. Wennberg, T.F. Hanisco, T.F. Jaegle, D.J. Jacob, E.J. Hints, E.J. Lanzendorf, J.G. Anderson, R.S. Gao, E.R. Keim, S.G. Donnelly, L.A. Negro, D.W. Fahey, S.A. McKeen, R.J. Salawitch, C.R. Webster, R.D. May, R.L. Herman, M.H. Proffitt, J.J. Margitan, E.L. Atlas, S.M. Schauffler, F. Flocke, C.T. McElroy, and T.P. Bui. Hydrogen radicals, nitrogen radicals, and the production of O<sub>3</sub> in the upper troposphere. *Science*, 279:49–53, 1998.
- [136] M.L. Wesely. Parameterization of surface resistances to gaseous dry deposition in regional-scale numerical models. *Atmospheric Environment*, 23(6):1293–1304, 1989.
- [137] S. Wessel, S. Aoki, P. Winkler, R. Weller, A. Herber, and H. Gernandt. Tropospheric ozone depletion in polar regions: A comparison of observations in the Arctic and Antarctic. *Tellus*, 50B:34–50, 1998.
- [138] X. Yang, R.A. Cox, N.J. Warwick, J.A. Pyle, G.D. Carver, F.M. O'Connor, and N.H. Savage. Tropospheric bromine chemistry and its impacts on ozone: a model study. *J. Geophysical Research*, 110(D23311,doi:10.1029/2005JD006244), 2005.
- [139] Y. Yokouchi, H. Akimoto, L.A. Barrie, J.W. Bottenheim, K. Anlauf, and B.T. Jobson. Serial gas chromatographic/mass spectrometric measurements of some volatile organic compounds in the Arctic atmosphere during the 1992 Polar Sunrise Experiment. *J. Geophysical Research*, 99:25,379–25,389, 1994.
- [140] Y. Yokouchi, L.A. Barrie, D. Toom, and H. Akimoto. The seasonal variation of selected natural and anthropogenic halocarbons in the Arctic troposphere. *Atmospheric Environment*, 30(10/11):1723–1727, 1996.
- [141] T. Zeng, Y. Wang, K. Chance, E.V. Browell, B.A. Ridley, and E.L. Atlas. Widespread persistent near-surface ozone depletion at Northern high latitudes in spring. *Geophys. Res. Lett.*, 30:2298, doi:10.1029/2003GL018587, 2003.



Die gesamten Veröffentlichungen in der Publikationsreihe des MPI-M  
„Berichte zur Erdsystemforschung“,  
„Reports on Earth System Science“,  
ISSN 1614-1199

sind über die Internetseiten des Max-Planck-Instituts für Meteorologie  
erhältlich:

<http://www.mpimet.mpg.de/wissenschaft/publikationen.html>





